Diss. ETH No. 14895

Multiple-Response Verification of a Distributed Hydrological Model at Different Spatial Scales

A dissertation submitted to the
SWISS FEDERAL INSTITUTE OF TECHNOLOGY (ETH)
ZÜRICH

for the degree of
DOCTOR OF NATURAL SCIENCE

presented by

Massimiliano Zappa

Dipl. Natw. ETH
born April 12, 1975
Citizen of Onsernone, Ticino

accepted on the recommendation of
Prof. Dr. Christoph Schär, examiner
Prof. Dr. Günter Blöschl, co-examiner
Dr. habil. Joachim Gurtz, co-examiner
PD Dr. Rolf Weingartner, co-examiner

November 2002

Abstract

The UNO declared 2002 as the "International Year of Mountains" and the UNESCO declared 2003 as the "International Year of Freshwater". Both initiatives show that the international organizations and the worlds of politics, economy and health care are highly interested to come to a deeper knowledge about the distribution in time and space of the water resources in mountainous environments. The water flow from mountainous river basins represents the only source of freshwater for a large part of the earth's population. Scientists are challenged to investigate past, present and future distributions of the water resources. The development of distributed hydrological models and the evaluation of alternative sources for meteorological forcing, such as general circulation (GCM) and regional climate models (RCM), is part of this research task, in particular in areas with limited availability of surface meteorological observations.

Mountainous catchments are very complex systems with respect to the spatial and temporal distribution of the water resources. The hydrological complexity is determined by the climatological and physiographic characteristics, which leads to great local and regional variety of possible hydrological response and discharge regimes. Models are generally evaluated at one specific scale and with respect to a reduced number of observed variables. A main objective of this thesis is thus the multiple-scale and multiple-response verification of a spatially distributed hydrological model. Thus, a series of case studies at different spatial and temporal scales was completed and evaluated. For this study, the PREVAH model was used. PREVAH is based on the concept of the hydrological response units (HRUs).

A key task was the assessment of the adequate grid size for distributed hydrological simulations in mountainous river basins. A discretization method based on two hierarchical grid-structures is developed to address this question. This allows combining spatial data with different resolution and identifying the key physiographic characteristics that affect discharge simulations. The results in a pre-alpine catchment indicate that the quality of the discharge simulations is sensitive to the resolution of the land-use properties. In the case of a high-alpine catchment, there was a significant decrease in the quality of the discharge simulation when the model was run with low-resolution topographic information. 500 m grid spacing resulted as a critical resolution for the discharge simulation in these mountainous catchments with areas around 100 km^2.

A series of experiments is conducted to determine the water balance components and discharge regime of seven Swiss catchments with areas ranging between 3 and 1700 km^2 for periods ranging between 8 and 20 years. These experiments at catchment scale were based on spatially and temporally interpolated hourly meteorological information and spatially distributed physiographic information with a basic resolution of 100x100 m^2. PREVAH was able to cope with a large variety of different discharge regimes within the Swiss Alps. This shows that the snowmelt, icemelt and runoff-generation modules are able to handle lowland, pre-alpine, alpine and high-alpine catchments.

The results include not only integral evaluations of the model results, but also analysis on the quality of single model components at plot-scale. A validation of soil moisture and evapotranspiration simulation was completed using the data set collected during the special observing period of the Mesoscale Alpine Programme (MAP-Riviera Project). The simulation of soil moisture and evapotranspiration was more accurate when the model was driven with the locally observed meteorological information than when driven by

meteorological values interpolated from data provided by surrounding stations of the Swiss meteorological service. The simulation of evapotranspiration with three conceptual parameterizations of the exchange processes between soil, vegetation and atmosphere showed a high correlation to the latent heat fluxes diagnosed using the Bowen ratio method. Additional multiple-response verification with the long-term hydrometeorological observation at the lysimeter site of the Rietholzbach catchment confirmed the quality of the soil module and evapotranspiration schemes of PREVAH.

This study also tested model components with different degrees of physical treatment and completed an intercomparison between a HRU-based conceptual model (PREVAH) and a gridded physically-based hydrological model (WaSiM-ETH). The intercomparison showed that the two models, despite different degrees of complexity, allowed for discharge simulations with similar quality in the pre-alpine Rietholzbach catchment and in the high-alpine Dischmabach catchment. The findings of this intercomparison study demonstrate that the goodness of the snowmelt module is of decisive importance for simulating runoff-generation in a spatially distributed manner. A case study in the Dischmabach catchment assessed the quality of three temperature-index and one energy balance based snowmelt model. The highest efficiency score was obtained by a temperature-index approach enhanced by a radiation term. A physically-based energy balance approach showed a stronger year-to-year variability in quality than the three methods based on the temperature-index approach.

The last part of the thesis focussed on the application of PREVAH at larger spatial scales. In a first experiment, PREVAH was used to investigate the interaction between climate conditions and the hydrological response of the Volga source area (Russia) by means of a model chain approach. The meteorological forcing provided by direct measurements, and experiments with a GCM and a RCM are used to drive PREVAH. An intercomparison against a PREVAH simulation driven by observations is used to evaluate the adequacy of using GCM and RCM experiments as alternative meteorological data sources for water balance studies. The results show that only the RCM provides suitable meteorological time series in this region of the Russian Plain. The GCM was not able to provide a plausible estimation of the seasonal precipitation pattern.

The second large-scale experiment with PREVAH evaluated a simulation involving the whole of Switzerland. The experiment simulates evapotranspiration, runoff and other components of the water balance for the 20-year period 1981-2000. PREVAH was driven by daily meteorological data obtained from the MeteoSwiss network. The resolution of the spatial physiographic data was 500x500 m^2. The evaluation included comparisons with monthly discharge rates, patterns of snow cover distribution from remote sensing observations, snow water equivalent data and data on the natural water balance of Switzerland recently published in the Hydrological Atlas of Switzerland.

The overall results show that the hydrological model PREVAH is a reliable tool for detailed hydrological studies in the Alpine region at different spatial scales and in catchments with different climatology and hydrological responses. The available results can provide valuable inputs to a wide range of other studies in the Swiss Alps. Future challenges and applications of the PREVAH model will focus on the improved spatially distributed assessment of the water balance of Switzerland and the use of these results for the management of water resources in the Alpine area.

Riassunto

L'ONU e l'UNESCO hanno proclamato rispettivamente il 2002 "Anno internazionale delle montagne" ed il 2003 "Anno internazionale delle acque dolci". Entrambe le iniziative dimostrano che le organizzazioni internazionali sono particolarmente interessate ad avere a una visione dettagliata della distribuzione spaziale e temporale delle risorse idriche, soprattutto nel caso di regioni montane. I deflussi di acque dolci provenienti da bacini imbriferi montani rappesentano, in molti casi, l'unica fonte d'acqua dolce per un grande parte della popolazione mondiale. Gruppi di ricercatori devono lavorare a favore della ricerca sulla distribuzione passata, presente e futura delle risorse idriche. Lo sviluppo di modelli distribuiti per la simulazioni idrologiche e la valutazione di risorse alternative di dati meteorologici, quali modelli della circolazione generale (GCM) e modelli climatici regionali (RCM) sono una parte del processo di ricerca, particolarmente nel caso di regioni dove la disponibilità di un numero adeguato di stazioni meteorologiche affidabili é ridotta.

I bacini imbriferi delle regioni montuose sono caratterizzati da una distribuzione spaziotemporale molto complessa delle risorse idriche. Dal punto di vista idrologico, questa complessità é generata dall'interazione tra le caratteristiche climatologiche e morfologiche della regione in esame. Questa interazione provoca un'evidente differenziazione nella dinamica dei processi idrologici e nella varietà di regimi di deflusso a livello locale e regionale. La qualità dei modelli a disposizione é di regola valutata paragonando un numero molto ridotto di osservazioni con i risultati delle simulazioni fornite dal modello stesso. In più, spesso, solo simulazioni in una specifica scala spaziale sono considerate rilevanti per la valutazione dei modelli. Uno degli obiettivi principali di questa tesi di dottorato é perciò una valutazione globale della qualità di un modello idrologico, testando molteplici opzioni per la valutazione delle simulazioni e delle varie sottocomponenti del modello stesso. Queste valutazioni sono state condotte tramite esperimenti e studi sia a diverse scale spaziali (punto, superficie, regione) sia a diverse scale temporali (valutazioni su dati orari, giornalieri, mensili, annuali). Tutti gli esperimenti compiuti utilizzano un unico modello idrologico: PREVAH. La struttura di PREVAH si basa sul concetto degli idrotopi (unità spaziali idrologicamente simili).

Uno dei compiti principali della tesi é la determinazione della risoluzione spaziale adatta per simulazioni idrologiche distribuite in bacini imbriferi montuosi. I risultati indicano che, in caso di bacini imbriferi prealpini, la qualità delle simulazioni dei deflussi dipende dalla risoluzione delle informazioni riguardanti lo sfruttamento del territorio. Nel caso di un bacino imbrifero alpino é stato possibile osservare che una corretta simulazione dei deflussi presuppone dettagliate informazioni riguardanti la topografia. L'uso di una risoluzione spaziale superiore a 500 metri é sconsigliata se si desiderano ottenere simulazioni dettagliate in bacini imbriferi con un'area di circa 100 km^2.

Una serie di esperimenti ha coinvolto sette bacini situati nelle Alpi svizzere. L'area di questi bacini varia tra i 3 ed i 1700 km^2. Gli esperimenti hanno considerato lassi di tempo lunghi da 8 a 20 anni. I risultati mostrano che PREVAH é stato in grado di descivere accuratamente i diversi aspetti del bilancio idrico e del regime di deflusso di questi sette bacini imbriferi. Questo conferma che le diverse componenti del modello sono adatte per lavori di ricerca in bacini imbriferi di carattere agricolo, prealpino, alpino e glaciale.

L'analisi puntuale della qualità del modello é avvenuta usando dati raccolti nell'ambito del progetto MAP-Riviera (Mesoscale Alpine Programme). Questi dati hanno permesso di

accertare la qualità del modello del suolo e del modello che descrive i processi interattivi tra il suolo, la vegetazione e l'atmosfera. La correlazione presente tra l'osservazione ed il valore simulato é elevata sia in caso dell'umidità del suolo, sia in caso dell' evapotraspirazione. L'uso di dati meteorologici locali ha fornito simulazioni più accurate rispetto a quelle basate sull'uso di dati meteorologici interpolati. Uno studio condotto parallelamente ha dimostrato che PREVAH é in grado di simulare correttamente la dinamica dei processi di infiltrazione, evaporazione, traspirazione percolazione e produzione di deflussi. Queste conclusioni sono basate su paragoni con le componenti del bilancio idrico di un lisimetro situato nel bacino di ricerca Rietholzbach.

Un alto punto focale di questa tesi é stata la intercomparazione di diversi tipi di modelli, basati su differenti concetti, talvolta astratti, talvolta fisicali. I risultati ottenuti con modello idrologico astratto (PREVAH) sono stati paragonati con quelli forniti da un modello più fisicale (WaSiM-ETH). Seppur molto diversi, entrambi i modelli hanno dimostrato di possedere un livello di qualità molto simile. Sia PREVAH che WaSiM-ETH riescono a riprodurre la complessità dei processi idrologici all'interno di due bacini imbriferi delle valli svizzere, Rietholzbach (di carattere prealpino) e Dischmabach (di carattere montano). Questo studio ha confermato che la qualità della simulazione dei deflussi dipende in gran parte dalla qualità dal modulo del modello che descrive l'accumulazione e lo scioglimento del manto nevoso. Uno studio specifico nel bacino Dischmabach ha valutato la qualità di 4 algoritmi che descrivono la dinamica del manto nevoso. I risultati migliori sono stati ottenuti utilizzando un modulo per la simulazione della coltre nevosa basato sulla parametrizzazione dei processi in funzione della temperatura dell'aria e delle variazioni giornaliere dell'irradiazione solare.

Gli ultimi due esperimenti inclusi nella tesi trattano l'applicazione di PREVAH per la simuazione del bilancio idrico di regioni con area oltre i 3000 km^2. PREVAH é stato utilizzato per determinare l'interazione tra la situatione climatica e la dinamica dei processi idrologici della regione delle sorgenti del Volga (Russia). PREVAH é stato inizializzato con dati meteorologici ottenuti da modelli atmosferici. L'uso di dati da un GCM e da un RCM al posto di dati osservati é valutato paragonando simulazioni con PREVAH inizializzate da dati meteorologici osservati. I risultati dimostrano che solo i dati forniti dal RCM sono compatibili con il tipo di clima osservato nelle pianure della Russia. L'uso del GCM non ha permesso di ottenere dati meteorologici plausibili. Il regime delle precipitazioni simulato con il GCM non coincide con quello osservato al suolo.

L'ultimo esperimento completato é rivolto alla determinazione del bilancio idrico e del regime dei deflussi per tutta la Svizzera durante il ventennio 1981-2000. La valutazione dei risultati comprende l'analisi della qualità della simulazione del manto nevoso tramite paragoni con immagini dell'estensione del manto nevoso da satellite. Anche dati del contenuto idrico equivalente del manto nevoso e dei deflussi mensili sono stati utilizzati per valutare altri aspetti di questo esperiemnto. Un test di plausibilità é stato completato tramite paragone tra i valori del bilancio idrico naturale pubblicati di recente nell'atlante idrologico svizzero e i valori del bilancio idrico naturale determinati con PREVAH.

La globalità dei risultati ottenuti in questa tesi mostrano che PREVAH é affidabile quale strumento per studi idrologici dettagliati in regioni montane. Questi studi possono fornire informazioni rilevanti per altre ricerche, anche a carattere non prettamente idrologico, nelle valli svizzere. Gli obiettivi futuri saranno mirati al miglioramento nella determinazione del bilancio idrico naturale della Svizzera, così da poter sfruttare le conscenze ed i risultati ottenuti per la gestione delle risorse idriche in Svizzera, nell'arco Alpino ed in altre regioni montuose della terra.

Content

1. Introduction

1.1. Motivation

The past, present and future distribution in time and space of the available water resources are a problem that interests the worlds of politics, economy and health care. Scientists have to investigate these issues by means of sound hydrological models. The number of available hydrological models and components for such models is large (Beven 2000) and every model is generally able to handle one or more aspects of the hydrological cycle, most commonly the runoff hydrograph, with some degree of agreement. Grayson and Blöschl (2001) state:

> " *.in catchment hydrology our historic interest has been more related to temporal patterns and in particular, that of streamflow.*[but] *there is a wide range of spatial arrangements present in hydrologic systems. But because of an interest in streamflow, that wonderful integrator of variability, we have until recently managed to avoid confronting the challenges of spatial heterogeneity. "*

and further Beven (2000) adds:

> " *The availability of discharge data is important for the model calibration. It is also an integrated measure in that the measured hydrograph will reflect all the complexity of flow processes occurring in the catchment. "*

The two statements are to some extent conceptually different. Is the hydrograph a reflection of the complexity of flow processes within a catchment or a '*wonderful integrator of variability'*? The feeling is that the hydrograph can reflect to some extent the macroscopic complexity of the runoff-generation processes, such as the gradual increase and decrease of discharge in alpine catchments during the snowmelt period, but integrate the small-scale variability of all the hydrological processes within the catchment. It is therefore not possible to fully evaluate the quality of a distributed hydrological model only by comparisons with runoff discharges.

Both quotations indicate how strongly catchment hydrology is linked to the idea that the priority of any model is its capability of computing discharge, basically regardless of what is happening within the catchment itself. The development of spatially distributed models did not largely change the attitude of hydrologist. Such models allow for the computation of the catchment "*internal reaction*". However, the results obtained with distributed models are summarized and compared with observed discharge rates. So, it happens that most of the scientific literature related to spatially distributed models basically presents model evaluations with respect to observed discharges.

The assimilation of suitable data for calibrating and evaluating distributed models makes new problems arise (Beven and Feyen 2002), since the availability of representative data sets is limited and mostly consist of point observations. Plot-scale observations are useful for a qualitative verification of distributed hydrological models. The indications yielded from such comparisons are, to some extent, questionable because of the different scale between measurement site (a point) and model (an area) (Blöschl and Sivapalan 1995, Blöschl 1999) and because of the disagreement between the actual world and its conceptual discretization within the model (e.g. topography, soil characteristics and land cover). Seibert and McDonnell (2001 and 2002) define such point-information as "*soft data*" and demonstrate their usefulness for multiple response and internal model verification.

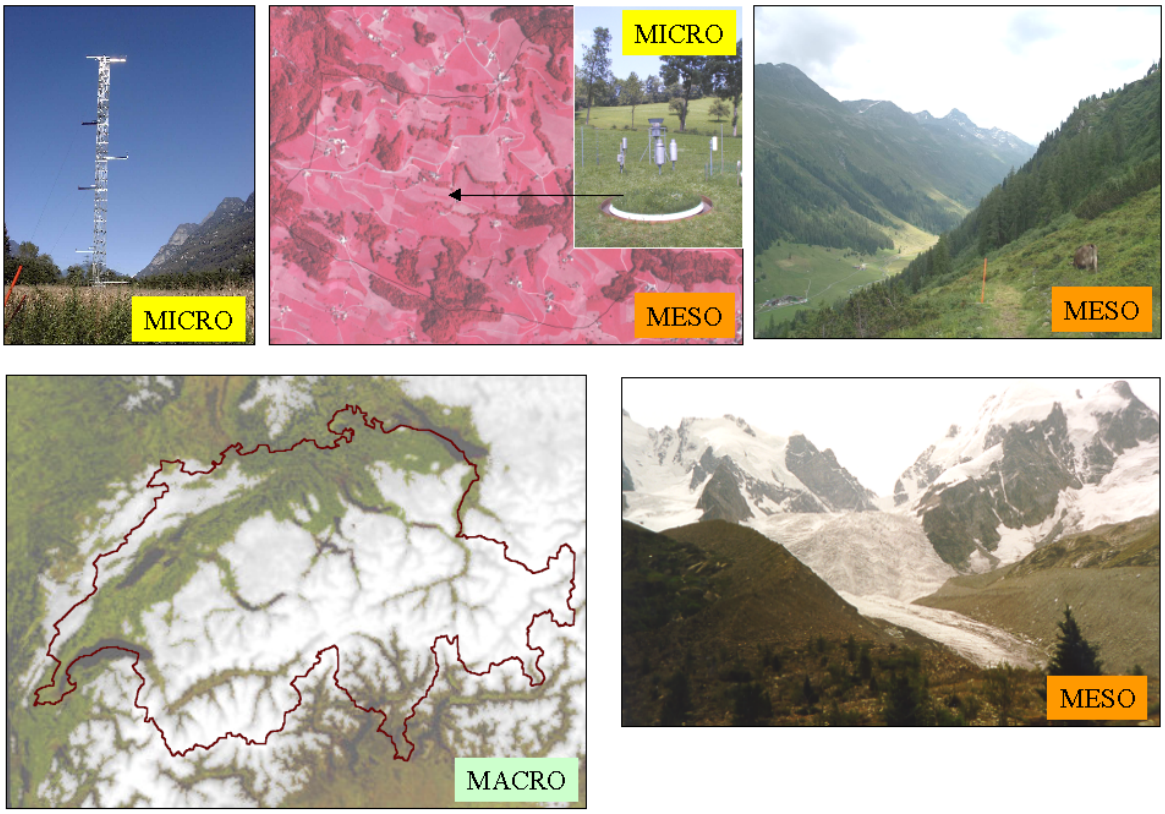

Figure 1.1 Views of the hydrological system Alps at different spatial scales. From top left clockwise: a meteorological tower in a alpine valley, an infrared airborne picture of the 3.3 km^2 hydrological research catchment Rietholzbach, the lysimeter site within the Rietholzbach catchment, a picture of the high-alpine valley Dischma, a picture of the partly glacerized Rosegbach catchment and a processed satellite shot of the snow-cover distribution in Switzerland (25 March 1998).

A way to handle the problem is to consider a hydrological model to be like a student who is learning several subjects and given exams for each subject to access to the next stage of his graduation. After graduation, the student is finally ready to contribute to the society. Similarly, the capabilities of a spatially distributed hydrological model must be tested in many different ways before adding further complexity. A thorough validated model can then being adopted to investigate practical problems and help increase the understanding of the processes governing the hydrological cycle.

Firstly consider the question from a Swiss perspective (figure 1.1). Switzerland, and particularly the its alpine regions, is a very heterogeneous system with respect to the spatial and temporal distribution of the different hydrological processes and of the water resources. Zooming from the macroscale to the alpine system it becomes evident that such heterogeneity is influenced by the local physiographic characteristics and, in some cases, by the presence of past-heritages like alpine glaciers. This leads to a great variety of possible hydrological responses and discharge regimes within this particular system. These result from the interaction between climate, topography, geology and many different kinds of anthropogenic activities. The investigation of such interactions by means of hydrologic models needs basic research activities at microscale and mesoscale. This allows for the acquisition of expertise for later macroscale model applications. Macroscale is obviously the scale in which both the decision making authorities and private companies (e.g. hydropower plants) are most interested in when discussing the

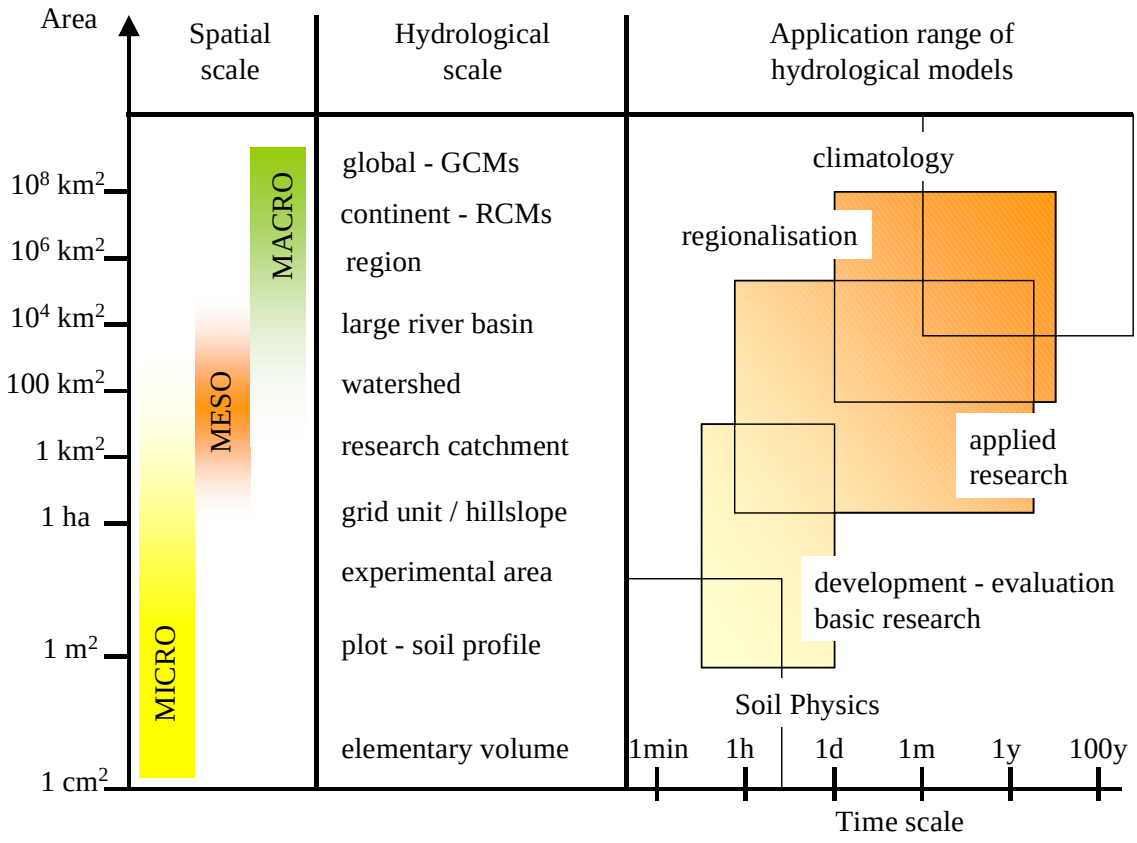

Figure 1.2 Application range of hydrological models at different spatial and temporal scales (plot based on a concept of Becker and Nemec 1987).

present and future management of water resources.

It is arduous to define the transition between micro-, meso- and macroscale (figure 1.2). In the case of watershed hydrology, it is useful to set such boundaries with respect to the area of the investigated system and the relevant time scales of the processes taking place within the system itself (Blöschl and Sivapalan 1995, Becker and Nemec 1987, Blöschl 2001). On the microscale, the model may be used to simulate the hydrological behaviour of a soil profile or for the assessment of processes taking place within an experimental area, which covers a few hectares. The research activities on this scale range allow for the development of the model, its components and the evaluation of its quality by means of a comparison with different hydrometeorological and soil physical quantities and with the observation of water fluxes and soil moisture content.

The application of hydrological models for investigating small, but highly equipped, research catchments (e.g. Kirnbauer *et al.* 2000) and mesoscale basins allows for the study of processes like snowmelt and runoff-generation. Such processes are characterized by strong spatial and temporal variability. Possible applications are the analysis of spatial patterns of snow-cover and soil moisture to investigate how distributed models can capture spatial variability (Grayson and Blöschl 2001). Similar approaches are used to evaluate snow-cover simulations at larger scales by means of snow-cover distribution patterns from satellite and/or airborne pictures (e.g. Strasser and Mauser 2001). The analysis of spatial patterns is so far one of the few effective ways to explicitly evaluate the quality of spatially distributed hydrological models, and to investigate the improved yielded by distributed models when compared to box and lumped models.

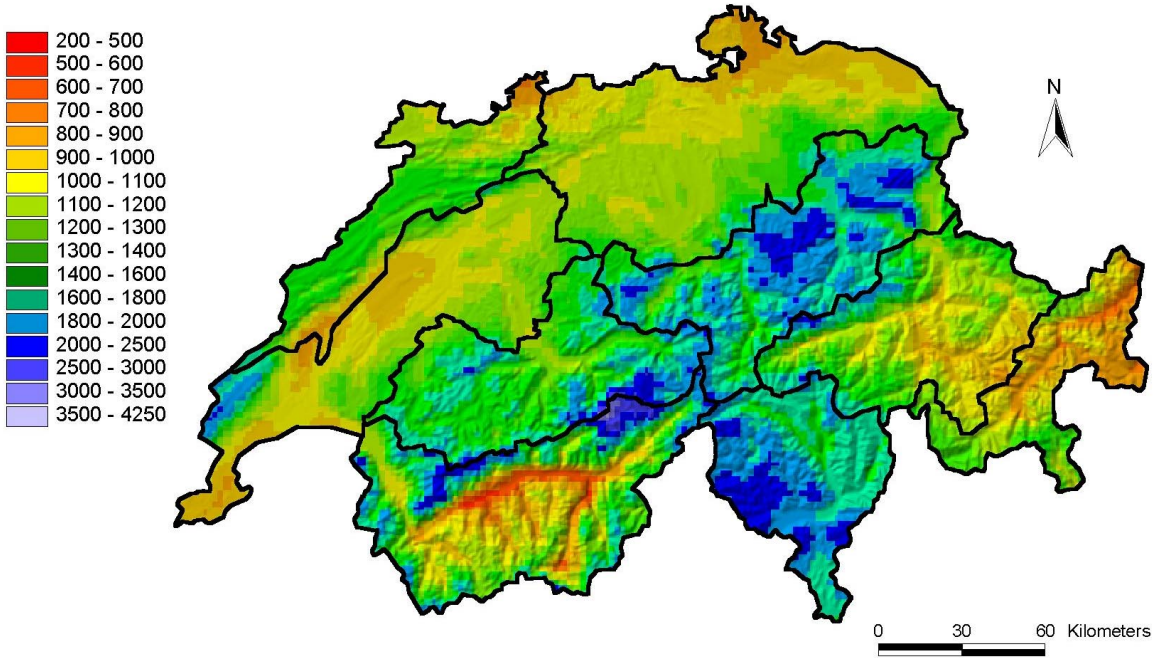

Figure 1.3 Precipitation climatology of Switzerland 1971-1990 [mm· y^{-1}]. Extract from the precipitation climatology of the European Alps by Schwarb *et al.* (2001).

With increasing area, the heterogeneity of the system increases. The regional climatological features become more evident. Streams with different discharge regimes merge and form large rivers whose hydrological behaviour integrates the signal of the various upstream sub-catchments. The simulations at large scales are characterized by feedbacks between hydrology and regional climatology. This opens possibilities for research work with coupled hydrologic and atmospheric models (e.g. Jasper 2001 and Kleinn 2002). One of the central tasks in this research field is the evaluation of the use of meteorological time series derived from experiments with atmospheric models for driving hydrological simulations. Such studies should help to acquire expertise for driving detailed hydrological simulations in large regions and in areas where the availability of reliable surface observations is limited.

The work of Schwarb *et al.* (2001) illustrates how important it is to account for the regional and sub-regional climatology to design any study related to surface water resources in the Alpine area. Figure 1.3 shows the precipitation climatology of Switzerland for the time range 1971 to 1990 overlapped by a subdivision of Switzerland into 9 climatological regions. The names of the units are declared in figure 3.1 and table 3.1. The differences from region to region and within regions are very important. Large differences may be noticed between the wet northern pre-Alps and the dry areas in the middle- and south-east. In the southern end of Switzerland, it can be observed that the valleys in the north-west part of the Ticino region (Valleys Maggia and Verzasca) are significantly wetter than the adjacent valleys in the north-east (Blenio and Mesox). In the region Wallis, there are ranges of average precipitation rates between 500 and up to 3000 mm per year at sites located less than 30 kilometres apart. The regional climatological features have to be considered when a distributed hydrological model is used for macroscale simulations. Both the meteorological information and the model parameterization need to be regionalized.

1.2. Aim of this study

A series of experiments at different spatial and temporal scales is evaluated. The experiments rely on the use of a spatially distributed hydrological model. The chosen model is PREVAH (*Precipitation-Runoff-Evapotranspiration HRU model*, Gurtz *et al.* 1999). It is based on the concept of the hydrological response units (HRUs), but has enough flexibility to also be run for a plot (a single HRU) or in gridded mode (as many HRUs as grid elements). One of the challenging issues of this work was the use of a large range of data for both model forcing and evaluation. Topical points were:

- the investigation of some critical issues in the model application at different spatial scales and with different spatial and temporal resolution.
- the testing of different solutions for the assessment of the model quality. This included the use of soil moisture data, lysimeter data, the eddy correlation technique for the measurement of latent heat flux, the Bowen ratio method for the computation of the latent heat flux, observations of the groundwater level, snow height, snow water equivalent, discharge observations, the Pardé coefficients, satellite observations of snow patterns. The combination of different options for model verification allowed a multiple response assessment of the model quality (Refsgaard 1997, Uhlenbrook and Leibundgut 2002, Gurtz *et al. 2003a*);
- the intercomparison of PREVAH with other models with a different degree of complexity and the analysis of different model components;
- the use of different sources of meteorological information. A hydrological model can be driven by meteorological time series obtained from point observations (instrumented meteorological towers) or assimilated from spatial and temporal interpolations of observations at surface stations within and around the region under investigation. The required meteorological input can also be provided by experiments with general circulation models (GCMs), climate models at regional scale (RCMs) and numerical weather prediction models (NWPs). Any model forcing data set can eventually be modified by means of climate scenarios.

The application of a unique model with all these sources of meteorological and hydrometeorological information was not previously experimented and should help to understanding the possible applications of complex hydrological models in the water resources management and research work at different scales.

The results of this work assess the suitability, strengths, possibilities and limitations of the chosen model at all considered scales. The PREVAH moved a step closer to becoming a tool for different kinds of studies related to water resources and consequent practical applications.

1.3. Literature review and state of the science

1.3.1 Distributed hydrological modelling in the alpine area

A key prerequisite for an appropriate simulation of hydrological processes is the development and application of physically congruous hydrological models, including careful parameterization, calibration and verification. In the last decades, the spatially distributed hydrological modelling became an established tool in catchment hydrology. The current models are used to study both the components and the possible changes of the hydrological cycle (Leavesley 1994). Beven (2000) gives an exhaustive review on the evolution of rainfall-runoff models up to the current state of the discipline. Following key points and papers can be emphasized:

- the concept of the rational method for the estimation of peak discharge developed in the second part of the 18th century;
- the first distributed approaches, published in the 1920's (e.g. Ross 1921);
- the idea of the unit hydrograph;
- the work of Horton (1933) for the parameterization of effective rainfall, saturation excess and infiltration capacity;
- the use of nomograms for determining storm runoff;
- the blueprint for physically-based hydrological simulations of Freeze and Harlan (1969);
- the development of *explicit soil moisture accounting models* (ESMA) such as the HBV model (Bergström 1976) and others (e.g. Franchini and Pacciani 1991);
- the TOPMODEL (Beven and Kirkby 1979);
- the conceptual separation of runoff-generation into components (Beven 1991, Gurtz *et al.* 2003a, Uhlenbrook and Hoeg 2003). A thorough review on scientific literature discussing runoff-generation is provided by Uhlenbrook (1999);
- the transition to fully distributed approaches (Ross *et al.* 1979, Abbot *et al.* 1986a and 1986b, Kirnbauer *et al.* 1994, Gurtz *et al.* 1999, Beven and Feyen 2002).

Pre-alpine and alpine catchments are characterized by highly variable morphology, soils and vegetation types and by pronounced temporal and spatial variations of the climatic elements (Klemeš 1990; Gurtz *et al.* 1999, Frei *et al.* 2000). Alpine discharge regimes depend, according to the location and elevation of the watersheds, on glacial melt, snowmelt, rainfall and their spatial and temporal superposition. The quality of the hydrological simulations depends on how the adopted models are able to describe and truly represent the heterogeneity of the hydrological system at the different spatial scales (Klemeš 1983, Blöschl and Sivapalan 1995). The availability of geographic information systems (GIS) and digital elevation models (DEM), the improved reliability, precision and resolution of meteorological and hydrological networks, combined with the availability of remotely sensed data collection, allowed the development and application of spatially distributed hydrological models within the alpine landscapes (Gurtz *et al.* 1999) and their calibration and evaluation with respect to observed temporal and spatial patterns (Grayson and Blöschl 2001).

1.3.2 Sensitivity of hydrological and atmospheric models to spatial resolution

The assessment of the model sensitivity to spatial resolution is central to the scientific community dealing with atmospheric research and catchment hydrology at all scales. Researchers using distributed rainfall-runoff models (Beven 2000, Singh and Woolhiser 2002, Refsgaard 1997) are particularly interested in evaluating the effects of the spatial

resolution of the physiographic information on the quality of hydrograph and water balance simulations (Singh 1997). The assessment of such interactions is essential since the small-scale variability of the processes leading to evapotranspiration and runoff generation is governed by the inhomogeneous, but to some extent organized, character of the physiographic properties within a catchment (Grayson and Blöschl 2000, Western *et al.* 1999) and by their interaction with the local and regional climatology (Gurtz *et al.* 1999). The generalization and aggregation of physiographic information inevitably leads to a loss in accuracy with respect to the description and parameterisation of the small-scale variability, which is particularly pronounced in the mountains where the choice of an adequate spatial resolution is of decisive importance for sound modelling experiments (Guert *et al.* 1997b).

Previous work had addressed some of these issues. Wood *et al.* (1988) demonstrated the existence of a representative elementary area (REA) for the simulation of runoff-generation by means of an experimental modelling approach. Their synthetic model realisations showed that the size of the REA is strongly influenced by the topography but less influenced by soils and variability of rainfall. More recent work with spatially distributed models (Zhang and Montgomery 1994, Schulla 1997, Kuo *et al.* 1999, Vàzquez *et al.* 2002, Haddeland *et al.* 2002) shows that the resolution of the spatial information available to the model considerably influences the simulation of soil moisture and discharge. Other studies were mainly focussed on the assessment of the hydrological simulations sensitivity to the digital elevation model resolution (Quinn *et al.* 1991, Wolock and Price 1994, Bruneau *et al.* 1995, Brasington and Richards 1998, Kenward *et al.* 2000, Higi and Musy 2000).

1.3.3 Assessment of the model quality at plot scale

Soil moisture and evapotranspiration are key elements of the water cycle. Their correct representation within hydrological models is essential for an accurate simulation of the exchange processes between soil, vegetation and atmosphere from the plot-scale up to the macroscale. The range of available land-surface schemes (LSSs) or SVATS (Soil – Vegetation – Atmosphere Transfer Schemes) to describe and simulate such interaction is very broad (Betts *et al.* 1996, Henderson Sellers *et al.* 1993, Schlosser *et al.* 2000).

The groundwork for intercomparison of LSSs with different degree of complexity includes the availability of detailed time series of observations from highly instrumented test sites (Schlosser *et al.* 1997, Aubinet *et al.* 2000, Mihailovic *et al.* 2000, Kirnbauer *et al.* 2000, Gurtz *et al.*, *2003*) and the launch of large international programs and projects like FIFE (Sellers *et al.* 1988), GEWEX (*Global Energy and Water Cycle Experiment*, Coughlan and Avissar 1996), BOREAS (*Boreal Ecosystems Atmosphere Study*, Sellers *et al.* 1997a), BALTEX (*Baltic Sea Experiment*, Raschke *et al.* 1998) and MAP (*Mesoscale Alpine Programme*, Bougeault *et al.* 2001). The development and reliability assessment of LSSs is requires comparisons with of hydrometeorological, biophysical and soil physical quantities as observed at the microscale. The validated LSSs are then scaled up and integrated within hydrologic models (Walko *et al.* 2000), RCMs, NWPs and GCMs. Sellers *et al.* (1997b) provide a comparative review of LSSs used in numerical models of the atmosphere, which are increasingly capable of representing the complex feedbacks of land-surface / atmosphere interactions. Spatially distributed hydrological models used to predict runoff in an entire catchment often use more simplified surface layer schemes to obtain the fluxes of sensible and latent heat from energy balance equations (e.g. Gurtz *et al.* 1999, Carlaw 2000, Zappa and Gurtz 2003).

1.3.4 Simulation of snow hydrology with spatially distributed models

The choice for temperature-index or energy balance based approaches for the computation of the snowmelt processes is a subject of frequent discussions in the scientific community dealing with snow hydrology and glaciology (WMO 1986, Ferguson 1999, Hock *2003*). The topical discussion includes the dilemma of using conceptual (Braun *et al.* 1994) or physically-based models (Abbot *et al.* 1986a, Beven 1989), the importance of the model structure (Braun *et al.* 1994, Klok *et al.* 2001, Zappa *et al. 2003*) and scaling issues (Blöschl and Sivapalan 1995, Blöschl 1999).

Klemeš (1990) discusses the differences between conceptual and physically-based snowmelt models with respect to their structure, need of data and calibration requirements. The more free parameters are available to fit the model for a selected catchment, the more it is possible to compensate the cumulative error caused by:

- observation of the target variables (discharge and snow water equivalents);
- parameterization (soil, physiographic and vegetation-specific parameters);
- conceptual representation of the hydrological processes (e.g., assumption of the linear response of storage reservoirs, separation between snow and rain, correction of precipitation);
- meteorological input data (plot-scale and / or interpolated).

Physically-based models, such as energy balance based snow models, tend to increase the a priori parameterization of the processes and to reduce the need of calibration to a minimum number of free parameters. This allows the transfer of experience from one catchment to another without starting the calibration again from scratch. The disadvantage is that an increased number of variables needs to be observed. Detailed snowmelt routines based on the parameterization of the energy balance are often integrated in land surface schemes. LSSs have been the target of several intercomparison studies at plot scale (Henderson-Sellers *et al.* 1996). Recent studies, focussing on the snow-cover, have been published by Slater *et al.* (2001), Essery *et al.* (1999), Strasser *et al.* (2002) and Gusev and Nasonova 2002.

Conceptual models, such as temperature-index based snow models, allow model application with fewer input variables. By tuning the free parameters the specifications of the catchment under investigation are captured. This generally increases the model performance within a catchment, but gives few indications for the transfer of the results to other regions. Measurement and spatial interpolation of air temperature with high resolution is easier to realize than detailed energy balance observations. Therefore, model users tend to apply temperature-index methods (Lang and Braun 1990, Hock *2003*) for spatially distributed hydrological simulations (Kirnbauer *et al.* 1994). Ohmura (2001) provides a thorough physically-based answer to the question why empirical temperature-based methods are effective, as generally shown in snow and ice melt computations. The temperature-index models perform that well, because the air temperature is a particularly representative diagnostic variable for the three major energy sources, which determine snowmelt and icemelt. These are the incoming longwave radiation, the absorbed global radiation and the sensible heat flux.

1.3.5 One way coupled use of atmospheric and hydrological models

One of the most important issues in catchment hydrology focuses on the evaluation and prediction of the impact of climate change on water resources. Wood *et al.* (1997) identify the role of hydrological modelling and model parameterization in relation to the

application of climate scenarios. Gyalistras *et al.* (1998), in focussing on the Alpine climate, described the kinds of scenarios required to analyse the possible feedback between climate change and social sciences, economy, glaciology, geomorphology, ecology and hydrology.

In the past decade, the one- and two-way coupling of different kinds of atmospheric models such as GCMs, RCMs (McGregor 1997) and NWPs (Jasper *et al.* 2002) with detailed hydrological models have become an important approach for investigations of climate change and its impact on the hydrological cycle. The high spatial and temporal resolution of meteorological inputs required for hydrological simulations implies the availability of accurate GCM, RCM and NWP experiments. Atmospheric models are able to integrate representative meteorological time series at the regional scale. One of the most promising applications of driving hydrological models with GCM, RCM or NWP data sets is the simulation of large watersheds with reduced networks of surface meteorological and hydrological observations. Scientific literature presenting studies that adopted similar approaches includes the works of Kouwen *et al.* (1996), Kite (1997), Kite and Habertland (1999), Krysanova *et al.* (1999), Benoit *et al.* (2000), Jasper *et al.* (2002) and Oltchev *et al.* (2002). Jasper (2001) and Kleinn (2002) provide a review on studies with coupled hydrological and RCMs / NWPs.

2. Methods

2.1. The hydrological model PREVAH

2.1.1 Spatial discretization: the HRU approach

When hydrological modelling is applied to different spatial units, the nature and size of the units must account for the complexity of the landscape and the accuracy required by modelling task (Gurtz *et al.* 1999).

The spatially distributed hydrological model PREVAH (Precipitation-Runoff-Evapotranspiration-HRU model) fulfils such requirements and was used for all the hydrological simulations that are incorporated in this work. The model can either be applied to each single grid cell or to an aggregation of spatially distributed grid cells, which are similar according to a set of structural and statistical differentiation characteristics. This implies a similar / homogeneous hydrological response, if the applied criteria for differentiation have a direct feedback with the most important processes controlling evapotranspiration and runoff-generation. Such an aggregation of hydrologically equal surface units is called a 'hydrological response unit' HRU (Ross *et al.* 1979, Engel 1996, Moore *et al.* 1993, Flügel 1997).

The HRU approach allows for the discretization of a catchment with an internally dynamical spatial resolution. The HRU size is smaller where the ensemble of the characteristics of the soils, land surface and topography shows higher spatial variability (see also table 3.1, Gurtz *et al.* 1997b and Zappa and Gurtz 2002). For plot-scale experiments, a single HRU is defined according to the characteristics of the site under investigation. For distributed simulations, a set of HRUs has to be defined. Different levels of information classes (figure 3.1) are introduced and used to generate the HRUs (Nemec 1993, Gurtz *et al.* 1999):

- the **level of the river system.** In particular the subcatchment areas and the channel network can be identified from the topography and the position of gauging stations;
- the **topographic level** is characterized by elevation, aspect (typically five classes: north, east, south, west or flat) and slope. The amount of energy available for evapotranspiration is strongly controlled by these factors in combination with surface albedo;
- the **level of the meteorological input variables.** The definition of meteorological sub-units is typically related to the delimitation of 100 meters elevation zones on the basis of the available digital elevation model (DEM). The use of other criteria for such differentiation is also possible;
- the **level of land-use characteristics** which are an important control on evapotranspiration as well as on processes involved in runoff-generation. In the case of glacerized catchments a further classification is required. The disposition of the grid elements with respect to the equilibrium line of the glacier (accumulation, ablation or ice-free area) has to be determined (Badoux 1999);
- the **level of soil properties and geology** includes field capacity, soil depth, permeability, groundwater recharge and storage characteristics. The extrapolation of those properties allows the description of the feedback between soil and water balance components.

The typical rules for generating a code for the definition of HRUs (figure 2.1) assign to an HRU all the grid elements in the same meteorological sub-unit, with similar aspect,

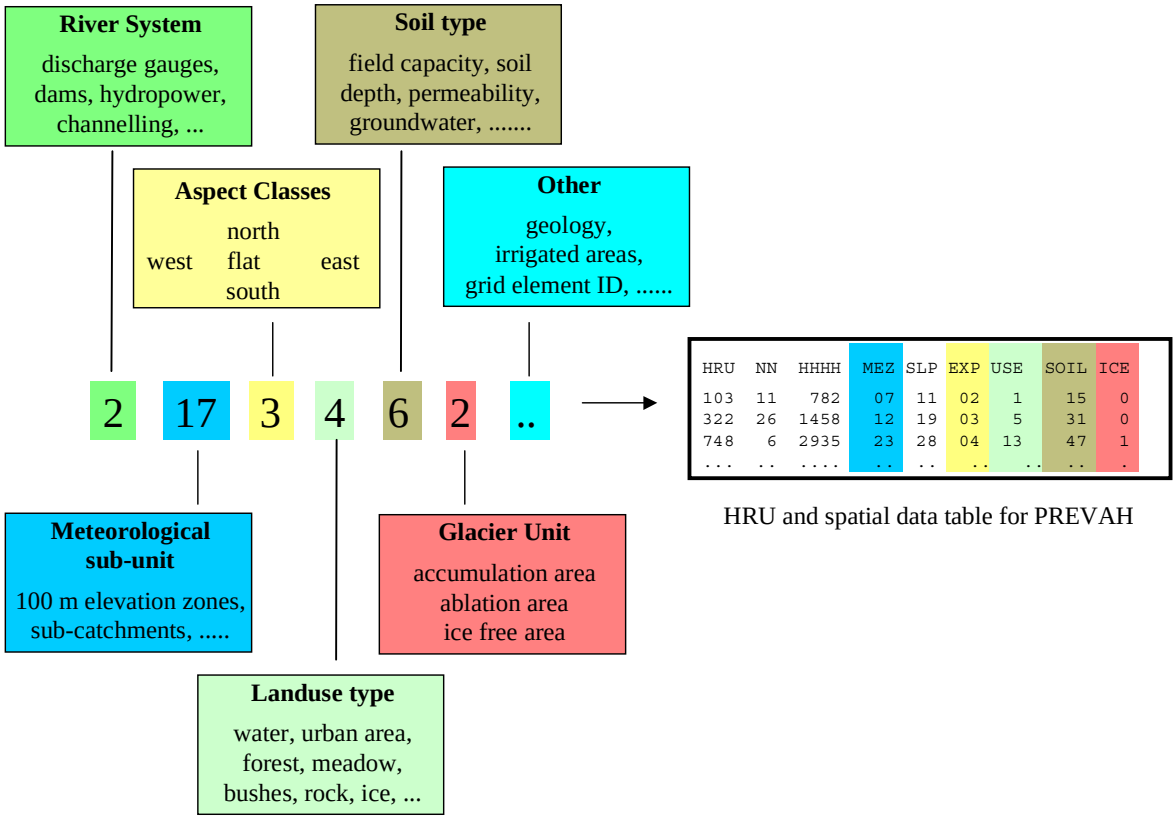

HRU and spatial data table for PREVAH

Figure 2.1 Preprocessing of spatial information for PREVAH including the possible criteria adopted for the aggregation of the HRUs.

same land-use classification and, eventually, same position with respect to the equilibrium line of a glacier. Grid-based simulations are also possible. In this case the rules for assembling the HRUs consist of making a code based on the level of the meteorological sub-units and the identifier of the raster elements (chapter 4).

The software package HYREU (Hydrological-Response-Units, Zappa 1999) was used to process GIS compatible spatial information and generate the HRUs. In comparison with the common GIS-applications HYREU, accelerates the preprocessing of the digital maps and the aggregation of HRUs. The preprocessing of the spatial digital information includes a complete topographic analysis (determination of slope, aspect, elevation zones, digital river network and other topographic characteristics), the possibility of summarizing the landuse classes to hydrological relevant classes and of assigning the parameterization of the soil properties from the map of the soil types. HYREU was designed to deal with a standard Swiss digital database (BFR 1980, BFS 1995, BFLT 1991), but was also adopted to process the database of spatial information for the Upper Volga catchment (Oltchev *et al.* 2002). HYREU stores all the HRU-specific spatial information needed for the simulation in a table that is assimilated by PREVAH at initialization.

Each HRU is provided with a set of parameters and relevant starting values, and is modelled separately. Such parameterization is based on information derived from the digital elevation model (elevation, exposure, slope, topographic index), soil maps (plant-available soil field capacity, soil depth, soil conductivity) and digital maps of landuse. For the determination of evapotranspiration, additional parameter values are introduced (Gurtz *et al.* 1999). The most important parameters that vary in time (monthly resolution) are: albedo, root depth, interception storage capacity, vegetation height, leaf area index (LAI), and minimum stomatal resistance of the various classes of vegetation.

The individual position of the HRUs within a catchment is not specified in model calculations, but tracked through the code of the HRU (chapter 4). The HRU code allows for the summary of the results for the whole catchment, and for the generation of spatially distributed grids of the simulated hydrological variables.

2.1.2 Temporal discretization

PREVAH always run at an internal time step of one hour. Depending on the choice of the evapotranspiration scheme up to six meteorological input variables are required:

- precipitation [mm per time step];
- air temperature [°C]. Air temperature is corrected for slope and aspect.
- global radiation [$W \cdot m^{-2}$]. Global radiation is also corrected for slope and aspect;
- relative sunshine duration [-];
- wind speed [$m \cdot s^{-1}$];
- relative air humidity [-] or water vapour pressure [hPa].

If only daily values of the meteorological elements are available, 24 identical values are assumed for every day in the case of air temperature, wind speed, water vapour pressure, relative humidity and precipitation. Daily values of global radiation are subdivided between sunrise and sunset according to the calculated potential clear-sky direct radiation (Schulla 1997, Hock 1999).

This assumption of uniform precipitation intensity and air temperature may principally affect the accuracy of the simulation of snow accumulation, snowmelt and runoff-generation. Zappa and Gurtz (2003) discuss this problem in the case of plot-scale simulations of soil moisture and evapotranspiration and conclude that the underestimation of the rain intensities leads to systematic errors in the computation of the soil water content but has a reduced effect on the estimation of daily evapotranspiration rates.

2.1.3 Meteorological information from surface observations

When PREVAH is driven by information obtained by an experimental meteorological tower, then the observations of the required meteorological inputs are directly adopted for plot and small-scale hydrological simulations.

Distributed hydrological modelling with PREVAH in Swiss mesoscale catchments is based on hourly observations of the climatic variables at different automatic weather stations run by MeteoSwiss. The used stations lie within or near the investigated area. In addition, meteorological information from a conventional weather station network is used. Such stations provide three readings of air temperature, wind speed and relative humidity daily and two readings of precipitation. Furthermore, a dense network of over 300 gauges distributed throughout Switzerland is available for the assimilation of detailed daily information on precipitation.

The procedure adopted for the spatial and temporal interpolation of observed meteorological information is described in Schulla (1997), Jasper (2001) and Klok *et al.* (2001). It is based on *altitude dependent regression* (ADR) and *inverse distance weighting* (IDW). In the preprocessing of the meteorological information, the data interpolation module of WaSiM-ETH is used. WaSiM-ETH is a grid-based hydrological model and allows for the interpolation of meteorological information for each grid element within the catchment under investigation (figure 2.2).

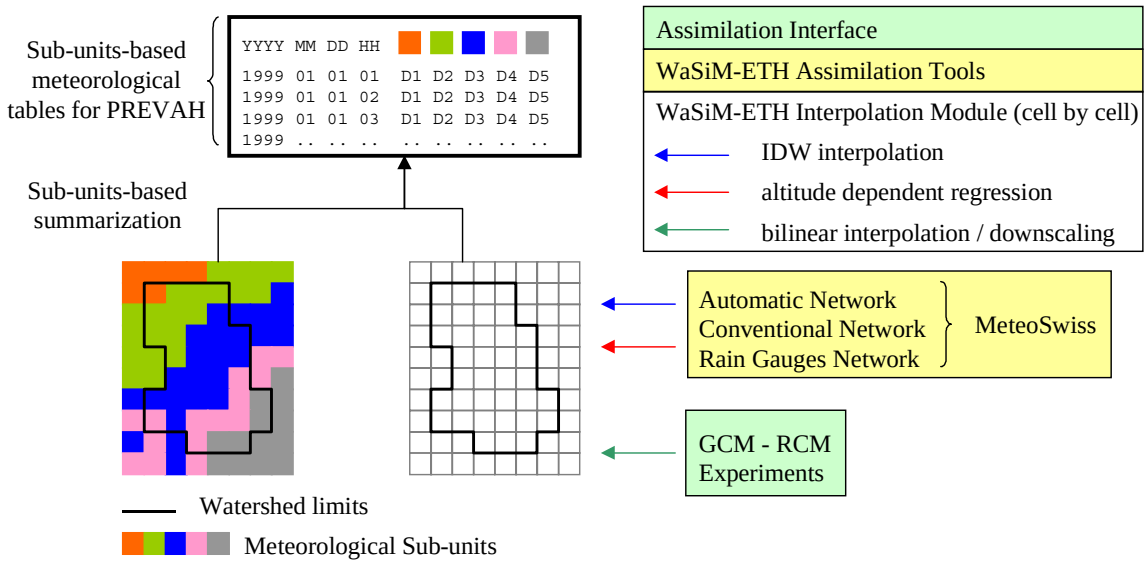

Figure 2.2 Assimilation of meteorological information for PREVAH using the interpolation module of WaSiM-ETH.

In the case of precipitation, the observations are separated into rain and snow before interpolation and corrected for the systematic, wind-induced measurement errors. The interpolation module of WaSiM-ETH determines, for every time step, an average value of each required climate element for all the defined meteorological sub-units in the catchment, as required by PREVAH (figure 2.2).

2.1.4 Use of meteorological information from atmospheric models

The application of PREVAH in the Upper Volga watershed (section 3.2.2 and chapter 6) required the assimilation of meteorological information from experiments with both a climate model at regional scale and an atmospheric GCM. The interpolation module of WaSiM-ETH also offers a suitable assimilation module. The grid elements of the GCM and RCM domains in the neighbourhood of the investigated area (e.g. fig. 3.5) are regarded as virtual surface meteorological stations and the meteorological information is then downscaled to the domain of the hydrological model by using bilinear technique (Schulla and Jasper 2000, Jasper 2001, Jasper *et al.* 2002, Kleinn 2002).

Gyalistras *et al.* (1998) discuss several methods for downscaling data from GCMs. In the case of grid point-based methods (as considered here) the use of individual GCM grid points is not particularly reliable in regions with complex topography such as the Alpine region. Such a restriction should not be that relevant within far reaching flat Upper Volga watershed.

2.2. The modules of PREVAH

Adjustment of precipitation

PREVAH offers the opportunity of adjusting precipitation by tuning two parameters (Gurtz *et al.* 1997a, Pos 2001):

$$P_{Rain} = P \cdot (1 - p_{Snow}) \cdot PKOR$$
$$P_{Snow} = P \cdot p_{Snow} \cdot SNOKOR \qquad (1)$$

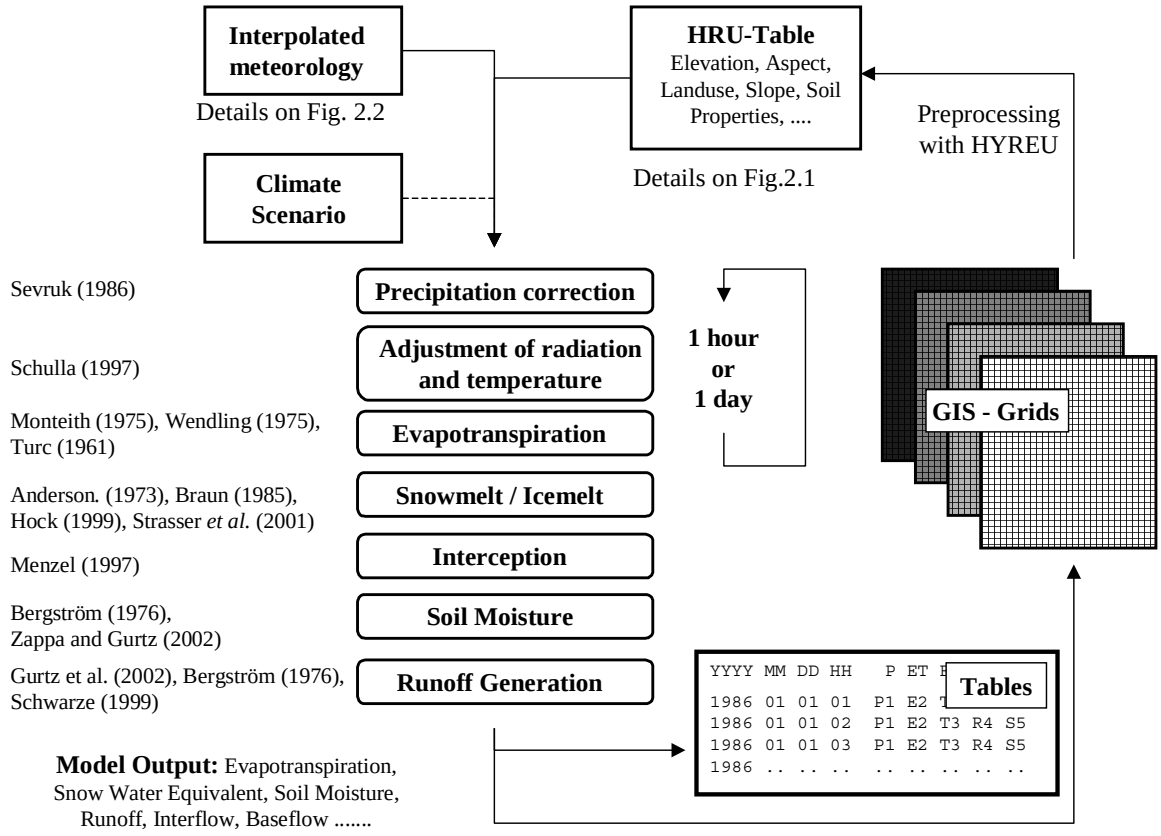

Figure 2.3 The flow chart of the PREVAH modules, including the assimilation of physiographic and meteorological information and the gridded or table-oriented model outputs.

P is the precipitation value obtained from a meteorological tower or provided by the interpolation module of WaSiM-ETH, P_{Rain} the adjusted rainfall, P_{Snow} the adjusted snowfall, p_{Snow} is the snow fraction (Eq. 2), *PKOR* and *SNOKOR* are two catchment specific tuneable parameters for rainfall and snowfall, respectively. Both parameters have to be determined during the calibration period. This allows for the minimization of the differences between observed and computed runoff rates and compensates for errors in the measurement, assimilation and interpolation of precipitation data (Sevruk 1986). The same factors may be utilized to scale *P* through consideration of a more detailed climatology as determined with other interpolation procedures (e.g. Schwarb *et al.* 2001). This procedure is presented in section 7.2.

The evapotranspiration module

Potential evapotranspiration is calculated following the Penman-***Monteith*** equation (Monteith 1965, 1975 and 1981). This widely used scheme relies on the Penman equation for potential grassland evapotranspiration (Penman 1948 and 1956). The adjustment to different surface characteristics or landuse types (including water bodies, urban areas and snow) is done by varying the albedo (Gurtz *et al.* 1999) and the stomatal resistances. The calculation of actual evapotranspiration is based on the simulated soil moisture deficit in the aeration zone. Two additional empirical schemes are implemented in PREVAH for the estimation of potential evapotranspiration: the ***Wendling*** equation (Wendling 1975, Schulla 1997, DVWK 1996), and the ***Turc*** equation (e.g. DVWK 1996). All the six previously listed meteorological variables are required to operate PREVAH using *Monteith*. For model runs configured for using *Wendling* or *Turc*, only information on

precipitation, air temperature and global radiation is needed. The equations of all three evapotranspiration schemes are summarized in Appendix A.

Snow accumulation module

A separation between snow and rain is made to determine snow accumulation. If the interpolated air temperature at 2 metres height T_a [°C] is lower than a calibrated threshold temperature T_{GR}, the phase of precipitation is solid. Otherwise, the phase of precipitation is liquid. A transition parameter (T_{TRANS}) can be adopted to define the air temperature range where the phase of precipitation is considered a mixture of rain and snow. The snow fraction (p_{Snow}) is given by:

$$p_{Snow} = \frac{T_{GR} + T_{TRANS} - T_a}{2 \cdot T_{TRANS}} \qquad (T_{GR} - T_{TRANS}) < T_a < (T_{GR} + T_{TRANS}) \qquad (2)$$

Snowmelt module

Four modular approaches for the spatially distributed computation of snowmelt are available:

a. The Positive Degree-Day Index (**PDDI**): This classical temperature-index method requires only the availability interpolated temperature data. If T_a is below a threshold temperature for snowmelt (T_0) then the melt rate (M) is zero. If T_a exceeds T_0 then the melt rate is calculated according to:

$$M = TMF_{PD} (T_a - T_o) \qquad (3)$$

The temperature dependent melt factor (TMF_{PD}) can be defined by a sinus shaped function of the threshold values between the annual maximum (set for June 21st) and minimum values (December 21st). In this differentiation, the seasonal variation of the solar radiation is taken into account (Braun 1985).

b. The Combination approach (**COMB**): Anderson (1973) extended the PDDI method introducing a combination of radiation melt for dry periods and advection melt for wet days. Radiation melt occurs when the melt is dominated by radiation energy. This occurs when the precipitation is less than threshold intensity. In that case snowmelt is calculated using Eq. (3). Advection melt occurs when rainfall exceeds threshold intensity. In this case a simple empirical parameterization of the energy balance, Eqs. (4.a)-(4.e), is applied for the computation of snowmelt (Braun 1985). The total snowmelt M is the sum of the melt rates given by long wave radiation (M_R), sensible heat flux (M_S), latent heat flux (M_L) and precipitation (M_P) :

$$M_R = f_R \cdot T_a \qquad (4.a)$$

$$M_S = (c_1 + c_2 \cdot u) \cdot T_a \qquad (4.b)$$

$$M_L = (c_1 + c_2 \cdot u) \cdot (e_a - 6.11)\, \gamma^1 \qquad (4.c)$$

$$M_P = f_P \cdot P \cdot T_a \qquad (4.d)$$

$$M = M_R + M_S + M_L + M_P \qquad (4.e)$$

f_R ($1.4 \cdot 10^{-8}$ m s^{-1} K^{-1}) and f_P (0.0125 K^{-1}) are parameterized constants; c_1 and c_2 are empirical model parameters and γ is the psychrometer constant.

c. The extended melt approach (**EMA**): Hock (1999) proposed the extension of the temperature-index approach under consideration of the daily potential direct radiation variations:

$$M = \begin{cases} (TMF_{EMA} + RMF_{EMA} \cdot I_0) \cdot (T_a - T_0) & T_a > T_0 \\ 0 & T_a \leq T_0 \end{cases} \quad (5)$$

I_0 is the site adjusted clear-sky direct solar radiation, TMF_{EMA} is a temperature dependent and RMF_{EMA} a radiation dependent melt factor. The inclusion of I_0 allows taking into account the pronounced daily cyclicity and the large spatial variability of the melt rates without increasing the required number of climate elements. The simulation of ice melt in the glacerized areas is also based on this approach.

d. The one-layer snow model **ESCIMO** (*Energy-Balance Snow Cover GIS-Integrated Model*) was developed for the hydrological simulation of the Weser catchment in Northern Germany (Strasser and Mauser 2001). It is designed as a physically-based model for the hourly simulation of the energy balance, the water equivalent and the melt rate of a snow-cover. The principle and most influential terms of the energy balance are the short and longwave radiation, the sensible and latent heat fluxes. The energy conducted by solid or liquid precipitation and a constant soil heat flux are also taken into account for the energy balance computation, even if their contribution is rather limited. The snow albedo is modelled using a function considering the age and the surface temperature of the snow pack (Rohrer 1994a and 1994b). For each time step the following scheme is adopted (Abbott *et al.* 1986a and 1986b): calculation of the energy balance, decision whether the precipitation is solid or liquid, estimation of the water mass and energy budget based on the hypothesis of zero snowmelt at the current time step, comparison of the total available energy with that sustained as snow by the total available mass at 273.16 K, calculation of the snowmelt produced by the available excess energy and a subsequent update of the mass and energy budgets. The number of free parameters is limited to the three. These control the simulation of the albedo and are the maximal albedo (ALB_{MAX}) and the parameters determining the ageing of the albedo (A_{POS} for positive and A_{NEG} for negative snow temperature). The mathematical representations of the simulated physical processes as used in ESCIMO are described in Strasser *et al.* (2002).

The glacial melt module

In the glacial melt module (Zappa *et al.* 2000, Klok *et al.* 2001, Verbunt *et al.* 2003), the amount of melting from the glacerized *HRU*s is calculated and the routing of melt water and possible liquid precipitation is determined. The glacerized surfaces are subdivided into a system of three linear reservoirs. A *HRU* is assigned to the *firn* reservoir if located above the *equilibrium line altitude* (ELA) of the glacier and, depending on the presence of snow-cover, to the snow or ice reservoir if located underneath the *ELA*. The melting from both snow and firn reservoirs is calculated within the snow sub-model with a degree-day approach. Melting from snow free ice areas IM is determined within the glacier sub-model following a modified temperature-index approach, including potential direct clear-sky solar radiation I_0 (Hock 1999):

$$IM = \begin{cases} (TMF_{ICE} + RMF_{ICE} \cdot I_0) \cdot (T_a - T_0) & T_a > T_0 \\ 0 & T_a \le T_0 \end{cases} \quad (6)$$

TMF_{ICE} and RMF_{ICE} are respectively a melt factor and a radiation coefficient that controls icemelt from glacerized HRUs below the ELA. The routing procedure is different for the defined reservoirs. Their content is transformed with calibrated storage and translation coefficients. The water from the firn reservoir is redirected into the groundwater reservoir and is then transformed within this reservoir to leave the catchment as baseflow (Badoux 1999). The outputs from snow and ice reservoirs are added to the fast and delayed surface runoff components.

The interception module

The filling of the interception storage is calculated as proposed by Menzel (1997). The interception model considers variations in interception storage as a function of the vegetation type. Evaporation of intercepted water occurs from vegetated surfaces, at the potential rate as long as the reservoir contains sufficient humidity. The surface depression storage capacity of rocky soils and urban areas is also defined for the calculation of direct evaporation. The equations of the interception module are summarized in Appendix A.

The soil module

Figure 2.4a presents the conceptual structure of the soil model in PREVAH, including the module of runoff-generation in the upper zone (*SUZ*) (Bergström 1976 and 1992). The link between the loss of water by evapotranspiration and runoff is given by the plant-available water storage in the aeration zone of the soil (*SSM*). The maximum storage capacity (*SFC*) is dependent on the soil depth (*Z*), the effective root-depth, and the plant-available field capacity of the soil (*AFC*). The inflow into the soil model (P_b) is supplied by the precipitation reaching the soil and by snowmelt. The non-linearity parameter *BETA* controls the redistribution of P_b between *SSM* and *SUZ*.

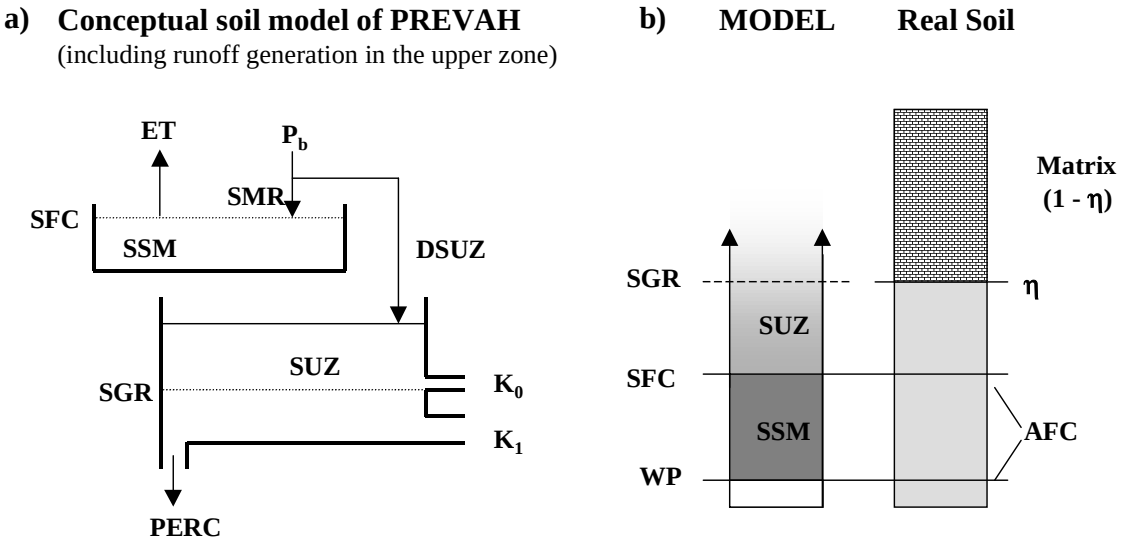

Figure 2.4 a) Conceptualisation of the soil model in PREVAH. b) Schematic conceptualisation of the real soil and of its parameterization in the hydrological model. Acronyms are defined in the text.

SFC regulates the inflow into the runoff-generation module (*DSUZ*):

$$DSUZ = P_b \cdot \left(\frac{SSM}{SFC} \right)^{BETA} \tag{7}$$

The soil moisture recharge (*SMR*) is the difference between P_b and *DSUZ*. *SMR* increases with increasing *BETA* (Uhlenbrook 1999). The generation of surface runoff and interflow is governed by the threshold parameter *SGR* and by the storage coefficients K_0 and K_1. The soil moisture is not explicitly calculated by PREVAH. Figure 3b shows how the description of the soil water content is conceptualized by PREVAH into three parts: the water content below the wilting point (*WP*), the content of *SSM* (limited by *SFC*) and *SUZ*. The water content below *WP* has to be added to the modelled *SSM* and *SUZ* to have a representative actual value of the soil moisture. The soil moisture as diagnosed in this way can be compared to the observed water content of the soil. The maximum water content of a soil profile is theoretically given by the porosity (η) and the soil depth (*Z*). The maximum value for *SUZ* is not assigned (fig. 3b). However the model structure implicitly allows values of *SUZ* above *SGR* only for a limited number of time steps, as governed by the storage coefficients K_0 and K_1 and by the rate of deep percolation *PERC*. The equations governing the water flows illustrated by figure 2.4 are presented in Appendix A.

Disaggregation and aggregation of the runoff components simulation

No suitable observation is available for the determination of the specific storage coefficients of each HRU. Thus, the free parameters of the runoff-generation module are obtained by comparison between the observed and simulated discharge at the catchment outlet. This would theoretically assume that a single large reservoir is defined for the whole catchment. This reservoir would collect the water flows and generate the runoff components after the scheme illustrates in figures 2.4 and 2.5. Contrarily, the concept implemented in PREVAH assigns to each HRU an own linear reservoir cascade. Being the reservoir cascade (figure 2.5) a linear system, it can be assumed, at a first stage, that each HRU is a catchment with equal area as the investigated domain. The same storage coefficients determined for the whole catchment are assigned to the single HRUs for the computation of the runoff components. The water flows yielded by the reservoir cascade of each HRU are then aggregated over the whole catchment, accounting of the portion of each single HRU to the total area of the catchment. Being the system linear, this additional disaggregation for the determination of runoff-generation does not change value of the simulated discharge. Becker and Braun (1999) define this disaggregation procedure as "fractional area concept", or "mosaic approach". Additionally, the disaggregation of the runoff components computation at the level of the HRUs also allows for the tracking of the local moisture content, when the soil water content is above field capacity. The local diagnosis of soil moisture for each HRU follows the scheme presented in figure 2.4 and discussed in the previous sub-section.

The runoff-generation module

Runoff-generation in mountainous catchments is characterized by high spatial, altitudinal and temporal variability. Such behaviour depends on the distribution of precipitation, snowmelt and glacial melt, evapotranspiration, soil moisture as well as on the spatial distribution of the physiographic properties (Frei *et al.* 2000, Gurtz *et al. 2003a*, Verbunt *et al.* 2003).

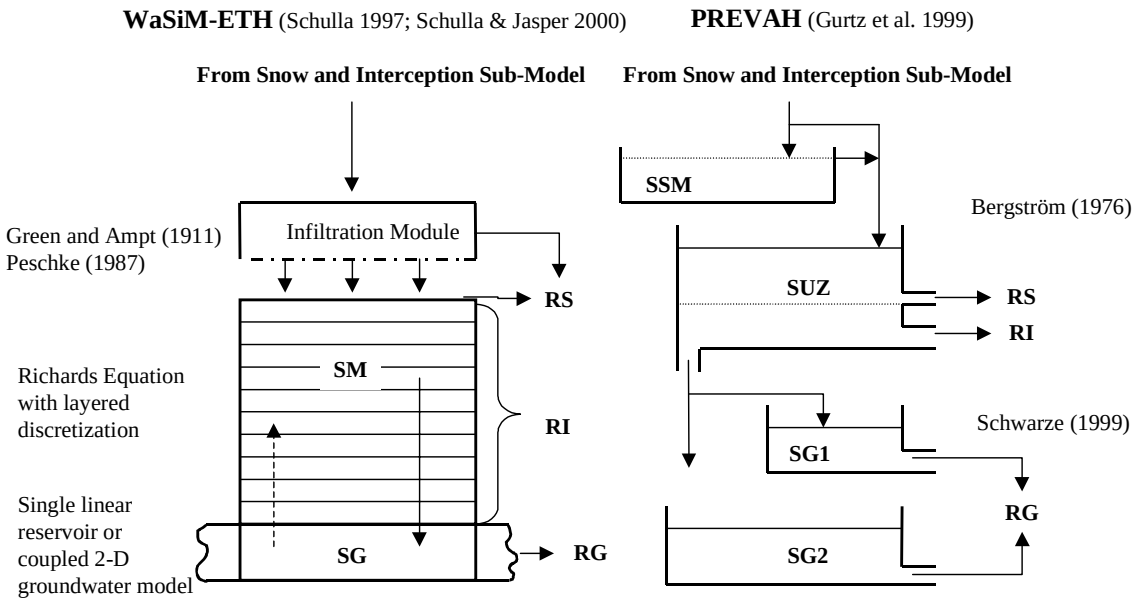

Figure 2.5 Schematic representation of the runoff-generation modules in WaSiM-ETH and PREVAH (Gurtz *et al.* 2003). All abbreviations are discussed in the text.

The fast surface runoff (RS) can occur in concurrence with rocky, impervious and frozen soil, in the case of water-saturated areas and by Hortonian runoff (Horton 1933, Uhlenbrook 1999). RS is governed by high rain intensities in pre-alpine catchments and by snow and ice melt in high-alpine catchments. The interflow (RI) is the most important runoff component in mountainous regions and is very sensitive to the soil characteristics (layering, differences in conductivity and storage capacity, slope and moisture). The portion of RI in total runoff decreases with increasing glacerization of the catchment (Verbunt *et al.* 2003). The baseflow (RG) is the slow and steadier runoff component in mountainous catchments. The main simulated RG portion occurs in winter depending on the characteristics of the defined groundwater storages and the amount of groundwater recharge.

The simulated relative portion of the runoff components depends on the philosophy of the model (Gurtz *et al.* 2003). The structure of the runoff-generation module of PREVAH is now discussed in parallel with the structure of the correspondent module in WaSiM-ETH (Schulla 1997, Schulla and Jasper 2000). The essential differences between the models lie in the degree of conceptualization of infiltration, percolation, interflow generation and groundwater recharge calculation (fig. 2.5). The effect of such structural difference on the discharge simulation is discussed in sections 5.2.2 and 5.3.1.

The soil model in WaSiM-ETH calculates the infiltration of water and the surface runoff-generation (RS) as proposed by Green and Ampt (1911) using a two-step model approach (Peschke 1987). The vertical flow of water in the unsaturated zone (SM) is calculated by the discrete Richards equation. Interflow (RI) is generated in predefined different soil layers depending on the suction, the drainable water content, the hydraulic conductivity and gradient as well as the flow density. In this study, the computation of baseflow (RG) with WaSiM-ETH is based on a single linear reservoir (SG). A coupling of WaSiM-ETH with a two dimensional groundwater model is also possible (fig. 2).

In PREVAH the soil water reservoir and the runoff storages are calculated in spatially distributed manner as a function of the plant-available soil moisture storage (SSM) content and of the soil characteristics of the HRUs. The submodels for runoff-generation

are derived from the HBV-model (Bergström 1976), but they were adapted to the HRU structure. The changes on the HBV structure allow the dynamic parameterization of every HRU according to its land surface and soil characteristics. The capacity of plant-available soil moisture storage (SSM) is limited by the average plant-available field capacity (SFC), and is related to the average soil depth or the average root depth within the grid elements summarized by a specific HRU. The land surface runoff (RS), the interflow (RI), and the percolation to the groundwater storage (SG1 and SG2) are generated in the upper runoff storage (SUZ). Baseflow (RG) is generated by the combination of two linear groundwater reservoirs (Schwarze *et al.* 1999) with a fast and a delayed component (fig. 2). The computation of all the previously described water fluxes occurs separately for each HRU. The storage coefficients for runoff-generation are catchment specific parameters that are estimated by calibration. Thus, each runoff component is transformed by its specific storage coefficient valid for the whole catchment. It should be also mentioned that the routing of the runoff components generated in the HRUs is assumed being instantaneous and implicitly governed by the storage coefficients of the runoff-generation module. This assumption is justified in small catchments, but represents a limitation in the case of simulation experiments at large scales. The equations governing the water flows within the runoff-generation module of PREVAH are summarized in Appendix A.

2.3. Calibration, evaluation and data analysis

2.3.1 Calibration and evaluation strategy

The available data sets for hydrological simulations in a catchment are divided into two not overlapping periods. If the global time series is longer than five years, at least three years are used as calibration period. The remaining period is used for the verification of the model quality without further adjustments of the tuneable parameters. The analysis of the hydrological behaviour of the catchment generally includes the entire available time series. The quality of the model simulation can be assessed by using different observed variables. The comparison of different outputs of a model run with selected observed variables allows a multiple-response verification of the model capabilities. Hydrometeorological observations available for model evaluation include:

- soil moisture time series;
- lysimeter data (evapotranspiration, percolation, storage changes);
- latent heat flux values observed by eddy correlation and computed through the Bowen ratio method;
- observed fluctuations of the groundwater level;
- records of snow height and snow water equivalent (Rohrer *et al.* 1994a and b);
- discharge observations;
- snow patterns derived by satellite observations (Apfl *et al.* 1995).

2.3.2 Calibration procedure

The calibration of PREVAH is completed manually. The model outputs are compared with observed values and evaluated by means of objective statistical criteria (Eqs. 8 to 12). The calibration periods for the different investigated catchments and locations are declared on table 3.1. The first year of the simulation period is generally adopted as an initialization period and then excluded from the evaluation. This decision is based on the uncertainty of the initial values for the snow water equivalent and for the water storages at initialization.

A graphical comparison between observation and simulation is made in the calibration phase for a subjective estimation of the simulation quality. This allows an expertise-based assessment of the model free parameters. As further index of the model quality the quantitative difference between computed and measured data is accounted and analyzed (e.g. between computed and observed average yearly discharge). The most sensitive catchment specific tuneable parameters to be calibrated are (see also figs. 2.4 and 2.5):

- the adjustment factors for snowfall and rainfall (Eq. 1);
- the parameters of the snowmelt modules (Eqs. 2 to 5);
- the parameters of the glacial melt module: TMF_{ICE} and RMF_{ICE} (Eq. 6);
- the non-linearity factor *BETA* controlling the soil moisture recharge (,Eq. 7);
- the threshold parameter *SGR* for the generation of surface runoff;
- the maximal storage SFB_{max} available for fast baseflow (Schwarze *et al.* 1999);
- the storage coefficients which govern the process of runoff-generation: *K0* for surface runoff, *K1* for interflow, *K2* for delayed baseflow, *K3* for fast baseflow;
- the percolation rate *PERC*;

2.3.3 Assessment of the quality of hydrological simulations

The objective statistical coefficients that were used to evaluate the simulated S with respect to the observed variables O are:

The empirical coefficient of correlation R_{os}:

$$R_{os} = \frac{\sum_{i=1}^{N} (S_i - \bar{S})(O_i - \bar{O})}{\sqrt{\sum_{i=1}^{N} (S_i - \bar{S})^2 \sum_{i=1}^{N} (O_i - \bar{O})^2}} \tag{8}$$

with $\bar{O}$ and $\bar{S}$ being the mean of the observations O_i and of the simulated S_i values respectively and N being the number of observations. R_{os} tends to the unity the more the simulated values have similar dynamics with respect to the observations.

The root mean square error RMSE:

$$RMSE = \sqrt{\frac{\sum_{i=1}^{N} (S_i - O_i)^2}{N}} \tag{9}$$

RMSE allows for the quantification of the magnitude of the deviation of the simulated from the observed values.

The mean absolute deviation MAD:

$$MAD = \frac{\sum_{i=1}^{N} |S_i - O_i|}{N} \tag{10}$$

MAD must be minimized in the calibration phase to obtain a better quantitative agreement for the simulated variable with respect to the observation.

*The efficiency score E_2 (*Legates and McCabe 1999, Nash and Sutcliffe 1970*):*

$$E_2 = 1 - \frac{\sum_{i=1}^{n} | O_i - S_i |^2}{\sum_{i=1}^{n} \left| O_i - \left[\frac{1}{n} \sum_{i=1}^{n} O_i \right] \right|^2} \tag{11}$$

E_2 quantifies the relative improvement of the model compared with the mean of the observations. Any positive value corresponds to an improvement. E_2 tends towards unity when S_i tends towards O_i. Further, the logarithmic formulation of E_2 (Schulla 1997, Hock 1999) is considered:

$$E_2^{\log} = 1 - \frac{\sum_{i=1}^{n} | \ln(O_i) - \ln(S_i) |^2}{\sum_{i=1}^{n} \left| \ln(O_i) - \left[\frac{1}{n} \sum_{i=1}^{n} \ln(O_i) \right] \right|^2} \tag{12}$$

The logarithmic efficiency score E_2^{log} gives valuable indications on the model performance in the case of discharge simulations during the low-flow periods in winter (Gurtz *et al.* 2001). The range of both E_2 and E_2^{log} is [-∞,1].

2.3.4 Analysis of the discharge regime: the Parde coefficient

The Hydrological Atlas of Switzerland (HADES, Weingartner and Aschwanden 1992) defines the discharge regimes as follows: "In general, 'regime' is used in a hydrological sense to refer to the relative or absolute variations of one element of the water cycle within a particular time period. 'Discharge regime' is used to designate the general hydrological behaviour of a river. The long-term average seasonal variations of runoff are referred here as regime. The regime can be described in terms of the dimensionless Pardé coefficients PC_i (Eq. 13, Pardé 1933)":

$$PC_i = 12 \cdot \frac{Q_i}{\sum_{i=1}^{12} Q_i} \tag{13}$$

where Q_i is the mean monthly runoff in month *i*. *i* ranges between 1 and 12. PC_i ranges between 0 and 12.

2.3.5 Analysis of categorical data by skill measures

Categorical, or conditional, statistics quantifies skill in the prediction of the occurrence of an event such as rainfall in one location or the presence of snow-cover within a pixel in an investigated domain. In such cases, a 2x2 verification method can be applied (table 2.1). The 2x2 verification problem (frequently yes/no, e.g. snow-covered / snow free) is the widest-known problem in this discipline (Doswell *et al.* 1990, Murphy and Epstein 1989, von Storch and Zwiers 1999). A variety of scores can be derived from table 2.1.

The accuracy:

$$ACC = \frac{(n_{11} + n_{00})}{n_{xx}} \tag{14}$$

The accuracy *ACC* is the number of correct forecasts for events and non-events divided by the total number of forecasts. The limits of this score are [0 to 1], the 'perfect' score is 1. *ACC* is greatly influenced by the most common category. For example, in a contingency table for snow-cover the 'snow free' events may greatly outnumber the 'snow-covered' events. *ACC* may therefore give misleading information about the skill of the forecast, particularly in lowland regions.

The probability of detection:

$$POD_1 = \frac{n_{11}}{n_{x1}} \qquad POD_0 = \frac{n_{00}}{n_{x0}} \tag{15}$$

Table 2.1 2x2 contingency table. Sim. 1 and Sim. 0 are simulations of the two possible observation classes. n_{11} are the so-called 'Hits', n_{10} the 'False Alarms', n_{01} the 'Missings' and n_{00} the 'Zeros'.

	Sim. 1	Sim. 0	Σ
Obs. 1	n_{11}	n_{01}	n_{x1}
Obs. 0	n_{10}	n_{00}	n_{x0}
Σ	n_{1x}	n_{0x}	n_{xx}

The probability of detection *POD* measures the success of the forecast in correctly predicting the occurrence or non-occurrence of events. *POD* is sensitive only to missed events, not to false alarms. The limits of this score are [0 to 1], the targeted score is 1.

The false alarm ratio:

$$FAR = \frac{n_{10}}{n_{1x}} \tag{16}$$

The false alarm ratio *FAR* measures the fraction of event forecasts that were actually non-events. *FAR* is sensitive only to false predictions, and not to 'missed' events. The limits of this score are [0 to 1], the optimal score is 0.

The bias score is defined as:

$$BIAS = \frac{n_{1x}}{n_{x1}} \tag{17}$$

The bias score *BIAS* measures the relative area (or frequency) of predicted and observed events, without regard to forecast accuracy. The limits of this score are [0 to ∞], the 'perfect' score is 1. A *BIAS* of 1 means the absence of bias; values above one indicate an overestimation of events; values below one indicate event underestimation. A perfect *BIAS* score indicates the predicted events frequency is the same as was observed; however, it may or may not be located in the same place (time or space). It suitability for the analysis of fields is therefore limited.

The threat score or the critical success index is given by:

$$CSI = \frac{n_{11}}{\left(n_{xx} - n_{00}\right)} \tag{18}$$

The critical success index *CSI* is the number of correct event forecasts divided by the number of cases forecast and / or observed. The limits of this score are [0 to 1], the optimal score is 1. The *CSI* has the advantage of not being dominated by no-events, as occurs for the simple accuracy *ACC*. A perfect score indicates that all events were perfectly forecasted, and all forecasts corresponded to observed events. Because it is sensitive to both false alarms and missed events, it gives a more representative idea of real accuracy both in situations where rare events are involved and in situations where the frequencies of 'event' and 'no event' are nearly equal.

Heidke skill score

'Skill scores' generally measure the improvement of a forecast over some reference forecast such as random chance, persistence or climatology. As such, they take into account the expected characteristics of the investigated target value in the sample set. One of such scores is the Heidke skill score *HSS*:

$$HSS = \frac{2 \cdot \left(n_{11} \cdot n_{00} - n_{01} \cdot n_{10}\right)}{n_{x1} \cdot n_{0x} + n_{1x} \cdot n_{x0}} \tag{19}$$

This is a measure of correct forecasts, with random correct forecasts removed. The reference forecast is random forecasting, subject to the constraint that marginal distributions of forecasts are the same as the marginal distributions of observations. The limits of this score are [-∞ to 1], the 'perfect' score is 1.

3. Studied locations, catchments and regions

3.1. Locations and catchments in Switzerland

3.1.1 General overview

PREVAH was adopted for hydrological simulations in several Swiss locations and catchments and also for the simulation of the whole of Switzerland (table 3.1 and fig. 3.1). Table 3.1 shows basic physiographic characteristics of these locations and catchments, starting with the smallest plot in Claro up to the different regions which where considered for the regionalization of the water balance simulation of Switzerland.

The digital information required for the analysis of the physiographic characteristics of catchments consisting of more than 1 HRU was derived, in the case of the Rietholzbach river and its tributaries Huwilerbach and Upper Rietholzbach, from a database prepared by Bohrer (1998) with spatial resolution of 50x50 m^2. The information for all other catchments was assimilated from a standard Swiss database of digital information with a basic grid size of 100x100 m^2. This database consists of:

- the digital elevation model RIMINI (BFLT 1991)
- the Swiss landuse / land cover statistic map ("Arealstatistik", BFS 1995)
- the soil capability maps ("Bodeneignungskarte", BFR 1980)

The next sub-sections describe in more detail three Swiss catchments that have been target of particular experiments in this work framework.

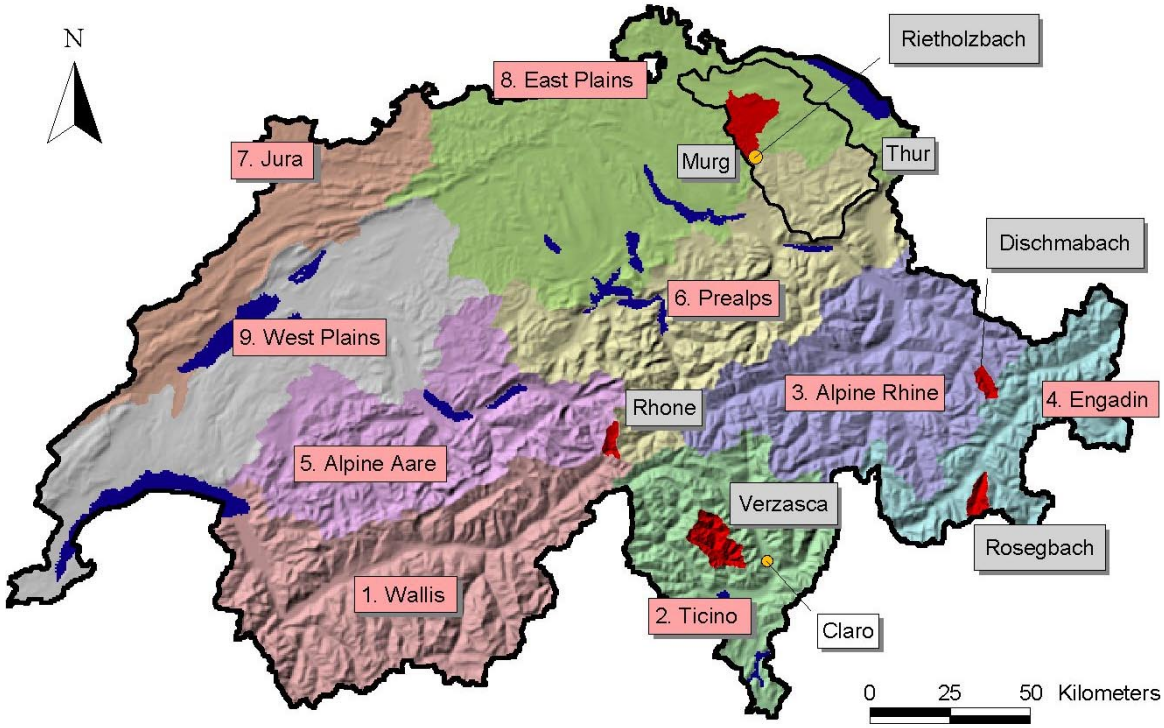

Figure 3.1 Overview of the considered Swiss regions (red flags), catchments (grey flags) and locations (white flags). A summary of the basic physiographic properties of all these locations is presented on table 3.1.

Table 3.1 Physiographic characteristics of all the investigated Swiss locations, catchments and regions. ICE is the portion of glacierized surfaces. N is the portion of north-faced, S of south-faced, E of eastern-faced and W of western-faced areas. A_{HRU} is the average area of the HRUs in hectares. All the catchments and locations noted with a star belong to the catchment of the river Thur.

Catchment	Period	Calibration	Area	Base Grid	Elevation [m. a. s. l.]	# 100 m zones	Dominant Landuse	ICE [%]	N [%]	S [%]	E [%]	W [%]	H [%]	A_{HRU} [hectares]
Claro	Jul-Nov 1999	August	1.00 m^2	--	250	--	100% Corn	--	--	--	--	--	100	1 HRU
Lysimeter *	1981-2000	93-98	3.14 m^2	--	755	--	100% Meadow	--	--	--	--	--	100	1 HRU
Huwilerbach *	1994-2000	94-95	0.12 km^2	50 m	746-891	2	82% Meadow	--	--	84	2	14	--	0.75
Up. Rietholz. *	1994-2000	94-95	0.9 km^2	50 m	745-950	3	76% Meadow	--	35	14	48	3	--	1.75
Rietholzbach *	1981-2000	93-98	3.2 km^2	50 m	682-950	4	73% Meadow	--	25	42	19	13	1	3.25
Rohne	1981-2000	90-93	39.7 km^2	100 m	1767-3582	18	30% Rock	47	11	38	19	32	--	9
Dischmabach	1981-2000	81-85 / 93-95	43.3 km^2	100 m	1668-3146	15	36% Pasture	2	24	30	7	39	--	13
Rosegbach	1991-1999	91-94	66.5 km^2	100 m	1766-4020	24	39% Rock	31	25	6	35	33	1	12
Verzasca	1991-1999	91-94	186 km^2	100 m	493-2836	25	29% Forest	--	21	29	25	25	--	30
Murg *	1981-1996	81-83	210 km^2	100 m	390-1031	8	55% Meadow	--	33	20	20	24	3	111
Thur	1981-1996	93-94	1703 km^2	100 m	356-2503	23	57% Meadow	--	31	25	--	--	--	78
Switzerland	1980-2000	--	41184 km^2	500 m	192-4463	44	32% Forest	3.1	27	22	23	25	2	162
1. Wallis			5613 km^2	500 m	371-4463	42	26% Rock	13	23	26	22	28	1	112
2. Ticino			3210 km^2	500 m	192-3258	32	46% Forest	0.7	20	27	27	26	--	137
3. Alpine Rhine			4371 km^2	500 m	478-3453	31	28% Pasture	1.5	25	27	23	25	--	112
4. Engadin			2572 km^2	500 m	627-3818	33	35% Rock	4.5	23	28	23	26	--	137
5. Alpine Aare			4390 km^2	500 m	375-4075	38	28% Forest	5.0	31	21	20	27	1	137
6. Prealps			4953 km^2	500 m	405-3519	32	27% Forest	2.1	29	25	21	25	--	137
7. Jura			2926 km^2	500 m	245-1550	14	42% Forest	--	32	19	30	17	2	250
8. East plains			7604 km^2	500 m	265-2013	19	57% Meadow	--	31	22	20	24	3	300
9. West plains			5545 km^2	500 m	343-1942	17	57% Meadow	--	26	23	22	25	6	250

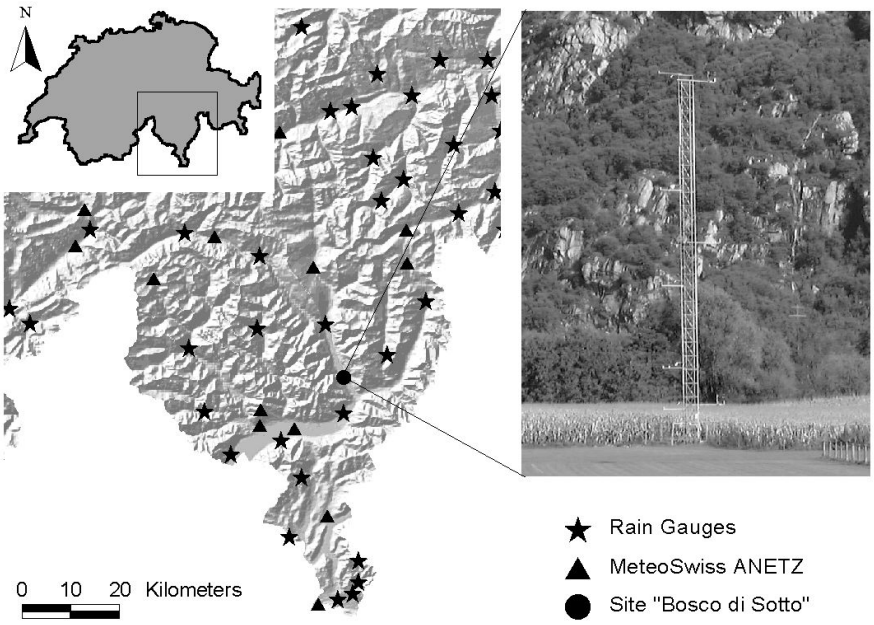

Figure 3.2 Location of the investigated MAP-Riviera site "Bosco di Sotto"

3.1.2 The MAP-Riviera field experiment

The *Mesoscale Alpine Programme* MAP is an international research initiative devoted to the study of atmospheric and hydrological processes over mountainous regions (Bougeault *et al.* 2001). The MAP research activities related to surface hydrology aim in particular to improve the understanding of orographically-influenced precipitation events and related flooding episodes and to improve the numerical prediction of moist processes in regions with complex topography, including interactions with land-surface processes (Binder 1996). These issues are investigated both through modelling (e.g. Benoit *et al.* 2002, Jasper *et al.* 2002) and field experiments (e.g. Ranzi 2001).

The *Ticino-Toce* watershed (CH-I) was one of the MAP test sites. During the *MAP Special Observing Period* (SOP, 15 September to 15 November 1999; Bougeault *et al.* 2001) boundary layer processes in highly complex topography were investigated in the *Riviera valley* in southern Switzerland (Rotach *et al.* 2003, Zappa and Gurtz 2003). This valley is midway between the "Lago Maggiore" and the Swiss central Alps (fig. 3.2). Unlike previous studies, the main focus of the *Riviera-Project* was on the turbulence structure and turbulent exchange processes at the valley surface. Owed to the anticipated spatial heterogeneity, a large number of turbulence probes were deployed on a cross-section through the valley (Matzinger *et al.* 2003). A light research aircraft with high temporal sampling resolution flew various patterns within the valley to yield information on the turbulence structure. Additional instrumentation such as a radio sounding system, a passive-microwave temperature profiler and a tethered balloon were operated during selected periods. The *Riviera Special Observing Period* **R-SOP** started on 24 July 1999 and lasted until the 10 November 1999.

The principal field survey area was located in the Riviera valley at the site "Bosco di Sotto" (fig. 3.2). The investigated soil profile was located at the edge of a cornfield. It consisted of a 40 cm deep humus layer (partly mixed with clean sand) followed by a 60 to 80 cm deep clean sand layer. Soil probes have been sampled at eight levels to determinate the porosity. The root zone of the corn reached 60 cm depth. Table 3.2 gives an overview of the soil characteristics up to 65 cm depth.

Table 3.2 MAP-Riviera: physical parameters of the investigated 650 mm deep soil profile.

Parameters	Symbol	Vol%	mm
Porosity	η	53	345
Field Capacity	SFC	30.5	198
Wilting Point	WP	6	39
Plant available field capacity	AFC	24.5	159

The porosity and the field capacity have been determined from the analysis of soil samples. The lowest observed soil moisture was 9 Vol%. The wilting point of was assumed being equal to 6 Vol%.

3.1.3 The hydrological research catchment Rietholzbach

The hilly pre-alpine research catchment Rietholzbach is located in the central part of the Thur river basin (tributary of Rhine) in north-eastern Switzerland with an area of 3.2 km^2 and the main water flow running west to east. The elevation ranges from 682 to 950 m a.s.l. It is primarily used as pasture (76%). The geology (fig. 3.3) is characterized by the tertiary deposits of the Upper Freshwater Molasse. Pleistocene sandy and silty gravel pockets of glacial moraines occur in the flat riparian zones along the creek (Vitvar 1998). A variety of soil types is observed: from less permeable gley soils to more permeable brown soils and regosols with relatively large soil water storage capacities. The soil depth exceeds 50 cm.

The Rietholzbach catchment (*http://www.iac.ethz.ch/research/riet/*) has been established and equipped in 1975/76 by the Laboratory of Hydraulics, Hydrology and Glaciology (VAW) of ETH Zurich under the supervision of Prof. H. Lang, Dr. B. Schädler and Dr. B. Sevruk. Since 1983 it was operated by the Institute for Atmospheric and Climate Science (ETH Zürich).

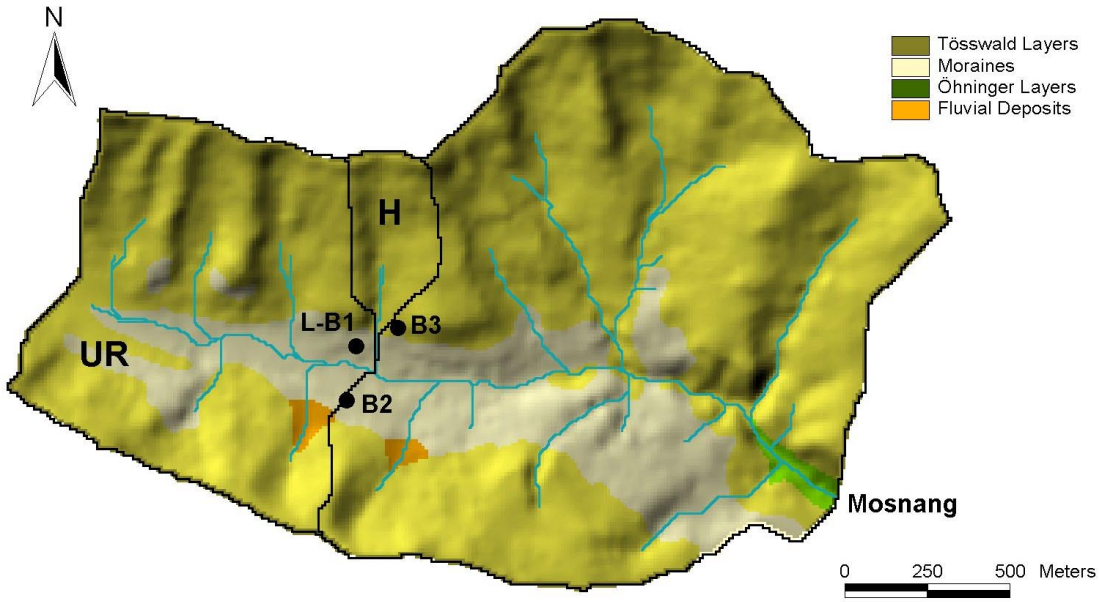

Figure 3.3 The hydrological research catchment Rietholzbach: 'H' indicates the Huwilerbach basin, 'UR' the Upper Rietholzbach basin. L-B1, B2 and B3 indicate the location of the lysimeter (L-) and of the three groundwater boreholes (B1, B2 and B3).

Table 3.3 Land-use classes in 4 investigated catchments (Gurtz *et al.* 2003).

	Dischmabach	Rietholzbach	Huwilerbach	Upper Rietholzbach
Water areas	0.3	-	-	-
Settlements	0.4	1.2	0.1	2.2
Deciduous forest	-	3.7	18.1	3.9
Mixed forest	-	19.2	-	16.9
Pine forest	2.4	2.0	-	-
Fruit orchard	-	0.9	-	0.3
Meadow	0.6	73.0	81.8	76.7
Wet areas	0.1	-	-	-
Bushes	7.1	-	-	-
Subalpine pastures	36.4	-	-	-
Alpine meadows	1.3	-	-	-
Gravel, pit / bare soil	15.8	-	-	-
Rock	33.5	-	-	-
Glacier	2.1	-	-	-

The purpose of this research catchment is to promote hydrological process studies, to support the development and parameterization of water balance and runoff models and to serve for educational purposes (Kirnbauer *et al.* 2000).

The catchment is equipped with a standard meteorological station, a weighting lysimeter, three runoff-gauging stations (Mosnang, Huwilerbach and Upper Rietholzbach), continuous time domain reflectometry TDR soil moisture measurements at different depths (Menzel 1997) and three access tubes for groundwater level observations (figure 3.3). The main streamflow gauge Rietholzbach Mosnang is part of the runoff network operated by the Swiss Federal Office for Water and Geology (FOWG).

The lysimeter container is made of synthetic material and has a diameter of 2.0 m. Its 3.14 m^2 surface is grass-covered. The structure, composition, cutting and fertilization of this meadow mainly reflect the conditions of the surroundings as advised by the WMO guidelines (WMO 1983). The container is filled with a (for this location) typical gley-brown soil and is 2.5 m deep. Between 2 and 2.5 m depth the container is filled with gravel to avoid that gley stuffs the drainage. The container sits on three weighting elements. The electronic scale has a resolution of 100 grams, which corresponds to a water column of 0.032 mm. This allows measuring very small water fluxes. The drainage water is collected at the bottom of the container in a barrel and its volume is measured with a tipping bucket. Evapotranspiration can be calculated through the water balance equation from the rain measurements, the drainage volume as well as the lysimeter weight changes (e.g. Menzel 1997, Moesch 2001, Gurtz *et al.* 2003c).

3.1.4 Characteristics of the high-alpine Dischmabach catchment

The Dischmabach catchment is located in the eastern part of Switzerland (fig. 3.4) in the transition zone between the wet northern Alps and the dry central Alps (de Jong *et al.* 2002). The river valley is oriented from south-south-east to north-north-west. The catchment has an area of 43.3 km^2, the elevation ranges from 1668 to 3146 m a.s.l.

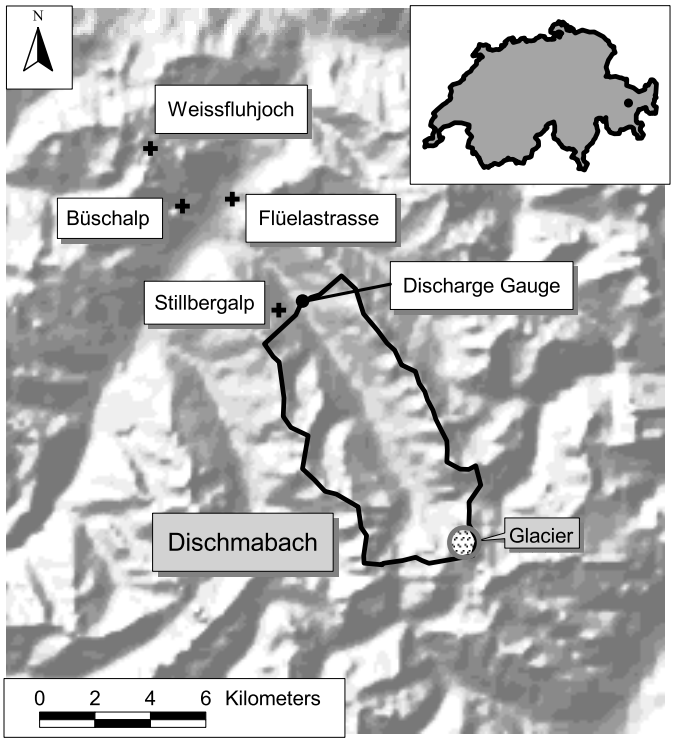

Figure 3.4 Location of four stations (crosses) for the observation of the snow water equivalent, of the discharge gauge and location of the Dischmabach catchment within the map of Switzerland (point in the upper right box).

In the lower part of the catchment snowfall represents approximately 40% of the total precipitation, while in the highest elevation zone more than 80% of the total precipitation consists of snow. In the lower parts snow accumulates between November and February. In the higher parts of the catchment snow accumulation can be observed from November until the end of April.

The basin represents the high-alpine region with sub-alpine, alpine and nival vegetation zones (table 3.3). 2.1% of the catchment area is glacerized. The crystalline underground consists of orthogneiss, paragneiss and amphibolites. The soils are less developed with soil depths mostly less than 50 cm. Riparian zones with groundwater storage occur along the creek at the valley bottom.

The only permanent hydrometeorological observations within the catchment are those of discharge and precipitation. However, at a few kilometres' distance, MeteoSwiss maintains the long-term fully equipped meteorological observatories of Davos (1590 m a.s.l.) and Weissfluhjoch (2690 m a.s.l.). The Institute for Snow and Avalanche Research SLF in Davos measures the snow water equivalent at four sites (fig. 3.4) in the neighbourhood of the Dischmabach catchment the 1st and 15th day of each month between November and July.

3.2. Investigated locations in the Russian plain

3.2.1 Usadievsky catchment

The grassland catchment Usadievsky (0.36 km^2) is located in the boreal forest region approximately 100 km north-east from the Upper Volga basin. Usadievsky ('USAD' on fig. 3.5) is located in the central part of the Valdai Hills (approx. 57.6 N, 33.1 E) in a region surrounded by boreal forest belonging to the catchment of the Valdai Lake. The discharge regime is governed by the snowmelt season in March-April.

The 18 years long (1966–83) set of atmospheric forcing and hydrological data was obtained from the Valdai Scientific-Research Hydrological Laboratory. This data set coincide with the data set used for the Land Surface Schemes (LSS) intercomparison project PILPS 2(d) presented in Schlosser *et al.* (1997). The hydrological records consist of total soil moisture in the soil top 100 cm, snow water equivalent, evaporation, runoff and groundwater table depth (table 3.4). The atmospheric data were originally sampled at 3-h intervals. The temporal downscaling below the 3h-sampling interval is described in Schlosser *et al.* (2000). The time series of short-wave radiation do not consist of direct measurement, but were diagnosed as reported in Schlosser *et al.* (1997). For the present study an hourly time step was used.

3.2.2 Upper Volga catchment

The large watersheds within the Russian plain are characterized by comparatively strong horizontal homogeneity, and by a substantially sparse surface observation network both in time (short time series) and space (low station density). An international project (Volga Forest) was launched to estimate the response of the water flows of the boreal forest region at the Volga's source area to climate changes (Oltchev *et al.* 2002). The variability of the boreal forest structure and the climatological-hydrological situation in the Upper Volga catchment (hereafter also referred as UV) has been described over the past 100-150 years. Upper Volga is located in the Moscow syncline that is part of the Precambrian Russian sheet and drained by the important rivers of Eastern Europe - Volga, Dnepr, Zapadnaya Dvina and Newa. This geological formation nearly corresponds to the Valdai Hills and has an area of about 70000 km^2. The Upper Volga basin up to the lake level station Selishe (214 m a.s.l.) has an area of about 3677 km^2 and it is approximately defined by the following co-ordinates: 56°20'-57°20' N, 32°00'-33°20'E (fig. 3.5). It includes the Volga source area, the depression part with large lakes and the surrounding elevations of the Valdai Hills. A dam and a weir at the outlet of Lake Volgo form the profile in Selishe. The elevation of Raswenitskiye Gory is 321 m a.s.l., the highest hill within the catchment.

Table 3.4 Valdai-Usadievsky: summary of the hydrological records for model calibration and evaluation within the period 1966-83.

Element	Calibration	Evaluation	Resolution	Reference
Evaporation	1966-1970	1971-1973	monthly	Schlosser *et al.* (1997)
Snow water equivalent	1966-1973	1974-1983	3-10 days	Schlosser *et al.* (1997)
Soil moisture	1966-1973	1974-1983	monthly	Robock *et al.* (1995)
Runoff	1966-1973	1974-1983	monthly	Schlosser *et al.* (2000)
Runoff	1966-1973	1974-1983	daily	Schlosser *et al* (2000)

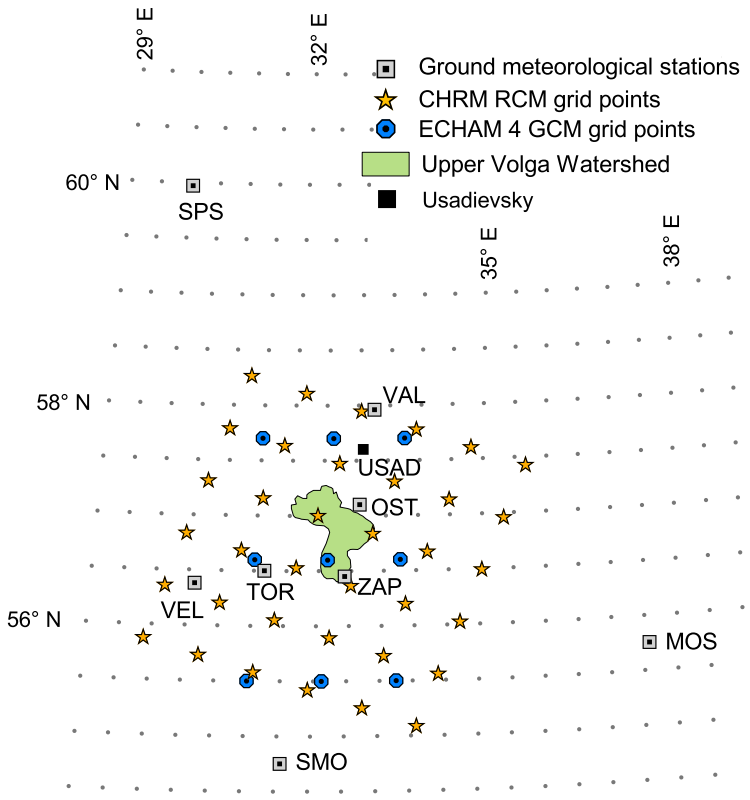

Figure 3.5 Location of the surface meteorological stations and of the representative grid points of ECHAM4 and CHRM in the surroundings of the Upper Volga catchment. See section 6 for details.

The most frequent soil type in the Upper Volga catchment is the mixed brown soil/podsol type on moraine deposits. The watershed is highly forested. The dominant forest type is the coniferous-mixed forest (54.2%), which is primarily composed of fir and birch trees. Broadleaf forests (7.1%) mainly consist of birch, alder, and aspen and willow trees. Wetland vegetation (8.5%) is composed of berries, grassland and pine trees. Grassland (19.4%) is partly used as pastures and is frequently located near the lakes (7.3%).

The climate is moderate-continental and characterized by considerable temperature differences between summer and winter periods. The mean long-term annual precipitation amount is 700-750 mm in the Western part and 650 mm in the eastern part (Tishenko *et al.* 1998). Long periods with temperatures below –20 °C are common. The water regime is continental, with a strong snowmelt influence. The melt season begins in the second part of March and ends about mid April.

A digital elevation model was constructed using the GIS ARC/Info by digitising a general geographical map. The original map has a 1:500000 scale and contain topographic contours with 20 m interval and separate information about elevation points. The interpolated DEM consists of a grid with 500 m spacing. Land-use, soil properties and geology were digitized from thematic maps of the catchment. The HRUs required for the use of PREVAH were aggregated according to the spatial differentiation of the land-use properties, of the soil types, of aspect and of the cell position within the available network of surface meteorological stations (fig. 3.5). The 14707 500x500 m^2 grid elements were summarized by 640 HRUs with an average area of 5.75 km^2 (23 grid elements).

4. The sensitivity of distributed hydrological simulations to the spatial resolution of physiographic data♦

4.1. Introduction

Two methods are most commonly adopted for the spatial discretization of a watershed (Singh 1997): (1) the grid-oriented approach; and (2) the response units approach (Ross *et al.* 1979, Moore *et al.* 1993). Grid-oriented hydrological models (Abbot *et al.* 1986, Klok *et al.* 2001) assimilate the spatial information for cell-by-cell simulations from grids with a prescribed spacing. Response units based models (Flügel 1995 and 1997, Gurtz *et al.* 1999, Becker and Braun 1999) rely on a physiographically-oriented discretization of the investigated domain into irregular-shaped hydrologically similar areas as determined by the ensemble of the soils, land surface and topographic characteristics.

The objectives of this study are: (1) the identification of the sensitivity of discharge simulations to the resolutions of the spatially distributed physiographic information, (2) the quantification of the relative importance of various physiographic data-sets for the quality of runoff-simulations, and (3) the determination of the critical grid-spacing for sound distributed hydrological simulation in mountainous environments. To address these questions a discretization approach based on a two-hierarchy grid resolution is proposed. The method allows combining spatial data with different resolutions.

A hydrological response units (HRUs) based model was used. The use of a conceptual HRU-based model was preferred to the use of a strictly gridded physically-based model because gridded physically-based models are not able to handle irregular spatial discretizations such as the here proposed two-hierarchical discretization. The used HRU-based model PREVAH (Gurtz *et al.* 1999) can handle both HRU and gridded spatial discretizations. This is the main prerequisite for handling spatial data different resolution.

The needed spatial information was assimilated from a database at 100x100 m^2 resolution consisting of a digital elevation model (DEM) (BFLT 1991); the Swiss landuse map (BFS 1995) and soil maps (BFR 1980). The experiments are based on observed hydrometeorological data for two test catchments in the Swiss Alps: the pre-alpine Murg; and the high-alpine Dischmabach catchment. PREVAH was calibrated basing on a HRU related catchment discretization (control experiment) and then run with other spatial discretizations without further parameter adjustments. This allowed also for testing the robustness of the model parameterization when changing the spatial resolution.

The quality of the hydrograph simulation was determined for all the experiments and compared with the model quality obtained in the verification period of the control experiment. The results are discussed based on previous work. A scale-independent equation is proposed for the determination of the critical grid-spacing in the framework of spatially distributed hydrological simulations.

4.2. A two-hierarchy discretization

Figure 1a shows the digital elevation model (DEM) and the boundaries of the Murg test catchment (210 km^2) at 100 m resolution.

♦ Paper in preparation for submission to *Hydrological Processes*. The related literature review is presented in section 1.3.3

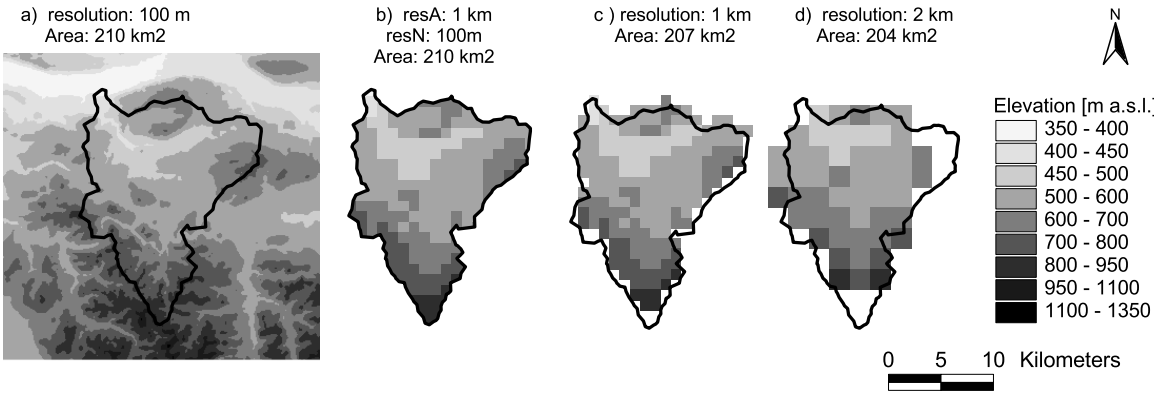

Figure 4.1 a) Digital elevation model of the Murg catchment at the maximum available 100 m resolution. b) Two-hierarchy resample to an actual resolution res_A of 1 km, and nominal resolution res_N of 100 m. c) Classic resample to 1 km resolution. d) Classic resample to 2 km resolution. The shape of the catchment computed from the elevation model at 100 m resolution is always kept in the foreground.

The catchment area computed with a classic resample to a 1 km spacing (figure 4.1c) is shifted in position and changed in dimension with respect to the boundary obtained from the basis map at 100 m resolution (fig. 4.1a). However, the obtained area still appears representative. The computation of a representative map of the test basin is problematic for classic resample to resolutions coarser than 1 km (figure 4.1d). A similar shortcoming was frequently observed in previous studies (Bruneau *et al.* 1995, Zhang and Montgomery 1994, Vazquez *et al.* 2002, Haddeland *et al.* 2002).

To resolve this shortcoming Kuo *et al.* (1999) proposed the addition of a scaling factor that ensures that no catchment area (or water flux) is added or lost while proceeding to spatial aggregation. The solution of Kuo *et al.* (1999) was not adequate for this study. A new kind of discretization is needed, which can also handle spatial information with different resolution, as for example detailed topographical information and coarse soil maps. Thus, a two-hierarchy discretization procedure was developed (figure 4.2).

The proposed procedure relies on the resolution reduction of the physiographic properties required for distributed hydrological simulations without increase in the basic grid-spacing. The digital representation of the most hydrologically relevant physiographic properties (elevation, land surface and soil characteristics) is taken at the highest available spatial resolution, here a 100 m grid-spacing (figure 4.1). Instead of proceeding with a classical resampling from a 100 m to a 1 km spacing (fig. 4.1c), it is proposed to maintain the basic 100x100 m^2 grid structure and to assign the average value (e.g. in the case of elevation, slope, aspect or soil depth) or the dominant class (e.g. in the case of land-use type) to all the grid elements within a 1x1 km^2 box (fig. 4.1b and figure 4.2). This allows for the distinction between a nominal resolution res_N (100 m, the resolution of the first hierarchy grid-cells) and an actual resolution res_A (1 km, the resolution of the second hierarchy box-structure). The computational compatibility between grids with different res_A settings is guaranteed by the common underlying first hierarchy discretization at res_N.

As figure 4.1b shows the two-hierarchy resample do not affect either the dimension or the position of the catchment boundaries with respect to figure 4.1a because the catchment area at the basic-resolution can be projected in the two-hierarchy structure. The spacing of the first-hierarchy elements, the grid cells, determine res_N.

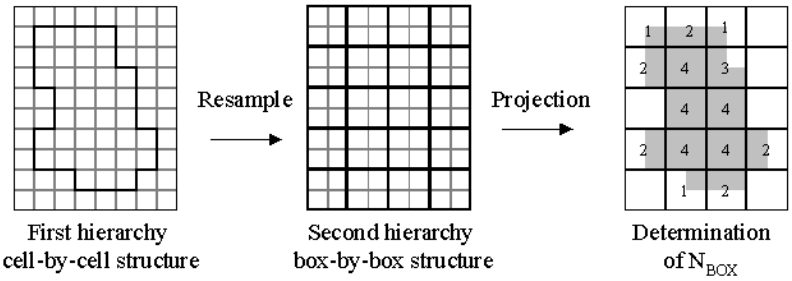

Figure 4.2 Stepwise generation of a two-hierarchy grid discretization and projection of the area of an idealized catchment in the box-by-box structure after the resample.

Boxes that are completely or partly included in a catchment comprehend a number of cells (N_{BOX}) equal to:

$$N_{BOX} = N_{MAX} - N_{OUT} \qquad N_{MAX} = \left(\frac{res_A}{res_N} \right)^2 \tag{20}$$

N_{MAX} is the maximum number of first hierarchy elements (the grid cells) in a second hierarchy box. N_{OUT} is the number of first hierarchy elements within a box excluded from the computational domain and can be determined projecting the catchment area delineated at res_A equal to res_N on the grid with lower res_A.

Figure 4.2 schematically shows the two-hierarchy resample of an idealized domain with res_N equal to one unit and res_A equal to two units. The domain consists of 20 second-hierarchy boxes, each composed by 4 first hierarchy elements. After projecting an idealized catchment boundary only five boxes are entirely included in the target area and have N_{OUT} equal to zero and N_{BOX} equal to four. Nine boxes are only partly included in the catchment with N_{OUT} and N_{BOX} ranging between one and three. With res_A equal to two, 14 boxes with a theoretical total area of 56 first hierarchy elements provide the spatial information for a box-by-box simulation. By projecting an idealized catchment area at res_N, only the 36 representative first hierarchy elements are accounted for hydrological simulations. It should be mentioned again that the spatial information of the elements within boxes with N_{BOX} below N_{MAX} is assigned considering the average characteristics of all the included first hierarchy elements.

4.3. Methods

4.3.1 Hydrological modelling and spatial discretization

The hydrological model PREVAH (*Precipitation-Runoff-Evapotranspiration-HRU* model) (Gurtz *et al.* 1999 and 2003a, Zappa *et al.* 2003) is used. The model relies on the aggregation of grid elements into HRUs (Moore *et al.* 1993, Flügel 1995). Figure 4.3a shows recommended rules for generating HRUs in mountainous environments (Gurtz *et al.* 1999). In the presented example, all the grid elements located in the same meteorological sub-unit, having similar aspect, same land-use classification and similar soil properties are assigned to a HRU. Equations (21a) and (21b) illustrates the formulation of the algorithm adopted for the generation of the code HRU^{ID}:

$$HRU^{ID}{}_{(i,j)} = \sum_{n=1}^{m} CLASS^{ID}(n)_{(i,j)} \cdot 10^{D_n} \tag{21a}$$

$$D_n = \begin{cases} \sum_{k=n+1}^{m} D^{ID}(k) & \text{for } n < m \\ 0 & \text{for } n = m \end{cases} \tag{21b}$$

HRU^{ID} is computed for all grid elements (i,j) located in the investigated domain. i defines the grid columns (e.g. the x co-ordinate in metric units or the longitude in degrees) and j defines the grid rows (e.g. the y co-ordinate or the latitude). m is the number of layers (physiographic properties) that are considered for generating HRU^{ID}. n is the identifier of a specific layer (table 4.1a). $CLASS^{ID}$ is a grid index where an integer number is assigned to every (i,j)-pair. That integer number represents a classification for a layer's attribute. A $CLASS^{ID}$ equal to '*3*' for the layer '*aspect*' means, as an example, that the (i,j)-pairs carrying this $CLASS^{ID}$ are south-exposed. The exponent D_n is required to build HRU^{ID} appending a layer $CLASS^{ID}$ to the $CLASS^{ID}$ of the next layers. D^{ID} is the number of digits occupied by a layer $CLASS^{ID}$ in the HRU^{ID}.

Table 4.1a shows a selection of physiographic layers for the generation of HRUs in mountainous catchments. In the presented example the HRU^{ID} can consider up to 100 meteorological sub-units (all the grid elements in the same 100 m range of elevation, in this experiment), land-use classes and soil types, and up to ten aspect classes. An idealized (x,y) grid element located in the lower part of the investigated domain (south-exposed, used as a pasture and characterized by sandy soils) can be identified by a HRU^{ID} equal to '*1532413*', using equation (21), and the idealized $CLASS^{ID}$ reported on table 4.1a. Other (i,j)-pairs may share that HRU^{ID}. Thus, they are assumed to have a similar hydrological response than the examined (x,y)-pair.

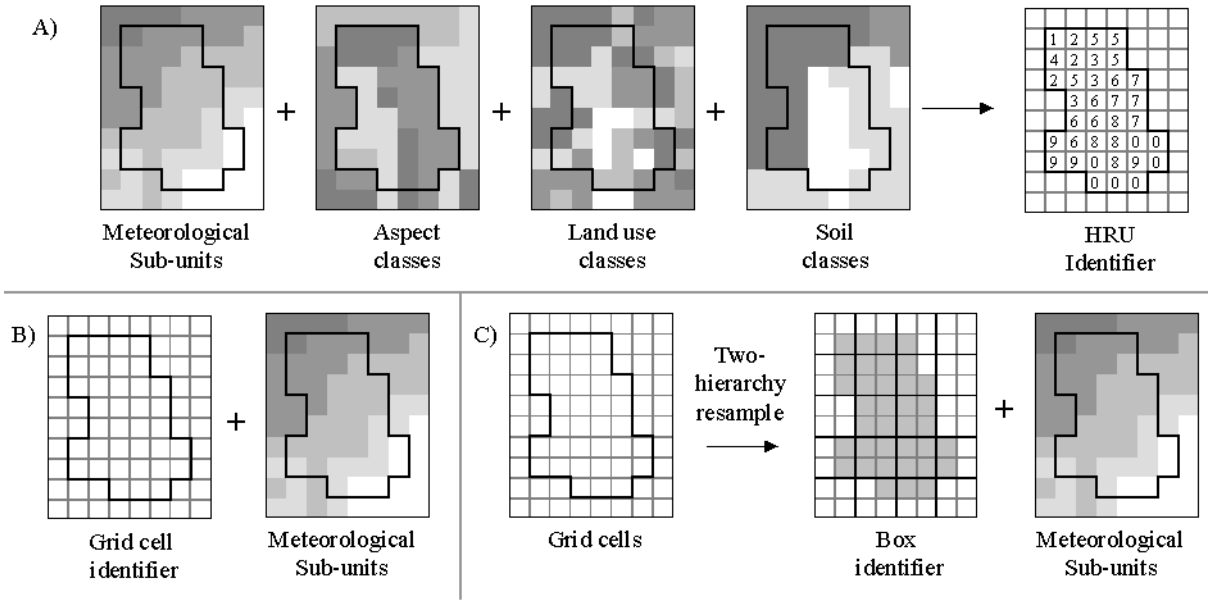

Figure 4.3 a) HRU based discretization of idealized domain for distributed hydrological simulations in mountainous environments. b) Cell-by-cell discretization. c) Box-by-box discretization after a two-hierarchy resample (see also figure 4.2).

Table 4.1 a) Recommended physiographic layers for the discretization of a mountainous catchment into HRUs. *n* is the identifier of the layer. $CLASS^{ID}$ is a grid containing for each *(i,j)* element, an integer number as an identifier for the attributes of a particular layer. D^{ID} is the required number of digits by a specific layer in the HRU-code. The right-part of the table shows the attributes $CLASS^{ID}_{(x,y)}$ for an arbitrary *(x,y)* grid point. b) Adopted layers for cell-by-cell and box-by-box discretization.

n	Layer	$CLASS^{ID}_{(i,j)}$	D^{ID}	(x,y)	$CLASS^{ID}_{(x,y)}$
a) HRU discretization					
1	Elevation zone	0-99	2	Valley floor	15
2	Aspect	0-9	1	South-exposed	3
3	Land-use	0-99	2	Pasture	24
4	Soil type	0-99	2	Sand	13
b) Cell-by-cell and box-by-box discretization					
1	Elevation zone	0-99	2	Valley bottom	15
2	Cell / Box identifier	0-99999	5	Identifier	56734

Both the grid cells and the second-hierarchy boxes (after the resample) fulfil the HRU definition: units (a grid cell, a box) with similar physiographic properties, and, therefore, hydrological response. Thus, PREVAH can handle a discretization of the catchment based on the cell-by-cell and box-by-box methods (figs. 4.3b and 4.3c). In the case of cell-by-cell and box-by-box model runs, an identifier is assigned to each cell, or to each box with grid cells included in the catchment, and combined with the defined meteorological sub-units (table 4.1b). In the presented example the arbitrary (*x,y*) grid element with the identifier '56734', located in the lower part of the catchments, has the HRU^{ID} '*1556734*'.

4.3.2 Test catchments

The pre-alpine *Murg* catchment belongs to the drainage system of the river Thur and is located in the north-eastern part of Switzerland. Its surface at the gauging station Frauenfeld is 210 km^2. The delineation of the HRUs considered the meteorological sub-units (8 elevation zones of 100 m range), aspect classes (5), land-use categories (10) and soil classes (5). Thus, on the level of the original grids at 100 m resolution 423 HRUs were generated, meaning an average area 0.71x0.71 km^2. Figure 4.4 shows that 20% of the HRUs consist of a single grid cell (0.1x0.1 km^2 area). However, there is a HRU that summarizes 1509 cells (3.88x3.88 km^2 area). More than 80% of the HRUs have a size ($=\sqrt{\text{area}}$) below average. Table 4.2 shows some physiographic properties at different res_A.

The average elevation is reasonably stable at every res_A. The smoothing of the highest and lowest elevation ranges is significant only at 10 km res_A. The aggregation of spatial information has a large influence on the composition of the dominant land-use classes. The portion of meadows increases from 55% at 0.1 km res_A to 90% at 10 km res_A. The portion of forested areas (27 %) is stable up to 0.5 km res_A and decreases to 10 % at the coarsest resolution. The frequency of north-exposed areas increases up to 93% with 10 km res_A. The influence of spatial aggregation on the average soil depth (SD) and plant available field capacity (PFC) is rather limited.

The high-alpine *Dischmabach* catchment is located in the eastern part of Switzerland and has a surface of 43.4 km^2, with a glacerized portion of 2.1%. The grid elements are aggregated into HRUs under consideration of the meteorological sub-units (16 elevation zones), aspect classes (5), land-use categories (11) and the equilibrium line altitude (ELA, 2700 m a. s. l.) of the glacier.

Table 4.2 Physiographic properties of the pre-alpine Murg catchment at different res_A (km). H_{MIN}, H_{MAX} and H_{AVG} are respectively the minimal, maximal and average catchment elevation. MU is the number of defined 100 m elevation zones (or meteorological sub units). S is the portion of south-exposed areas and N the portion of north-exposed areas. The portion of the three hydrologically dominant land-use classes is also given. PFC is the average plant-available field capacity in Vol% and SD the average soil depth in meters.

res_A	Unit	res_A 0.1	res_A 0.3	res_A 0.5	res_A 1.0	res_A 2.0	res_A 10.0
H_{MIN}	[m a.s.l]	395	395	394	397	393	461
H_{MAX}	[m a.s.l]	1023	980	960	952	918	826
H_{AVG}	[m a.s.l]	593	593	593	593	594	586
MU	[-]	8	7	7	7	7	5
S	[%]	20.3	18.7	18.2	15.8	16.6	0
N	[%]	32.5	36.1	38.7	41	47.6	93.3
Meadow	[%]	55.2	65	67.5	76.3	81.8	89.6
Forest	[%]	26.7	27.1	26.7	20.9	17.1	10.4
Urban	[%]	10.1	6.4	5.2	2.8	1.1	0
PFC	[Vol%]	14.7	14.7	14.7	14.9	14.4	14
SD	[m]	1.5	1.5	1.5	1.6	1.6	1.4

The 4340 grid elements at basic resolution are summarized by 334 HRUs. This means an average size of 0.36x0.36 km^2 (fig. 4.4). One of four HRUs consists of a single grid cell. Contrarily there is a HRU that summarizes 116 cells (1.07x1.07 km^2 area). Approximately 75% of the HRUs have a resolution below the average resolution.

Table 4.3 shows the physiographic properties of the catchment with different res_A. The average elevation is not affected by the aggregation to a coarse res_A. A large smoothing of the highest and lowest limits of the elevation range can already be observed at 0.5 km res_A. This causes a reduction of relevant 100 m elevation meteorological sub-units (MU).The aggregation of spatial information has limited influence on the composition of the dominant land-use classes up to 1 km res_A.

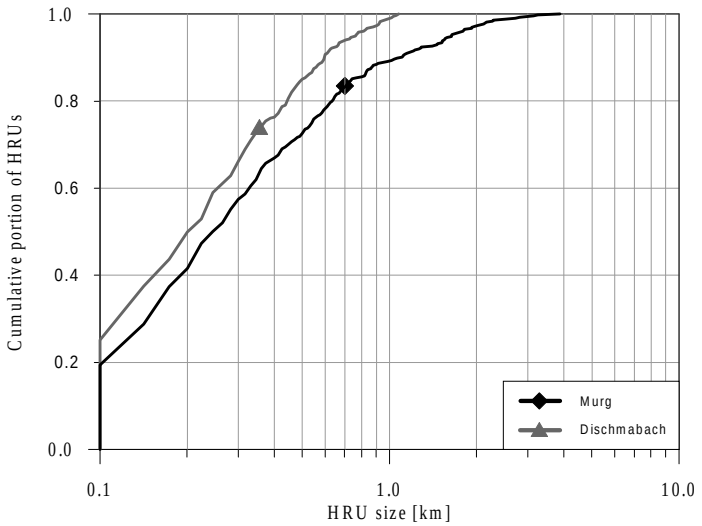

Figure 4.4 Cumulative portion of HRUs exceeding a certain size ($=\sqrt{area}$). The symbols indicate the average HRU size in the Murg (black line) and Dischmabach (grey line) catchments.

Table 4.3 Physiographic properties of the high-alpine Dischmabach catchment at different res_A (km). Legend as table 4.2.

res_A	Unit	res_A 0.1	res_A 0.3	res_A 0.5	res_A 1.0	res_A 2.0	res_A 5.0
H_{MIN}	[m a.s.l]	1677	1696	1691	1808	1922	1917
H_{MAX}	[m a.s.l]	3130	3063	2978	2932	2920	2724
H_{AVG}	[m a.s.l]	2380	2380	2379	2381	2380	2381
MU	[-]	16	15	14	12	11	9
S	[%]	7.2	6.6	4.5	2.3	0	0
N	[%]	22	23.5	25.4	29.6	20.7	59.6
Rock	[%]	33.5	33.4	33.8	33.7	40.4	29.4
Meadow	[%]	36.4	43.4	45.1	52.5	59	70.1
Glacier	[%]	2.1	1.7	2.1	1.5	0.2	0
PFC	[Vol%]	3.3	3.2	3.2	3.4	3.3	3.6
SD	[m]	0.28	0.25	0.25	0.21	0.15	0.17

The portion of south-faced areas decreases constantly with decreasing res_A, while the portion of north-exposed areas only increases at 5 km res_A. The average soil depth (SD) decreases with decreasing res_A, while the average plant available field capacity (PFC) increases slightly at coarse res_A.

4.3.3 Meteorological information

The processing of meteorological information is presented in section 2.1.3. For the experiment presented here an hourly forcing was used. An average value of the different climate variables was interpolated for all meteorological sub-units of the two catchments. Since the applied spatial aggregation causes a generalization of the spatial information, it should be mentioned that the number of relevant meteorological sub-units decreases with decreasing resolution of the digital elevation model (MU on tables 4.2 and 4.3).

Meteorological information is available for the period 1981-1996 for the Murg catchment and for the period 1981-2000 for the Dischmabach catchment.

4.3.4 Experimental settings and evaluation

PREVAH was calibrated on the exclusive basis of model runs relying on the HRU discretization, defined as *MHRU* for the Murg catchment and *DHRU* for the Dischmabach catchment (table 4.4). Model runs with cell-by-cell and box-by-box discretizations with the calibrated parameters from the HRU-based control runs were then performed with res_N equal 0.1 km and res_A ranging between 0.1 (cell-by-cell) and 10 km.

In a first phase the spatial data were processed adopting a uniform res_A. Then different res_A were alternatively introduced to allow for the assessment of the contribution of a particular physiographic characteristic to the change in simulation quality. Table 4.4 summarizes the experimental settings.

The statistical scores used for the evaluation of the experiments are defined in section 2.3.2. To evaluate the response to the change in resolution the following additional dimensionless score is introduced:

$$dE_2 = 100\% \cdot \left(\frac{E_2(res_A)}{E_2(HRU)} - 1 \right) \tag{22}$$

Table 4.4 Experimental settings for the catchments Murg (left) and Dischmabach (right). TOPO denotes the res_A [km] of the topographic information, USE of the land-use, and SOIL of the soil properties maps.

Murg	TOPO [km]	USE [km]	SOIL [km]	Dischmabach	TOPO [km]	USE [km]	SOIL [km]
MHRU	0.71*	0.71*	0.71*	DHRU	0.36*	0.36*	0.36*
M100	0.1	0.1	0.1	D100	0.1	0.1	0.1
M300	0.3	0.3	0.3	D300	0.3	0.3	0.3
M500	0.5	0.5	0.5	D500	0.5	0.5	0.5
M1000	1.0	1.0	1.0	D1000	1.0	1.0	1.0
M2000	2.0	2.0	2.0	D2000	2.0	2.0	2.0
M10000	10.0	10.0	10.0	D5000	5.0	5.0	5.0
MTOPO	2.0	0.3	0.3	DTOPO	5.0	0.1	0.1
MSOIL	0.3	0.3	2.0	DSOIL	0.1	0.1	5.0
MUSE	0.5	2.0	0.5	DUSE	0.1	5.0	0.1

(*) The average size of the HRUs is an average of the size of the 423 HRUs that are distinguished for the Murg and of the 334 HRUs that are distinguished for the Dischmabach catchment. See also figure 4.4.

dE_2 is the increase or decrease in the simulation quality (Eq. 11) at a specific res_A with respect to the simulation quality attained by the control run based on the HRU discretization.

4.4. Results

4.4.1 Calibration runs

Table 4.4 shows the catchment specific model parameters obtained after the manual calibration of PREVAH. Figure 4.5 shows the observed and simulated hourly hydrograph in the calibration year 1983, as obtained running PREVAH with the model parameters declared in table 4.5 and the spatial information assimilated from the HRU related discretization (control runs *MHRU* and *DHRU*).

Table 4.4 Calibrated model parameters obtained during the control experiments with HRU-related discretization for the Murg and Dischmabach catchments.

Parameter	Murg	Dischmabach	Unit
Temperature threshold for snowfall	0.0	0.0	[°C]
Temperature range for snow-rainfall	0.5	0.5	[K]
Threshold temperature for snowmelt start	0.5	-0.5	[°C]
Temperature melt factor for snow	$8.7 \cdot 10^{-9}$	$9.3 \cdot 10^{-9}$	[m s^{-1} K^{-1}]
Radiation melt factor for snow	$5.6 \cdot 10^{-11}$	$7.5 \cdot 10^{-11}$	[m^3 s^{-1} W^{-1} K^{-1}]
Temperature melt factor for ice	-	$5.8 \cdot 10^{-9}$	[m s^{-1} K^{-1}]
Radiation melt factor for ice	-	$5.0 \cdot 10^{-11}$	[m^3 s^{-1} W^{-1} K^{-1}]
Soil moisture recharge parameter	5.5	4.5	[-]
Storage coefficient for surface runoff	16	16	[h]
Storage coefficient for interflow	60	300	[h]
Storage coefficient for baseflow	2000	3200	[h]
Deep percolation rate	0.14	0.09	[mm $\cdot$ h^{-1}]

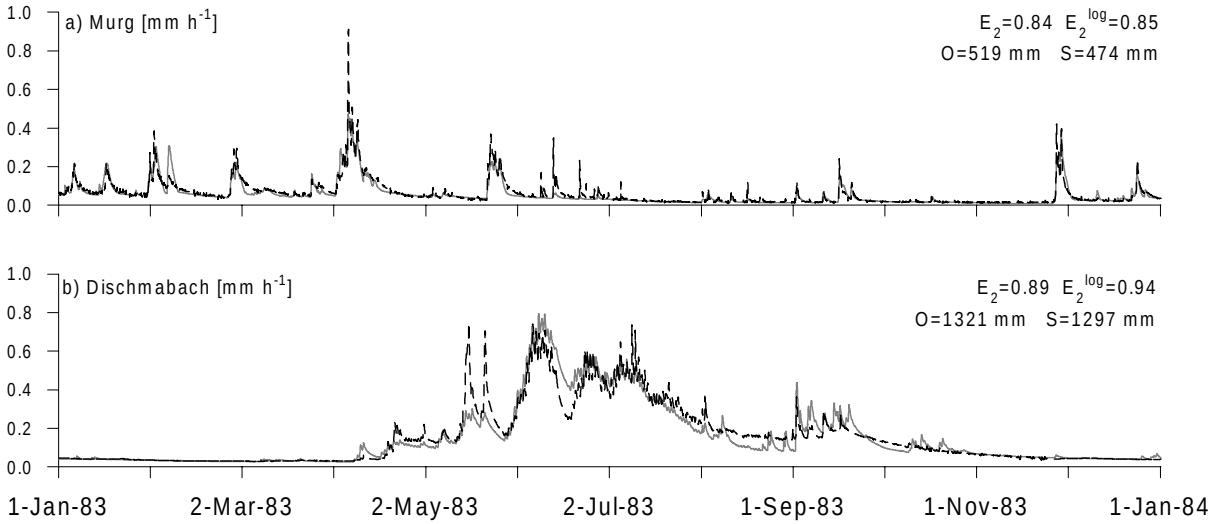

Figure 4.5 Observed (O, dashed black line) and simulated (S, grey line) hourly hydrograph in the calibration year 1983.

In both basins the attained E_2 and E_2^{log} efficiencies are above 0.8, which indicates that the model parameters allow a fair reproduction of the runoff-generation dynamics during both high- and low-flow periods.

The calibration period included, in the case of the Murg catchment, the years 1981-1983 (table 3.1). The model is able to capture the pre-alpine character of the discharge regime of the river Murg (fig. 4.5a), governed by precipitation in winter and by evapotranspiration and soil moisture deficit in summer. A serious problem is the difference between observed (O) and simulated (S) total runoff, which equates to 45 mm (or 8.6%) in 1983.

For the Dischmabach catchment, two calibration periods were defined: 1981-1985 and 1993-1995 (Zappa *et al.* 2003). The temporal dynamics of runoff-generation is well reproduced by means of the model parameters for the two periods. The hydrograph (fig. 4.5b) is characterized by low water flows in winter during the phase of prevailing snow accumulation and by a typical high-alpine snowmelt period between April and July with internal daily fluctuations of the discharge, as governed by the daily cyclicity of air temperature and incoming short-wave radiation. The difference between observed and simulated discharge is small (26 mm or 1.9%).

4.4.2 Murg catchment: evaluation period

The 13-year period 1984-1996 was considered for the evaluation of the experiments. The quality of the hourly hydrograph simulation is highest with a homogeneous res_A of 100 m (E_2 0.869) and decreases gradually with decreasing res_A (table 4.6 and figure 4.6a). The efficiency score range of all the individual years widens with coarser resolution. The spread is 0.17 (0.75 to 0.92) at res_A 300 m and *0.25* (0.67 to 0.92) at res_A 10 km. If the elevation model data are processed at 2 km res_A (keeping all other data at 300 m res_A) the attained efficiency scores remains high at 0.864. The achieved efficiency score decreases to 0.854 only when the land-use information is aggregated to 2 km res_A. The decrease of E_2^{log} for the *MUSE* experiment is more pronounced. The efficiency score lowers from 0.860 at res_A 500 m to 0.844 if only the land-use is resampled at 2 km res_A. Figure 4.6b shows that the year-by-year difference between simulated (*S*) and observed (*O*) discharges fluctuates around zero up to res_A 500 m. At coarser res_A the average bias between *S* and *O* increases up to 36 mm$\cdot$ y^{-1} at 10 km res_A (table 4.6).

Table 4.6 Results of the statistical analysis and average simulated runoff (R) and evapotranspiration (ET) in the Murg catchment (precipitation approx. 1165 mm· y^{-1}) in the evaluation period. E_2 and E_2^{log} are two scores of efficiency. S-O is the difference between the computed and observed discharge.

	E_2 [-]	E_2^{log} [-]	S-O [mm· y^{-1}]	R [mm· y^{-1}]	ET [mm· y^{-1}]
MHRU	0.865	0.858	3.0	588	572
M100	0.869	0.864	5.7	591	569
M300	0.865	0.862	2.6	588	572
M500	0.863	0.860	1.8	587	573
M1000	0.858	0.851	12.7	598	562
M2000	0.848	0.838	24.7	609	550
M10000	0.843	0.830	36.7	622	523
MTOPO	0.864	0.860	6.9	592	567
MSOIL	0.864	0.859	2.0	587	573
MUSE	0.853	0.844	22.9	608	552

The results of the *MUSE* model run confirm that this behaviour is owed to the decreasing res_A of the land-use information. This reaction is caused by the different parameterization of meadows when compared to forests (Gurtz *et al.* 1997a and 1999).

The aggregation to low-resolution spatial information causes the decrease in the portion of forested and urban areas in the catchment (table 4.2), while the portion of grassland increases. Meadowland has a lower leaf area, and consequently interception capacity, than both broadleaf and evergreen forests, and retains less precipitation.

Thus, an increasing portion of meadowland in low res_A experiments causes the decreasing of interception and consequently a decrease in actual evapotranspiration (table 4.6). This implies a higher availability of water for infiltration and runoff-generation. The coarsening of the land-use information from 500 m to 2 km res_A causes an increase of 3.6% in the average computed runoff (table 4.6).

Additionally the average root depth of meadowland (approximately 60 cm) is much smaller than the parameterized roots depth of forests (1.5 m). If the root depth is smaller than the soil depth, the amount of soil moisture available to the vegetation for evapotranspiration depends linearly on the root depth. Otherwise, the soil depth limits the amount of plant available soil moisture. Therefore, forested areas have a larger availability of water for evapotranspiration than meadowland if the soil depth exceeds 60 cm. Table 4.2 shows that the average soil depth in the Murg catchment is approximately 1.5 m. A larger availability of moisture allows larger evapotranspiration rates in the case of forests when compared to meadowland.

This coupled sequence of processes is the main cause of the observed decrease in discharge simulation quality in the Murg catchment with physiographic data at low res_A with respect to the *MHRU* run.

Figure 4.6d illustrates that the cumulative difference between the average monthly runoff rates of various experiments and the ones computed during the *MHRU* model run almost steadily increases during the average hydrological year (October to September) if res_A exceeds 1 km. The experiments *MTOPO* and *MSOIL* are only slightly different from the experiments with res_A between 100 and 500 m.

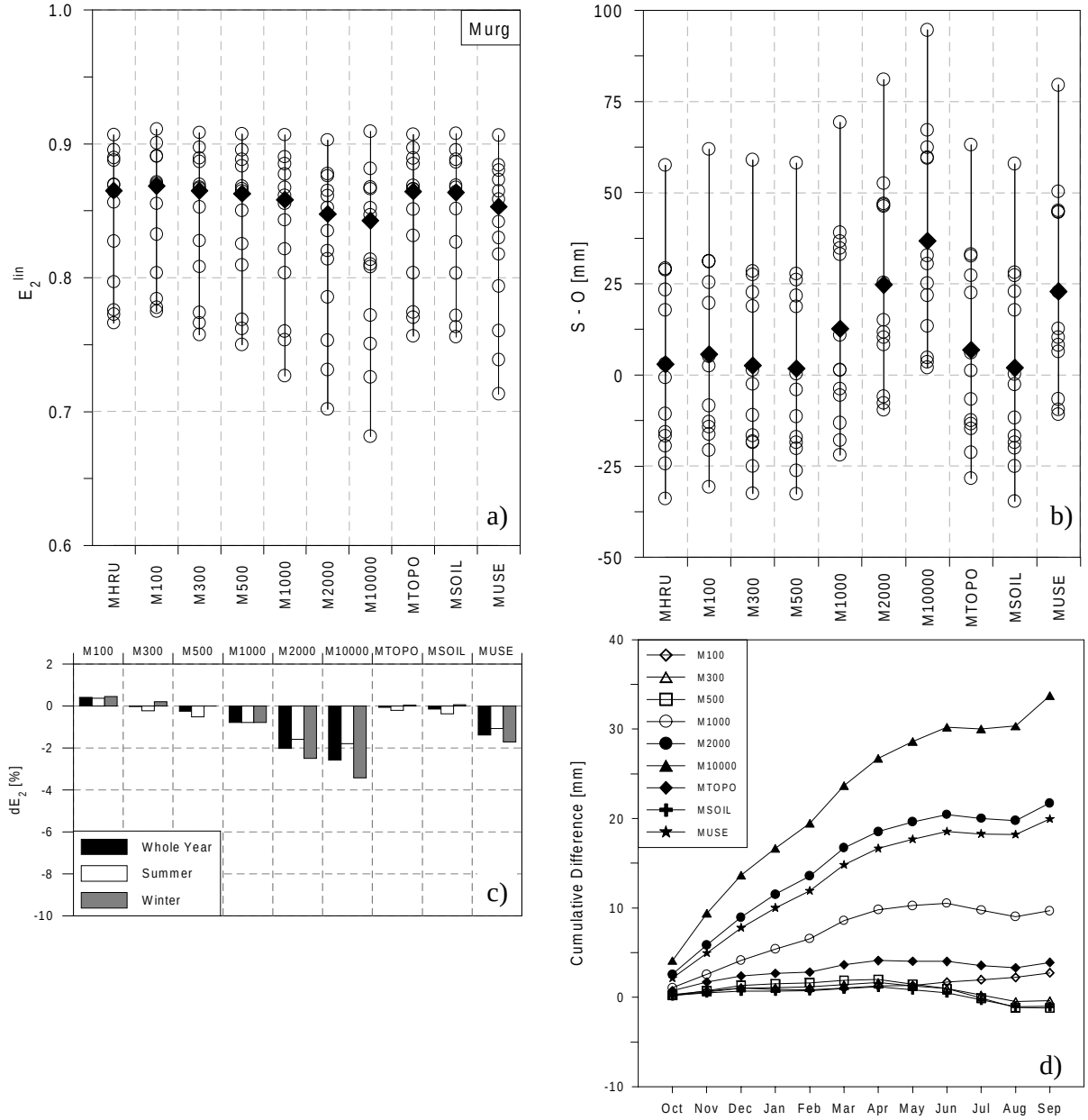

Figure 4.6 Discharge simulations at the Murg catchment in the evaluation period: (a) Year-by-year (circles) and global (diamonds) linear efficiency score of all experiments (table 4.4, left) when compared to observed discharge. (b) Year-by-year and average deviation of the simulated (S) from the observed (O) runoff. (c) Percentual deviation of the efficiency score obtained by the experiments at different res_A from the efficiency score obtained with the HRU-discretization for summer, winter and the whole year. (d) Cumulative average difference of the monthly runoff computed at different res_A to the runoff computed with the HRU discretization.

Again, it is evident that the difference between *MHRU* and *M2000* is mainly caused by the reduced res_A of the land-use characteristics (*MUSE*). The deviation in percentage (dE_2) of the efficiency score of the experiments at various res_A (table 4.4, left) from the efficiency score of the *MHRU* run for summer (April-September in the case of the Murg catchment), winter and for the whole year (see also Eq. 22) is presented in figure 4.6c. dE_2 is close to zero up to 1 km res_A. The differences are small even if the calibration of the model parameters was completed on the exclusive basis of the *MHRU* experiment. This shows that the assigned model parameters are also adequate for cell-by-cell simulations and for

model runs at coarser res_A. At larger res_A a negative dE_2 can be observed, which indicates a reduced efficiency score with respect to the *MHRU* control experiment and to observations (fig. 4.6a). dE_2 is slightly more negative in winter than in summer. This is caused by the seasonal parameterisation of the physiological properties of the land-use. A great part of the dE_2 at 2 km res_A (*M2000*) is caused by the reduction in resolution of the land-use properties (*MUSE*). The sensitivity to the res_A of the soil and topographic characteristics is limited.

4.4.3 Dischmabach catchment: evaluation period

The accounted evaluation period included the years 1986 to 1992 and 1996 to 2000. Figure 4.7a and table 4.7 show that PREVAH is able to simulate the hourly runoff hydrograph with nearly stable efficiency score until 1 km res_A (E_2 of 0.891). The simulation quality rapidly decreases thereafter with decreasing resolution. In the case of the Dischmabach, E_2^{log} is much less sensitive to the change in resolution than E_2. This indicates that the low-flow phases in winter can be simulated with similar agreement at all considered res_A. The topography has the highest sensitivity for a reliable simulation of the runoff hydrograph in the Dischmabach. The model performance decreases considerably when only the information of the digital elevation model data is aggregated to 5 km res_A. When only the land-use or the soil properties are considered having a 5 km res_A, the achieved efficiency score is just slightly lower than at 100 m res_A. At low resolution, the topography is smoothed and the range of elevation from the valley bottom to the top considerably reduces. At both 0.1 and 2 km res_A, the average elevation given by the digital elevation model is 2380 m a. s. l. (table 4.3). The lowest point of the catchment is located at 1677 and 1922 m a. s. l. and the highest point at 3130 and 2920 m a. s. l., respectively. The timing of the snowmelt season and the shape of the discharge hydrograph in the Dischmabach catchment is strongly coupled with the passing of the 0° isotherm through the different elevation zones in the period from March until June (Zappa *et al.* 2003).

The decrease in quality is caused by the change in distribution of the catchment portion in each elevation zone and by the smoothing of the highest and the lowest elevation zones in model runs with low-resolution topographic data.

Figure 4.7a presents the year-by-year Nash-Sutcliffe coefficient for the different experiments in the Dischmabach catchment. The overall quality of the simulation decreases with decreasing resolution.

Table 4.7 As table 4.5, for the Dischmabach catchment (Precipitation approx. 1445 mm· y^{-1}).

	E_2 [-]	E_2^{log} [-]	S-O [mm· y^{-1}]	R [mm· y^{-1}]	ET [mm· y^{-1}]
DHRU	0.895	0.912	-34.3	1183	235
D100	0.895	0.910	-37.2	1180	237
D300	0.895	0.910	-38.0	1179	239
D500	0.895	0.912	-34.6	1182	237
D1000	0.891	0.907	-48.5	1168	241
D2000	0.867	0.897	-39.3	1178	230
D5000	0.842	0.881	-37.6	1179	228
DTOPO	0.852	0.897	0.8	1218	209
DSOIL	0.896	0.907	-32.1	1185	235
DUSE	0.891	0.902	-50.8	1166	245

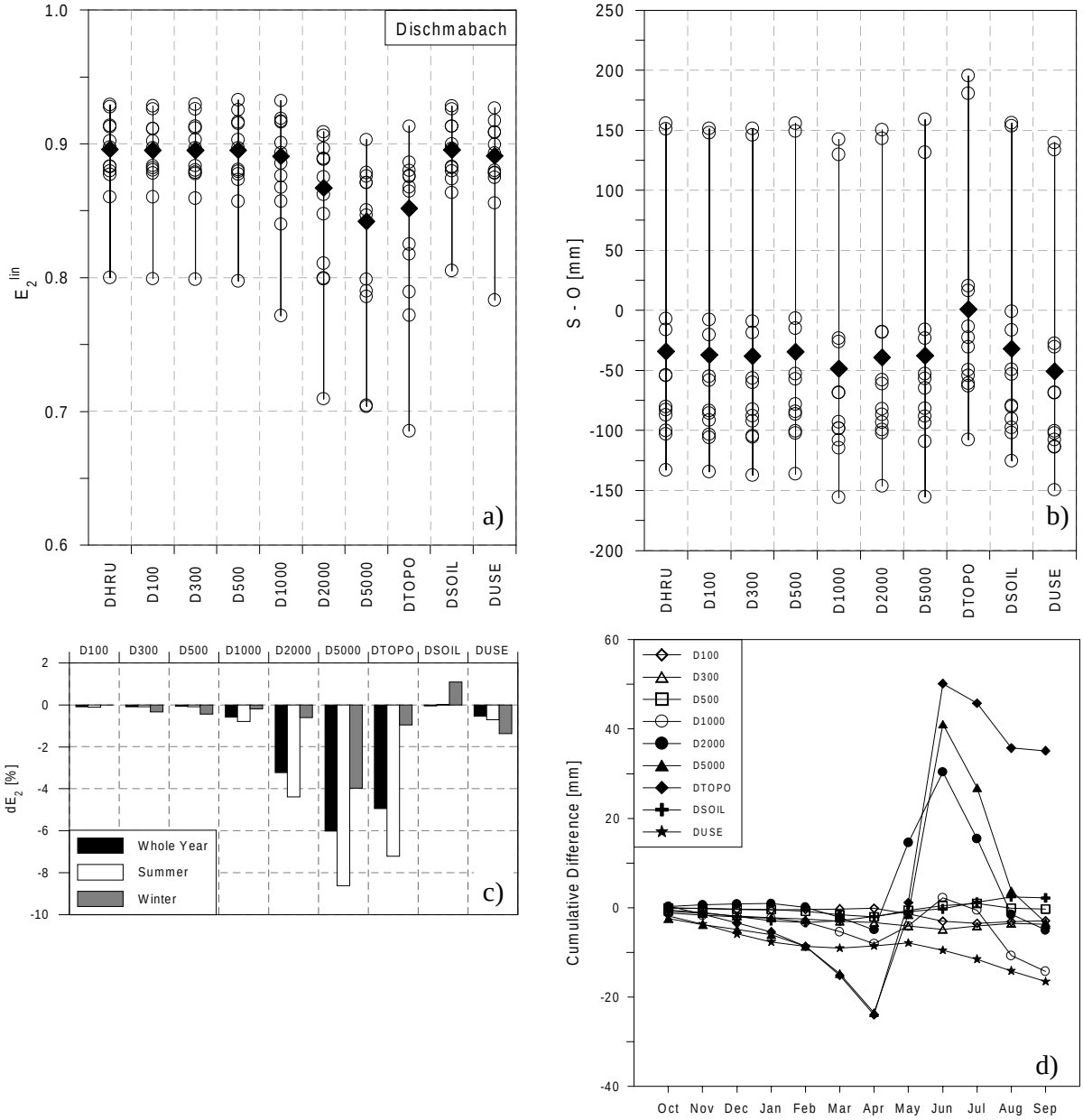

Figure 4.7 Discharge simulations at the Dischmabach catchment in the evaluation period: (a) Year-by-year (circles) and global (diamonds) linear efficiency score of all experiments when compared to observed discharge. (b) Year-by-year and average deviation of the simulated (S) from the observed (O) runoff. (c) Percentual deviation of the efficiency score obtained by the experiments at different res_A from the efficiency score obtained with the HRU-discretization for summer, winter and the whole year. (d) Cumulative average difference of the monthly runoff computed at different res_A to the runoff computed with the HRU discretization.

The range between years, with better and poorer agreement to the observation, spreads considerably. If the simulation at 5 km actual resolution is compared to the simulation with only topography at 5 km resolution, it is evident that most of the quality decrease with respect to the simulations at higher resolution can be explained with the change of resolution of the topographic information. This particular behaviour in the Dischmabach catchment is owed to the dependency of its discharge regime to air temperature and snowmelt. The differences in the year-by-year agreement between simulated and observed total discharge (*S-O*) are rather limited (fig. 4.7b). Beside the *DTOPO*

experiment, the range of *S-O* is between -150 and 150 mm. The average difference *S-O* ranges between -30 and -50 $mm \cdot y^{-1}$ (table 4.7). The diverging behaviour of *DTOPO* is implicitly owed to the different resolution adopted for the topographic information in that particular experiment. Taking only the information of the elevation model at low resolution, and maintaining the resolution of the land-use data at the highest resolution causes that a larger part of the glacerized HRUs is assigned to the ablation area of the glacier. After the end of the snowmelt season, larger melt rates from the ablation area of the glacier are computed. The *DTOPO* experiments therefore shows higher total runoff. This experimental shortcoming is confirmed by figure 4.7d. The cumulative difference between the *DHRU* and the *DTOPO* experiments during the hydrological year (October to September) varies between -25 mm in April and 50 mm in June. Different from the other experiments, a final bias of about 35 mm is present in the case of the *DTOPO* experiment. A similar shortcoming is also present in the case of the *DUSE* and *D1000* experiments. The reduction of glaciated areas after the aggregation of the land-use information causes a lower amount of glacial melt and therefore a bias with respect to the cumulative discharge of *DHRU*.

Figure 4.7d also allows the further explanation for the sensitivity of the Dischmabach catchment to the resolution of the topographic information. The bias between the average runoff generation at high resolution and at coarse resolution is zero up to the beginning of the snowmelt season, when it then turns negative. This means that the snowmelt season begins earlier if high-resolution physiographic data are used. Afterwards the bias slowly becomes positive and is again close to zero after the end of the snow melt season in August. This means that the snowmelt season ends earlier in model runs at low resolution. This behaviour can be explained with the smoothing of the elevation in the model runs at coarse resolution. After the resample, the lowest elevation zones are higher on average and therefore the period with air temperature above the melting point comes later. The highest regions are smoothed. Thus, the period with positive air temperature arrives earlier and causes an earlier end of the snowmelt season.

The sensitivity of the results differs considerably from summer (March-August in the case of the Dischmabach catchment) to winter (figure 4.7c). The discharge regime exhibits significantly higher sensitivity to the change in resolution in summer than in winter. This is owed to the strong dependency of the catchment discharge to air temperature. This behaviour has a strong feedback with the spatial and temporal pattern of snowmelt-governed runoff-generation. Figure 4.7c confirms that the decreasing resolution of the topography (*DTOPO*) alone explains the reduced performance for experiments at low resolution (*D2000* and *D5000*). Figure 4.7c shows that the aggregation to low resolution soil information leads to a slight improvement in the discharge simulation in winter. The aggregation to low resolution soil properties causes a reduction by one third of the average soil depth in the catchment (table 4.3). This may mean that a reduction of the thickness of the soil layer involved in the exchange processes between vegetation and atmosphere in winter could also improve the quality of the discharge simulation at higher resolution. A simple process-based explanation for such behaviour is suggested.

The long periods with air temperatures below 0°C in high-alpine catchments may cause the freezing of the water molecules in the soil and therefore a reduction of the available porosity and infiltration capacity. PREVAH needs information on the soil depth SD and the plant available field capacity (PFC) to parameterize the maximum content of soil moisture storage. A reduction of SD and/or PFC in winter is a conceptually indirect way to account for soil freezing, since both soil freezing and lower SD/PFC values cause a reduction of room in the unsaturated zone of the soil. Thus, the enhancement of PREVAH with a module for the simulation of soil freezing and thawing processes (e.g. Gusev and

Nasonova 2002) could improve the description of the runoff-generation processes in high-alpine catchments during winter.

4.5. Discussion

The problem of the critical grid-size for distributed hydrological simulation has been investigated here. Zhang and Montgomery (1994) analyzed the aggregation of the topographic information, and determined by investigating two catchments with area below 2 km^2, that a grid-size of 10 m is an adequate compromise for simulating a wide range of geomorphic and hydrological processes. Bohrer (1998) computed the water balance of the 3.2 km^2 Rietholzbach catchment with spatial resolutions ranging from 10 and 100 meters. The investigations indicated that a 50x50 m^2 resolution was most suitable for spatially distributed hydrological simulations. A study of Brasington and Richards (1998) determined that the accuracy of model predictions for a 4.5 km^2 basin in Nepal might lose agreement when the resolution of the elevation model exceeds 100 meters.

The work presented in the previous sections shows that the critical grid-size for distributed hydrological simulations in both alpine catchments is between 500 meters and 1 kilometre. Vàzquez *et al.* (2002) assessed an optimal grid resolution of 600 meters for the simulation of the hydrological response of a catchment having approximately 600 km^2 area. Schulla (1997) showed that the critical grid-size for discharge simulations of the large pre-alpine / alpine Thur catchment (Switzerland, 1700 km^2) is 2 km.

Table 4.8 shows the recommendations for the adequate / critical grid size in the framework of distributed hydrological simulations in catchments with area ranging between few hectares and more than 1000 km^2. Figure 4.8 visualizes the recommendations declared in table 4.8 in a log-log plot. A power function is fitted to the eight available recommendations:

$$\log \beta = 0.61 \cdot \log(\alpha) - 3.84 \qquad \text{or} \qquad \beta = 0.021 \cdot \alpha^{0.61} \tag{23}$$

where α [km^2] is the area of the considered catchment and β [km] the diagnosed critical grid size. The explained variance r^2 on the obtained power function is 0.91. The standard error σ of the logarithmic residuals is 0.62.

Table 4.8 Summary of recommended critical grid spacing for geomorphic and hydrological simulation in catchments with different surface area.

Reference	Catchment area α [km^2]	Grid size β [km]	Label
Zhang and Montgomery (1994)	0.3	0.01	1
Zhang and Montgomery (1994)	1.3	0.01	1
Bohrer (1998)	3.2	0.05	2
Brasington and Richards (1998)	4.5	0.10	3
this study	43.3	0.50	4
this study	210	0.50	4
Vàzquez *et al.* (2002)	600	0.60	5
Schulla (1997)	1700	2.00	6

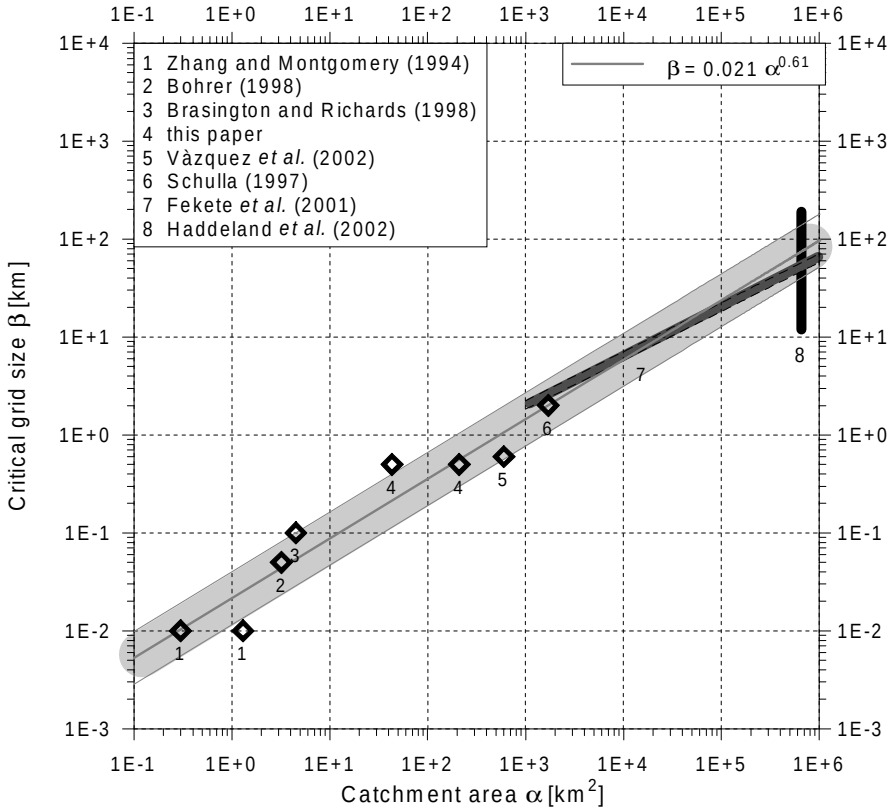

Figure 4.8 Visualization of the declared critical grid size β as a function of the catchment area α. A grid size below the value indicated by the computed regression (thick grey line) indicates an increase of computational time without increase of model ability. A grid size above the value diagnosed by the proposed log-log regression may cause a significant reduction in ability in the simulation of hydrological processes within the investigated catchment. The dark grey area indicates the recommended grid size proposed by Fekete *et al.* (2001). The black area represents the range of grid sizes adopted by Haddeland *et al.* (2002) for the simulation of the discharge from two macroscale basins.

A more general formulation of equation 23 accounts the standard error σ:

$$e^{(-3.84-\sigma)} \cdot \alpha^{0.61} \leq \beta \leq e^{(-3.84+\sigma)} \cdot \alpha^{0.61} \qquad (24)$$

Equation 24 (light grey area in figure 4.8) defines the range where the allowed critical resolution β [km] may be exceeded in catchments with area α [km^2] between 1 hectare and 10000 km^2. A homogeneous catchment with a surface of 100 km^2 has, intuitively, a larger critical grid size than a relatively inhomogeneous catchment of the same dimension. It is therefore necessary to be aware that the difference in the critical size between catchments of similar area is also determined by the small-scale variability of the physiographic properties. Thus, after equation 24 the critical grid spacing for the simulation of hydrological processes within a catchment having an area of one hectare may range between 3 and 10 m. The simulation of the hydrological response for a catchment having an area of 10000 km^2 may become critical if the adopted grid-spacing ranges between 3 and 10 km.

It is to be expected that a resolution lower than the one recommended by the right term of equation (24) may lead to a reduced quality in the simulation results. If the adopted model resolution is higher than recommended by the left term of equation (24), it is to be

expected than the additional computational time would only bring limited improvements in the quality of the hydrological simulations.

The extrapolation of equation (23) and (24) for macroscale catchments exceeding 10000 km^2 area is not advisable. Fekete *et al.* (2001) show that a minimum number of 200 to 300 grid cells is required to capture the individual physiographic characteristics of large river basins. The dark grey area plotted in figure 4.8 visualizes the resolution that is needed to satisfy Fekete's assumption for catchments larger than 100 km^2. The formula proposed in this study for assessing the critical grid size (Eq. 23) and the assumption of Fekete *et al.* (2001) nearly coincides in the case of catchments between 10000 and 100000 km^2 area. For even larger catchments, it is to be expected that the allowed resolution diagnosed by equation (23) may be too large for a sound description of the catchment characteristics. Such assertion is confirmed by the study of Haddeland *et al.* (2002). In the cited study, the water balance of two large American catchments (approx. 650000 km^2) was simulated with a grid spacing varying approximately between 12 and 140 km^2 (black area in figure 4.8). Equation (24) diagnoses that the critical grid size for a 650000 km^2 large catchment is between 40 and 140 km. The results of Haddeland *et al.* show that the generation of direct runoff is very sensitive to the change in spatial resolution and that reliable discharge simulations in model runs with low resolution are only attained if a reparameterization of the variation of precipitation with elevation is adopted. Thus, the critical grid size for macroscale catchments may be overestimated by equations (23) and (24).

4.6. Conclusions

The application of the proposed distinction between actual res_A and nominal resolution res_N allows representative hydrological simulations in small catchments at coarse resolution. Furthermore, it allows the identification of the relative sensitivity of the different physiographic properties to the performance decrease in low-resolution simulations. The experiments with PREVAH showed that the critical resolution, namely where the model performance begins to sink significantly, is approximately 500x500 m^2 in the case of both the investigated Dischmabach and Murg catchments. A grid resolution up to 500x500 m^2 appears to be suitable in the framework of detailed spatially distributed hydrological simulations in the alpine region.

It was proven that the model parameters determined by calibration with model runs relying on an HRU discretization are robust and allow an accurate simulation of discharge without additional calibration up to the critical resolution of 500x500 m^2. If this conclusion is considered from the opposite point of view, an important positive technical feedback may arise from the whole experiment. Modellers may use a coarser grid resolution in the calibration phase and save CPU-time. This would also allow obtaining representative configurations of calibrated model parameters for high-resolution model runs. Thus, the number of model runs requiring CPU-time may be minimized (e.g. Zhang and Montgomery 1994, Haddeland *et al.* 2002). In the case of the Murg catchment the MUSE experiment (100x100 m^2 resolution) required approximately 80 times more CPU-time than the MHRU experiment, also related on a basic grid resolution of 100x100 m^2. This proves that the aggregation of grid-cells to HRUs is a very efficient, and method for detailed distributed hydrological simulations. At the same time the use of a HRU discretization allow saving CPU-time.

It was demonstrated that the reason for a decreasing model efficiency score in the simulation of hourly discharges is different for the two investigated catchments. In the case of the prealpine Murg catchment, the efficiency score of the runoff simulations is

sensitive to the aggregation of the land surface properties and is not affected by the decrease in resolution of the information linked to the soil and topography. The aggregation of the land-use information causes a significant change in relative portion of the different land-use classes. The increase of meadowlands at the expense of forested areas causes a reduction in evapotranspiration and an increase of total runoff. The correct representation of the relative portions of the land-use classes is a key condition for the simulation of the hydrological cycle in pre-alpine catchments.

The experiments in the high-alpine Dischmabach catchment showed that there is a very significant decrease in the quality of the discharge simulation when the topographic information is smoothed. The sensitivity to changes in the spatial resolution of the soil and land surface characteristics appears limited. An inaccurate representation of the topographic information leads to an inadequate representation of the processes that have a strong variation with altitude. A smoothed elevation model causes a delayed onset of the snowmelt season to be delayed in the lowest parts of the catchment and an early end of the snowmelt season in the upper parts of the basin.

Thus, the simulation of the hydrological cycle at a coarse resolution may be improved by the reparameterization of the key processes involved in the process of runoff-generation. In the case of pre-alpine landscapes, large-scale models should account for the sub-grid distribution of the land-use information. In the case of high-alpine landscapes, a sub-grid parameterization of snow accumulation and snowmelt processes are required. Such parameterization should be able to anticipate the beginning of the snowmelt season in low elevation ranges and to delay the end of the snowmelt in the highest elevation ranges.

Finally, an equation based on the recommendations published in recent literature was proposed for the formulation of the critical grid spacing for spatially distributed hydrological simulations. The representative range for the presented tentative equation includes catchments with an area ranging between 1 hectare and 10000 km^2.

5. Applications and experiments at different scales

5.1. Applications at the plot-scale

5.1.1 Model assessment at the MAP-Riviera site♦

Field observations

In the framework of the MAP-Riviera field experiment (Section 3.1.2) the soil water content of a corn field at "Bosco di Sotto" (fig. 3.2) was measured hourly with a Tektronix-TDR-System. With the Time Domain Reflectometry technique (TDR), it is possible to measure the changes in the relative dielectric properties of the soil in relation to the changes in the soil water content to determinate the soil's volumetric water content (Topp *et al.* 1980, Menzel 1995). Six TDR probes (fig. 5.1) and three temperature probes (thermocouples) were buried into the soil at different depths (5 to 120 cm depth) to obtain a representative profile of the vertical changes of soil temperature and water content. The TDR signals were analyzed as proposed by Roth *et al.* (1990). A meteorological tower at the same location was equipped to observe data at different levels (fig. 3.2). From 12 August 1999 to 10 November 1999, the following variables were collected using a time resolution of 30 minutes and then aggregated to hourly data (data set **TOWER**):

- the vertical profile of air temperature, relative humidity and wind speed (1.5 m, 3 m, 6 m, 12 m, 19 m, and 28 m heights);
- net radiation, global radiation, outgoing short-wave radiation, and incoming and outgoing long-wave radiation at 1.5 m height;
- the soil heat flux;
- precipitation at 3 m height with a Tognini gauge.

Figure 5.1 Instrumentation at the site "Bosco di Sotto". Left: asymmetric ultrasonic anemometer combined with a fast-response krypton hygrometer. Right: soil moisture detection by TDR-probes.

♦ The results presented in section 5.1.1 are part of the paper "Plot-scale simulation of soil moisture and evapotranspiration during the 1999 MAP-Riviera campaign" by M. Zappa and J. Gurtz. The paper is submitted to *Hydrology and Earth System Sciences.*

The data from the 1.5 m and 6 m heights of the meteorological tower were used for the computation of the Bowen ratio (β) (Bowen 1926) and assessment of the latent heat flux (Konzelmann *et al.* 1997, Zappa *et al.* 2001). The quality and physical consistency of the energy fluxes diagnosed from β were analyzed as proposed by Ohmura (1982) and similarly to Konzelmann *et al.* (1997) and Müller (1989). Konzelmann *et al.* (1997) assessed that the relative uncertainty of the Bowen ratio method for the computation of the hourly turbulent fluxes ranges between 10% and 20%. This method assumes that the energy balance at the investigated site is closed (Ohmura 1982).

Data from stations surrounding the Riviera valley (up to 50 km from the site "Bosco di Sotto", fig. 3.2) were used to create a representative hourly data set (**$ANETZ_H$**) for the location under investigation covering the period from July to November 1999 (R-SOP). Appendix B shows the results of the intercomparison between the TOWER and $ANETZ_H$ data sets (Zappa and Gurtz 2003).

Simulation of soil moisture and latent heat flux

The tuneable parameters were calibrated on the period 12 to 31 August 1999 using the data set TOWER and *Monteith* for the computation of ET (table 5.1) and following the procedure illustrated in section 2.3. The hydrological model was operated using the meteorological data collected at the 3 m level on the tower. The remainder of the R-SOP was used to validate the quality of the conceptual soil model of PREVAH (figure 2.4). Secondly, the model was run with the same set of free parameters using the meteorological time series $ANETZ_H$. The quality of the model simulation was assessed by comparing the observed soil moisture and latent heat flux with values obtained from the simulation. Table 5.2 shows a month-by-month overview of the statistical performance of the soil moisture simulation at the site "Bosco di Sotto" for both runs. The quality of the simulation using the TOWER data is very high in both periods of calibration and evaluation. R_{OS} and E_2 are above 0.8 and the average RMSE is low.

The month-by-month performance of the model indicates that the quality of the TOWER simulation is constantly high during the whole R-SOP period. The calibrated free parameters allow a good description of the dynamic of soil moisture recharge and consumption. The results of the simulation based on the $ANETZ_H$ data set are also satisfying. With exception of the month of August, the statistical analysis of the $ANETZ_H$ run with respect to the observed soil moisture gives similar results to the TOWER run.

Table 5.1 Definition of selected state variables of the hydrological model and declaration of the calibrated tuneable model parameters.

Parameter	Symbol	Unit	Value	Type
Inflow in the soil model	P_b	$mm \cdot h^{-1}$	-	state variable
Evapotranspiration	ET	$mm \cdot h^{-1}$	-	state variable
Water storage in the aeration zone of the soil	SSM	mm	-	state variable
Inflow in the runoff-generation module	DSUZ	mm	-	state variable
Water storage in the upper zone	SUZ	mm	-	state variable
Non linearity parameter	BETA	-	6.5	tuneable parameter
Threshold parameter for surface runoff	SG	mm	30	tuneable parameter
Storage coefficient for surface runoff	K_0	h	3	tuneable parameter
Storage coefficient for interflow	K_1	h	75	tuneable parameter
Deep Percolation	PERC	$mm \cdot h^{-1}$	0.08	tuneable parameter

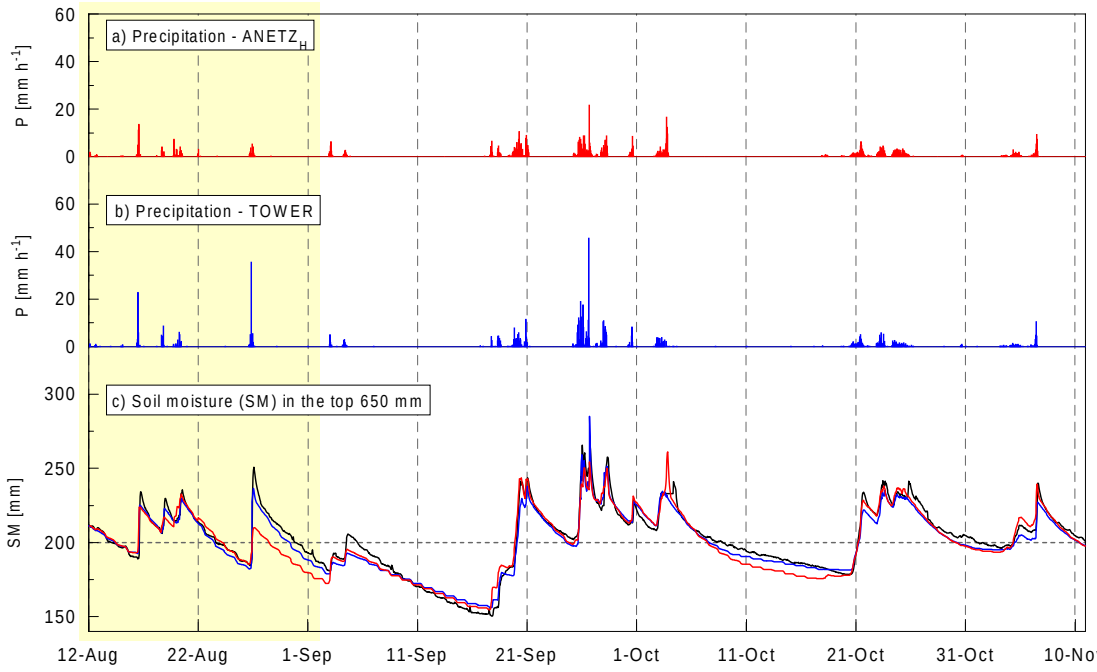

Figure 5.2 Soil moisture simulation. The light yellow background indicates the calibration period. a) Hourly precipitation rates of the ANETZ$_H$ data set. b) Hourly precipitation rates of the TOWER data set. c) Observed hourly soil moisture (black line), simulation with TOWER (blue line), simulation with ANETZ$_H$ (red line).

The model performance in August with the ANETZ$_H$ data set is clearly affected by the event on 26 August. The RMSE in August is more than double that calculated for the ANETZ$_H$ run (10.4 mm) with respect to the TOWER run (4.4 mm). Both R_{OS} (0.73 vs. 0.96) and E_2 (0.38 vs. 0.89) confirm this behaviour. On 26 August, a very active convective cell caused heavy precipitation in the area surrounding the investigated area (figure 5.2b). This rainfall event was characterized by very high rain intensities (up to 35 mm·h$_{-1}$) and caused a rapid increase in soil water content (figure 5.2c). Since this heavy event was very localized, it was not possible to reconstruct it accurately using the data from the MeteoSwiss network (fig. 5.2a).

The result of this lack of information on rain rates and intensities caused an underestimation of the soil moisture recharge in the ANETZ$_H$ simulation. This situation lasted until the next small precipitation event on 4 September (fig. 5.2).

Table 5.2 Statistical analysis between observed and simulated soil moisture (hourly data) in the case of the model runs with the TOWER and the ANETZ$_H$ time series. The statistical indices R_{OS}, E_2 and *RMSE* are defined in section 2.3.3.

Data set	Variable	Unit	August	September	October	November	Period
TOWER	R_{os}	-	0.96	0.98	0.98	0.98	0.98
ANETZ$_H$	R_{os}	-	0.73	0.97	0.97	0.93	0.95
TOWER	E_2	-	0.89	0.96	0.89	0.81	0.95
ANETZ$_H$	E_2	-	0.38	0.95	0.87	0.80	0.88
TOWER	RMSE	mm	4.41	5.63	4.41	4.10	4.81
ANETZ$_H$	RMSE	mm	10.40	6.26	6.27	4.20	7.20

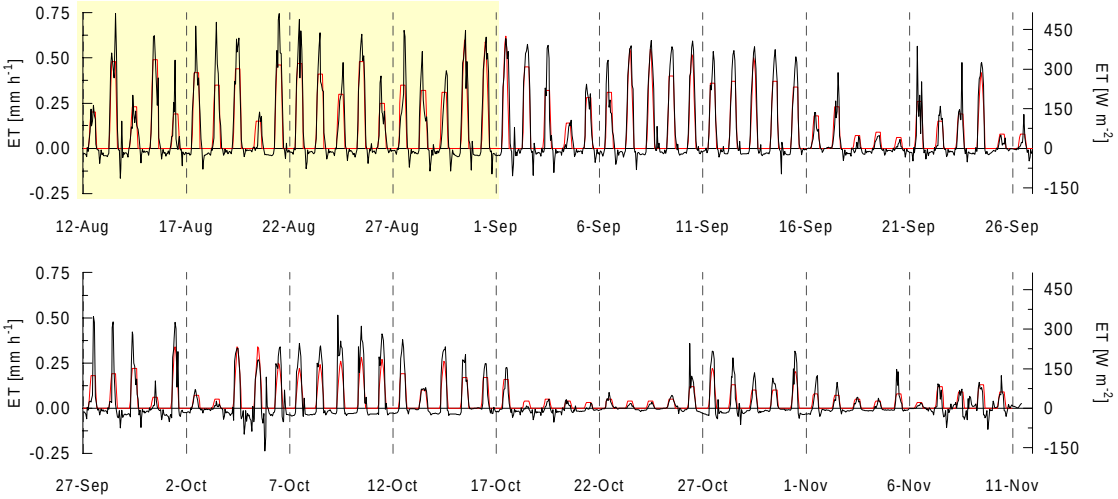

Figure 5.3 Simulation of evapotranspiration. The light yellow background indicates the calibration period. The black line indicates LE computed by Bowen Ratio, the red line the simulation with TOWER.

This was characterized by advective precipitation and was therefore easier to be reconstructed by interpolation. The following dry period is characterized by an underestimation of the depletion of soil water content for the TOWER data set. The observed soil moisture after the third week of September can be accurately modelled using both meteorological time series. However there is another important variation between the two runs during the dry phase after the rainfall on 4 October. The soil water content simulated using $ANETZ_H$ (RMSE 6.3 mm in October) dries more than both the observed and the simulated values from the TOWER (RMSE 4.4 in October). After the harvesting of the cornfield on 27 October, the model is capable to follow the moisture content changes accurately. At this time, the cornfield is only covered with bare soil and stubble.

The latent heat flux data computed using the Bowen ratio (LE-β) from the observed vertical profile of air temperature and relative humidity were used to quantify the quality of the evapotranspiration as simulated by the hydrological model for the "Bosco di Sotto" site. Figure 5.3 shows a comparison between LE-β and the corresponding values simulated by PREVAH driven using the TOWER data set (*Monteith* was used for this specific analysis). The qualitative comparison between LE-β and the simulation is very good, having R_{OS}=0.92 and E_2=0.83. The fluctuation in magnitude of hourly evapotranspiration from day-to-day is caused by the alternation of dry and wet weathering periods. This behavior is accurately reproduced.

PREVAH computes the hourly evapotranspiration between sunrise and sunset from the daily evapotranspiration values as a function of precipitation and radiation (Gurtz *et al.* 1997a). This is the main reason for the underestimation of hourly evapotranspiration during the day and for the absence of condensation during the night (negative latent heat flux). The model is only valid for the qualitative estimation of hourly evapotranspiration. The model, however, does not diagnose the accumulation of dew on the canopy. This phenomenon was observed regularly after cloudless nights.

Figure 5.4 and table 5.3 show the comparison between the daily LE-β and the daily ET computed using different model runs. The last (E_2 to LE-β) and second last lines (R_{OS} to LE-β) in table 5.3 show the statistical analysis of both figures 5.4a. and 5.4b.

Table 5.3 Statistical analysis between observed and simulated evapotranspiration / latent heat flux (daily data) for the six model runs. The cumulative evapotranspiration between 12 August and the indicated dates is given in mm. See the body of the text for further details.

Method Meteo	LE-β TOWER	*Monteith* TOWER	*Wendling* TOWER	*Turc* TOWER	*Monteith* $ANETZ_H$	*Wendling* $ANETZ_H$	*Turc* $ANETZ_H$
15 Aug.	10.7	9.9	9.8	10.3	13.4	10.5	11.0
30 Aug.	50.6	41.7	47.2	49.8	57.2	51.1	53.8
15 Sept.	94.9	77.7	90.7	92.8	106.0	96.5	98.9
30 Sept.	106.6	91.0	106.8	110.3	130.0	115.3	119.0
15 Oct.	124.8	108.6	131.2	130.0	162.9	142.2	141.6
30 Oct.	130.1	119.0	141.4	139.7	176.2	152.0	151.2
10 Nov.	133.4	127.2	150.1	146.6	188.9	161.5	158.9
R_{os} vs. LE-β	-	0.83	0.96	0.97	0.77	0.93	0.95
E_2 vs. LE-β	-	0.67	0.88	0.90	0.35	0.81	0.85

Figure 5.4a. shows a scatter-plot between LE-β and ET-TOWER for the three schemes used to compute ET. The simulated daily ET is better aligned along the 1:1 line when PREVAH is configured to use *Turc* and *Wendling* for estimating ET. However, low LE-β values tend to be overestimated while high values tend to be slightly underestimated. If *Monteith* is used a significant underestimation of the LE-β values can be observed. Some large positive outlying points erroneously compensate this systematic underestimation in days with low LE-β and relatively high wind speed. This indicates that in days with low energy availability and high wind speed, the ET computed by *Monteith* is poorly correlated with LE-β. *Wendling* and *Turc* don't take wind speed into consideration and keep a high correlation with LE-β, which is also doesn't account wind speed.

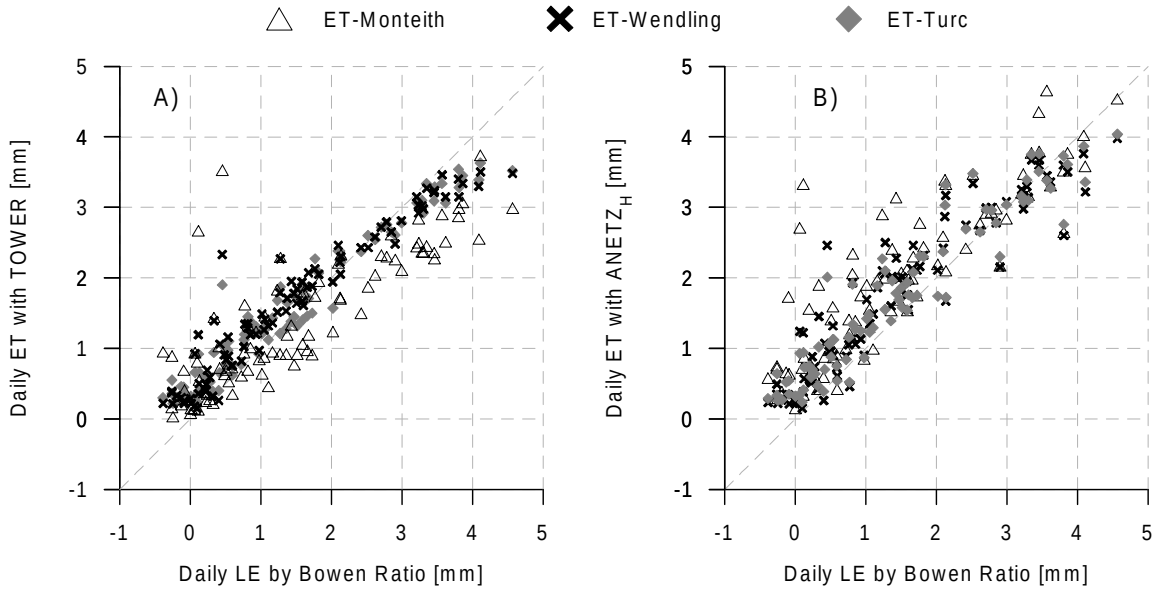

Figure 5.4 Comparison between the daily latent heat flux (LE) computed by Bowen Ratio and the simulated daily evapotranspiration (ET) between 12 August and 10 November 1999 with three evapotranspiration schemes. A) Model run with the TOWER data set. B) Model run with the $ANETZ_H$ data set.

Figure 5.4b. is similar to figure 5.4a. Here $ANETZ_H$ is used instead of TOWER for the simulation of ET with PREVAH. Also in this case the use of *Turc* and *Wendling* leads to better correlation to LE-β than using *Monteith* (table 5.3). Both the objective statistical analysis (smaller R_{OS} and E_2) and the subjective visual comparisons indicates a larger scatter of the simulated ET-values with respect to the 1:1 line values in the case of the simulation using the $ANETZ_H$. Both R_{OS} and E_2 decrease largely when using *Monteith* for evapotranspiration. This indicates problems in the spatial interpolation of the meteorological elements other than precipitation, global radiation and air temperature (i.e. wind speed and water vapour pressure).

The quantitative agreement between LE-β and the different simulated values is shown on table 5.3. The cumulative LE-β and simulated ET of 6 model runs (values in mm) is calculated at regular time intervals between 15 August and 10 November 1999. Only one model run (*Monteith*-TOWER) underestimates the cumulative LE-β during the considered period. Larger ET values are computed using the $ANETZ_H$ data set than with TOWER. The overestimation of LE with the *Monteith*-approach and interpolated meteorology is very large (more than 30%), even when the three main climate elements are in good agreement with the TOWER data set (See Appendix B). The main reason for the increase in ET between the TOWER and the $ANETZ_H$ experiments lies in the amount of available precipitation for soil moisture recharge and runoff-generation.

Comment

The adopted methods for the spatial interpolation of the meteorological data have proved to be accurate for air temperature and global radiation (Appendix B). An accurate interpolation of precipitation was only possible in case of advective rainfall events. The temporal dynamics of rainfall intensities for thunderstorms and local convective precipitation events was not accurately modelled. The underestimation of the rain intensities leads to systematic errors in the computation of the soil water content. Such systematic errors disappear as soon as both the modelled soil zone and the real soil zone reach field capacity during a persisting advective precipitation event. The development of a more robust method for spatial rainfall interpolation should be considered for the hydrological model for both plot-scale and spatially distributed applications.

Both the statistical and the subjective visual analysis showed that PREVAH has a simple but well performing conceptual soil model. The good results during the phase of calibration were confirmed by both the analysis of the validation period and the simulations with interpolated meteorology. The assessment of the quality of the soil model is only possible when detailed specific observations are available at the plot-scale. This underlines the importance of performing process-related investigations both in instrumented research catchments and within the framework of term-projects like MAP.

The performance analysis of three simple parameterizations for evapotranspiration showed better correlation to observations when the local meteorology is used. The hydrologic modellers community generally used approach of Penman-Monteith resulted in poorer correlations than the more conceptual parameterizations after Wendling and Turc. The reasons for such partial failure of the Penman-Monteith scheme should be found in the preprocessing and assimilation of the interpolated wind speed data. Wendling and Turc have the additional advantage that less climate data are needed. However, their usefulness for spatially distributed simulation is scarce, since there is little chance for parameterization of these two schemes for different land use types. This limitation is not present for the Monteith approach, which is therefore preferred by modellers if all the required meteorological data are available.

5.1.2 Use of long-term records from a hydrometeorological experimental site♦

The lysimeter of the hydrological research catchment Rietholzbach provides valuable data for multiple-response model evaluation. The lysimeter only has vertical flows. Although the original concept beyond PREVAH is the simulation of both lateral and vertical flows, in this case the model is adopted for the simulation of vertical flow. The parameters of the runoff-generation module (figures 2.4 and 2.5) were adjusted to reproduce the vertical flows at the lysimeter site. The water balance of the lysimeter is available for the period 1976 to 2000 (Moesch 2001).

The presented analysis considers the period 1983 to 1998. The statistical analysis between computed and observed elements of the lysimeter water balance is summarized in table 5.4. The simulated monthly outflow (R), evapotranspiration (ET) and storage change (ΔS) show a high correlation with the respective observations. All the elements of the lysimeter water balance are slightly overestimated. The efficiency score E_2 is above 0.80 in the calibration as well as in the evaluation period. ET is reproduced slightly better in the evaluation period, both R and ΔS in the calibration period.

Figure 5.5 shows the temporal pattern of observed and simulated R, ET and ΔS. The model is able to capture the year-to-year variability of the observations and the alternation of dry and wet seasons. The largest gap is present in the case of ET in the summertime, which is often overestimated by the model. Another shortcoming is the accuracy of the simulation of ΔS when snow accumulation and snowmelt events are involved. Such behaviour is evident in the winters 1988/89, 1990/91 and 1996/97. The model stores too much water and shows reduced outflow when compared to the observations. The simulated ΔS values in December are higher than the storage changes of the lysimeter.

Table 5.4 Multiple response evaluation of PREVAH with records from the lysimeter of the Rietholzbach catchment for the period 1983 to 1998. The calibration is declared in table 3.5. R is the lysimeter outflow, ET the evapotranspiration, ΔS the storage change.

	Period	Unit	R	ET	ΔS
Monthly Records					
R_{OS}	entire	-	0.917	0.973	0.833
E_2	entire	-	0.876	0.937	0.861
E_2	calibration	-	0.896	0.914	0.891
E_2	evaluation	-	0.862	0.949	0.842
Average	observation	mm· month^{-1}	86.1	43.9	0.6
Average	simulation	mm· month^{-1}	86.9	46.6	-0.2
Daily Records					
E_2	entire	-	0.651	0.780	
E_2	calibration	-	0.686	0.752	
E_2	evaluation	-	0.630	0.796	
Average	observation	mm· day^{-1}	2.79	1.44	
Average	simulation	mm· day^{-1}	2.85	1.53	

♦ The work presented in section 5.1.2 is included in the paper " Long-term hydrometeorological measurements and model-based analyses in the hydrological research catchment Rietholzbach " by J. Gurtz *et al.*. The paper is accepted for publication in the *Journal of Hydrology and Hydromechanics.*

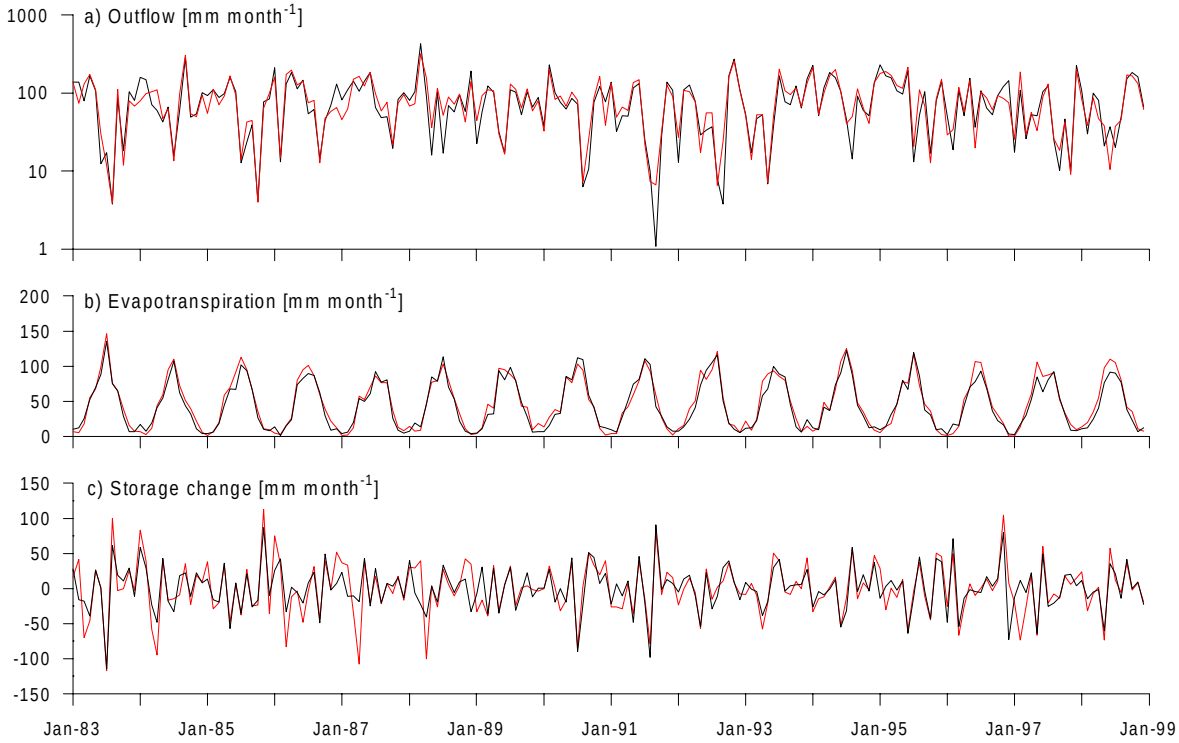

Figure 5.5 Simulation of the lysimeter monthly water balance elements: a) outflow. b) evapotranspiration. c) storage change. Observed values are black, simulated values are in red.

Later in winter, the water stored by the model is released and causes lower ΔS values than the observations. Thus, the observed outflow is underestimated. The analysis of daily records also shows that the model efficiently reproduces the daily time series of outflow and evapotranspiration. The achieved E_2 in the calibration and evaluation periods are above 0.6 (table 5.4). The E_2 range is 0.09-0.78 in the case of the lysimeter outflow and 0.69-0.84 for ET.

Figure 5.6 visualizes the daily time series of four observed and simulated hydrometeorological variables for the two-year period 1994-1995. Observations of the soil water content by TDR measurements are available since 1994 (Menzel 1995 and 1997). Albedo was computed on the basis of observations of incoming and reflected short-wave radiation at 2 p.m. and used to diagnose the presence of snow-cover within the period January 1993 up to April 1998.

The computed albedo at 2 p.m. is compared to the simulated snow water equivalent (fig. 5.6a). The visual qualitative correspondence is satisfying. The average albedo at 2 p.m. during snow-free periods (e.g. May to October 1995) is below 0.2. An albedo above 0.3 is assumed diagnosing snow-cover presence. In the period between 1993 and 1998 (October to April only) there are 350 days that meet this assumption. In 343 of those cases the model also shows presence of snow. In another 221 cases, the model indicates the presence of snow while the albedo is below 0.3. The *CSI* (Eq. 18) of the prediction of snow presence when compared to albedo values is 0.60 (maximum 0.72 in 1997, minimum 0.47 in 1994). In more than 500 cases between October and April of the considered years, the model simulated absence of snow and the albedo was below 0.3. The comparison with albedo outlines that PREVAH tends to predict snow-cover for a too long period.

Figure 5.6b shows a comparison between computed and observed daily evapotranspiration. The ET simulation shows a high quality as confirmed by the statistical analysis (table 5.4), E_2 is 0.79 in both 1994 and 1995. The largest biases are found in winter,

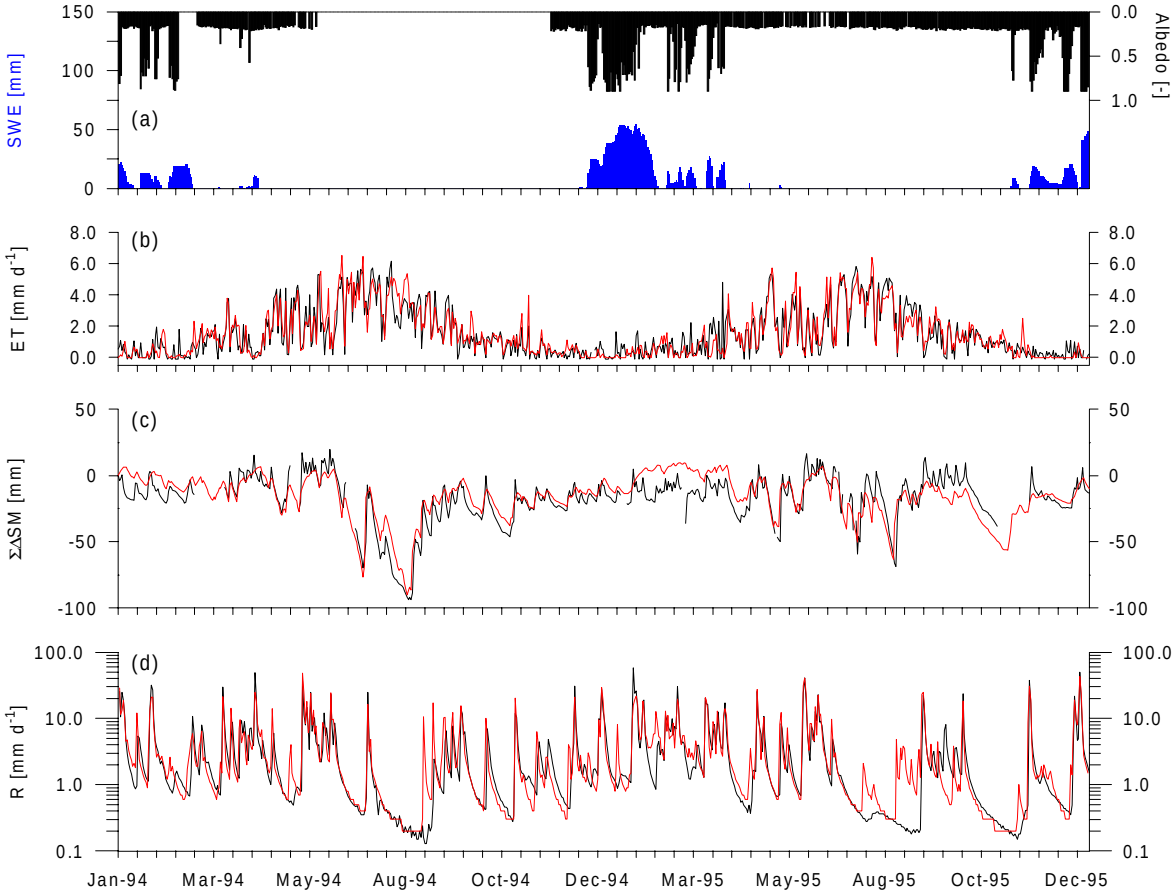

Figure 5.6 Daily values of observed (in black) and simulated (in red and blue) hydrometeorological variables for the lysimeter site in the Rietholzbach catchment (1994 and 1995): a) observed albedo at 2 p.m. (right axis) and simulated snow water equivalent (SWE, left axis). b) lysimeter and simulated evapotranspiration ET. c) cumulative soil water content changes (ΣΔSM) observed within the lysimeter by the TDR technique and simulated with PREVAH. d) observed and simulated lysimeter outflow.

where both problems in the collection of reliable evaporation data from the lysimeter and of assessing the latent heat flux from the snow-cover in the model lead to a decrease in correlation between observations and simulations. The day-to-day fluctuations of ET in summer are caused by the alternation of dry and wet weather periods and are reproduced with good quality.

The simulation of the changes in soil water content (ΣΔSM) since January 1994 (fig. 5.6b) is compared to the observed ΣΔSM. The temporal pattern of ΣΔSM is closely related to ET. The model can capture the temporal dynamics of ΣΔSM for the presented two-year period. The differences are caused by shortcomings in the model approach for the separation between soil water recharge and runoff-generation, by uncertainties in the observation, and by divergences between the interpolated precipitation and the precipitation actually falling on the lysimeter. Another shortcoming of the model is the overestimation of ΣΔSM during and after snowmelt periods

Further the simulated lysimeter outflow shows good agreement with observations. E_2 is above 0.7 in both 1994 (0.73) and 1995 (0.76). The obtained E_2^{log} is 0.65 in both years. As figure 5.6d shows, the determination of the lysimeter outflow is particularly difficult in the dry periods. Both figures 5.6c and 5.6d indicates that the lysimeter retains water after

intense rainfall events and shows a very reduced reaction to precipitation after dry periods in summer. The model is not able to describe those particular behaviours of the lysimeter. Since the lysimeter container is separated from its environs and has no lateral hydraulic connection with the 'free' soil, it is difficult to assess to what extent its reaction to precipitation is similar to the one of a natural soil profile.

Comment

The analysis of the model quality at plot-scale allowed for the separate testing of the quality of several model-components with observed data other than the generally adopted discharge data. The multiple-response evaluation, as performed for the lysimeter, site allows for reliable assumptions on the suitability of the different model components and, therefore, indicates the way for further improvements in the spatially distributed simulation of runoff-generation and other hydrological processes. The results show the usefulness of lysimeter data for the assessment of the quality of the components of hydrological models. The lateral flows present in a natural soil profile are not possible in the lysimeter container. Therefore, the outflow from a lysimeter is not suitable as an indicator of the runoff-generation processes dynamics.

5.2. Applications in hydrological research catchments

5.2.1 Multiple response verification in a hillslope catchment

The data set of the hydrometeorological research station Valdai-Usadievsky (Schlosser *et al.* 1997) was used for studies at the grassland hillslope catchment Usadievsky. A multiple response validation of PREVAH was completed. The records were divided into sub-periods for calibration and evaluation with the available observed hydrological time series (table 3.4). Such simulations allowed the calibration and evaluation of PREVAH in a location with similar climatology as the Upper Volga catchment, which was the target of the EU-INCO Copernicus Volga Forest project (Oltchev *et al.* 2002). Owing to the reduced data availability in the Upper Volga region (only precipitation, air temperature and global radiation were available), and in order to transfer the calibrated model parameters at Usadievsky to the whole Upper Volga catchment the approach of *Wendling* (1975) was selected for estimating the evapotranspiration.

The calculated water balance elements at Usadievsky expressed as annual average between 1966 and 1983 are: 757 mm precipitation, 300 mm runoff and 451 mm evapotranspiration. Approximately 60% of the precipitation leaves the system by evapotranspiration and 80% of the total runoff is generated by snowmelt (238 $mm \cdot y^{-1}$).

Table 5.5 and figure 5.7 summarize the results of the multiple response verification. The analysis is based on monthly values of discharge R, evapotranspiration ET, soil moisture change ΔSM and on 238 observations of the snow water equivalent SWE. The correlation coefficient R_{OS} between simulations and observations is above 0.8 for the four considered hydrometeorological variables for the entire 18-year period and both the periods of calibration and evaluation. PREVAH is able to capture the hydrological dynamics of the different components of the water cycle in Usadievsky catchment. The computed averages are in the exception of soil moisture in good agreement with the observation. The average soil moisture change since 1966 is underestimated by about 10 mm. Such differences are mainly owed to the systematic underestimation of ΔSM in winter, where the processes of soil water freezing and thawing play an important role in the hydrological regime at these latitudes (Gusev and Nasonova 2002). PREVAH do include a module for the consideration of such processes. In the summer, the simulation of ΣΔSM shows better agreement to the observed values.

Table 5.5 Multiple response verification of PREVAH with records from the hillslope catchment Usadievsky. The calibration and evaluation periods are declared in table 3.4. R is the monthly runoff, SWE the snow water equivalent, ET the evapotranspiration and ΣΔSM the change of soil moisture in the catchment with respect to the value in January 1966. The statistical indices R_{OS}, E_2, *MAD* and *RMSE* are defined in section 2.3.3.

		Unit	R	SWE	ET	ΣΔSM
Records	entire	-	211	238	96	211
R_{OS}	entire	-	0.937	0.879	0.885	0.844
R_{OS}	calibration	-	0.927	0.858	0.900	0.857
R_{OS}	evaluation	-	0.948	0.916	0.856	0.830
Average	observation	$mm \cdot month^{-1}$	26.7	82.3	38.1	-15.7
Average	simulation	$mm \cdot month^{-1}$	25.6	88.6	36.7	-31.6
E_2	entire	-	0.875	0.624	0.777	0.530
RMSE	entire	$mm \cdot month^{-1}$	15.2	30.0	16.7	25.8
MAD	entire	$mm \cdot month^{-1}$	9.3	22.3	10.8	20.4

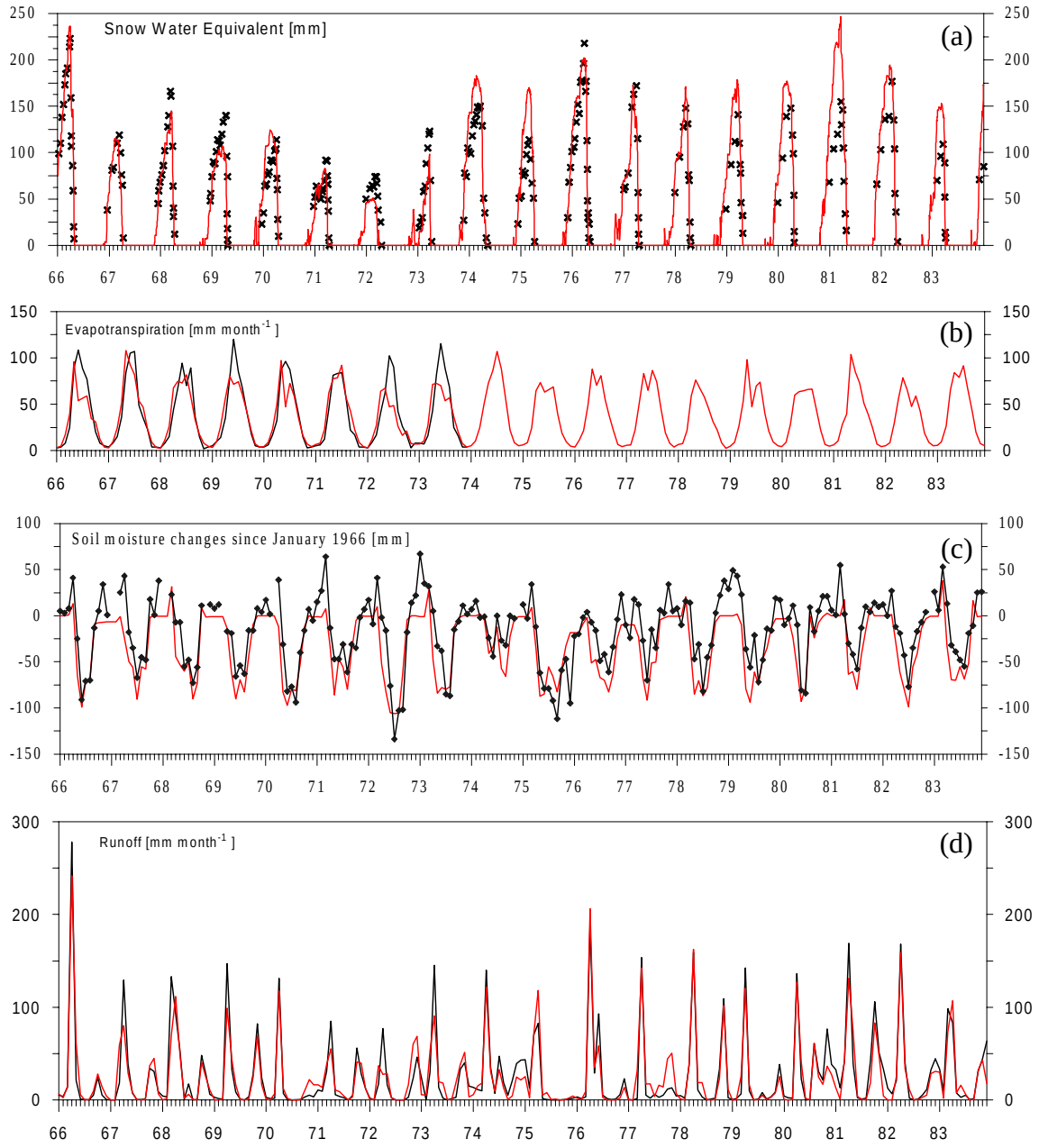

Figure 5.7 Comparison between four observed hydrometeorological values (black lines) and the simulations with PREVAH at the hillslope catchment Usadievsky (red lines) within the period 1966 to 1983: a) snow water equivalent. b) evapotranspiration. c) soil moisture changes (ΣΔSM) since January 1966. d) monthly runoff.

In figure 5.7, the observed monthly observations are plotted against the simulated values. Figures 5.7a to 5.7d confirm that the hydrological model is able to simulate the temporal pattern of all four available hydrometeorological observations with good agreement. Figure 5.7a visualizes the observed and simulated snow water equivalent time series. Snowmelt was computed here with the PDDI approach (Eq. 3). The timing of both the snow accumulation and snowmelt period are captured with fair accuracy. However, both *RMSE* and *MAD* (table 5.5) indicate that the total snow amounts are not always of the correct magnitude order. There are several years before 1974 where PREVAH underestimates the snow water equivalent. After 1974, the model overestimates the snow amounts more frequently. Figure 5.7b shows that the evaporation observations are only

conditionally in good agreement with the simulation. Despite the high correlation R_{OS} and Nash and Sutcliffe score E_2, the observations are not well fitted by the model. The slight overestimation in spring is probably owed to excessive radiation forcing and the neglecting of soil freezing. The overestimated drying of the soil in spring causes reduced water availability in summer and therefore an underestimation of evapotranspiration in June and July. Figure 5.7c shows a comparison between the observed and simulated soil moisture content as a difference from the value at initialization of the simulation in January 1966. Simulated values are diagnosed at the end of each month, as described in figure 2.4. Observed values were monitored "near the end of each month" (Schlosser *et al.* 1997). The qualitative correspondence between records and simulated values is reasonably satisfying, as confirmed by the statistical evaluation (table 5.5). The model in many cases, underestimates the absolute value, mainly in the winter phase when the soil's freezing and thawing processes have a dominant role. The model tends to dry too early at the beginning of the vegetation period. At that time in the year the soil is probably still partly frozen and limits evaporation. Finally, figure 5.7d shows the comparison between observed and simulated monthly runoff rates. The statistical analysis justifies the consideration that the qualitative and quantitative agreement is high.

The agreement between the daily observation and simulation of the discharge rates is less trustworthy (table 5.6). In the calibration period, both E_2 and E_2^{log} are above 0.5, which is a generally accepted minimum target that indicates an effective simulation. In the calibration period, the simulated total runoff overestimates the observation by 9 mm per year. The analysis of the evaluation period is twofold. E_2 increases and is well above 0.6, while the E_2^{log} agreement sinks below 0.4. The simulated runoff in the evaluation period is more than 20 mm per year lower than the observations. The efficiency score of the simulation of the whole period 1966-1983 reflects this opposite behaviour between the calibration and evaluation periods.

Figure 5.8 shows examples of runoff hydrograph simulations at Usadievsky for two four-year periods, the first 1967-1970 in the calibration period, the second 1977-1980 in the evaluation period. The statistical analysis of both periods is included in table 5.6. The model quality is, in some cases, good and poor in others. The model is always able to reproduce the timing of the main melt season. Less satisfying is the reproduction of runoff-generation in late summer and autumn and, in general, all peak-flows are underestimated.

Table 5.6 Verification of the daily discharge simulations in the hillslope catchment Usadievsky. S-O is the difference between the computed *S* and observed *O* discharge.

Period	E_2 [-]	E_2^{log} [-]	*S* [mm· y^{-1}]	*O* [mm· y^{-1}]	*S-O* [mm· y^{-1}]
1966-1983	0.61	0.45	300	308	-8.4
1966-1973	0.54	0.51	277	268	9.1
1974-1983	0.66	0.37	317	340	-22.5
1967-1970	0.59	0.51	260	267	-7.0
1977-1980	0.68	0.38	316	326	-10.3
Winter	0.62	0.19	220	232	-12.4
Summer	0.40	0.45	80	76	4.0

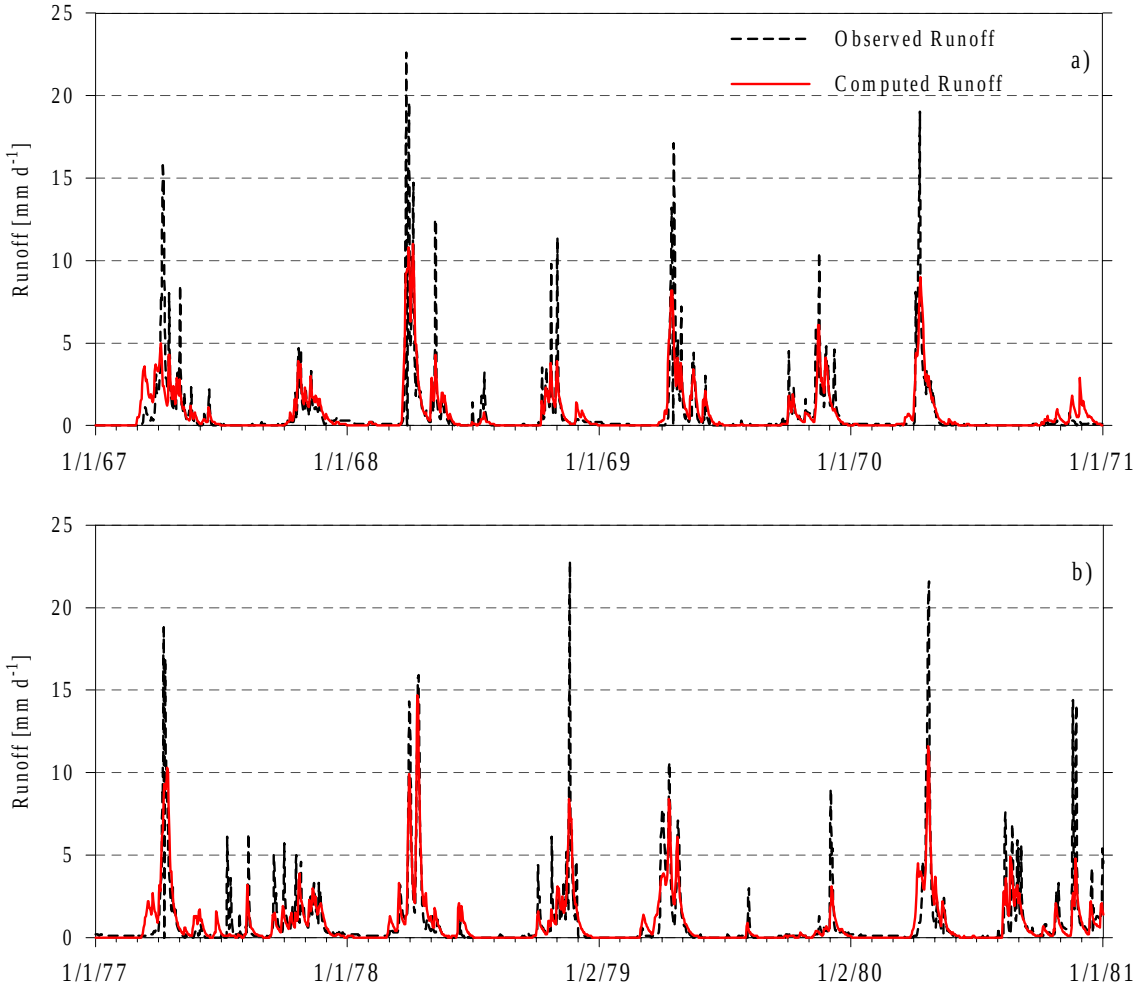

Figure 5.8 Daily observed (black line) and simulated (red line) hydrograph at the hillslope catchment Usadievsky in: a) four years of the calibration period. b) four years of the evaluation period.

The separate analysis of the model quality in summer and winter shows a further opposite behaviour. The peak-flows are better captured between November and April than between May and October. The simulation of low-flows is mostly efficient in the summer half year.

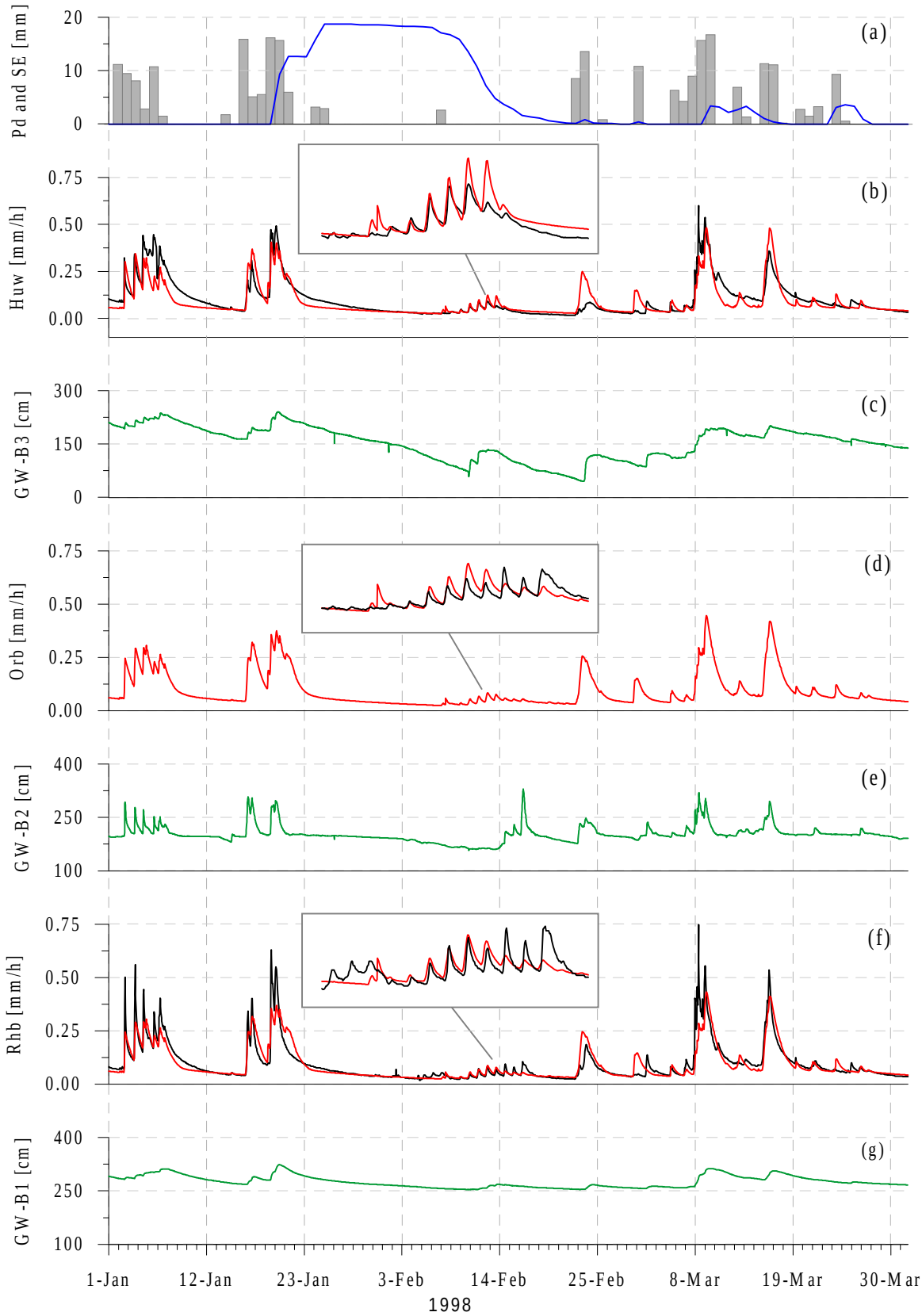

Figure 5.9 Rietholzbach - 1 January to 31 March 1998 with PREVAH: a) Bars: Interpolated daily precipitation (P); Blue line: simulated snow water equivalent (SE). b) Huwilerbach: Black: measurement; Red: simulation. c) Groundwater table height, borehole B3. d) as b) for Upper Rietholzbach. e) Groundwater table height, borehole B2. f) as b) for Rietholzbach. g) Groundwater table height, borehole B1. The 'zoomed' snowmelt event on e), d), and f) refers on the period between 5 February and 18 February.

5.2.2 Simulations results in the pre-alpine catchment Rietholzbach♦

Simulation of winter processes

Field measurements and simulations by PREVAH for Rietholzbach and its subcatchments (table 3.3 and fig. 5.9) between January and March 1998 provided valuable information concerning the improvement of modelling the runoff-generation processes in the winter season. Figures 5 and 5.10 illustrate the influence of topography on the snowmelt processes. PREVAH starts to simulate snow accumulation during the precipitation event of 19 January. By 25 January an average of about 19 mm snow water equivalent (SE) is accumulated within the catchment (fig. 5.9a and fig. 5.10).

Snowmelt begins after the small rainfall on 6 February. The event starts in the 84% south-exposed subcatchment Huwilerbach (Plot b and relative 'zoom') with a stronger reaction and finishes at least three days earlier than in the whole (42% south-exposed) Rietholzbach catchment (Plot f in fig. 5 and 'zoom'). PREVAH is able to reproduce this behavior fairly well, especially the earlier melt of the snowpack within the Huwilerbach subcatchment (see Plots b, d and f on fig. 5.9 and fig. 5.10). Such detailed snowmelt simulation is only possible if a radiation-based approach is used together with a temperature-based approach to determine the hourly snowmelt rate and the daily fluctuation respectively. A similar approach is proposed by Hock (1999) for snowmelt on glacerized surfaces.

Figure 5.10 illustrates the changes of the spatial snow water equivalent distribution during the snowmelt event under consideration. Between two phases of approximately homogeneous snow-cover distribution it can be observed that the hydrological model is able to consider topography and aspect for the processes linked to the snowmelt generation. After the snowfall events between 20 January and 5 February (fig. 5.9a) the catchment is homogeneously covered by snow with water equivalents increasing from 12 to 27 mm as a function of the increasing elevation. In the following days the model simulates higher snowmelt rates within the south-exposed part of the catchment. The Huwilerbach (H) sub-basin is practically snow-free on 11 February, while the north-exposed slopes in the upper part of the catchment (UR) still have up to 20 mm snow water equivalent. This behavior is confirmed by the runoff and groundwater level measurements illustrated in figure 5.9. Three boreholes for groundwater table monitoring (fig. 5.10) are used to show the groundwater reaction to percolation processes and to lateral drainage in winter. Borehole B1 is situated in the riparian glacial moraines with reduced hydraulic conductivity and shows a mean residence time of 28 months (Vitvar 1998). The other two boreholes are located in the Tertiary deposits of the Freshwater Molasse, one (B2) in a north- and the other (B3) in a south-exposed hillslope. For those boreholes, much shorter residence times of 9 and 12 months respectively have been estimated. A delayed reaction of the groundwater levels can be seen during the main melt period in mid February. The rise of groundwater level at the south-exposed B3 begins two days earlier than at B1 and 4 days earlier than at B2 (figs. 5.9c, 5.9e and 5.9g). The stronger reaction of B3 and, especially, of B2 indicates an important influence of interflow (figs. 5.9a and 5.9e) linked to both snowmelt and precipitation. The B1 reaction indicates the riparian groundwater mixing (figs. 5.9a and 5.9g).

♦ Sections 5.2.2 and 5.3.1 are reprinted from the paper "A comparative study in modelling runoff and its components in two mountainous catchments" by J. Gurtz *et al.* The paper is published in *Hydrological Processes,* **17**, pp. 297-311 as a part of a special issue on "*Runoff generation and implications for river basin modelling*".

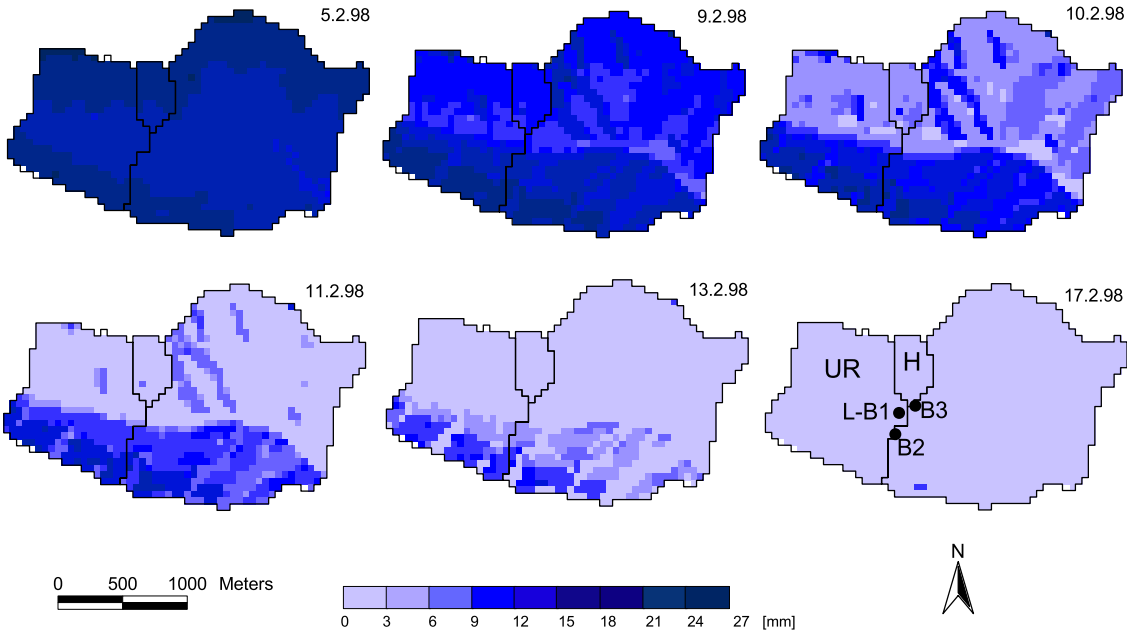

Figure 5.10 Rietholzbach - February 1998: spatial distribution of snow water equivalent at the end of six selected days. On the lowest right map 'H' indicates the Huwilerbach basin, 'UR' the Upper Rietholzbach basin. L-B1, B2 and B3 indicate the location of the lysimeter L- and of the three groundwater boreholes B1, B2 and B3.

It can be concluded that the spatially distributed application of the snow model within PREVAH is a valid approach to determine the spatial and temporal distribution of melt-water-induced runoff-generation within mountainous catchments with complex topography.

Simulation of the water balance

The mean annual water balance elements recorded by the grass-covered lysimeter are 1576 mm precipitation, 529 mm evapotranspiration and 1049 mm percolation outflow (table 5.7) for the period 1981-1998. The averaged monthly values are presented in figure 5.11. The calculated evapotranspiration for the lysimeter site is 20 mm higher, whereas the observed outflow is lower than the runoff calculated by PREVAH. This evapotranspiration bias is partly owed to the defined assumptions in the method for determining the lysimeter water balance. During rainy hours (> 0.1 mm precipitation) lysimeter evapotranspiration is neglected. This can lead to an evapotranspiration loss, mainly in warm wet months (fig. 5.11). Similar simulations for the whole catchment, as obtained using PREVAH and WaSiM-ETH, produce between 580 and 590 mm average annual evapotranspiration and about 1010 mm average annual runoff, compared with the 1013 mm average annual observed runoff (table 5.7). The higher catchment evapotranspiration is caused by the relatively high portion of south-exposed slope areas and by the presence of forest areas with high transpiration rates in the catchment (table 3.3).

About 50% of the computed runoff is generated with both models by interflow. The analysis of the runoff components during flood events using environmental tracers showed similar results (Vitvar 1998). Compared with PREVAH, WaSiM-ETH generates a clearly higher surface runoff portion and a lower baseflow portion.

Table 5.7 Measured and modelled mean annual water balance (P = precipitation, ET = evapotranspiration, R_{sim} = simulated runoff, R_{obs} = observed runoff), including simulated runoff components (RS = surface runoff, RI= interflow, RG= baseflow), storage change (DS) and obtained averaged efficiency score for the simulation of hourly discharges.

Method	Location	P	ET	R_{sim}	R_{obs}	RS	RI	RG	DS	E_2	E_2^{log}
Measured	Lysimeter	1576	529	-	1049	--	--	--	--	--	--
PREVAH	Lysimeter	1570	549	1020	1049	--	--	--	--	0.610	--
PREVAH	Rietholzbach	1593	583	1010	1013	73	561	376	0	0.713	0.890
WaSiM	Rietholzbach	1596	587	1011	1013	385	494	132	-2	0.796	0.825
PREVAH	Dischmabach	1446	234	1250	1260	141	707	402	-38	0.871	0.934
WaSiM	Dischmabach	1384	211	1243	1260	204	750	289	-70	0.877	0.885

A better linear criterion of efficiency E_2 is obtained by the WaSiM-ETH simulations, whereas PREVAH simulations allow a better logarithmic criterion of efficiency E_2^{log}. This implies that the land surface runoff is underestimated by PREVAH and slightly overestimated by WaSiM-ETH, whereas the baseflow is simulated more realistically by PREVAH. The reasons for these differences are related to the different runoff-generation approaches (See fig. 2.5).

In spite of these different approaches and of the different simulated contributions of each runoff component, both the applied models are able to reproduce the seasonal cycle of the observed runoff at the gauging station and of the measured evapotranspiration at the lysimeter site (fig. 1.1). The snow accumulation and snowmelt dominate the runoff from December until April (fig. 5.11), while the evapotranspiration strongly influences the runoff-generation processes from April until September. Apart from some heavy precipitation events in summer, the seasonal distribution of precipitation and evaporation causes groundwater recharge mainly, in autumn, early winter and during the period with maximal precipitation in June.

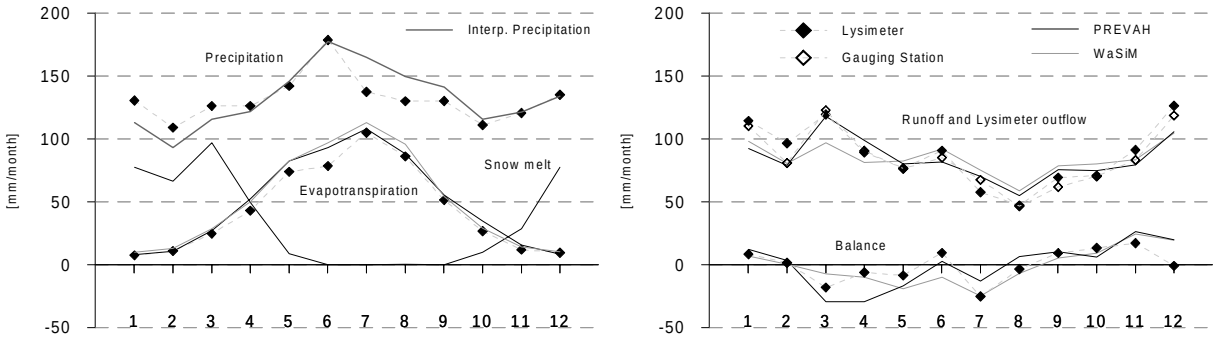

Figure 5.11 Rietholzbach - monthly average of the main water balance components for the period 1981-1998: the dotted grey line with filled squares indicates the lysimeter measurement; the continuous black line indicates the simulation results with PREVAH; the continuous grey line indicates the simulation results with WaSiM-ETH; the dotted grey line with void squares indicates the runoff measurement at the outlet station.

5.3. Applications at catchment scale

5.3.1 Simulation results in the high-alpine Dischmabach catchment

Simulation of the water balance

The application of PREVAH for the period 1981-1996 leads to the following mean annual water balance elements in the Dischmabach catchment: 1440 mm precipitation, 230 mm evapotranspiration and 1250 mm runoff. The simulated runoff is close to the measured 1260 mm (table 5.7). Owing to the different parameterization of the vegetation and soil characteristics and to the different handling of the incoming meteorological variables, WaSiM-ETH shows slightly smaller values for precipitation and evaporation than PREVAH. The average catchment snow portion in precipitation is about 70%.

The simulated mean seasonal distribution of water balance elements and runoff components is presented in fig. 5.12. A strong temperature dependency of the runoff regime is obvious. The temporal distribution of runoff is strongly influenced by snow accumulation and snowmelt, while the seasonal precipitation pattern has two maxims. The high precipitation amounts during summer are superimposed over the main melt period (SNOW on fig. 5.12a) and the combined effects therefore cause a single large runoff maximum in June and July (fig. 5.12a).

The model intercomparison outlines differences in the achieved values of the logarithmic efficiency criterion E_2^{log}. The smaller values for WaSiM-ETH indicate a lower accuracy for baseflow simulation (figs 5.12a and c). Figures 5.12b-d show the differences in the simulated runoff components caused by the differently structured soil and runoff-generation modules (fig. 2.5). WaSiM-ETH produces a higher portion of surface runoff RS and interflow RI.

This allows a better reproduction of the hourly runoff fluctuations, as confirmed by the obtained linear efficiency criterion E_2 (table 5.7). The lower interflow RI and baseflow RG contribution of WaSiM-ETH between May and July when compared to PREVAH is partly compensated by higher surface runoff amounts.

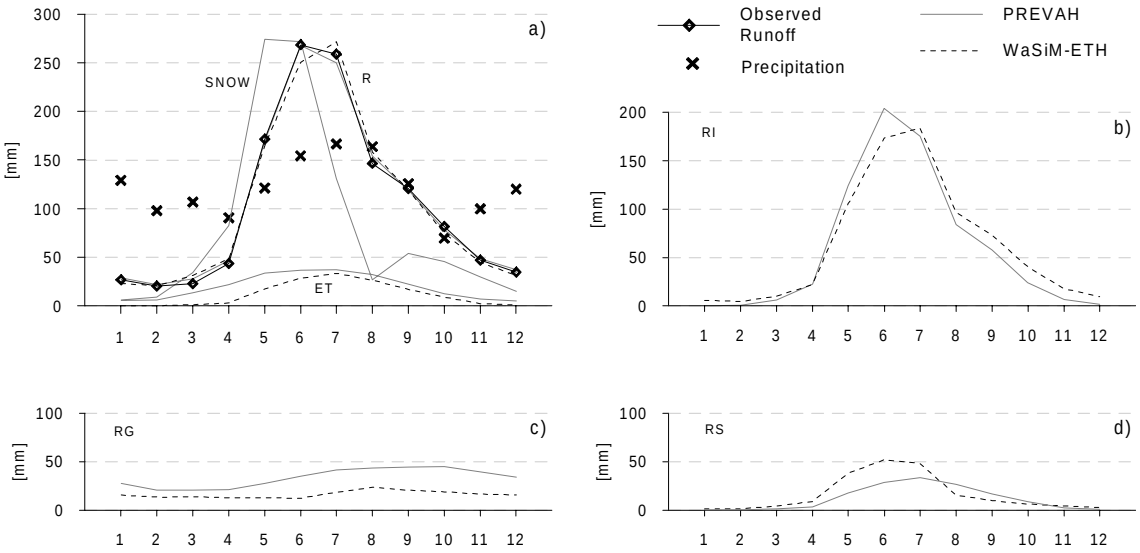

Figure 5.12 Dischmabach - monthly average of the main water balance and runoff components for the period 1981-1996: a) observed and simulated runoff (R), Evapotranspiration (ET), Precipitation (P) and Snowmelt (SNOW). b) Interflow (RI), as simulated by WaSiM-ETH and PREVAH. c) Baseflow (RG). d) Surface runoff (RS).

The higher interflow generation of WaSiM-ETH in autumn is mainly compensated by much lower baseflow amounts and by slightly lower surface runoff-generation. This proves that in the WaSiM-ETH the quick baseflow component is assigned to the interflow as lateral outflow from deep soil layers above the groundwater level (fig. 5.12b). Only the slow component is classified as baseflow RG from the groundwater storage (fig. 5.12c).

5.3.2 Evaluation of four routines for snowmelt modelling♦

PREVAH was operated for water balance simulations in the Dischmabach catchment alternating the four snowmelt modules presented in Section 2.2.

The model calibration was performed manually. The basis calibration of the runoff-generation module (using the PDDI snowmelt module) included the period 1993-1995 (Gurtz *et al.* 2003a). The calibration period for the detailed snowmelt simulation was 1982-1985. The procedure of the model calibration was presented in Section 2.3. The year 1981 was adopted as initialization period and was therefore excluded in the evaluation phase because of the uncertainty of the initial values for the snow water equivalent and for the water storages within the catchment at the initialization of the simulation. The calibration effort differed, depending on the method chosen for the snowmelt computation.

Table 5.8 Data requirement and calibrated parameters of the snowmelt and runoff modules.

	Unit	PDDI	COMB	EMA	ESCIMO
SNOWMELT MODULE					
Required Input		T_a, P	T_a, P, e_a, u	T_a, P	T_a, P e_a, u, G, SSD
T_{GR}	[°C]	0.0	0.0	0.0	0.0
T_{TRANS}	[K]	0.5	0.5	0.5	
T_0	[°C]	-0.5	-0.5	-0.5	
$TMF_{PD\text{-}MIN}$	[m s^{-1} K^{-1}]	2.8· 10^{-8}	2.2· 10^{-8}		
$TMF_{PD\text{-}MAX}$	[m s^{-1} K^{-1}]	5.8· 10^{-8}	5.8· 10^{-8}		
c_1	[m s^{-1} K^{-1}]		2.2· 10^{-8}		
c_2	[K^{-1}]		1.1· 10^{-8}		
TMF_{EMA}	[m s^{-1} K^{-1}]			9.3· 10^{-9}	
RMF_{EMA}	[m^3 s^{-1} W^{-1} K^{-1}]			7.5· 10^{-11}	
ALB_{MAX}	[-]				0.90
A_{POS}	[h^{-1}]				0.07
A_{NEG}	[h^{-1}]				0.02
RUNOFF MODULE					
K_0	[h]	8	8	16	16
K_1	[h]	370	370	300	300
K_2	[h]	3200	3200	3200	3200
PERC	[mm· h^{-1}]	0.09	0.09	0.09	0.09

♦ The results related to the Dischmabach catchment presented in sections 5.3.2 and 5.3.3 are reprinted from the paper "Seasonal water balance of an alpine catchment as evaluated by different methods for spatially distributed snow melt modelling" by M. Zappa *et al.* The paper is published in *Nordic Hydrology*, Volume 34(3).

Table 5.9 Simulation performances between observed (O) and simulated (S) hourly discharge. Left columns: Calibration period (1982-1985 and 1993-1995). Right columns: evaluation period (1986-1992 and 1996-2000).

	Calibration Period			Evaluation Period		
	E_2	S [mm·y^{-1}]	$S - O$ [mm·y^{-1}]	E_2	S [mm·y^{-1}]	$S - O$ [mm·y^{-1}]
PDDI	0.867	1328	33	0.880	1205	-12
COMB	0.864	1330	35	0.865	1208	-9
EMA	0.882	1327	32	0.896	1203	-14
ESCIMO	0.862	1330	35	0.840	1193	-24

A sensitivity test of the parameters controlling the separation between rain and snow was also part of the calibration phase (Pos 2001). Table 5.8 gives an overview of the calibration of the free parameters within the snowmelt modules. The difference in the calibrated runoff parameters is rather limited (COMB and PDDI have slightly different storage coefficients for the generation of surface runoff and interflow when compared to EMA and ESCIMO). It is therefore expected that the differences in quality found in the four runs be caused in the first instance by the quality of the respective snowmelt modules.

Statistical performance of the snowmelt approaches

Table 5.9 shows the mean annual simulation results of all four snowmelt approaches. The left hand part only considers the period of the calibration of the snow modules (1982-1985) and of the runoff-generation module (1993-1995). The right hand part summarizes the statistical performance in the validation periods (1986-1992 and 1996-2000). Additionally, the mean annual differences between the simulated (S) and the observed (O) discharges are indicated for both periods.

Only ESCIMO shows a slightly worse simulation in the validation period than in the calibration period. To some extent this difference is caused by an outlying point (the year 1992) in the validation period (figure 5.13). The PDDI and the COMB approaches show almost identical efficiencies during the calibration period, however, the more simple PDDI shows slightly better results in the validation period. The EMA performs well in general with an E_2 of 0.891 over the whole period. The sum of the differences between simulated and observed discharge rates is 0.3%. Table 5.9 exemplifies that the difference between simulation and observation is positive in the calibration period and negative in the validation period. This is also shown in the other three snowmelt modules. The cause of this behavior is not completely understood. A minor correspondence was found between this change of sign in the differences and the mass balance of the Silvretta glacier (Dyurgerov 2002), which is located some 15 kilometres north-east from the Dischma valley. The average mass balance of the Silvretta glacier is -95 mm· y^{-1} in the years where PREVAH was calibrated and -420 mm· y^{-1} in the validation years. Thus, years with limited negative, or positive, mass balance at Silvretta glacier are found more often in the calibration than in the evaluation period. The model might therefore slightly overestimate the runoff rates in years with moderate ice melt and underestimate the runoff rates in years with high ablation rates.

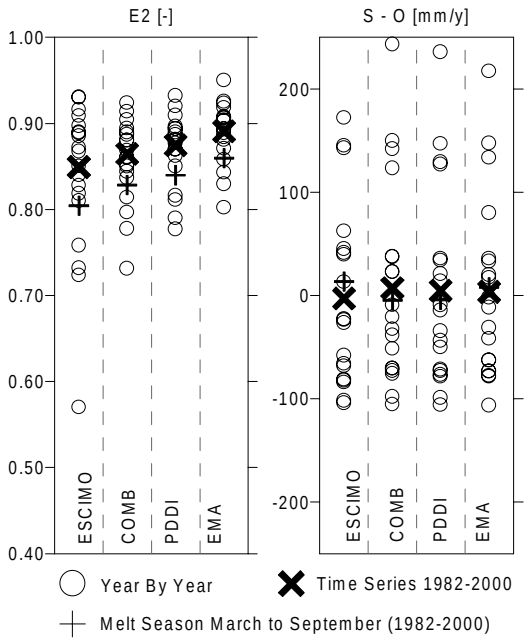

Figure 5.13 Variability of the simulation performances. Left: Statistical efficiency. Right: Bias between observed (O) and simulated discharges (S).

The analysis of the year-by-year variability of the model efficiency (fig. 5.13) brings further indications. The ESCIMO simulation is characterized by a very large difference of efficiency from year to year with E_2 ranging between 0.57 and 0.93 and a standard deviation of 0.09. The other three methods show a reduced range between the years with the highest and the lowest E_2 with standard deviations below 0.05. Evident differences for E_2 are shown in the evaluation of the annual time series and those of the period of March to September. E_2 during the melt season shows higher values in the case of EMA (0.86) and lower values in the case of ESCIMO (0.8).

The average difference between observations and simulations (1982-2000) is smaller than 1.0% for any of the four simulations, which is even lower than the measurement error, which is expected to be about 5%. The deviation in the single years can be up to ±10%. ESCIMO shows the smallest standard deviation (87 mm) of the year-by-year deviation from the observations and a better long-term balance between observed and simulated runoff. The COMB and the PDDI runs have the largest range between years with negative and positive difference between observed and simulated discharge (standard deviation above 95 mm, figure 5.13, right). Figure 5.13 shows that the balance during the snowmelt season is less accurate in the case of ESCIMO, which is a relevant negative aspect of the overall performance of the model. This result indicates the importance of the statistical analysis of the results, not only for the whole period but also for the sub-periods that are more relevant for the processes under investigation.

Discharge simulations

Figure 5.14 allows some general considerations of the catchment discharge regime. The runoff-generation is strongly governed by the processes of snow accumulation and snowmelt. Rainfall shows to have some influence on the discharge regime only between June and October. The mean role of sublimation / evapotranspiration is limited.

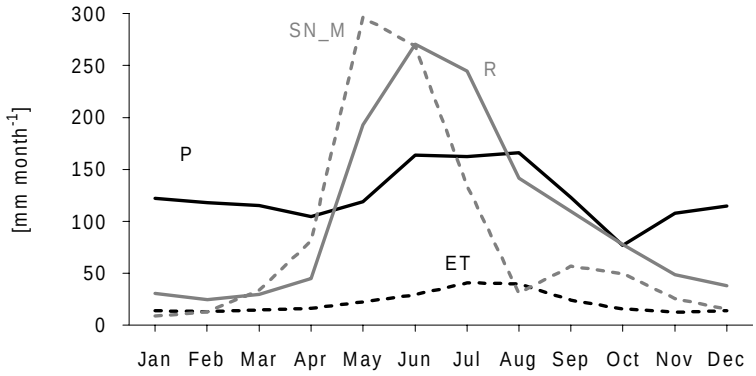

Figure 5.14 Average seasonal course (1982-2000) of the main water balance elements simulated with PREVAH and the EMA snowmelt module. P is the interpolated precipitation, R the discharge, ET the sublimation / evapotranspiration and SN_M the snowmelt.

The snowmelt amounts indicate that 60 to 70% of the catchment precipitation occurs as snowfall underlining the importance of the snow model quality for the hydrological simulation in the Dischmabach.

Table 5.10 indicates that the simulated water balance elements of each of the four PREVAH runs show only limited differences. The different precipitation correction adopted for rain and snow (Sevruk 1986) combined with the different portions of snow and rain computed with Eq. (2) causes the difference between the average precipitation for all model runs using the temperature-index based methods (1493 $mm \cdot y^{-1}$) and the ESCIMO model run (1464 $mm \cdot y^{-1}$) This happens because ESCIMO doesn't consider a temperature range to separate rain and snow (table 5.8).

Figure 5.15 shows the quality of the simulated discharge regime. All snowmelt methods allow a good reconstruction of the average monthly discharge. The average standard deviation of the monthly runoff rates (given in mm per hour) is also well reproduced. This indicates that the models simulate the discharge variability correctly. However, all the methods used show a too large average standard deviation between January and March, which is an indication for isolated small snowmelt events in late winter and in early spring, which are not confirmed by the observations. This behavior is caused by the strict parameterization of the model, which is constant for the whole catchment throughout the year. A higher threshold temperature T_{GR} at lower elevation zones when compared to higher parts of the catchment would probably eliminate this discrepancy between simulation and observation. In addition, ESCIMO tends to have problems simulating the discharge variability in May, at the onset of the main melt season.

Table 5.10 Simulated water balance (WB) over the period 1982-2000. P is the interpolated precipitation, R the discharge, ET the sublimation / evapotranspiration and SN_M the snowmelt. WB is equal to P minus R minus ET. All units are $mm \cdot y^{-1}$.

Model	P	SN_M	ET	R	WB
PDDI	1493	1010	258	1251	-16
COMB	1493	1014	256	1253	-17
EMA	1493	1031	254	1249	-11
ESCIMO	1464	977	246	1243	-25

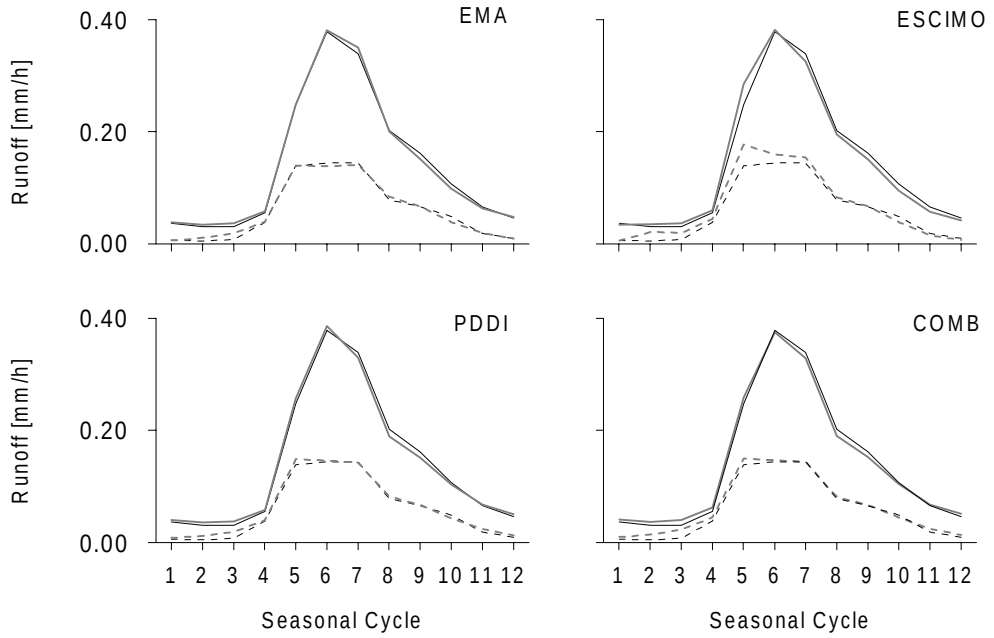

Figure 5.15 Observed (black) and simulated (grey) average monthly discharge (full line, in $mm \cdot h^{-1}$) and the respective average standard deviation (dashed, in $mm \cdot h^{-1}$) from January to December.

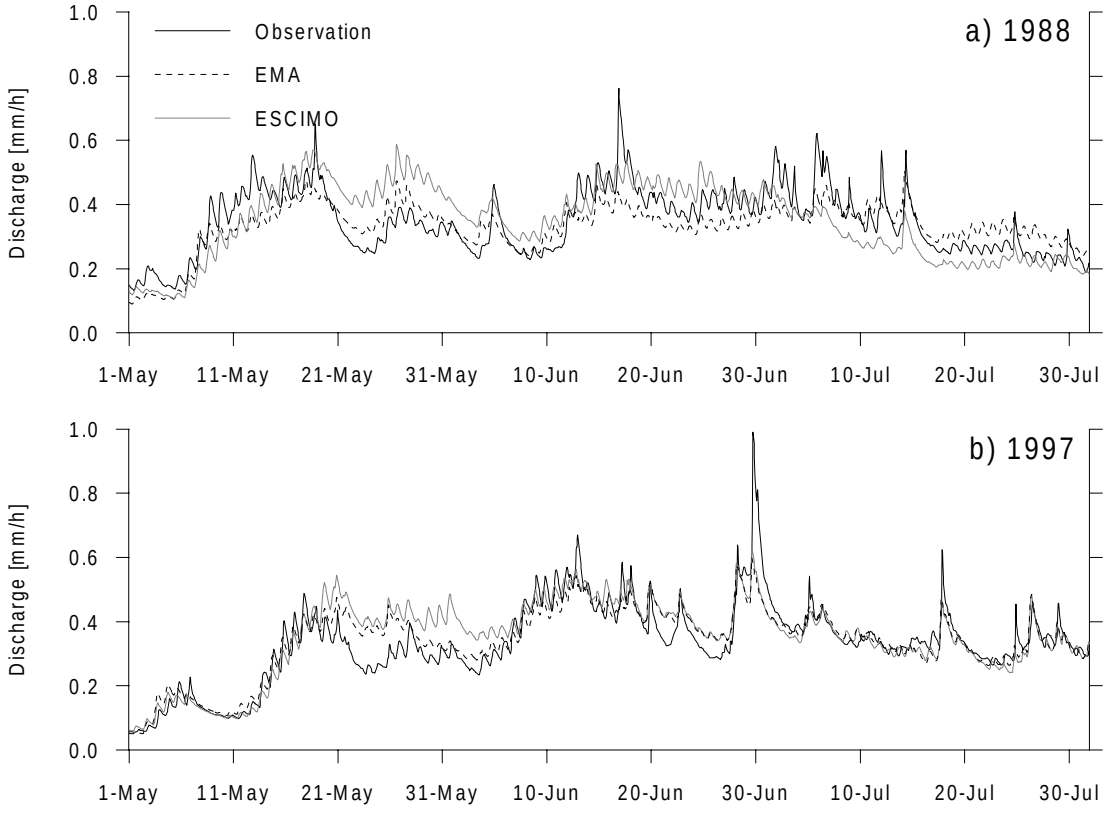

Figure 5.16 Hourly runoff hydrograph of Dischmabach between May and July in 1988 (a) and 1997 (b).

The efficiency analysis, the comparisons of the discharge regimes and of the simulated water balance elements indicate that all snow models considered are suitable for snowmelt computation in this alpine catchment. The EMA has a limited requirement for meteorological data, but is able to determine the strong daily cyclicity of the snowmelt. The simple energy balance parameterization of COMB increases its requirements for data and its need for parameter calibration when compared to PDDI and EMA. However, the results show that in the case of the Dischmabach catchment this complexity does not bring any improvement in the discharge simulation. ESCIMO requires a large amount of meteorological data and is based on a strict parameterization of the energy balance. This reduces to need for calibration, but in all ESCIMO yields the poorest statistical performance.

Figure 5.16 presents the hourly runoff hydrograph between May and July in 1988 and 1997. The graph shows how the runoff regime is characterized by daily fluctuations that are reproduced reasonably well by the ESCIMO and EMA simulation. The amplitude of the fluctuations is larger in May, when most of the runoff is generated between 2100-2500 m a.s.l., than in July, when the highest snowmelt rates occur above 2600 m a.s.l. (figs. 5.18 to 5.21). Both models capture this behavior, which is probably caused by the gradual reduction of water supply by snowmelt owed also to a smaller extension of snow-covered areas later in the melt season.

ESCIMO shows the tendency to accelerate the course of the snowmelt season (fig. 15). As also previously observed ESCIMO generates too much runoff between 20 May and 10 June both in 1988 (E_2 May-July = 0.31) and 1997 (E_2 = 0.69) and, especially in 1988, tends to underestimate the runoff later in the melting season.

The EMA shows a better performance than ESCIMO in both 1988 (E_2 May-July = 0.58) and 1997 (E_2 = 0.80). The largest bias is also in the case of EMA related to the period of snowmelt onset in the elevations between 2100 and 2500 m a.s.l.

Simulation of the snow water equivalent

The Institute for Snow and Avalanche Research (SLF) in Davos measures the snow water equivalent (SWE) at four sites (fig. 3.4) in the neighbourhood of the Dischmabach catchment the 1st and 15th day of each month between November and July. None of these sites is located within the catchment. Therefore, the observations have been compared to the simulated snow water equivalent of an HRU with similar elevation and aspect as the station under consideration. Only the Stillbergalp station showed to be representative for the evaluation of the results in the Dischma valley. For the stations Flüelastrasse, Büschalp and Weissfluhjoch the simulated SWE is considerably lower than the observations, although the observed and simulated timing of snow accumulation and snowmelt correspond well to ESCIMO and EMA (Pos 2001). These three stations are situated in a neighbouring valley with different orientation than the Dischma valley. The different orientation causes a larger amount of precipitation on the slopes to the north-west of Davos (fig. 3.4) when compared to the Dischmabach catchment.

Only the Stillbergalp site was therefore suitable for a quantitative comparison with simulated SWE. The simulated SWE (fig. 5.17) for deadlines in consecutive 15-day intervals fits well for the Stillbergalp site, which is located less than one kilometre away from the HRU used for the model evaluation. The average timing of the seasonal course of snow accumulation and melt is fairly good. The SWE simulations with ESCIMO and with the EMA are similar. However, ESCIMO (correlation R_{OS} = 0.82) fits slightly better in the observed values than EMA (R_{OS}= 0.79). The two melt models have a similar efficiency during three winters with different snow conditions, as well as the in the case of the 'average winter' (fig. 5.17):

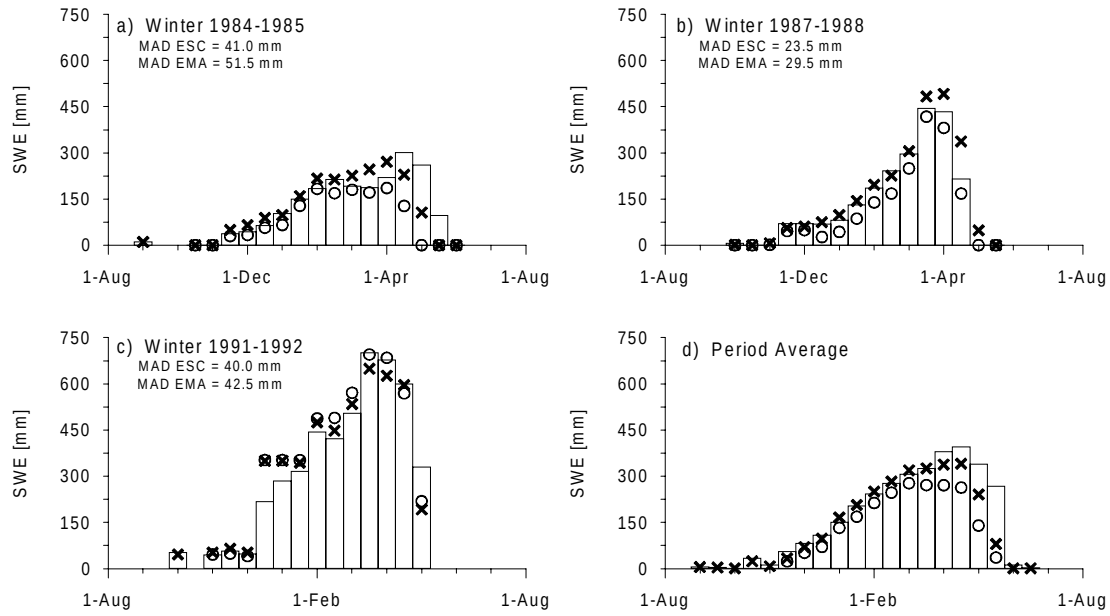

Figure 5.17 Stillbergalp (1970 m a.s.l.): Three winters and the period average (1982-2000) of the observed (bars) and the simulated (symbols) snow water equivalent (SWE) are shown. The crosses identify the ESCIMO simulation, the circles the EMA simulation. The mean absolute deviation (MAD) between simulations and observation during the three winters is also given.

- The winter of 1984-1985 has little snowfall and snow accumulation. Both ESCIMO and EMA reproduce the accumulation phase well, but they terminate the melt season too early;
- The winter of 1987-1988 was dry until mid-February, when many snowfall events followed until the end of March. EMA underestimates the observed SWE throughout this winter. ESCIMO shows a good agreement with the observations during the whole winter. In both cases the course of snow accumulation and ablation is well captured;
- The winter of 1991-1992 was characterized by a large accumulation of snow. The two snow models succeed well in the reconstruction of the features of the hydrological processes in this winter with 'extreme' snow conditions;
- The overall quality of the SWE simulation (winters 1982-2000) is better with respect to the accumulation phase than with respect to the ablation phase. Both models simulate the timing of both phases of the snowpack cycle very well. However, ESCIMO and, to a larger extent, EMA underestimate the average amount of snow stored during the winter at Stillbergalp and show too high melt rates in May.

In all the three discussed winters the SWE simulated with ESCIMO show a smaller mean absolute deviation (MAD) than SWE determined with EMA with respect to the observed values (figs. 5.17a, b and c). Considering the overall performance, ESCIMO is capable of capturing the local climatological characteristics of Stillbergalp with a higher reliability than EMA. This is owed to the fact that in ESCIMO only the snow albedo simulation is controlled by catchment-specific parameters, while in the case of EMA the local features can only be captured by the site adjusted clear-sky direct solar radiation.

Summary and conclusions

Four methods for the spatially distributed simulation of snow hydrology at catchment scale have been compared. All of them appear to be suitable to compute the runoff hydrograph of an alpine catchment with runoff regime governed by snowmelt. This is confirmed by the year-to-year analysis of the model efficiency as well as by the analysis of the water balance. The quality of the results obtained from the calibration and validation is similar.

The three temperature-index based methods showed to a great extent similar efficiencies, however, the inclusion of the potential clear-sky radiation appears to be an evident improvement in the reconstruction of the daily runoff hydrograph fluctuations without the need of additional observations with respect to the classic PDDI approach. Since the potential clear-sky radiation is subject to high spatial and temporal variations, it can be concluded that the improved efficiency is owed to the important role played by topography for the spatial and temporal distribution of snowmelt (and runoff) generation. If the interest is limited to daily or monthly discharges, then all of the temperature-index based methods are suitable. In lowland regions where such daily fluctuations of the discharge rates are smaller and rain-on-snow events more frequent it is probably less evident that EMA is superior to both PDDI and COMB.

The simulation based on ESCIMO is characterized by a very large variation in quality from year to year. This variability is better captured by the temperature-index methods. The physically based structure of ESCIMO is more sensitive to the quality of the meteorological input than the conceptual structure of temperature-index based approaches, since the latter allow the calibration of more free parameters. During the transition period, when the temperature of the snowpack is close to melting condition, considerable errors in the (ESCIMO) simulation of melt rates can occur even owed to comparably small uncertainties in the meteorological variables: mainly the phase of the precipitation, rain or snow, has a significant consequence on the energy balance. In this respect the fix threshold temperature for the distinction between rain and snow and that melting conditions occur only at isothermal state of the entire snowpack at 273.16 K can be shortcomings of ESCIMO. Nevertheless, the model structure can't account for the uncertainties of the input data.

The simulation of snow water equivalent was more successful with ESCIMO, since an energy balance based model considers better the local characteristics of the specific catchment unit (grid cell or HRU). The application of ESCIMO instead of a temperature-index based model causes a 20-30% increase in the computational time. However, this increase in computational time is not supported by an increase in quality of the hydrological simulations.

5.3.3 Altitudinal dependence of the water balance elements

Analysis in the Dischmabach catchment

Figure 5.18 shows the average monthly spatially interpolated 2 meters air temperature and precipitation at different elevation zones. Figure 5.19 shows the computed contribution of the different elevation zones to the catchment snowmelt for the months of April to July for both the energy balance based snowmelt module ESICMO and the temperature-index-based snowmelt module EMA. In April the total catchment melt originates from levels between 1600-2000 m a.s.l. where the average air temperature is above the 0° isotherm.

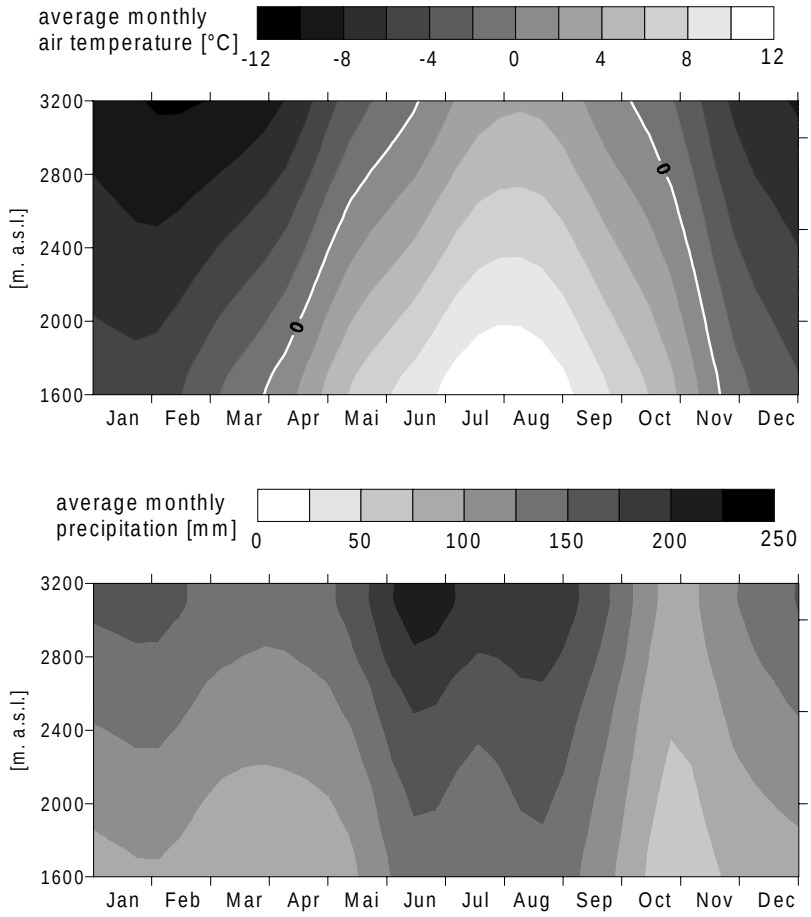

Figure 5.18 Dischmabach, 1982-2000: Monthly averages of 2 meters air temperature and precipitation at the different 100 m elevation zones.

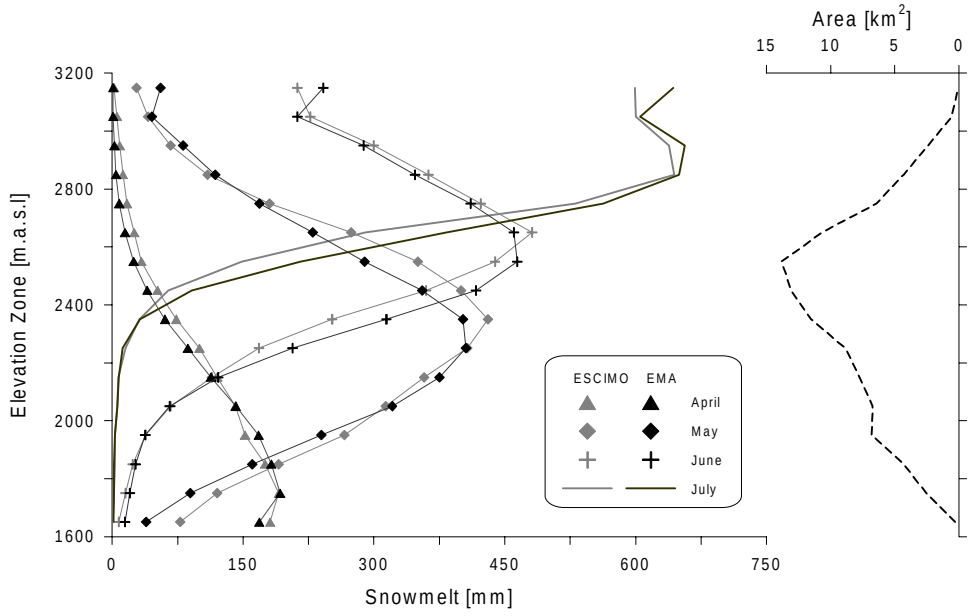

Figure 5.19 Left: Average altitudinal distribution of the simulated snowmelt (1982-2000) for the months April to July determined using ESCIMO (grey) and the extended melt approach (EMA, black). Right: Catchment area at each elevation zone.

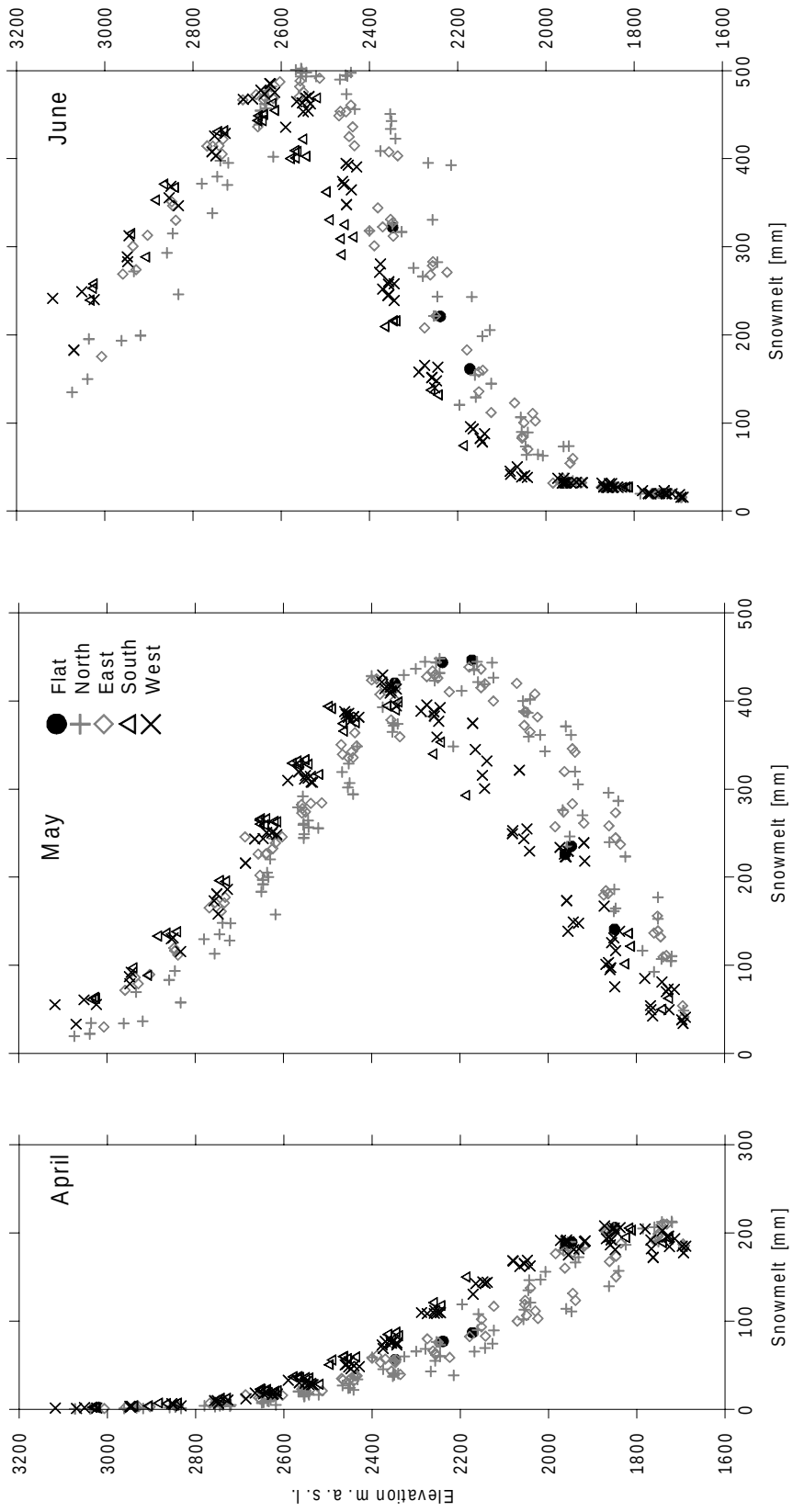

Figure 5.20 Monthly snowmelt of the HRUs with respect to elevation and exposure (symbols). HRUs representing water surfaces are not plotted, since snow accumulation is not allowed for such HRUs. The data are based on the simulation with the extended melt approach over the period 1982-2000.

In May the elevation range with maximum snowmelt shifts to 2100-2500 m a.s.l., where the largest part of the catchment is located (right hand plot in fig. 5.20). This explains the increase in runoff between the 1 and 31 of May (fig. 5.16). The runoff maximum in the

Dischmabach is caused by a superposition of the main snowmelt season in the area between 2100-2800 m a.s.l. and the period with maximum rainfall (fig. 5.18).

Figure 5.20 presents the altitudinal dependence of the snowmelt in the months of April to June as simulated with EMA (each symbol represents a HRU and its aspect). In April the south and west exposed HRUs between 1900 and 2400 m a.s.l show larger average snowmelt rates than the north and west exposed areas. In May the average snowmelt occurs between 1900 and 2400 m a.s.l., mainly in the north and east exposed HRUs. Above 2400 m a.s.l. the west and south exposed HRUs show higher snowmelt than north and east exposed HRUs. This behavior is caused by the different amounts of energy available for the melting processes with respect to elevation and aspect. This process is well understood for north and south-exposed HRUs, but is worth further discussion in the case of the east and west exposed HRUs, which theoretically get the same amount of potential radiation. The differences are a result of the temporal shift between the radiation input in the east and west-oriented slopes. East-oriented slopes already dispose of direct solar radiation early in the morning (maximum at approximately 10 a.m.), when the surface air temperature is often below melting point. West-exposed areas receive direct radiation later (maximum income at about 15 p.m.), when the air temperature is more often above melting point. These differences are hydrologically relevant when the daily air temperature cycle fluctuates around the melting point.

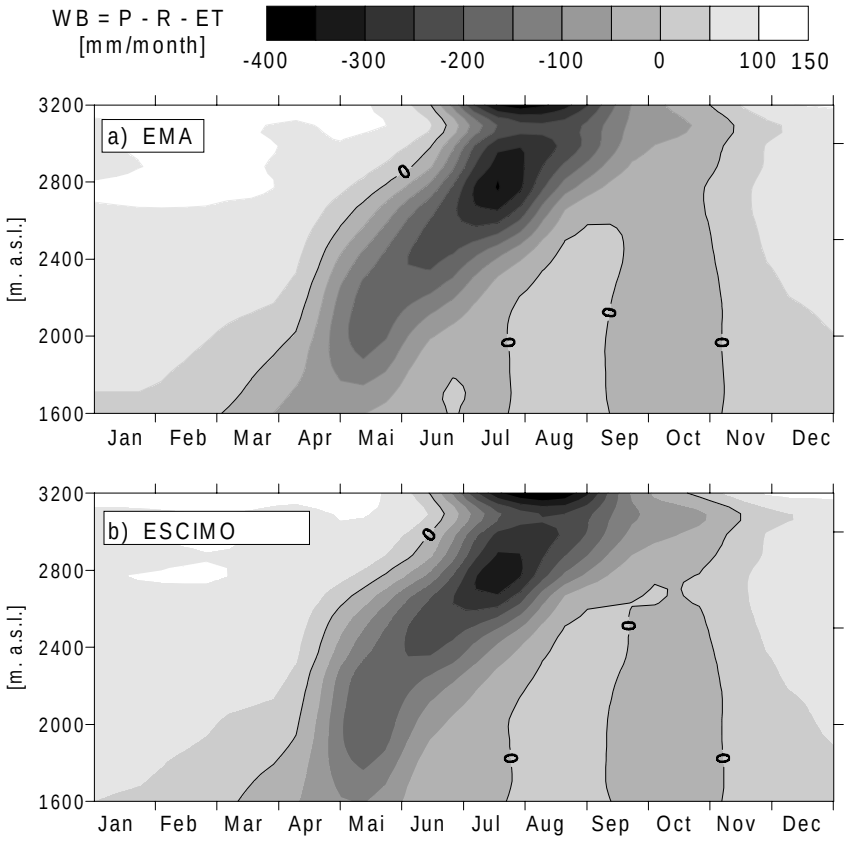

Figure 5.21 Dischmabach, seasonal water balance, 1982-2000: The water balance at each elevation zone (WB) was computed subtracting the simulated runoff (R) and the simulated evapotranspiration (ET) from the interpolated precipitation (P). (a) average simulated monthly water balance with respect to elevation determined by using the extended melt approach (EMA). (b): as a) using ESCIMO.

Figure 5.21a illustrates the altitudinal dependence of the average monthly water balance in the case of the EMA snowmelt module. The period with a positive water balance (increase of water storage) differs considerably with respect to the elevation and is governed by both the snowmelt season, the annual course of precipitation and surface air temperature (fig. 5.18). At 1700 m a.s.l, the water balance is negative (release of water) in March, while above 3000 m a.s.l. this happens after May. This demonstrates the temporal shift of the snowmelt season onset with respect to the elevation. The large negative balance at 2800 m a.s.l. in July and August is owed to the presence of bare ice areas in the ablation zone of the glacier which generate a considerable amount of glacial melt. Figure 5.21b demonstrates that the difference between ESCIMO and EMA in the computed monthly water balance is limited. ESCIMO shows a more negative water balance in May below 2700 m a.s.l. and in August above 3000 m a.s.l. Above 2400 m a.s.l. the water balance of July is more negative in the case of EMA. This indicates that in the case of EMA the ablation zone of the glacier is clear of snow earlier than for ESCIMO and that therefore higher glacial melt rates are computed.

The topographic structure, the seasonal air temperature gradient and the seasonal distribution of precipitation are the main factors, which control the discharge hydrograph. The period after the 0° C air temperature isotherm passes the elevation zones with the largest parts of the catchment area is the condition for the highest runoff rates. The level of the runoff maximum is additionally increased if the seasonal precipitation maximum coincides with the snowmelt period in the largest part of the catchment, as was the case in the investigated Dischmabach catchment. The analysis of the seasonal altitudinal distribution of the water balance is of great interest to the management of water resources in alpine catchments such as the optimization of the production of electricity with hydropower or for the planning of new hydropower plants. The results show that PREVAH is a suitable tool to cope with such questions.

Analysis in the Thur catchment ♦

Figure 5.22 illustrates the ET computed by PREVAH for the different HRUs that were defined for simulation of the water balance of the Thur catchment (1981-1996). The classification of HRUs into the two aspect classes clearly reveals the high amounts of ET on south-exposed slopes, with their higher radiation and temperature input when compared to those HRUs on north-exposed slopes. The influence of exposure is strong even though it is superimposed with the evaporation demand of various land-use. The mean annual ET varies most frequently between 450 and 650 mm. In the sub-alpine and alpine areas up to 2500 m a.s.l., ET can fall to values as low as 200 to 400 mm per year. The lowest computed ET rates occur on north exposed HRUs with rocky or urban surfaces or alpine meadows. The maximum ET rates occur on south exposed forest areas and wetlands (fig. 5.22). Between these extremes, the following land-use categories give a sequence of increasing ET rates: orchards, bushes, and meadows. Within each land-use category, the ET depends, to a great extent, on the available amounts of water and/or the slope of the HRU. All vegetation types are characterized by a distinct decrease of ET with increasing elevation, owed to the decreasing transpiration capability of the predominant types of vegetation (which is controlled by the physiological properties of the vegetation) and to the plant available soil water depending on the storage capacity and the actual

♦ The work presented in this sub-section is included in the book chapter "Advanced applications of distributed hydrological models in mountainous catchments" by J. Gurtz *et al.* The book "Climate and Hydrology in Mountain Areas" is edited by C. de Jong *et al.* and scheduled for print in fall 2003.

level of saturation. On rocky and urban land surface areas, the evaporation is limited by the surface depression storage capacity. Additionally the dependence of ET on altitude is strongly influenced by the albedo through its effect on short-wave radiation. Land surface characteristics, vegetation cover and snow-cover determine albedo. The increasing duration of snow-cover causes a decrease of the energy amount available for ET (Gurtz *et al.* 1999).

Figure 5.23a shows the average monthly-interpolated air temperature at different elevation zones of the Thur catchment. Figure 5.23b shows the same for average monthly precipitation. Figures 5.23c and 5.23d illustrates the altitudinal dependence of the average monthly evapotranspiration and water balance (WB = P - R - ET) as computed with PREVAH (period 1981-1996). The period with a positive water balance (water storage within the catchment) differs considerably with respect to the elevation and is governed by the annual course of precipitation and surface air temperature.

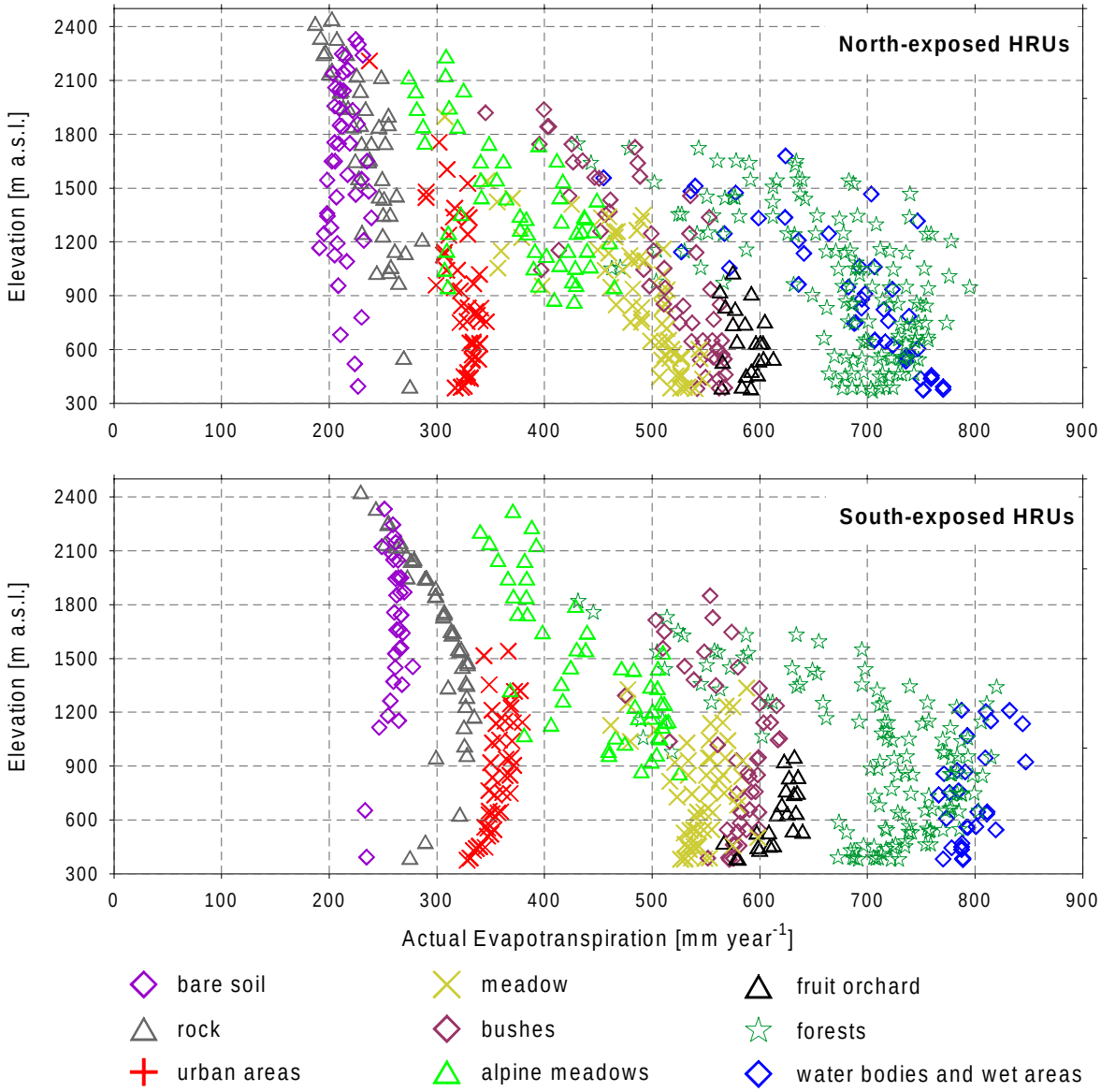

Figure 5.22 Mean annual actual evapotranspiration as a function of elevation for different land-uses and divided into two exposure classes for the Thur basin (1981-1996).

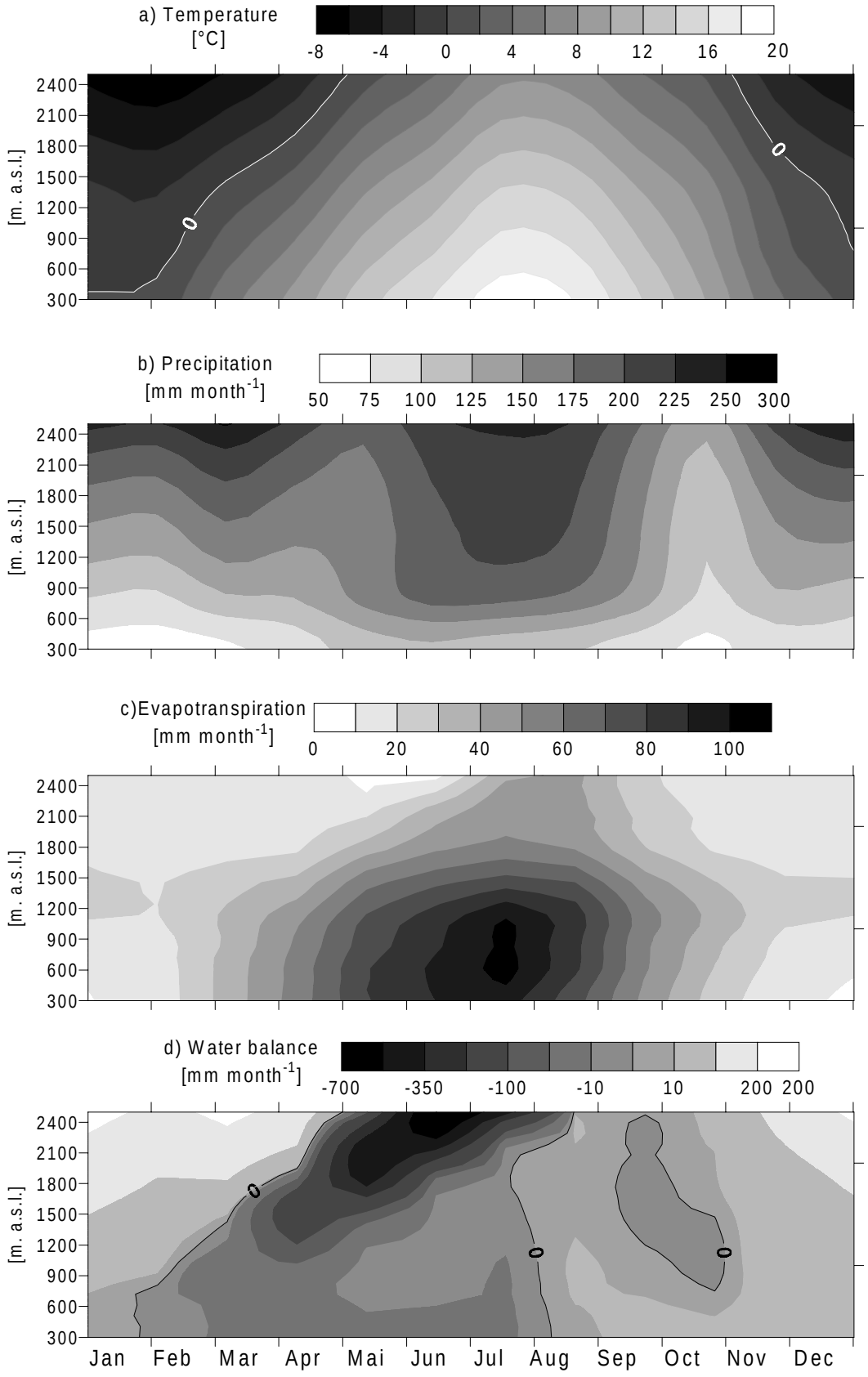

Figure 5.23 Thur catchment, 1981-1996: a) monthly averages of air temperature at the different 100 m elevation zones. b) monthly averages of precipitation. c) actual evapotranspiration. d) water balance computed subtracting the simulated runoff and evapotranspiration from the interpolated precipitation.

In the elevation range below 1000 m a.s.l., the water balance is negative (release of water from the catchment) between February and August, while above 2000 m a.s.l. WB is below zero only after April. This demonstrates the temporal shift when the snowmelt season begins with respect to elevation and the longer snow accumulation phase at higher altitudes. At approximately 1000 m a.s.l., the discharge regime is observed to turn gradually from a lowland regime (governed by rainfall and evapotranspiration) into an alpine regime (governed by air temperature and snowmelt). This transition is marked by the more negative WB below 700 m a.s.l. between March and July as a consequence of the limited runoff-generation and high evapotranspiration rates. With increasing altitude, the regime is observed to be more influenced by the duration of the accumulation and ablation phase of the snow-cover. The snowmelt season ends in the higher altitudes between July and August. The positive WB in the lowest altitudinal range later in August is caused by the seasonal maximum of precipitation (fig. 5.23b). This allows the replacement of the water losses by ET from the previous warm months. The slight negative balance in September and October in the altitudes above 1000 m a.s.l. is owed to the reduced precipitation rates in that period and to the fact that the alpine vegetation is fully developed after the end of the snowmelt season in August, which causes water losses by evapotranspiration (fig. 5.23c). This region is characterized in winter by frequent temperature inversions. The more or less similar average temperature in the region below 1000 m a.s.l confirms this. The frequent lowland fog below 1000 m a.s.l. reduces the incoming radiation and the average sunshine duration and, therefore, also evapotranspiration. The higher rates of ET in the elevation range between 1000 and 1700 m a.s.l. is therefore caused not only by the local climatology but also by the soils at those elevations which have very high water storage capacity and therefore more moisture available to the vegetation for transpiration. The higher portion of evergreen needle-leaf vegetation (coniferous forest) when compared to lowland regions (Gurtz *et al.* 1999) is also responsible for the higher computed evapotranspiration.

5.3.4 Model reliability for different alpine discharge regimes

The purpose of this section is the demonstration of the runoff-generation module quality in catchments with different hydrological regime (table 5.1, Weingartner and Aschwanden 1992). The hypothesis is that the quality of the runoff-generation module is not guaranteed if the simulations only allow the correct reproduction of a particular type of discharge regime at one particular scale. To test this hypothesis PREVAH was used in different alpine catchments, which are characterized by different climatology, physiography and surface area (table 2.1, figures 1.3 and 3.1). The sub-periods that were considered for calibration and evaluation, respectively, are declared in table 3.1.

The Murg and the Rietholzbach catchments drain into the Thur River (Gurtz *et al.* 1999). Detailed information on the Thur catchment and sub-catchments, and on the Dischmabach catchments, has already been presented in section 3.1. The Verzasca catchment is representative for the climate of the Southern Alps (Zappa 1999, Jasper 2001). The high-alpine Rosegbach catchment is partly glacerized and located in the dry Engadina valley (Zappa *et al.* 2000). The Rhone catchment is a heavily glacerized catchment located in the very wet north-eastern part of Wallis (fig. 1.3, Klok *et al.* 2001).

Table 5.11 shows that the average precipitation at the Murg catchment is less than half when compared to the Rhone catchment. The average evapotranspiration of the Murg catchment is four times larger than at the Rhone catchment.

Table 5.11 Average water balance ($mm \cdot y^{-1}$) of several catchments. (P = precipitation; ET = simulated evapotranspiration; S = simulated runoff; O = observed runoff;). The Nash-Sutcliffe efficiency score for the simulation of daily discharge is indicated. The declared classification of the discharge regime follows Weingartner and Aschwanden (1989).

Catchment	Period	P	ET	S	O	E_2	E_2^{Log}	Regime
Rietholzbach	1981-2000	1597	555	1043	1019	0.83	0.89	Pluvial
Murg	1981-1996	1146	541	599	601	0.89	0.87	Pluvial
Thur	1981-1996	1467	556	905	899	0.85	0.89	Pluvial-Nival
Verzasca	1991-1998	2107	311	1816	1849	0.89	0.94	Nival-Pluvial
Dischmabach	1982-2000	1493	254	1245	1250	0.89	0.93	Nival
Rosegbach	1991-1998	1208	337	1464	1461	0.93	0.95	Glacial
Rhone	1981-2000	2531	150	2354	2406	0.92	0.93	Glacial

The statistical analysis demonstrates that the model is able to capture the hydrological regime of a large spectrum of catchments with good quality. The E_2 and E_2^{log} between the observed and simulated daily discharge is, in all cases, above 0.8 for periods ranging between 8 and 20 years. Figures 5.24 and 5.25 show the simulated daily hydrograph of 1994 for the seven catchments listed in table 5.11.

In the small pre-alpine Rietholzbach catchment (3.2 km^2) PREVAH is able to reconstruct the temporal pattern of the discharge regime. The regime here is governed by rainfall in winter and evapotranspiration in summer. The discharge is slightly overestimated during low-flows periods. The ratio between precipitation and discharge is approximately 0.66. One third of the average catchment precipitation leaves the catchment through evapotranspiration.

The Murg catchment (210 km^2) is located a few kilometres north of the Rietholzbach catchment. The river has a typical runoff regime of the Swiss midland plains. Runoff generation is basically rainfed and limited by the high evaporation demand in summer. The hydrological response of the Murg catchment is characterized by a lower variance between peak and low-flows when compared to the Rietholzbach catchment. The simulations show that PREVAH can describe the different hydrological response of those two pre-alpine catchments. The average precipitation in the Murg catchment is more the 25% lower than in the Rietholzbach catchment. About 45-50% of the precipitation leaves the catchments as evapotranspiration, while only 50-55% of the precipitation input activates the runoff-generation processes.

The larger catchment of the Thur (1703 km^2) is characterized by both a midland rainfed regime in the lowland sub-catchments (including the Murg river) and an alpine snowmelt governed regime of the upland sub-catchments (fig. 5.23). Thus, the discharge hydrograph shows a large contribution of discharge from snowmelt in the upland part between March and May. In the remainder of the year, the hydrological response of the Thur River is governed by rainfall and evapotranspiration, as in the Murg catchment, as confirmed by the intercomparison of the discharge hydrograph in 1994 (fig. 5.25). The average water balance of the Thur is similar to the water balance of the Rietholzbach catchments. Up to 35-40% of the precipitation leaves the system by evapotranspiration. Approximately 60-65% of the available water resources contribute to the catchment discharge. As described in the previous section, the snowmelt and runoff-generation modules of PREVAH are able to capture this duality in the discharge regime of the Thur catchment and can reasonably reproduce the snowmelt governed phase of the hydrograph in spring and the rainfed peak-flows in the remainder of the year.

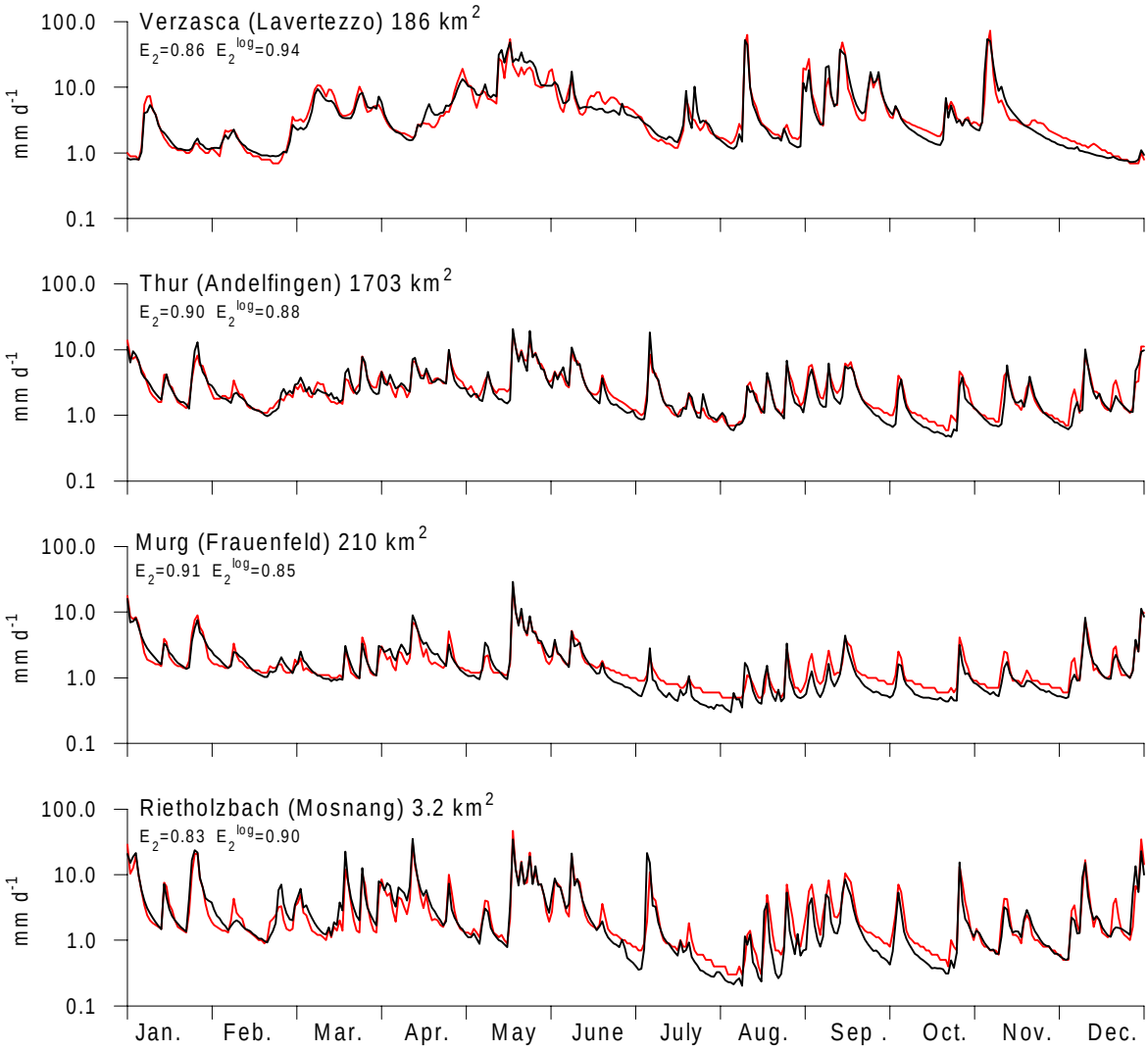

Figure 5.24 Comparison of the observed (black line) with the simulated (red line) daily hydrograph for two pre-alpine and two alpine catchments in 1994. E_2 and E_2^{log} are the achieved linear and logarithmic Nash and Sutcliffe score, respectively.

Such duality in the Thur catchment is caused by the differences in the local climatological and physiographic characteristics between the lowland and the upland regions. The fact that PREVAH is able to capture this duality without showing any decrease in the computed efficiency score for the simulation of daily discharges (table 5.11) speaks for the flexibility of the implemented snowmelt and runoff-generation modules.

The discharge regime of the alpine Verzasca catchment (186 km^2) is also characterized by a dual response. Weingartner and Aschwanden (1989) classify such a hydrological regime as meriodional (south-alpine) nival-pluvial regime (table 3.11). The seasonal precipitation pattern (e.g. Zappa 1999 and Jasper 2001) is characterized by a first maximum in May, which superimposes the high contribution of snowmelt to the total discharge. The summer season is characterized by high evapotranspiration and reduced runoff-generation. The second precipitation maximum in autumn is responsible for the second peak in the seasonal discharge pattern. The precipitation regime in autumn is often characterized by high rainfall intensities and can lead to flash floods. The response of the Verzasca catchments to heavy rainfall events is investigated by Jasper (2001).

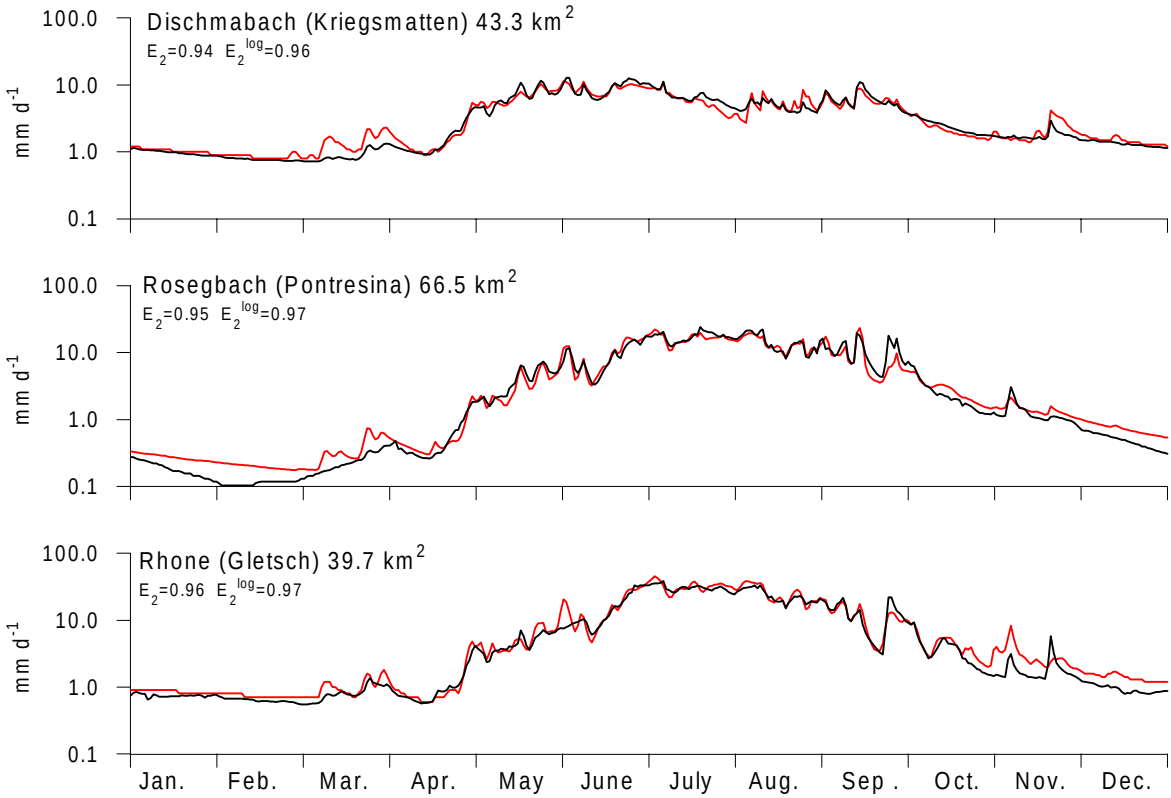

Figure 5.25 Comparison of the observed (black line) with the simulated (red line) daily hydrograph for three partly glacerized high-alpine catchments in 1994. E_2 and E_2^{log} are the achieved linear and logarithmic Nash and Sutcliffe score, respectively.

Also in the case of the Verzasca catchment PREVAH is able to cope with the spatial and temporal variability of the runoff-generation processes and can reproduce the discharge regime with good quality. The average precipitation is larger than in the case of the Thur, Murg and Rietholzbach catchments. More than 80% of rainfall is transformed into discharge. Evapotranspiration is limited and represents less than 20% of the available rainfall.

In the alpine/high-alpine Dischmabach catchment (43.3 km^2) the great part of runoff-generation occurs during the snowmelt season. As presented in previous sections PREVAH can efficiently reproduce the temporal pattern of the discharge regime of the Dischmabach catchment. The maximum runoff is reached in June-July when snowmelt-runoff is supported and integrated by rainfed runoff-generation (Zappa *et al.* 2003). The average catchment precipitation is low when compared to the Verzasca catchment and to the alpine parts of the Thur catchment (e.g. fig .1.3). The portion of average catchment precipitation that is transformed to runoff is above 80%.

The simulation of the discharge regime of the Rosegbach catchment (66.5 km^2) required the implementation of a glacial melt module in PREVAH (Badoux 1999, Zappa *et al.* 2000). This module allows the estimation of icemelt from glacerized areas in the ablation part of a glacier, and the computations of firn melt. The average precipitation of the Rosegbach catchment is approximately 20% lower than the average precipitation in the Dischmabach catchment and less than half of the precipitation in the Rhone catchment. The large contribution of glacial melt to the catchment discharge causes that the average runoff (1464 mm·y^{-1}) exceeds the average catchment precipitation by approximately 20% (table 5.11). Also accounting of evapotranspiration, it should be concluded that glacial melt from the

glacerized portion of the catchment below the glacier equilibrium contributes to the total discharge with a water column of approximately 650 $mm \cdot y^{-1}$. The comparison between the hydrograph of the Dischmabach and Rosegbach catchments shows that, in the case of the Rosegbach (30% glacerized) catchment, glacial melt maintains a high catchment discharge rates after the end of the main snowmelt season, while in the Dischmabach catchment (2.1% glacerized) the quantitative contribution of icemelt to the generation of runoff is more reduced. The pattern of the hydrograph is mainly determined by precipitation. Runoff generation is mainly rainfed.

The last considered catchment is the high-alpine Rhone catchment (39.7 km^2) with a glacerized portion of 47%. The runoff volume in the Rhone catchment clearly exceeds the values of the Dischmabach and Rosegbach catchments as a result of higher precipitation (2531 $mm \cdot y^{-1}$). This causes a high accumulation of firn in the magnitude of approximately 30 $mm \cdot y^{-1}$ within the catchment. This implies that the Rhone glacier is growing. Verbunt *et al.* (2003) discuss the application of the WaSiM-ETH model in three partly glacerized catchments and concluded that the interpolated meteorological information provides, in the case of precipitation in high-alpine regions, a very uncertain value. At high elevations the lack of detailed measurements represent a great problem. The precipitation amounts must be extrapolated from observations at lower altitudes and this implies the assumption that the vertical gradients of precipitation are constant up to more than 4000 m a.s.l. The analysis proposed by Verbunt *et al.* shows that there is some evidence that the vertical gradients of precipitation may decrease or even become negative at elevations above 2700 m a.s.l. This would lead to a decrease of the catchment's average precipitation and to a more realistic estimation of the water balance. This conclusion agrees with the considerations of Schädler and Weingartner (2002b). Their estimates for the water balance elements of Swiss basins with area ranging between 100-200 km^2 based on observed discharges and simulated evapotranspiration (Menzel *et al.* 1999) also indicates that a reduction of the precipitation gradients should be accounted in the case of several alpine and high-alpine regions.

5.4. Conclusions

This chapter demonstrated the importance of simulation experiments at different spatial scales for the development, calibration and multiple-response evaluation of distributed hydrological models.

The analysis of the model quality at plot-scale allowed for the separate testing of the quality of several model-components with observed data other than the generally adopted discharge data. In situ measurements and special investigations in selected sites (section 5.1) and small research catchments (section 5.2) are essential for a realistic and successful parameterization, calibration and evaluation of distributed hydrological models. The multiple-response evaluation, as performed for the lysimeter site and for the Usadievsky catchment, allows more reliable assumptions on the suitability of the different model components and, therefore, indicates the way for further improvements in the spatially distributed simulation of runoff-generation and other relevant hydrological processes.

A sound and reliable process-oriented hydrological modelling of mountainous catchments needs to consider the spatial differences in topography, land-use, land cover, soil characteristics and meteorological variables. The application of PREVAH for the simulation of alpine catchments with different discharge regimes (section 5.3) allowed for the evaluation of different key features that a hydrological model has to cope with for the spatially distributed simulation of the hydrological cycle.

The presented results indicate that the significance of snow accumulation and snowmelt and their spatial distribution increases with increasing altitude. As a result, the quality of the estimated runoff-generation strongly depends on the snow model quality. An intercomparison between four different snowmelt modules showed that the discharge regime of an alpine catchment can be successfully estimated with both temperature-index (both classic or enhanced with a radiation term) and energy balance-based approaches (Zappa *et al.* 2003).

The intercomparison between PREVAH and the hydrological model WaSiM-ETH (Gurtz *et al.* 2003a, Klok *et al.* 2001) demonstrated that the estimated portions of the different runoff components are affected by the physiographic and climatic specifications of the catchments and by the structure of the used models. The WaSiM-ETH physically-based structure has a larger flexibility in the separation of surface runoff from interflow, but includes the fast baseflow component as delayed interflow from the lowest unsaturated soil layers. This causes a limited flexibility and lower simulation performance during dry periods than the two groundwater reservoirs approach adopted in PREVAH. The application of the PREVAH model shows good performance within pre-alpine and alpine catchments with comparatively reduced computational time. WaSiM-ETH allows a higher reliability for the simulation of high-flows. The required computational time for grid-based WaSiM-ETH is approximately three times higher than for HRU-based PREVAH (Gurtz *et al.* 2003a).

PREVAH is able to cope with the variety of discharge regimes within the Swiss Alps (Weingartner and Aschwanden 1992). This is possible since the snowmelt, icemelt and runoff-generation modules have proven to be adequate in lowland, pre-alpine, alpine and high-alpine catchments. The acquired expertise allows for the conclusion that PREVAH is a reliable tool for spatially distributed hydrological simulations in mountainous environments. The next step will be using PREVAH for the simulation of the hydrological regime in larger catchments. The first experiment at a large scale is presented in chapter 7.

6. Use of meteorological forcing from atmospheric models♦

6.1. The Volga Forest project

The Volga Forest project was launched to estimate the response of the water flows of the boreal forest region at the Volga's source area (Russia) to climate changes. This region is drained by the most important rivers of the Eastern Europe and has an enormous ecological importance (Oltchev *et al.* 2002). Within Volga Forest the involved research groups co-operated in order to describe the variability of the boreal forest structure and of the climatological-hydrological situation in the Upper Volga catchment over the past 100-150 years (section 3.2.2). The principal finding of the project are summarized in Oltchev *et al.* (2002). This chapter presents the contribution of the IACETH Zürich to the Volga Forest project. Aim of this contribution was the evaluation of the use of meteorological time series generated by RCM and GCM experiments as a forcing for an hydrological model and to assess the feasibility of performing longer term water balance studies from such experiments. Thus, PREVAH was forced by meteorological information from surface observations, from an atmospheric GCM and from a RCM. Section 6.2 describes briefly the atmospheric models used. The data sets are presented in section 6.3. The procedure used for the assimilation of meteorological information from atmospheric models is presented in section 2.1.4. The results of the data analysis are given in section 6.4. The calibration and validation of the hydrological simulations and the water balance simulations for control (labelled hereafter CTRL) and scenario (labelled hereafter SCEN) climate conditions are presented in section 6.4 followed by a discussion of the results and the conclusions in section 6.5.

6.2. Atmospheric models and experiments

6.2.1 The general circulation model ECHAM4

The experiments with the ECHAM model series (Roeckner *et al.* 1996) are an example of a high-resolution application of a GCM for the investigation of climate change on the global scale. Several experiments (Wild *et al.* 1998) have been carried out jointly by the Max Planck Institute (Hamburg, Germany) and the Institute for Atmospheric and Climate Science ETH. Climate change experiments at high resolution were performed to obtain scenarios at the highest horizontal resolution currently used in climate modelling. The horizontal discretization of this model is given by spherical harmonics, and the resolution consists on a triangular truncation T106, corresponding to a grid resolution of 1.1°. Since it is not feasible to run such a high resolution GCM over several decades as required in transient climate change experiments, a 'time-slice' methodology was adopted (Wild *et al.* 1997). The experiments were realized for both present day and $2xCO_2$ conditions with associated sea surface temperature and sea-ice distributions derived from a transient scenario run at T42 resolution (2.8°) coupled to an ocean model (Roeckner *et al.* 1999). This scenario takes into account a gradual increase in CO_2 and other greenhouse gases basing on the IPCC Scenario IS92a (IPCC 1992). The considered climate change experiment is representative for the decade 2041-2050.

♦ A paper entitled: "Water balance studies driven by observation, GCM, RCM simulations and climate change scenarios: a study in the Volga's source region " is in preparation.

6.2.2 The regional climate model CHRM

A model for the simulation of meteorology and climatology on the regional scale was developed from the operational limited-area weather forecasting model of the German and Swiss weather services (Majewski 1991). The Climate High Resolution Model CHRM is based on the operational high-resolution is used for climate simulations and case studies with 56 km and 14 km grid-spacing (Lüthi *et al.* 1996). The model grid is a regular latitude/longitude grid with a rotated pole and a hybrid vertical co-ordinate. The integration domain encompasses Europe, the Mediterranean Sea and the North Atlantic Ocean. It embraces a full package of physical parameterization (Vidale *et al.* 1998) including a mass-flux scheme for moist convection, Kessler-type microphysics, a land surface scheme with three soil layers. Vertical diffusion and turbulent fluxes is based on the flux-gradient approach. The model is driven at the lateral boundaries by observed data (ECMWF Re-Analysis, ERA, Gibson *et al.* 1997) available on a grid with 1.1° resolution (T106) and assimilated every 6 hours. Studies of regional processes relevant to water-cycle impacts of vegetation changes and global warming have been carried out (Frei *et al.* 1998, Heck *et al.* 2001, Kleinn 2002, Vidale *et al.* 2003).

6.3. Meteorological and hydrological data sets

6.3.1 Valdai-Usadievsky data set

The Valdai-Usadievsky data set is presented in section 3.2.1 and is summarized in table 3.4. A thorough description of this data set is provided by the scientific literature related to the Land Surface Schemes (LSS) intercomparison project PILPS 2(d) (Schlosser *et al.* 1997 and 2000, Slater *et al.* 2001, Gusev and Nasonova 2002).

6.3.2 Upper Volga data set

Records from eight surface meteorological stations of the Russian Meteorological Service are available (fig. 3.5 and table 6.1). The stations Ostashkow and Toropetz are located outside the Upper Volga catchment. They allow the interpolation of the meteorological records over the axis west-east throughout the catchment. The station Zapovyednyik is located at the southern end of the target area. For these three stations the Tver State University has provided daily meteorological data for the period 1993-1996. Daily and three hourly data of two further stations, Smolensk and Velikie Luki, were obtained from the NDP-048 database (Razuvaev *et al.* 1995).

Table 6.1 Available information from surface meteorological stations (P: precipitation, T: air temperature, W: wind speed, RH: relative humidity, C: cloud cover, GR: global radiation).

Station	Fig 3.5	P	T	W	RH	C	RG
Ostashkow	OST	X	X	X	X	X	
Toropetz	TOR	X	X	X	X	X	
Zapowednyi	ZAP	X	X	X	X	X	
Smolensk	SMO	X	X				
Velikie Luki	VEL	X	X				
Valdai	VAL	X					
Moscow	MOS	X	X				X
St. Petersburg	SPS						X

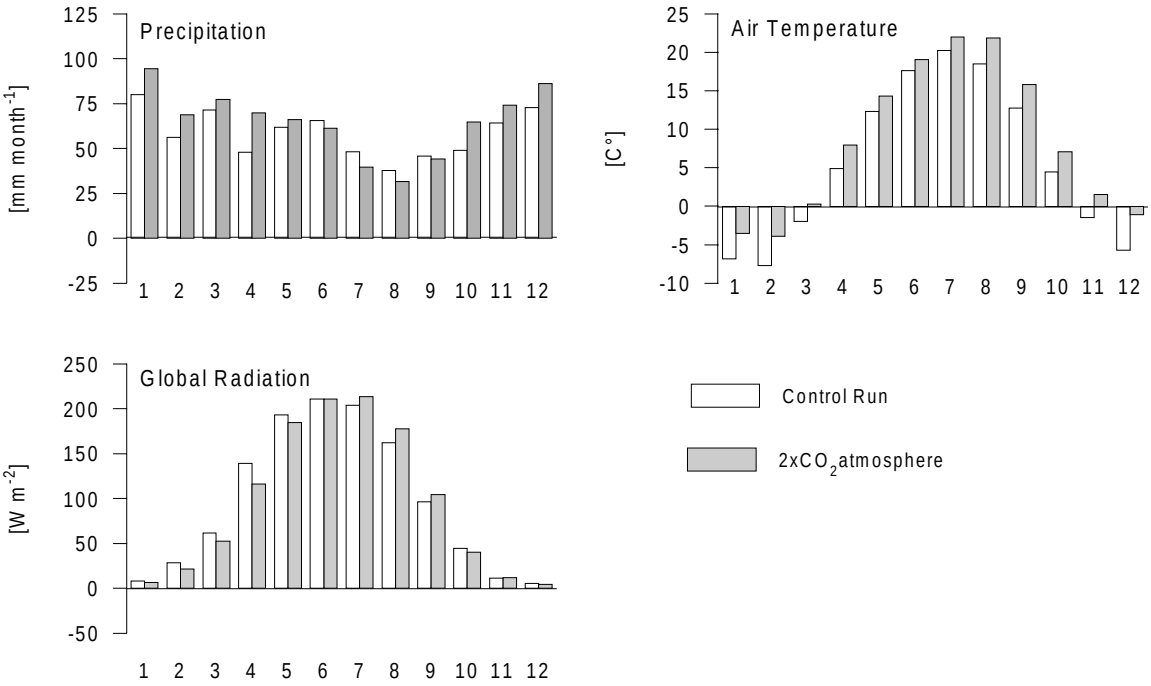

Figure 6.1 Monthly averaged ECHAM4 outputs of the control and scenario runs for precipitation, air temperature and global radiation in the Upper Volga region.

In addition precipitation data for the station Valdai have been used. Since no information on global radiation at the mentioned stations was available, the radiation records from the stations Moscow and St. Petersburg had been taken instead. Those records were obtained from the world radiation data centre in St. Petersburg (WRDC 1993). The hydrological data record necessary for the model evaluation consist of the lake level fluctuations records at the dam Selishe. The Tver State University has provided the daily records for the modelling period 1993-1996. This data set will be referred hereafter as UV_{CTRL}.

6.3.3 Determination of the climate scenario

ECHAM4 was used to compute climate scenarios for the Upper Volga area. An integration over 10 years of the ECHAM4 T106 experiment for present conditions ('control run') was compared with an experiment assuming a doubled CO_2 content in the atmosphere. (IPCC 1992). Only the grid points closest to the research area have been accounted for the computation of the climate scenario (figure 3.5). The location of the Upper Volga region was defined through a square of 9 points (latitudes 57.7 N, 56.6 N and 55.5 N - longitudes 31.5 E, 32.625 E, 33.75 E). The current climate conditions in the region of the Upper Volga were assessed through monthly averages of precipitation, air temperature and global radiation. The month-to-month difference between the control run and the $2xCO_2$ run was also obtained from the ECHAM4 experiments. This allowed the diagnosis of the possible climate changes in the target area. Figure 6.1 shows the obtained monthly averages from the GCM experiments for air temperature, global radiation and precipitation. The deviation of the scenario run from the run for the region of the Upper Volga area is also indicated. The ECHAM4 experiments indicate that the total amount of precipitation should increase by about 11% (from 700 to 780 mm per year). A significant difference arises between summer and winter (table 6.2).

Table 6.2 Mean changes of selected climate values in the winter half year according to a 2xCO_2 scenario experiment with ECHAM4 (ΔP = Percentual change of precipitation, ΔT = change in air temperature in °C, ΔGR = Percentual change of global radiation).

	Nov	Dec	Jan	Feb	Mar	Apr	Winter
$SCEN_{ID}$	11	12	1	2	3	4	-
ΔP [%]	15.4	18.3	18.2	22.4	8.2	45.6	19.9
ΔT [°C]	3.0	4.7	3.3	3.8	2.2	3.1	3.3
ΔGR [%]	1.2	-17.9	-17.1	-23.7	-14.8	-16.7	-16.3

Table 6.2 (continued) Mean changes of selected climate values in the summer half year and in average for the whole year

	Mai	Jun	Jul	Aug	Sep	Oct	Summer	Year
$SCEN_{ID}$	5	6	7	8	9	10	-	-
ΔP [%]	6.5	-6.4	-17.9	-16.4	-3.9	32.3	-0.3	11.0
ΔT [°C]	2.0	1.5	1.7	3.3	3.1	2.7	2.4	2.9
ΔGR [%]	-4.4	0.0	4.7	9.7	8.2	-9.7	2.3	-1.8

In the period May to October no mayor changes should be expected in the total amount of the precipitation (-0.3%). A considerable increase can be observed for April, while an important reduction of the precipitation amount is expected between June and September. A mean increase of 20% in the precipitation amount in the winter is predicted. The mean increase of the air temperature may be about +2.9°C (maximum of +4.7°C for December and minimum of +1.7°C for July). The changes in the global radiation may be smaller and more important in the winter half year (-16.3%).

This scenario with monthly resolution was assimilated by the hydrological model to update the available meteorological information to the predicted climate and to analyse the feedback between the climate changes as diagnosed by ECHAM4 and the changes in the temporal pattern of the water budget. The defined climate scenarios are be assimilated at each time step *t* to modify the meteorological information used for the control simulations. Following procedure is adopted to modify the control data sets:

$$P_{SCEN}(t) = P_{CTRL}(t) \cdot \Delta P(SCEN_{ID})$$

$$T_{SCEN}(t) = T_{CTRL}(t) + \Delta T(SCEN_{ID}) \qquad (25)$$

$$GR_{SCEN}(t) = GR_{CTRL}(t) \cdot \Delta GR(SCEN_{ID})$$

P_{SCEN}, T_{SCEN} and GR_{SCEN} are the values of the meteorological forcing after the modification determined by the climate scenario. The values of the control (*CTRL*) meteorological information on precipitation *P*, air temperature *T* and global radiation *GR* serves as basis for the application of monthly-based modifications (ΔP, ΔT, ΔGR). $SCEN_{ID}$ is an identifier for the monthly-based changes declared in table 6.2. Model experiments based on meteorological information modified after Eq. 25 are labelled hereafter as 'SCEN'.

6.3.4 The ECHAM4 forcing

The 10 years ECHAM4 integration with control climate served not only for the determination of monthly-based scenario, but was also applied for water balance and runoff simulations. The 10 year data set is adopted as a representative meteorological forcing for the Upper Volga region. The nine grid points within the domain of ECHAM4 in the surroundings of the target region (fig. 3.5) have been regarded as 'virtual' surface meteorological observation sites. The 10 years ECHAM4 experiment (hereafter referred as GCM_{CTRL}) has a temporal resolution of six hours and was applied to drive water balance and runoff simulations with PREVAH.

6.3.5 The CHRM forcing

The adopted CHRM meteorological forcing for the hydrological simulations, hereafter referred as RCM_{CTRL}, was provided from an experiment over more than 6 years (September 1987 until the end of 1993) with a three hours temporal resolution (Vidale *et al.* 2003). Only the period 1988-93 was processed for offline coupled hydrological simulations with PREVAH. Similarly to the previously considered GCM-based forcing, 36 representative points within the CHRM domain were considered and regarded as 'virtual' surface meteorological station (fig. 3.5). CHRM does not provide directly values for the global radiation; the latter was diagnosed from the short wave radiation budget and the albedo.

6.4. Intercomparison of the meteorological data sets

Prior to the application of the meteorological data derived from the GCM and RCM experiments for hydrological simulations, it was essential to determine the suitability of the climatology that these models are reproducing, even if the relevant averaging period is restricted to just 10 and 6 years respectively. The average seasonal cycle of precipitation, air temperature and global radiation was calculated for GCM_{CTRL} and RCM_{CTRL} and compared to long term measurements at one surface meteorological station: Zapovyednyik (1970-1998) in the case of air temperature and precipitation and Moscow (1964-89, data from GEBA; Gilgen and Ohmura 1999) in the case of global radiation.

The average annual precipitation (table 6.3 and fig. 6.2b) is 721 mm at Zapovyednyik, 808 mm using the RCM_{CTRL} forcing and 660 mm in the case of the GCM_{CTRL} forcing. The quality of RCM_{CTRL} is satisfying. An overestimation of precipitation occurs between January and April, when compared to the surface stations. Since the observed precipitation was not corrected for measurement error (Sevruk 1997) this overestimation can be judged as a positive result of the RCM. The period with maximal precipitation is shifted from July to June. The reproduction of the precipitation seasonal cycle is the most evident and preoccupying shortcoming of the GCM_{CTRL}. The winter precipitation is overestimated, while the precipitation maximum in the summer is completely missed.

The average air temperature during the considered periods (table 6.3 and fig. 6.2c) is 3.9 °C at Zapovyednyik, 4.2 °C in the case of RCM_{CTRL} and 5.6 °C in the data set GCM_{CTRL}. Except for January and February, RCM_{CTRL} computes a temperature cycle, which is in good agreement with the surface stations over the whole year. The differences in winter might be caused by the snow albedo parameterization. The defined constant albedo 0.7 for snow (fig. 6.3) is probably too low and causes an excessive warming of the atmospheric boundary layer when snow-cover is present in the investigated region. GCM_{CTRL} shows higher quality than RCM_{CTRL} in winter, but fails to reproduce the climatology of temperature in the summer.

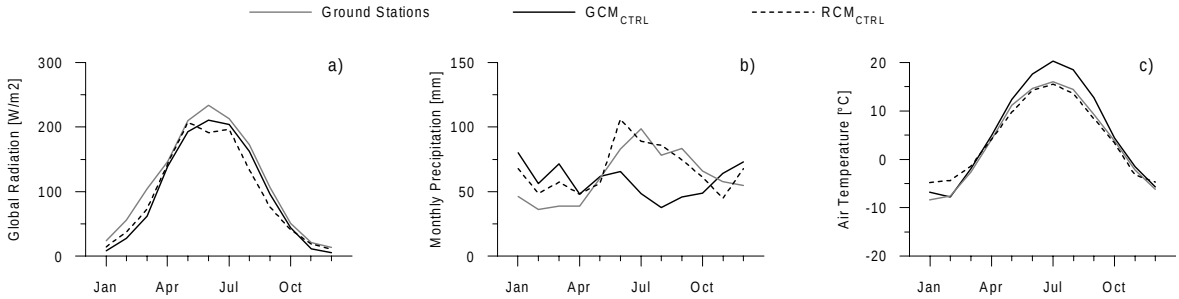

Figure 6.2 Upper Volga: seasonal cycle of global radiation (a), precipitation (b) and air temperature (c) for the available time series of the considered meteorological data sets.

The low precipitation amounts in the summer cause lower evapotranspiration and an excessive warming and flux of sensible heat in the atmosphere surface boundary layer. Thus, the average air temperature is overestimated. The annual-average incoming solar radiation is 113 Wm^{-2} at Moscow, 108 Wm^{-2} at St. Petersburg, 95 Wm^{-2} within RCM_{CTRL} and 97 Wm^{-2} with GCM_{CTRL} (table 6.3 and fig. 6.2a). In comparison to the surface stations in Moscow and St. Petersburg, both CHRM and ECHAM4 tend to underestimate global radiation by about 15 Wm^{-2} throughout the year.

Since ERA fields drive CHRM, a day-to-day comparison with observations is possible. The 1993 time series of RCM_{CTRL} have been compared to observations 1993.

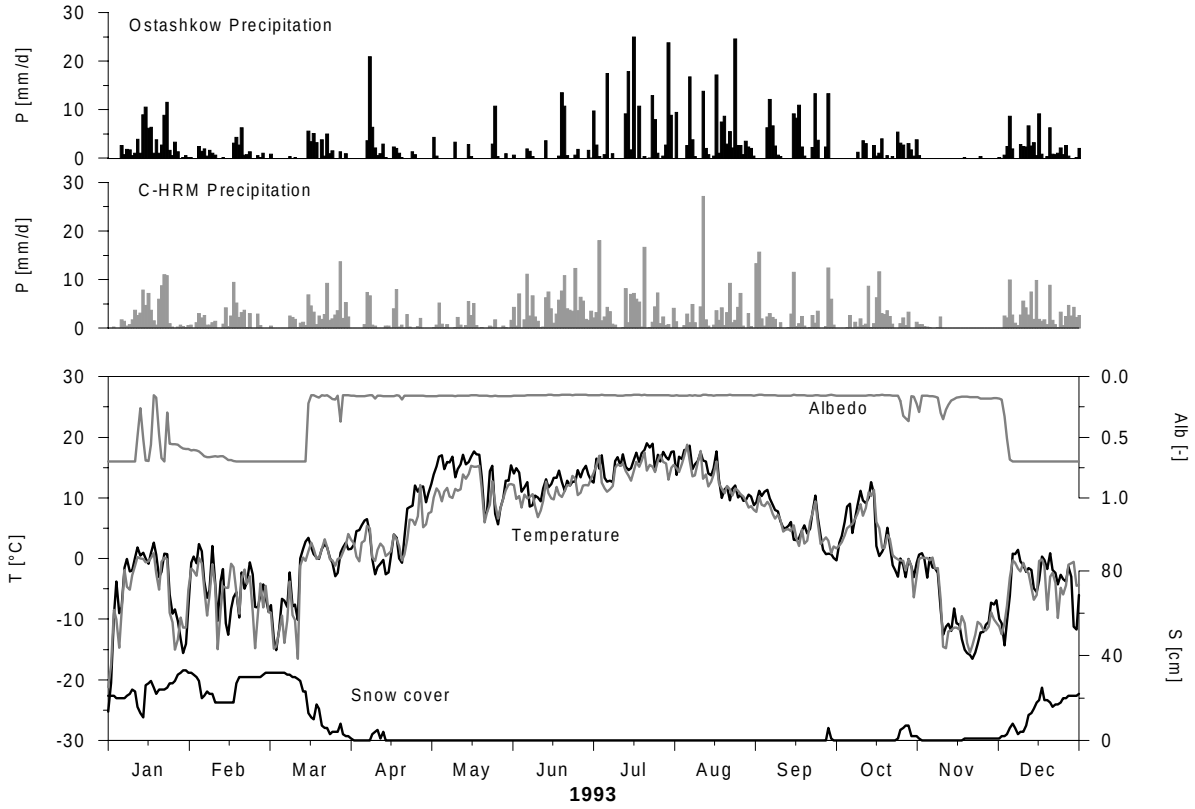

Figure 6.3 Upper Volga, 1993: comparison of daily precipitation (P), average air temperature (T), snow-cover depth (S) and albedo (ALB) between the surface station Ostashkow (black lines and bars) and the CHRM-Grid point closest to the surface station (grey lines and bars).

Figure 6.3 shows the comparison between the surface station Ostashkow and the CHRM point located in the centre of Upper Volga catchment (fig. 3.5). The averaged daily temperature records at Ostashkow are nearly identical to the model record, except for an underestimation between mid March and end June. RCM_{CTRL} describes correctly both the cold weather period in November and the large temperature fluctuations in September and October. The intercomparison of the precipitation records show less positive results. In spite of a general overestimation of the precipitation frequency in June, both series have similar patterns. The alternation of wet and dry periods is well reproduced throughout the year. If the modelled albedo is compared with the snow depth records, it is obvious that CHRM is also able to reproduce accurately the temperature and precipitation induced changes of the land surface characteristics. This suggests that RCM_{CTRL} represents useful data source for driving hydrological simulations. The discrepancy in spring and summer precipitation do partly relate to the reduced predictability in this season (Vidale *et al.* 2003) that partly invalidates day-to-day intercomparison.

6.5. Water balance simulations results

6.5.1 Calibration and evaluation at the Valdai-Usadievsky research catchment

This topic is presented and discussed in section 5.2.1.

6.5.2 Evaluation within the Upper Volga catchment

A model evaluation was performed based upon UV_{CTRL}. Unfortunately this validation was limited by the absence of an accurate quantitative knowledge on the runoff at the outlet point of the catchment (Selishe dam). Figure 6.4b shows a comparison of the 1994-95 lake inflow simulations and the recorded lake level changes.

Additionally figure 6.4a illustrates the time series of the simulated snow water equivalent, simulated plant available soil moisture and daily precipitation.

A qualitatively good correspondence is present between the lake level fluctuations and the simulated runoff (equivalent to the lake inflows) during the main snow-melting phase (R_{OS} of 0.58 between February and June). The surface runoff and interflow contribute to the total runoff until shortly after the beginning of the lake level decrease. The slow baseflow component allows the water supply to the lake during the summer phases with decreasing surface level and water storage of the lake. Except for two melting events that are simulated for March 1994 but were not recorded as lake level increase; the melt season was reproduced in both years with reliable temporal correspondence. An important runoff response to precipitation occurs only shortly after the end of the snowmelt season. At this time the soil is nearly saturated and still partly frozen and water cannot infiltrate in the soil.

Similar precipitation events in autumn cause a different response from the catchment. The water can infiltrate and refills the soil, which were dried by evapotranspiration during the summer. The simulated plant available soil moisture depletion is correlated with the lake level decrease between June and September (R_{OS} of 0.47). In the summer precipitation never compensates evapotranspiration, but reduces the lake level decrease and allows a partial recovery of the soil water content. The generation of quick runoff components occurs again in autumn when the rainfall nearly allows for the attainment of soil saturation. In this case, the lake level increase until the beginning of the cold season when the lake surface is frozen. This happened between mid December 1994 and mid February 1995.

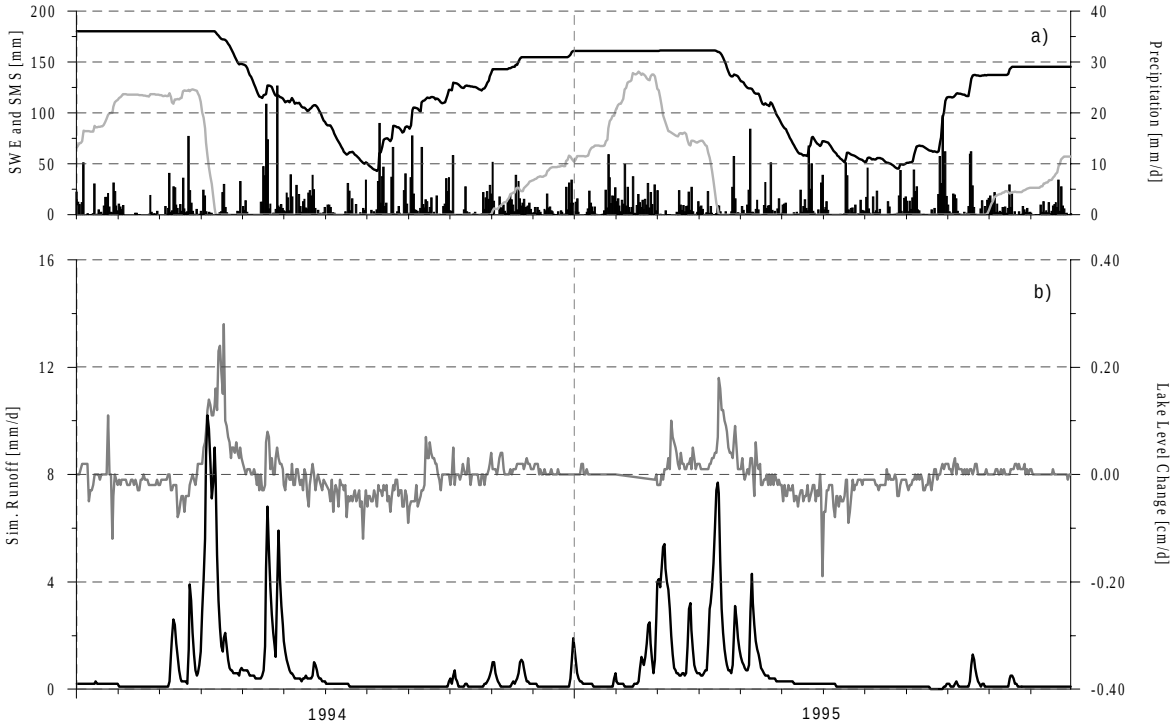

Figure 6.4 Upper Volga, daily values 1994-95: a) comparison between measured lake level changes (right axis, grey line) and the simulated runoff (left axis, black line). b) time series of the interpolated precipitation (right axis, bars), simulated snow water equivalent (SWE, left axis, grey line) and simulated plant available soil moisture storage (SMS, left axis, black line).

6.5.3 Upper Volga simulation

Figure 6.5 summarizes the simulated seasonal pattern of six elements of the hydrological cycle. Those results were obtained forcing PREVAH with the control data sets UV_{CTRL}, RCM_{CTRL} and GCM_{CTRL}. Figure 6.6 shows the corresponding results if the considered monthly averaged climate scenario (SCEN) is applied to modify the meteorological information (Eq. 25). Figure 6.7 shows the differences between the seasonal cycle computed using the climate scenario and the one computed for control climate conditions. The yearly averaged elements of the water balance obtained by all the experiments in the Upper Volga catchment with PREVAH are presented in table 6.3.

Table 6.3 Yearly averages of air temperature (T), global radiation (GR), precipitation (P), simulated actual evapotranspiration (ET), total runoff (R) and quotient snowmelt to total runoff (SR, in percent of the total runoff) for both measured records and simulation results.

Catchment	Meteorology	T [°C]	GR [Wm-2]	P [mm]	ET [mm]	R [mm]	SR [%]
Valdai Hills	Surface stations	3.9	113	721	--	--	--
Usadievsky	US_{CTRL}	3.7	139	757	451	300	70%
Usadievsky	US_{SCEN}	6.6	136	822	449	376	55%
Upper Volga	UV_{CTRL}	4.1	114	717	462	255	74%
Upper Volga	UV_{SCEN}	7.0	112	763	478	294	52%
Upper Volga	GCM_{CTRL}	5.6	97	660	397	266	108%
Upper Volga	GCM_{SCEN}	8.5	95	730	408	327	71%
Upper Volga	RCM_{CTRL}	4.2	95	808	431	367	69%
Upper Volga	RCM_{SCEN}	7.1	93	861	452	410	33%

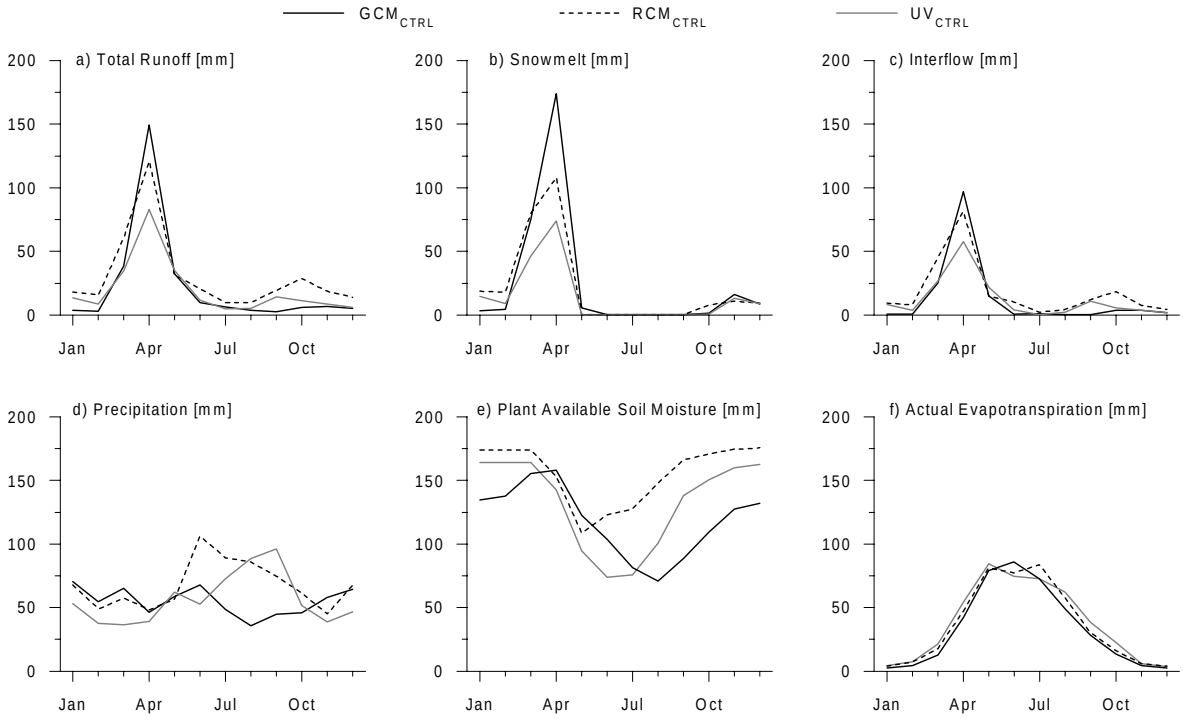

Figure 6.5 Average seasonal cycle of water balance elements as obtained by PREVAH under control climate conditions using the data sets as representative meteorological forcing. Abbreviations are defined in the text.

Lake areas were parameterized to compute potential evapotranspiration over the whole year and not considered for the computation of the average plant available soil moisture on figs. 6.4 through 6.7.

Present climate conditions

Figure 6.5a shows that the seasonal pattern of the simulated total runoff has different average values, because of the different seasonal distribution and total amount of precipitation (fig. 7.d and table 6.3). The high winter precipitation rates of GCM_{CTRL} causes a large accumulation of snow and higher snowmelt rates, when compared with the other data sets (fig. 6.5b). All the data sets reproduce a similar distribution of the maximum runoff during the main melt season, although the application of RCM_{CTRL} and GCM_{CTRL} indicated a slightly anticipated begin of the melt season compared to UV_{CTRL}. This can be better evaluated by examining the snowmelt distribution in the period between February and May (fig. 6.5b). This qualitative agreement can be explained by the similarity of the average temperature in March-April, which governs the temporal occurrence of the snowmelt season. The small temperature differences in January and February cause an anticipated melting of snow when RCM_{CTRL} and GCM_{CTRL} are used for model runs.
The runoff maximum in autumn is owed to the seasonal distribution of precipitation. The application of UV_{CTRL} shows a second runoff maximum in September, in agreement with the precipitation maximum. The other two model runs show higher runoff rates in October-November, when precipitation and infiltration exceed evapotranspiration. This allows the increase of the soil moisture content and interflow generation (fig. 6.5c and 6.5e).

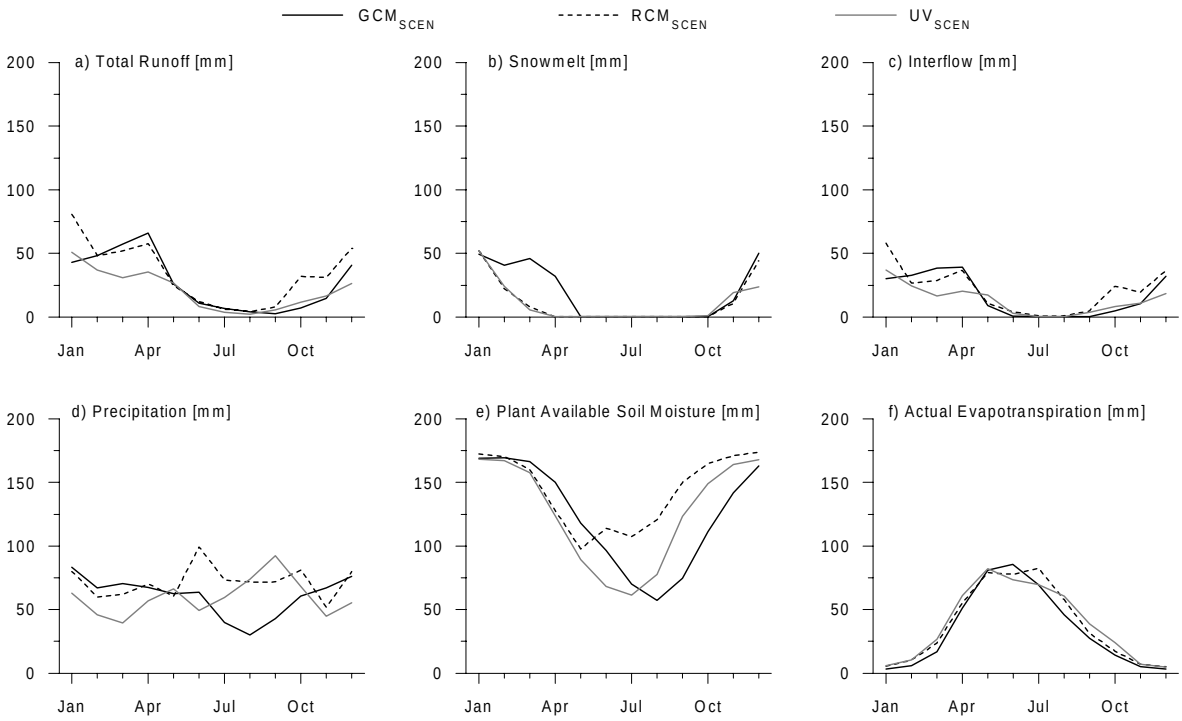

Figure 6.6 Average seasonal cycle of water balance for climate scenario conditions. Abbreviations are defined in the text.

Since evapotranspiration dominates the hydrological cycle in the summer, groundwater recharge occurs only during a limited range of time during the melt period and in late autumn. A good agreement of the seasonal evapotranspiration cycle results from all PREVAH runs. The ratio of evapotranspiration to precipitation ranges between 53% (RCM_{CTRL}) and 64% (UV_{CTRL}). The air temperature differences in the summer (GCM_{CTRL}) and the biases of incoming solar radiation in winter and summer periods are responsible for the seasonal contrasts.

The differences are owed to the seasonal precipitation distribution contrasts and are most obvious if the computed plant available soil moisture cycles are compared one to another (fig. 6.5e). With higher averaged precipitation amounts shortly after the end of the melt season (fig. 6.5d); RCM_{CTRL} produces higher soil moisture storage than UV_{CTRL} and GCM_{CTRL} throughout the summer season.

The low precipitation amounts of GCM_{CTRL} between July and October cause a reduced soil moisture recharge in autumn and therefore a soil moisture deficit during the winter, which is not compensated until the snowmelt period in March and April. This also explains why the calculated snowmelt exceeds the simulated runoff by 8% (table 6.3). The elevated snow accumulation in winter and the reduced recharge in autumn cause considerable water amounts from snowmelt to contribute to the soil moisture recharge instead of contributing to runoff-generation. This behaviour is not present in the simulations with the other data sets. In such cases the computed soil water content approximately reaches the plant available field capacity already before the onset of the snow accumulation.

Scenario climate conditions

UV_{SCEN}, RCM_{SCEN} and GCM_{SCEN} rely on the application of the available monthly averaged scenario (Eq. 25 and table 6.2).

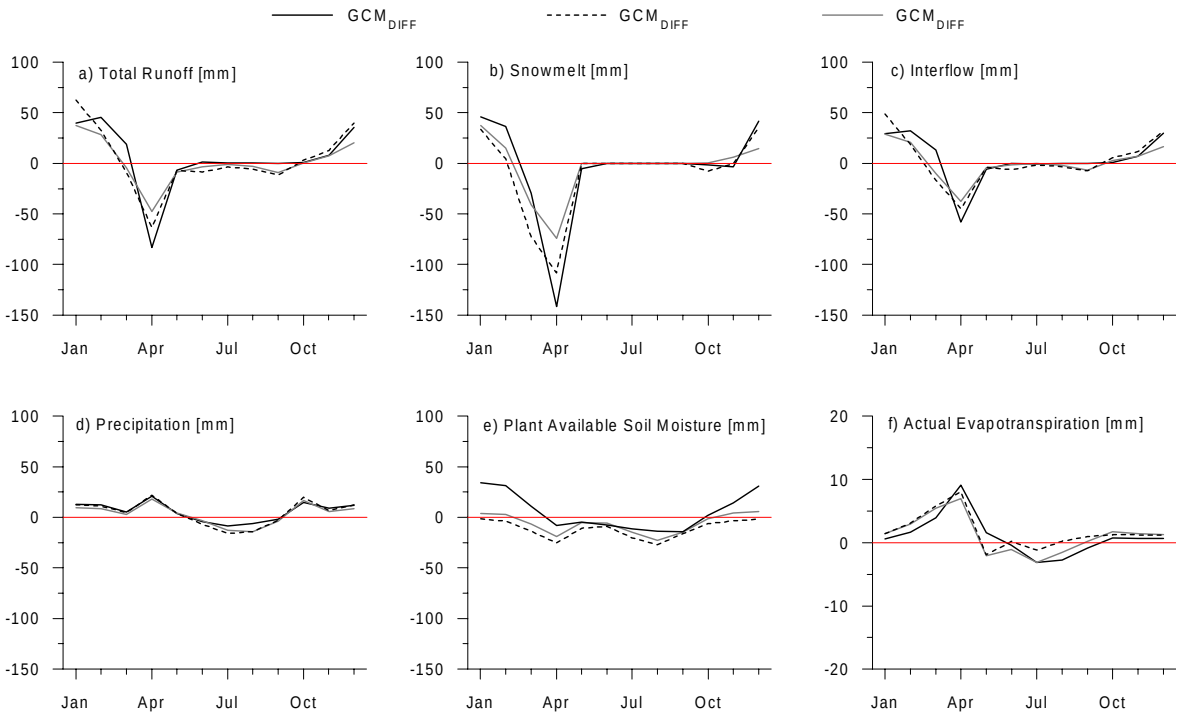

Figure 6.7 Average differences (DIFF) within the seasonal cycle of water balance elements between scenario (SCEN) and control (CTRL) climate conditions. Abbreviations are defined in the text.

The computed average runoff regime has changed. The seasonal runoff maximum in spring appears to be reduced and runoff-generation may be more evenly distributed throughout the winter (figs. 6.5a and 6.6a). The low runoff-generation in summer seems not to be affected by the applied climate scenario. The dissimilarities between the various simulations (fig. 6.6) are not owed to the seasonal distribution of the calculated soil moisture storage (fig. 6.5e and 6.6e). Such differences are mainly owed to the missing correspondence of the main melt season (fig. 6.6b), which originates from the temperature biases in January and February (fig. 6.2c). All the model runs point out that the main melt season may be shifted from April to an earlier month: January in the case of UV_{SCEN} and RCM_{SCEN}, while the simulation driven by GCM_{SCEN} calculates snowmelt amounts in the same quantity range between December and April.

This important temporal difference in the end date of the melt season affects the whole water balance simulation and explains the significant disagreements between simulations with the different meteorological forcing. The precipitation increase resulted in an in crease of the total runoff (up to 34% more in the case of GCM_{SCEN}), but only a limited growth of the actual evapotranspiration (maximum 5% more in the case of RCM_{SCEN}).

The higher average temperature throughout the year causes an important decrease of snow accumulation. The runoff portion originated from the snowmelt is drastically reduced if the ECHAM4 scenario modifies the current meteorological information. As indicated in table 6.3 the ratio of the snowmelt to the total runoff is reduced by at least 20% using any of the three data sets, and in the case of RCM_{SCEN} even by 36%.

The effect of the surface albedo decrease following an earlier absence of snow-cover causes an actual evapotranspiration increase in late winter and early spring (fig. 6.7f). All the simulations driven by scenario data sets show reduced evapotranspiration in the summer, caused by both the decrease in rainfall (fig. 6.7d) and the earlier depletion of the soil moisture content in spring. This is a consequence of the snowmelt season earlier end.

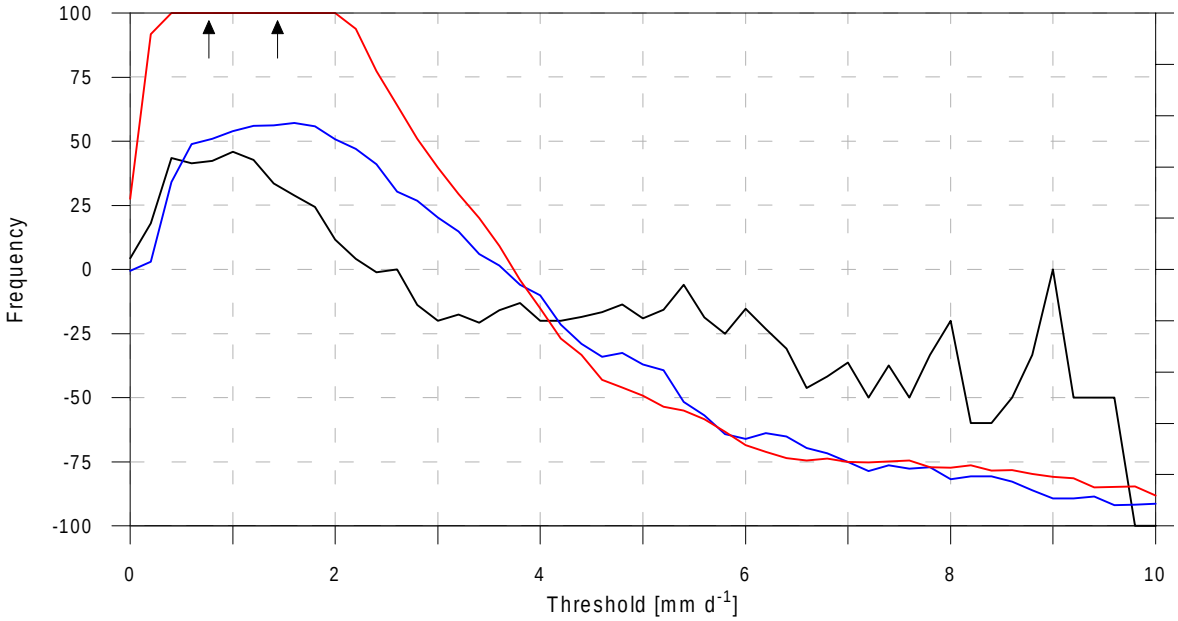

Figure 6.8 Changes in the relative frequency of daily discharge rate exceeding a specific threshold. Black are the changes between UV_{SCEN} and UV_{CTRL}, red the differences between GCM_{SCEN} and GCM_{CTRL} and blue the differences between RCM_{SCEN} and RCM_{CTRL}.

An important plant available soil moisture storage increase as a consequence of the precipitation changes in the winter half-year is obvious in GCM_{SCEN} (fig. 6.7e). The increased runoff-generation in autumn (figs. 6.6c and 6.7c) is owed to the predicted seasonal precipitation increase and also caused by the decrease of the snowfall portion in that period. The additional rainfall allows a faster soil moisture content recovery that leads to increased runoff sensitivity to precipitation and secondarily slightly higher actual evapotranspiration (figs. 6.7c and 6.7f). Also the GCM_{SCEN} experiment determines that soil field capacity may be approximately reached before the start of winter (fig. 6.6e). As already discussed this was not the case for the simulations driven by GCM_{CTRL} (fig. 6.5e).

6.6. Discussion

The experimental use of PREVAH with meteorological forcing information from the ECHAM4 general circulation model and the regional climate model CHRM shows contradictory results. It has been shown that the average climatology from atmospheric models is fairly similar to the measurements at surface stations within the Valdai Hills area in the case of air temperature and global radiation. The most important limitation is the very poor representation of the seasonal cycle of precipitation. Such differences are caused in the case of CHRM by the limited available averaging period (six years) and presumably by uncertainties in the parameterization of convective precipitation. The GCM fails in reproducing adequately the seasonal cycle of precipitation, presumably owed to the difficulties in reproducing the Atlantic storm track and the propagation of synoptic systems into the continent.

The use of meteorological information from different sources allows qualitatively reliable analysis on the water balance and runoff regime of the Upper Volga catchment. The presented simulation experiments showed that climate change might cause an important temporal redistribution of the water resources at the Volga source area as a

result of the high sensitivity of snow-cover to temperature changes. The flood frequency might be positively affected by the reduction of snow accumulation, allowing a temporal redistribution of runoff, less dependent upon winter temperature and more dependent on winter precipitation. Figure 6.8 demonstrates that the relative frequency of daily runoff events exceeding 4 $mm \cdot d^{-1}$ might decrease of about 20%. In opposition the frequency of daily discharge between one and two $mm \cdot d^{-1}$ might increase of more than 20%.

The runoff-generation in the winter half year might no longer be limited to the main melt season in March-April but could be more evenly distributed over the whole period December to April.

7. Internal multiple-response verification of a water balance and runoff regimes simulation for the whole of Switzerland

7.1. Introduction

The simulation experiments with PREVAH discussed in the previous chapters basically rely either on an integral evaluation of the model quality at the catchment outlet by means of comparison to discharge observations, or on comparisons to plot observations of hydrometeorological records that might be located outside the investigated catchment (e.g. section 5.3.2). The evaluation of the quality of the simulation within the catchment domain was shortly addressed in section 5.2.2. in the framework of the simulation of a radiation-governed snowmelt event in the Rietholzbach catchment and its sub-catchments Huwilerbach and Upper Rietholzbach. With increasing area of the investigated domain, the number of integral observations decreases and, at the same time, those observations become valuable information for multiple-response internal evaluation.

The last experiment of this thesis therefore addresses the use of PREVAH for the spatially distributed simulation of a macroscale domain. The water balance and discharge regime for the whole of Switzerland (hereafter referred as CH-experiment) was determined for the 20-year period 1980-2000.

The CH-experiment partly relies on the set of daily meteorological data prepared by Menzel *et al.* (1999) for the determination of the mean annual actual evapotranspiration of Switzerland within the period 1973-1992, who used it to drive the TRAIN-Model (*Tra*nspiration-*In*terception Model, Menzel 1999). This set of daily meteorological observations includes all climate variables needed to run PREVAH except, for observed global radiation. Menzel *et al.* (1999) diagnosed the global radiation based estimates of the clear-sky direct radiation and spatially interpolated sunshine duration (Schulla 1997). The standard automatic stations of MeteoSwiss monitor global radiation only since 1980. The required information on observed global radiation was prepared for the period 1980-2000.

Table 7.1 Basic experimental settings of Menzel *et al.* (1999) and of the presented simulation experiment for the whole of Switzerland.

	MENZEL *et al.* (1999)	CH-experiment
Model	TRAIN	PREVAH
Investigated period	1973 – 1992	1981 – 2000
Spatial resolution	1 x 1 km^2	500x500 m^2 aggregated to HRUs
Time resolution	Input: 1 day Model internal: 1 day	Input: 1 day Model internal: 1 hour
Land-use classes	7 classes	17 classes
Meteorological information	absence of observed global radiation	availability of observed global radiation use of a precipitation climatology to adjust the spatially interpolated precipitation
Regionalization	9 regions	9 regions based on 2^{nd} -order streams
Meteorological sub-units	100 m elevation zones within the 9 regions	200 m elevations zones within the 2^{nd}-order streams of the 9 regions
Results	one evapotranspiration map	up to one map per day of the main components of the water cycle

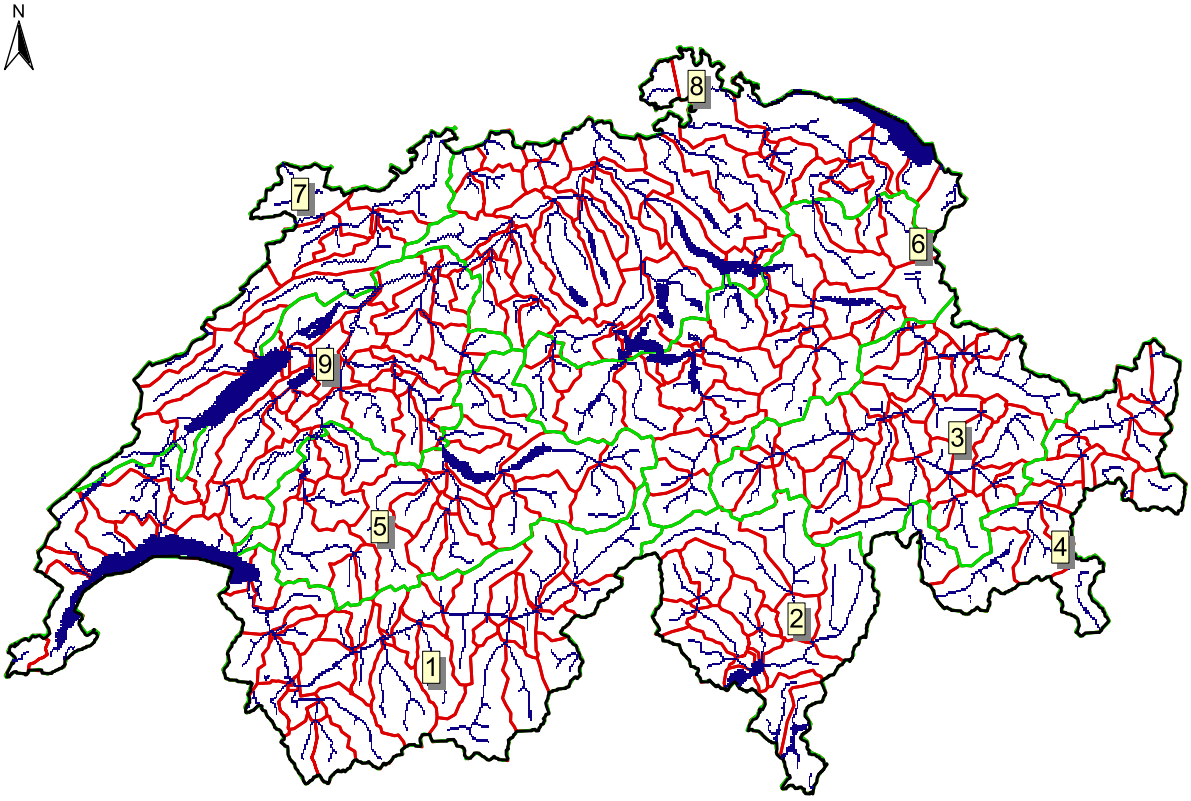

Figure 7.1 Regionalization of the meteorological information into 9 main climatological regions (green borders) and into 2nd order streams (red borders). Labels are declared in table 3.1.

The data set of the other meteorological variable was completed by preparing the missing period 1993-2000.

Table 7.1 indicates the differences in the experimental settings between the investigations of Menzel *et al.* (1999) and the CH-experiment. The CH-experiment considers the 21-year period 1980-2000, whereby 1980 was adopted as a initialization period and disregarded for evaluation purposes.

PREVAH was driven by daily meteorological data. The considered basic grid-spacing of 500x500 m^2, which is a reliable resolution for the investigation of a catchment with pre-alpine and high-alpine characteristics (chapter 4). To account for the main regional climatological differences, the domain of Switzerland was subdivided into nine climate units (figure 3.1 and 7.1 and table 3.1): (1) Wallis, (2) Ticino, (3) Alpine Rhine, (4) Engadin (the smallest region with 2572 km^2 area), (5) Alpine Aare, (6) Prealps, (7) Jura, (8) East Plains (the largest region with 7604 km^2 area) and (9) West Plains.

Each climate unit was considered, at a first stage, as a large catchment. A set of HRUs was determined for each climate unit based on further meteorological sub-units, aspect and land-use. The position of the grid elements with respect to the equilibrium line of glaciers was also taken into account to distinguish between pixels in the accumulation and ablation zone of glaciers. The meteorological sub-units within the nine climate units were defined on the basis of:

- the contributing area of 2nd-order streams (figure 7.1);
- the different 200 meters elevation zones within a specific 2nd order stream.

More than 2500 meteorological sub-units were considered. The average size of the meteorological units is approximately 16 km^2. The adopted spatial differentiation of the

meteorological information assumes that all the HRUs in the same climate unit, same contributing area of a 2nd-order streams and same 200 meters elevation zone are characterized by identical climatology.

Similarly to all previously discussed experiments with PREVAH, air temperature and global radiation are adjusted according to the slope and aspect of each HRU. Snowmelt and glacial melt were computed after the method proposed by Hock (1999) and defined by equations 5 and 6 (section 2.2).

7.2. Parameterization of the precipitation bias correction

The precipitation fields generated by the interpolation module of WaSiM-ETH from measured precipitation are not directly suitable for large-scale hydrological simulations. The techniques used (section 2.1.3) are not capable of capturing the regional climatological difference from region to region and internally to the defined climate units. A bias is present between observed and interpolated precipitation fields. Such a bias can be estimated by comparing simulated with observed discharges. For this experiment, the bias correction of precipitation (equation 1 in section 2.2.) is not tuned to obtain a good correspondence between observed and simulated discharges since none of the defined climate units can rely on representative undisturbed discharge observations.

The spatial distribution of precipitation published in the maps of yearly precipitation climatology for the Alps (1971-1990), prepared by Schwarb (2001, figure 1.3), was used to parameterize the bias correction for the precipitation fields interpolated by WaSiM-ETH. The map of Schwarb *et al.* (2001) relies on the data set prepared and described by Frei and Schär (1998), and is based on precipitation data that were not corrected for measurement errors. The systematic rain-gauge bias (Sevruk 1985) was corrected as proposed by Sevruk and Kirchhofer (1992). The correction of precipitation is identical both for liquid and solid precipitation. Spatial and gauge bias factors are introduced to adjust the daily precipitation data at each meteorological sub-unit. This is achieved by:

$$P_{PREVAH}^{i,d} = k_{gauge}^{i} \cdot k_{spatial}^{i} \cdot P_{WaSiM}^{i,d} \tag{26}$$

where i is the identifier of a specific meteorological sub-unit (MU). $P^{i,d}_{PREVAH}$ [mm·d^{-1}] is the adjusted daily precipitation. $P^{i,d}_{WaSiM}$ [mm·d^{-1}] is the daily precipitation at every MU as interpolated through WaSiM-ETH. $k^{i,}_{gauge}$ and $k^{i,}_{spatial}$ are two factors that relate to corrections associated with systematic rain-gauge and spatial biases, respectively. More specifically:

$$k_{gauge}^{i} = \frac{P_{corrected}^{i}}{\left(P_{corrected}^{i} - P_{correction}^{i}\right)} \tag{27}$$

where $P^{i}_{corrected}$ is the average corrected precipitation [mm·y^{-1}] in a MU after Kirchhofer and Sevruk (1992) and $P^{i}_{correction}$ the average correction [mm·y^{-1}] in a MU after Sevruk and Kirchhofer (1992).

The spatial bias correction $k^{i,}_{spatial}$ is obtained from the high-resolution precipitation climatology of Schwarb (2001) as:

$$k_{spatial}^{i} = \frac{P_{Schwarb}^{i}}{P_{WaSiM}^{i}} \tag{28}$$

where $P_{Schwarb}$ is the average precipitation [mm·y^{-1}] in a *MU* after Schwarb (2001) P^{i}_{WaSiM} is the biases average precipitation [mm·y^{-1}] in a *MU* as obtained using WaSiM-ETH in the period 1981-2000. Note that both $k^{i,}_{gauge}$ and $k^{i,}_{spatial}$ do not depend on the season, but are calculate for every sub-unit *i*.

7.3. Calibration strategy

The calibration strategy differed from the generally adopted calibration procedure (section 2.3). Since every climate unit (figures 3.1 and 7.1) was considered as a catchment and simulated separately by PREVAH, nine sets of model parameters must be calibrated.

A great part of the PREVAH tuneable parameters (section 2.3.2) are assumed to be catchment specific. It should be mentioned, at this point, that such an assumption might be sustainable in the case of microscale and mesoscale catchments, but may lead to large uncertainties and errors in macroscale model applications. This is mainly owed to the difficulty in the spatial interpolation of meteorological information for large-scale catchments, and to the lack of a spatially distributed parameter sets. Another disadvantage is the uncertainty of methods to parameterize the tuneable parameters according to the local characteristics of the HRUs and/or meteorological sub-units. This causes that a model parameter, such as the non-linearity parameter for the separation between runoff-generation and soil moisture recharge (section 2.2), is identical for all the HRUs within a climate unit. As an example: the simulation of a forested HRU located in the southern part of the climate unit Ticino at 600 m a.s.l. is governed by the same set of tuneable parameters also adopted for the simulation of a rocky HRU located at 2500 m a.s.l. in the northern part of the same climate unit.

Being aware of the above experimental shortcomings and restrictions, an objective was set. The main goal of the CH-experiment was to obtain a good agreement between observed and computed natural discharge regimes in different gauged sub-catchments of the climate units. Aschwanden and Weingartner (1985) published the Parde coefficients (equation 13 in section 2.2) and defined the discharge regime for more than 80 undisturbed Swiss catchments. A selection of 33 sub-catchments was considered to calibrate and evaluate the CH-experiment. The selection included the catchments whose area, average elevation and portion of glacerized areas (FOWG 2000) were reliably represented within the 500x500 m^2 data set of physiographic information used in this study (table 7.2).

The Swiss Federal Office for Water and Geology (FOWG) provided the monthly discharge rates. The Parde coefficients for the time range 1981-2000 were determined for the 33 considered catchments. For the catchment Schächen (basin label 12), only the period 1985-2000 was available and for the catchment Verzasca (label 32), the period 1990-2000 was available. The snowmelt and runoff-generation modules were tuned by comparing the observed and computed regimes, which were defined by the dimensionless Parde coefficients. The parameters of the snowmelt module were additionally tuned to allow for a good correspondence to two observed NOAA-AVHRR spatial patterns of snow-cover (15 February 1993 and 25 March 1998).

7.4. Analysis and evaluation

7.4.1 Data sets for internal multiple-response verification

The verification of the CH-experiment relied on the following data sets:

- monthly time series (1981-2000) of the discharge from 33 catchments, provided by FOWG (as a continuous data set and as a deviation from the average regime);
- snow water equivalent observations from more than 100 locations in Switzerland during the period 1981-1993 (Rohrer *et al.* 1994a and 1994b). The data set consists of 5 observations per winter (1 January, 1 February, 1 March, 1 April and 1 May). Approximately 65 observations per station are available;
- more detailed observations of the snow water equivalent in four locations within the landscape surrounding Davos (figure 3.4) for the period 1981-2000 ("SLF Messdaten © SLF 1999");
- 20 spatially distributed fields of the snow-cover distribution for the whole of Switzerland. This data set was provided by the MFB-GeoConsulting GmbH (Bern). The fields were processed from remote sensed observations with the NOAA-AVHRR satellite. The same fields are described by Apfl *et al.* (1995);
- the data from the lysimeter in Rietholzbach (section 5.1.2);
- the evapotranspiration map of Menzel *et al.* (1999);
- the results of Schädler and Weingartner (2002a and 2002b) on the Swiss natural water balance 1961–1990.

7.4.2 Evaluation of the discharge simulations

Due to the particular calibration procedure adopted in this experiment, the representativity of the average discharge regime within the period 1981-2000 for the verification of the model quality is questionable. The Parde coefficients influenced the manual assessment of the tuneable parameters. Therefore, the average signal of the monthly discharges cannot be used as an indicator for the model verification since no separate evaluation period was defined. However, the Parde coefficients are dimensionless and the bias correction for precipitation was parameterized a priori (eqs. 26 to 28). The volume bias between observed and simulated monthly mean discharge can therefore be adopted for model evaluation. The average monthly observed discharge was not considered for model tuning. Thus, the Nash-Sutcliffe score E_2, based on monthly values, can be used to evaluate the model quality. E_2 quantifies how the simulation is a better estimate of the observations than the period averaged observation (eq. 11).

Figure 7.2 shows to what extent the average monthly discharges, obtained after model calibration, and corresponds to the observed regime. The calibration allowed for the attainment of a plausible agreement between the observed and computed regimes in most of the considered catchments with undisturbed regime (catchment 17 is not plotted). The range of the typical Swiss regime types is wide (16 types after Weingartner and Aschwanden 1992):

- glacial and glacial-nival regime: catchments 1 to 8;
- nival regime: catchments 9 to 16;
- pluvial-nival regime: 17 to 21;
- pluvial regime: 22 to 28;
- meridional (south-alpine) regimes (both pluvial and nival): 29 to 33.

Table 7.2 Catchments selected for the calibration and verification of the CH-experiment. The basin label indicates an identifier for the catchments. F is the area in km^2, H is the average elevation in meters and G is the glacerized portion in percent.

Basin label	River	Gauge	FOWG (2000)			CH-experiment		
			F [km^2]	H [m]	G [%]	F [km^2]	H [m]	G [%]
1	Rhone	Gletsch	38.9	2719	53	38.5	2663	46.1
2	Massa	Blatten / Naters	202	2920	65.9	190.7	2924	68.7
3	Lonza	Blatten	77.8	2630	35.7	78.5	2676	35.7
4	Rosegbach	Pontresina	66.5	2716	31.1	64.7	2659	27
5	Simme	Oberried	35.7	2370	34.7	35.5	2303	21.1
6	Berninabach	Pontresina	107	2617	18.8	109.5	2599	19.4
7	Hinterrhein	Hinterrhein	53.7	2360	22.1	53.5	2400	22.9
8	Lütschine	Gsteig	379	2050	17.3	385.7	2080	17
9	Dischmabach	Davos	43.3	2372	2.3	43.25	2394	1.2
10	Reuss	Andermatt	192	2280	6.4	189.2	2269	5.5
11	Julia	Tiefencastel	325	2190	0.9	318.5	2209	0.4
12	Schächen	Bürglen	95.1	1800	3.7	110.7	1773	3.2
13	Plessur	Chur	263	1850	0	265.7	1868	0
14	Allenbach	Adelboden	28.8	1856	0	29	1869	0
15	Grande Eau	Aigle	132	1560	1.8	134	1566	0.7
16	Muota	Ingenbohl	316	1360	0.1	309	1343	0
17	Sitter	Appenzell	74.2	1252	0.1	76.2	1361	0
18	Thur	Stein	84	1448	0	84.7	1408	0
19	Emme	Emmenmatt	443	1070	0	445.5	1070	0
20	Kleine Emme	Malters	448	1070	0	477.2	1042	0
21	Urnäsch	Hundwil	64.5	1085	0	65	1125	0
22	Goldach	Goldach	49.8	833	0	50.5	817	0
23	Broye	Payerne	392	710	0	398.5	721	0
24	Langeten	Huttwil	59.9	766	0	64	767	0
25	Murg	Wängi	78	650	0	76.7	638	0
26	Töss	Neftenbach	342	650	0	340.2	629	0
27	Ergolz	Liestal	261	590	0	262.2	584	0
28	Mentue	Yvonand	105	679	0	100.5	682	0
29	Calancasca	Buseno	120	1915	0.7	119.7	1958	1.9
30	Poschiavino	La Rösa	14.1	2283	0	15	2317	0
31	Ticino	Piotta	158	2060	1.8	158.5	2063	2.5
32	Verzasca	Vogorno	233	1550	0	188.5	1663	0
33	Cassarate	Pregassona	73.9	990	0	70	946	0

During the periods considered by Weingartner and Aschwanden (1989) all the selected catchments were undisturbed. However, in the case of the considered period 1981-2000, several sub-catchments (nr. 7, 10, 11 and 31) were strongly influenced by anthropogenic activities, mainly by water diversion to hydropower plants. The qualitative intercomparison between observations and simulation shows that the largest part of the pluvial regimes in the sub-catchments located in the north-alpine plains can be described by PREVAH after the calibration of the model parameters.

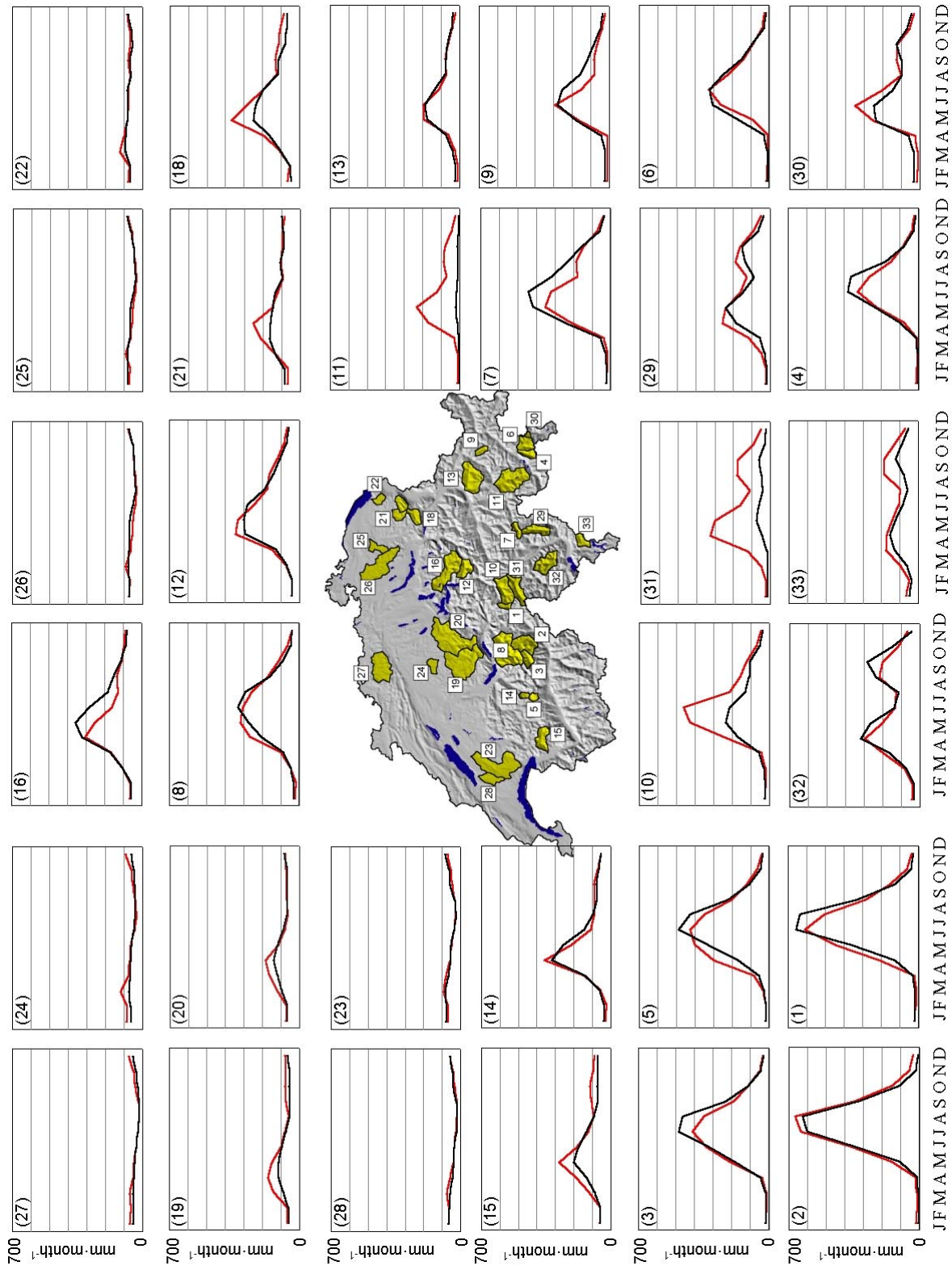

Figure 7.2 Observed and computed discharge regime for 32 Swiss catchments. The identifier of the catchments is specified in table 7.2. Catchments 7, 10, 11 and 31 are disturbed.

In many pre-alpine and alpine catchments, there are evidences that the amount of winter precipitation is underestimated (catchments 3, 4, 9, 16) or overestimated (catchments 12, 18 to 21 and 24). The typical meridional two maximum regimes are

governed by the south-alpine climatological characteristics. PREVAH is able to describe this regional behaviour correctly. In the case of some catchments in the south-alpine climate unit with meridional regime, the precipitation amounts are either overestimated (nr. 29, 30, and 33) or underestimated (nr. 32) throughout the year.

The determination of when the snowmelt season begins is the most deceiving aspect of the CH-experiment. The results show that a slightly wrong timing is present in the case of several sub-catchments (nr. 1, 5, 6, 8, 15, 29 and 33). This is the main negative feedback related to the regionalization of the model parameters to the whole climate units. The representativity of the snowmelt (and glacial melt) parameters at regional scale is not guaranteed when temperature-index based approaches are used (section 5.2.2). Such approaches show the best efficiency score when they are locally calibrated on the basis of detailed discharge observations. In the case of the sub-catchment Rhone (nr. 1), the large difference between actual (53%) and the parameterized (46.1%) glacerized portion may be responsible for the underestimation of the discharge between June and August.

The evaluation of the observed and computed discharge regime of the disturbed catchments allows for an estimation of the impact of dams and hydropower plants on the natural spatial and temporal distribution of the water resources in alpine environments. This strong impact is exemplary shown in the case of the river Julia (nr. 11). The present discharge regime consists of prescribed minima flows that the hydropower plants have to release in the river. The actual natural discharge regime would be similar to the regime observed for the Dischmabach and Plessur catchments (nr. 9 and 13).

The left-hand side of figure 7.3 visualizes a scatter plot of the obtained Nash and Sutcliffe coefficient E_2 versus the obtained average deviation between simulated (S) and observed (O) discharge for the considered catchments (labels). Two of the disturbed catchments are not plotted (E_2 below –15 and a volume error exceeding +70% between S and O).

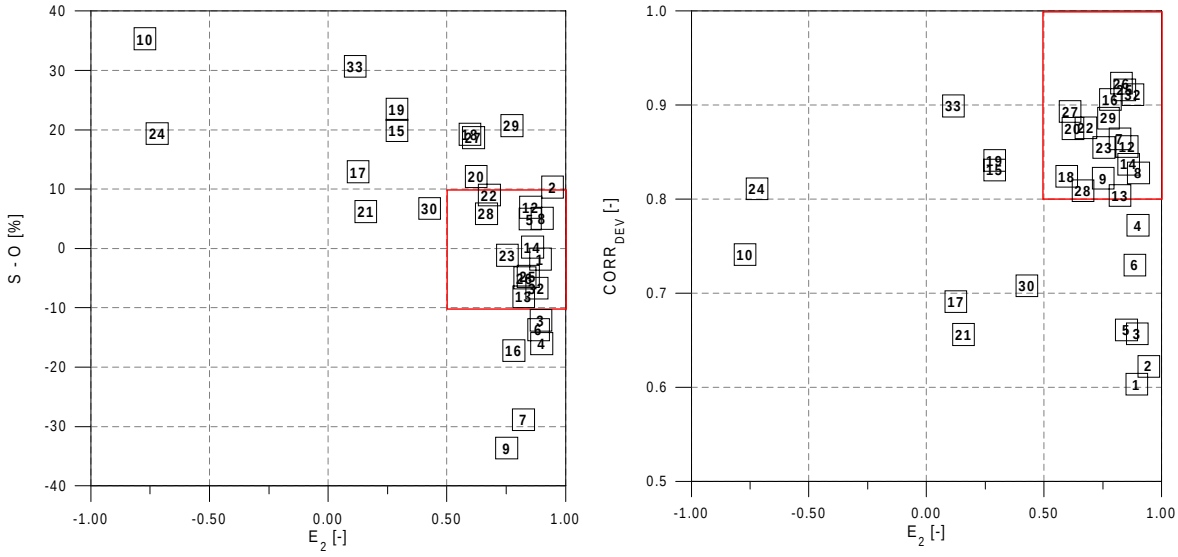

Figure 7.3 Discharge simulation in 33 catchments for the period 1981-2000. The labels are specified in table 7.2. Left: the obtained Nash and Sutcliffe efficiency score E_2 versus the obtained percentual deviation of the simulated (S) from the observed runoff (O), averaged over the entire period. Right: E_2 versus the obtained correlation ($CORR_{DEV}$) between the simulated and observed monthly deviations from the average computed, and observed, discharge regime, respectively (fig 7.2). The reason for the two red boxes is discussed in the main text.

The graph shows that PREVAH results have an efficient simulation in 12 of the sub-catchments; E_2 is above 0.5 and the absolute volume error between *S* and *O* is below 10%. Another 11 catchments are characterized by E_2 above 0.5, but the observed discharge is either underestimated (6 cases) or overestimated (5 cases) by more than 10%. This indicates a low accuracy of the assimilated precipitation fields. For 6 undisturbed catchments, PREVAH is not able to provide an efficient simulation (E_2 below 0.5) even though, in two cases, the volume error between *S* and *O* is below 10%. This speaks for the inadequacy of the assumed identity in the free model parameter within a climate unit.

The right-hand side in figure 7.3 shows E_2 versus the obtained correlation $CORR_{DEV}$ between simulated and observed month-by-month deviations from the average discharge regime (figure 7.2). $CORR_{DEV}$ indicates the model's capability for capturing the observed year-to-year deviation from the average regime. PREVAH is able to accurately describe the year-to-year variability ($CORR_{DEV}$ above 0.8) in the case of the largest part of the catchments with E_2 above 0.5. When E_2 is above 0.5, it is interesting to notice that $CORR_{DEV}$ is below 0.8 only in the case of heavily glacerized catchments (nr. 1 to 6). This leads to the conclusion that an E_2 clearly above 0.5 is not necessarily a guarantee for an efficient simulation of the year-to-year variability of observed discharge in high-alpine glacerized catchments. This behaviour is slightly less apparent for the climate unit Engadin (basins 4 and 6) than for the climate unit Wallis (basins 1 to 3) and Alpine Aare (basin 5).

For four of the eight sub catchments with E_2 below 0.5, PREVAH computes monthly discharge rates with $CORR_{DEV}$ above 0.8 when compared to observed values. That means that the problems are not due to the climatological representativity of the meteorological sub-units discretization but to the parameterization of the physiographic properties or to the reduced local representativity of the calibrated free parameters.

7.4.3 Verification of the local estimation for snow-cover and snow water equivalent

A second kind of internal verification of the results provided by the CH-experiment is the comparison of the simulated snow-cover and snow water equivalent to values yielded by a dense network of local observations of snow water equivalent. The data set used was prepared by Rohrer *et al.* (1994a and 1994b). The observed snow water equivalents were used for both a qualitative and quantitative model evaluation.

Figure 7.4 spatially displays how the model was able to predict the presence of snow-cover. Both the local observation and the correspondent pixel in the investigated domain were considered snow-covered when the snow water equivalent exceeded 1 mm. A correct prediction of snow-cover means that both the location and the pixel are either snow free (‘Zeros’, red portion on figure 7.4) or snow-covered (‘Hits’ blue portion on figure 7.4). ‘False alarms’ (light grey) mean an overestimation of snow-cover presence. ‘Misses’ (dark grey portion) indicates that the model is free of snow, while the observation indicated presence of snow.

In almost all locations, the portion of correct predictions is significantly larger than the portion of errors. A tendency to overestimate the snow-cover events is mostly evident along the pre-alpine hills of the climate units East Plains and West Plains and on the valley floors of the other regions. The overestimation, in some cases, is certainly caused by the fact that the pixel in the model may be located at a higher altitude than the location where the observation is made. In some locations, for the same reason, there is an underestimation in the presence of snow-cover (the pixel has a lower elevation than the respective location). Since the network of observed snow data shows a good spatial distribution within the nine climate units, it can be concluded that the quality of the regional snow-cover simulation with PREVAH is reasonably accurate.

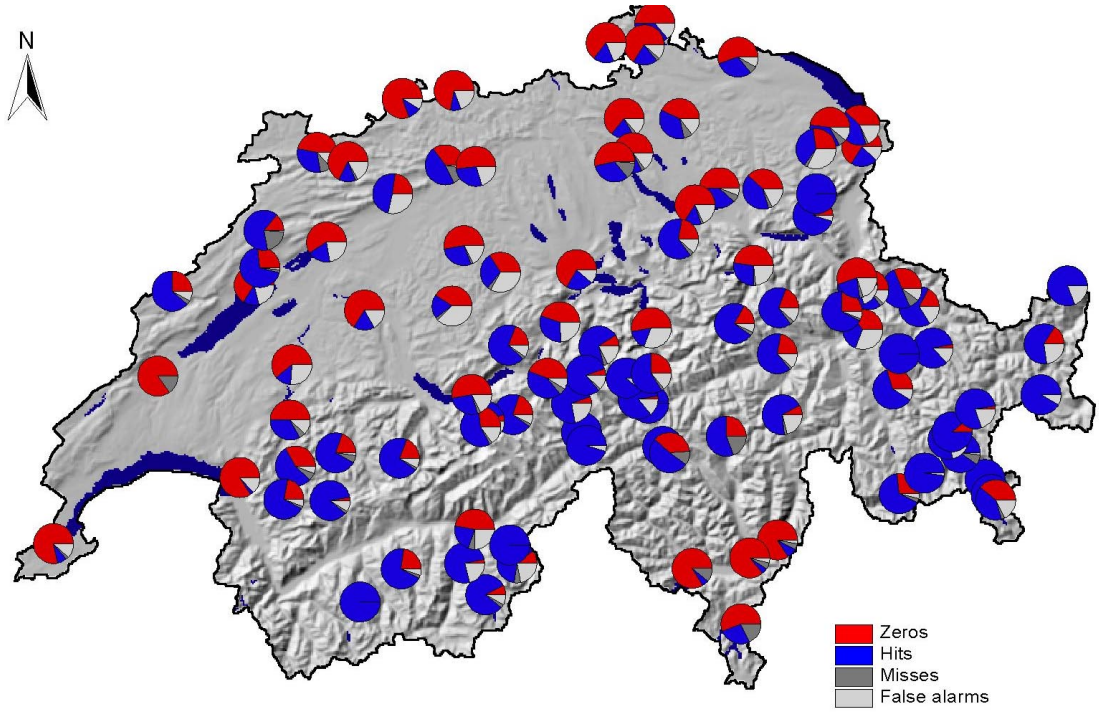

Figure 7.4 Simulation of the snow-cover presence (snow water equivalent > 1 mm) in the period 1981-1993 evaluated through comparisons to a dense network of local observations. The red portion defines the 'Zeros' (table 2.1, absence of snow is estimated correctly), the blue portion the 'Hits' (presence of snow is estimated correctly), the dark grey portion the 'Misses' (snow-cover only in the observed location) and the light grey portion the 'False alarms' (snow-cover only in the model output);

Figure 7.5 shows a quantitative analysis of the results presented in figure 7.4. Figure 7.5a shows the relation of the computed accuracy of the snow-cover prediction (section 2.3.5) at each of the 103 considered locations to the calculated correlation coefficient R_{OS} (section 2.3.3) between the respective actual values of the snow water equivalent (SWE). The symbols additionally indicate the difference in meters between the elevation of the pixel within the 500x500 m^2 grid of the digital elevation model and the elevation at the observed location. Although the achieved accuracy of the model is in the case of all the considered locations above 0.6, only one-third of them shows a R_{OS} between simulated and observed values above 0.8. Lower R_{OS} values occur not only where the bias in elevation between model pixel and target location is high, but also in the case of stations where the correspondence with respect to elevation is good. The low correlation is caused by both the over-/underestimation of the observed snow water equivalent and by uncertainties in the parameterization of the free parameters of the snowmelt module, which were assumed to be constant within a specific climate unit. The use of daily meteorology instead of the usually available hourly meteorological input may also cause a reduction in the snowmelt module quality. The simulation of snow accumulation is very sensitive to the daily cycle of air temperature. The temperature-index approach with an enhancement through a radiation term (Hock 1999) performs with higher reliability with an hourly meteorological input.

Figure 7.5b visualizes the quantitative comparison between observed and simulated snow water equivalent (SWE). The simulation shows the broad tendency to overestimate the observed SWE, in few a cases by a factor of 10.

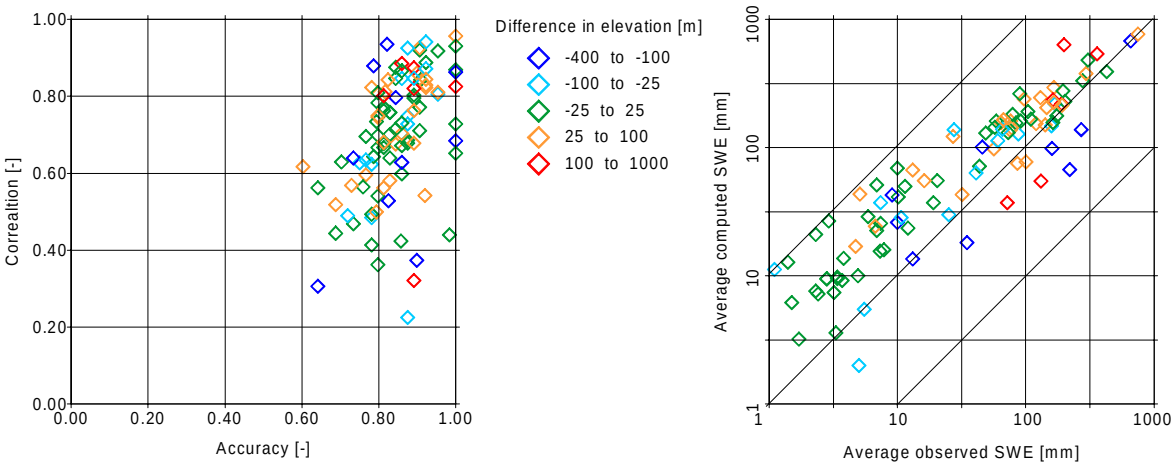

Figure 7.5 (a) Relation of the accuracy of the snow-cover presence simulation to the correlation between observed and computed time series of the snow water equivalent at 103 Swiss stations. (b) Comparison between the average observed and computed snow water equivalent (SWE). The colour of the symbols visualizes the magnitude of the difference in elevation between the pixel considered in the investigated domain and the station.

This tendency is not only observed in the case where the simulated pixel has a large difference in elevation with the observed location, but also concerns the pixels where such bias is below 25 meters. The comparisons shown in figure 7.5 indicate that the agreement between the observed and simulated snow water equivalents is positive only from a qualitative viewpoint. The quantitative agreement is somewhat poor. An overestimation of the observed SWE also speaks for an overestimation in precipitation during winter, and for possible errors in the local interpolation of the air temperature. Schwarb (2001) and Schädler and Weingartner (2002b) came to similar conclusions. They speculate that the adopted rain gauge bias correction (eq. 27) is much too high in some alpine and high-alpine areas.

Figure 7.6 shows the simulated and observed snow water equivalent at four sites within the landscape surrounding Davos (fig. 3.4). The sites are monitored by the Institute for Snow and Avalanche Research (SLF) in Davos ("SLF Messdaten © SLF 1999"). Observations are available for the period 1981 to 2000 at the stations Flüelastrasse (actual elevation 1560 m a.s.l., model elevation 1540 m a.s.l.), Büschalp (1960 m a.s.l., model 1767 m a.s.l.), Stillbergalp (1970 m a.s.l., model 2162 m a.s.l.) and Weissfluhjoch (2540 m a.s.l., model 2554 m a.s.l.).

The analysis of the 20 years time series outlines that, at the station Flüelastrasse where the model elevation agrees well with the actual elevation, the observed and simulated SWE pattern show good agreement. The SWE is slightly underestimated in the winters 1980/1981, 1982/1983 and 1998/1999. A small overestimation in the observed SWE is present in the winters 1990/1991 and 1991/1992. The timing of the snowmelt season is reproduced with fair accuracy.

At the station Büschalp, the elevation of the model point is 200 m lower than the actual elevation of the station. This lack of representativity considerably affects the agreement between the observed and simulated SWE. The simulation of PREVAH for the location systematically underestimates the observed SWE. This is a good example for the reason why point-observations are only conditionally reliable for the assessment of the quality of spatially distributed models. This shortcoming occurs mainly when the spatial discretization relies on low-resolution physiographic information.

Figure 7.6 Comparison of observed (black crosses) and simulated (red line) snow water equivalent SWE at four locations within the landscape surrounding Davos in the time range 1981-2000. "SLF Messdaten © SLF 1999".

At the station Stillbergalp, the same shortcoming is present. In this case, the elevation of the model point is 200 m higher than the actual elevation of the station. Due to this bias, a systematic overestimation of the observed SWE is expected. However, there is no evidence for any systematic overestimation. The simulated records fit the observations. This agreement actually indicates that the model underestimates the local value of the SWE. The simulated monthly discharges for the Dischmabach catchment (basin 9 in figure 7.2, see also figure 3.4) also indicated that the average winter precipitation assimilated by PREVAH underestimates the actual precipitation amounts in this landscape.

The latter observation is confirmed by the evaluation of the quality of the SWE simulation for the station Weissfluhjoch, where no relevant bias is present between the model elevation and its actual elevation. Beside the winters 1986/87, 1990/91 and 1994/1995, the estimated SWE shows the general tendency to underestimate the observations. The shape of the time series of estimated SWE show a good correspondence with the shape of the observed SWE.

7.4.4 Verification of simulated snow-cover patterns by means of remotely sensed images and categorical statistics

The information on snow-cover distribution, provided by earth observation satellites, enhances the more general view on the snow-cover obtained through point measurements

(see previous section). The use of observed spatial patterns represents the future of the evaluation of distributed hydrological models. Grayson and Blöschl (2001) presents a selection of recent case studies, where the quality of hydrological models was assessed by comparing recorded and simulated fields of hydrological variables, such as soil moisture fields and snow-cover pattern fields. The comparison between observed and simulated spatial patterns of the snow-cover distribution is one of the most currently adopted methods for the explicit verification of spatially distributed hydrological models. Blöschl *et al.* (1991) showed a model verification based on the comparison between an air photo of a partly snow-covered alpine landscape and the projection of simulated snow-cover data on the digital elevation model of that landscape. Wigmosta *et al.* (1994) and Strasser and Mauser (2001) determined the quality of the spatially distributed simulation of the snow-cover of large watersheds by comparing a picture of the snow-cover distribution detected by the NOAA / AVHRR satellite with simulated fields. Cline *et al.* (1998) assimilated several LANDSAT TM (Thematic Mapper) scenes and investigated the snow accumulation distribution in a small mountain basin by means of a coupled approach between remote sensed imagery and physically-based snow-cover modelling. Blöschl *et al.* (2002) verified a spatially distributed snowmelt model with 12 remotely sensed images of the SPOT XS satellite. Thus, they determined where the model shows systematic underestimations, and overestimations, of snow-cover and snow-water equivalent, respectively.

For this study a set of 20 processed spatial patterns of the snow-cover distribution for the whole of Switzerland could be accessed. The satellite data were detected by NOAA (National Oceanic and Atmospheric Administration). The images were sensed with the wide-angle AVHRR (Advanced Very High Resolution Radiometer) scanner. The snowfields were drawn from the remotely sensed images by means of digital image processing and GIS (Apfl *et al.* 1995). Apfl *et al.* (1995) analyzed these fileds to investigate the variation of the snowline in Switzerland during the winters 1983 / 1984 and 1993 / 1994. Their results are published in the Hydrological Atlas of Switzerland. The selection of the 20 spatial patterns is determined by the data source.

The spatial resolution of the remotely sensed snow patterns fields is 1x1 km^2. The conversion of the fields into the adopted 500x500 m^2 structure was completed by splitting the original 1x1 km^2 grid elements into four identical 500x500 m^2 grid elements. This procedure is a source of uncertainty in the case of grid cells where the snow-covered pixels are surrounded by one or more snow free pixel and vice versa. The pixels representing large water bodies were not considered in the analysis of the recorded spatial patterns. This is owed to the fact that PREVAH directly transforms the snow amounts falling on pixels classified as water body into input for the runoff-generation modules. The information included in the processed satellite images is a binary signal: either is a pixel snow free ('zero') or snow-covered ('one'). The agreement between observed and simulated snowfields was assessed by means of categorical statistics (Section 2.3.5). All the simulated fields were also transformed into binary fields: 'zero' in the case of a snow free pixel (snow water equivalent $\leq$ 1 mm) and 'one' in the case of snow-covered pixels (snow water equivalent > 1 mm). The choice of threshold for the generation of binary fields (1 mm) from simulated snowfields was set without any sensitivity analysis to the observed fields.

As mentioned above, the analysis of two NOAA / AVHRR images of the snow-cover (15 February 1993 and 25 March 1998) was considered for the manual assessment of the free parameters of the snowmelt module. Figure 7.7 shows two examples of the snow-cover distribution simulation in Switzerland. The model captures the observed snow-cover patterns with high accuracy in both April and June 1984; the largest uncertainties are present in the pre-alpine area and in the climate unit Jura.

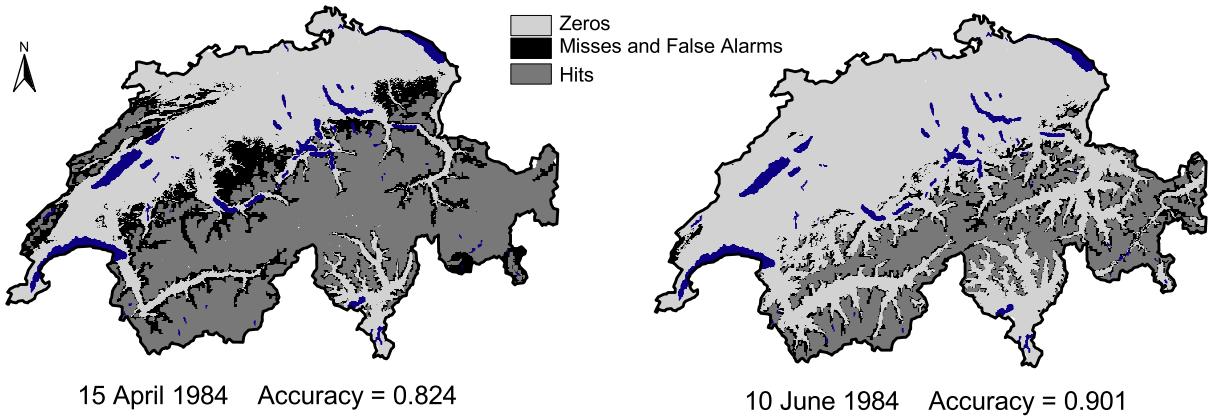

Figure 7.7 Observed (NOAA-AVHRR) and simulated patterns of the snow-cover distribution in Switzerland for two deadlines in spring 1984. Large water bodies (blue) are not counted in the analysis. The accuracy after equation 14 is also indicated. The 'Zeros' and the 'Hits' indicate correct forecasts.

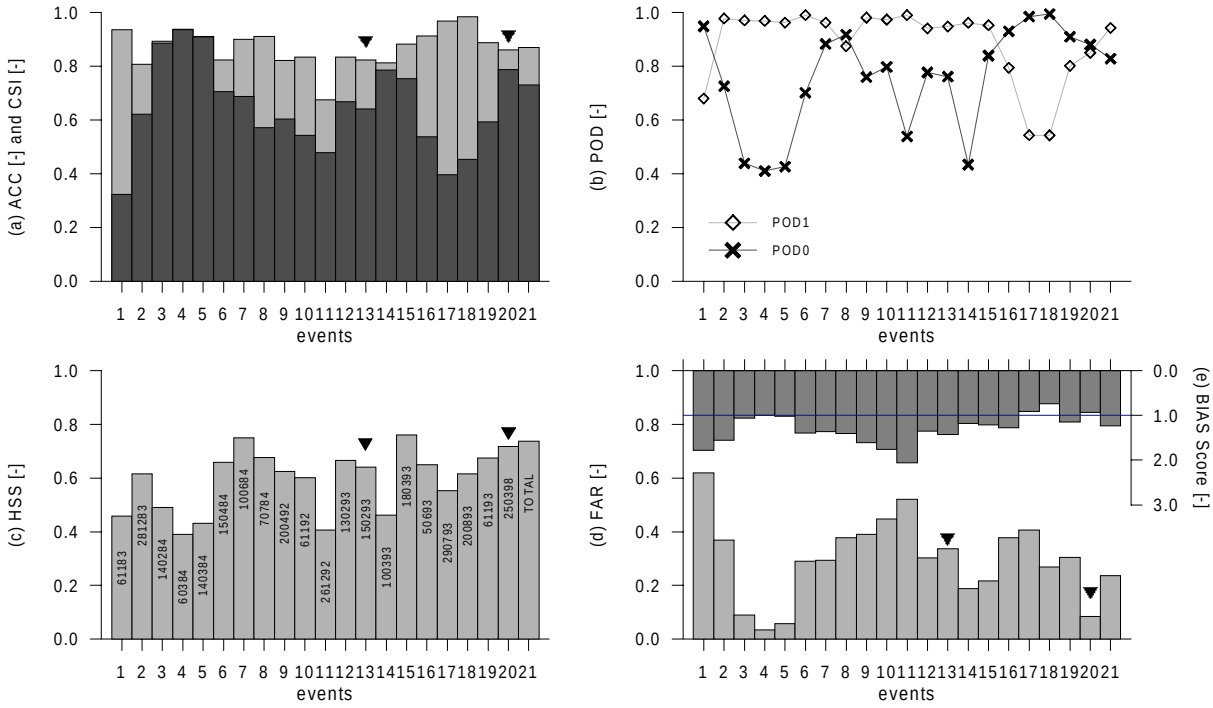

Figure 7.8 Categorical statistics (section 2.3.5) between 20 simulated snow-cover patterns and 20 snow patterns observed by the NOAA-AVHRR satellite. The two events labelled with a triangle were considered for the manual calibration of PREVAH. (a) Accuracy (ACC) and Critical Success Index (CSI). (b) Probability of detecting 'Hits' (POD1) and 'Zeros' (POD0). (c) Heidke skill score (HSS). (d) False alarm ratio (FAR). (e) Bias score (BIAS).

In more than 80% of the pixels the model correctly represents the presence or absence of snow-cover in both April and June. In the presented example, PREVAH was able to capture the ablation of snow within the Swiss Alps with good quality.

Figure 7.8 shows a detailed comparison between the 20 satellite images and the corresponding observed fields. Figure 7.8a displays the attained accuracy (ACC) and CSI score (critical success index) of the simulated fields when compared to the NOAA / AVHRR images. With the exception of the field on 26 December 1992 (very large

overestimation of snow covered pixels), the accuracy score between observed and computed fields is above 0.8. The integral accuracy for all pixels and considered events is 0.87. The CSI score is not sensitive on the snow free events ('zeros'). A CSI lower than ACC means that the cases of snow-covered pixels are either overestimated or underestimated. Thus, if the probability of detecting snow-covered pixels POD1 (fig. 7.8b) and the false alarm ratio FAR are high (fig. 7.8d) then snow-cover is overestimated. If the probability of detecting snow free pixels POD0 is high (fig. 7.8b) and CSI is low, the snow free cases are overestimated. The average POD1 is 0.94, while the average POD0 is only 0.83. This means that the high POD1 is due to a systematic overestimation of snow-covered pixels. This indication is confirmed by the average BIAS score of 1.23 (figure 7.8e). Of the 20 events, 14 show a clear positive BIAS score and only 3 a negative BIAS score. The analysis of the snow-cover patterns confirms the results of the above presented model verification by means of local observations of the snow water equivalent (figure 7.4 and 7.5): PREVAH tends to overestimate snow-cover.

An event where the snow free pixels are much more than the snow-covered pixels has a larger random predictability than an event with an equal distribution of pixel with / without snow. The Heidke Skill Score HSS (figure 7.8c) allows for the quantification of the improvement yielded by the model with respect to a random forecast quality, as guaranteed by the marginal distribution of events and non-events in the observed and simulated fields. Thus, HSS is a more representative score for the relative quality in the simulation of the various events. HSS exceeds 0.4 in all considered events. This indicates that the model predicts a minimum of 40% of the not randomly predictable pixels correctly. This speaks for the integral quality of PREVAH in representing the snowfields in those two winters with large availability of remotely sensed snow-cover pattern images.

Categorical statistics can also be adopted for the determination of the average spatial quality of the snow-cover predictions. Figure 7.9 displays a pixel-by-pixel verification of the agreement between the simulated fields and the remotely sensed images. Figure 7.9a shows the attained accuracy at all the 500x500 m^2 pixels in the investigated domain. Figure 7.9b shows the respective bias score. Opposite to the accuracy that is defined for all pixels, the bias score is defined only if snow-cover is detected for at least one of the satellite scans (equation 17 and table 2.1 in section 2.1). Such a condition is not met in the lowest elevation ranges of the climate unit Ticino and in the surroundings of the Lake of Geneva and Constance. The accuracy values closest to the optimal value ‘1’ are found in the plains, where snow-cover is seldom, and in the highest elevations of the Alpine mountains, where snow-cover is always present. Accuracy values below 0.5 represent less than 1% of the pixels. Again, the largest uncertainties are located in the northern pre-alpine landscapes of the Alpine ridge. Other critical locations are the hills in the transition zone between the valley’s plains and the upper part of the valley’s slopes. This behaviour is mostly evident in the climate units Wallis and Alpine Rhine. There are several plausible reasons for such a disagreement: an over / underestimation in precipitation, uncertainties in the determination of the local temperature gradients, and in the determination of the model free parameters. An overestimation of snow-cover frequency in wind-exposed and / or very steep locations may also be caused by the missing parameterization of snow drift processes (e.g. Blöschl *et al.* 2002) in PREVAH. Analogously, snow-cover may be underestimated in locations protected from strong winds and in depressions in the landscape where the drifted snow deposits.

The analysis of the bias score map (figure 7.9b) allows for further interpretations. The bias score is closest to the desired value 1 in the highest elevation ranges, in the climate unit Jura and in the more rural parts of the large plains in the north-alpine climate units. The critical regions identified in the case of the accuracy map (figure 7.9a) are confirmed.

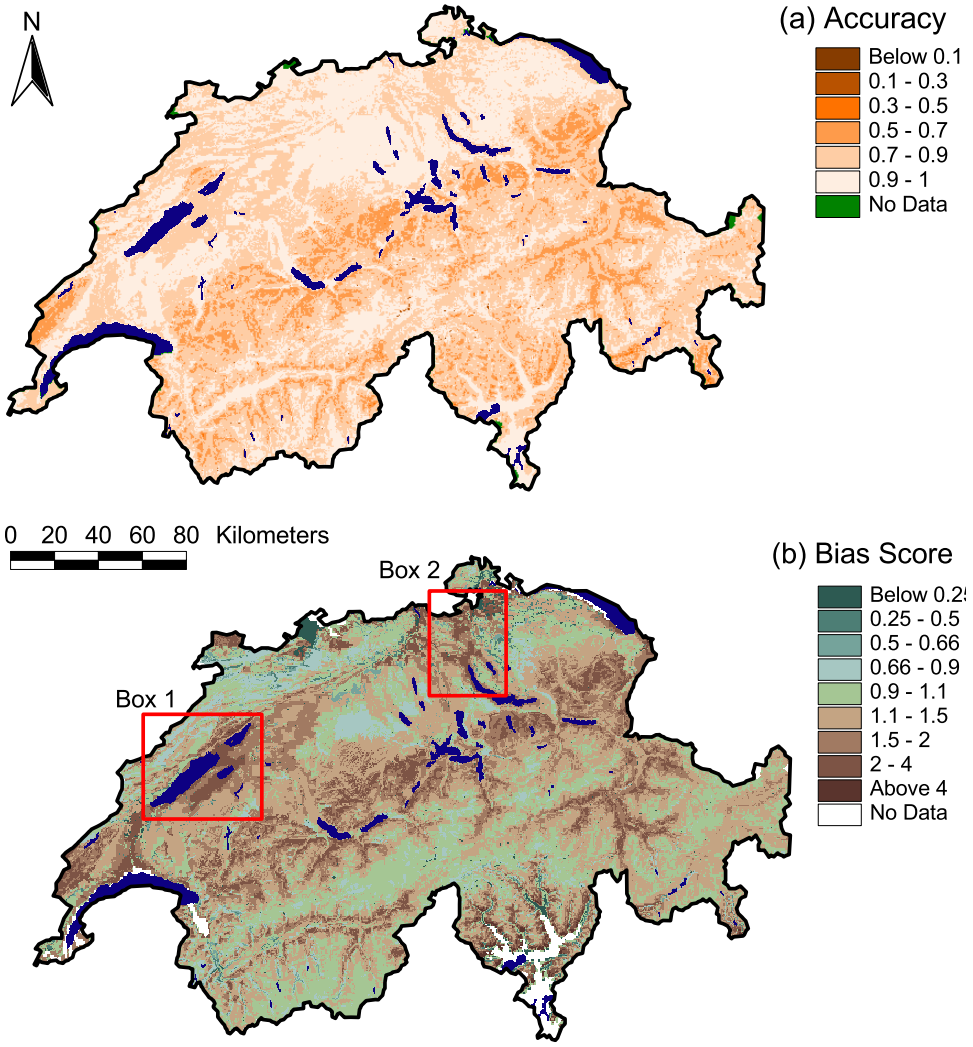

Figure 7.9 Pixel-by-pixel categorical statistics between 20 observed (NOAA-AVHRR) and simulated patterns of the snow-cover distribution in Switzerland. Upper plot: local accuracy for each pixel. Lower plot: local bias score. The bias score is not defined ('no data') in the pixels that were always snow free when a satellite image was scanned. The two sub-domains in the red boxes are discussed in more detail in the main text.

The most intriguing features of the bias score map are the bias values clearly above 1.5 in the regions east of the three lakes (Neuchâtel, Biel and Murten, box 1 in figure 7.9b), and in the urban and industrial surroundings of Zürich (box 2 in figure 7.9b). The large lakes are, in winter, generally much warmer than the advected air masses. The regions surrounding those lakes are influenced by the microclimate of the lakes, which can lead to higher air temperatures in the lower parts of the atmospheric boundary layer. Since west-winds are dominating in northern Switzerland, it is suggested that the blowing wind mixes with warmer air on the lake surfaces and influences the processes of snow accumulation and snowmelt in the eastern surrounding regions.

This could be a climatological explanation for the observed overestimation of snow-cover in box 1. PREVAH do not account for possible feedbacks between the winter temperatures of the lake surface and the microclimate of the surrounding regions.

A similar explanation may also be plausible for box 2. Here, the local microclimate is governed by both the Lake of Zürich and by urbanization.

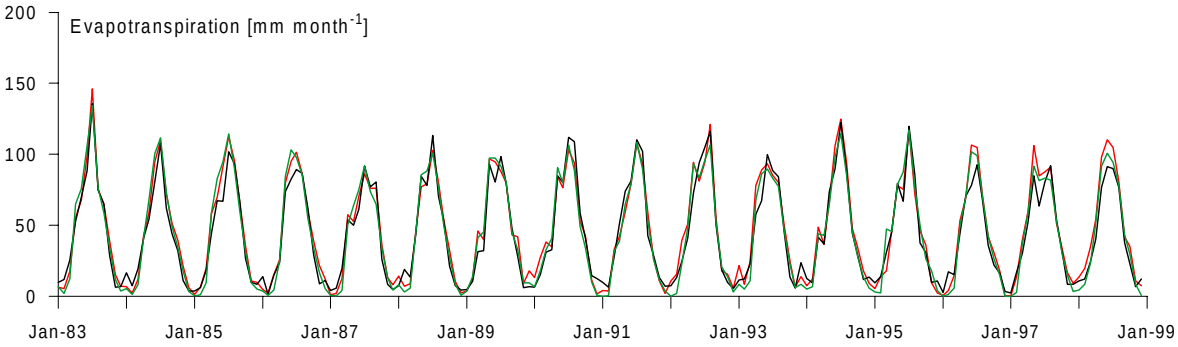

Figure 7.10 Comparison between the evapotranspiration observed at the Rietholzbach lysimeter site (black line) and the simulated values of both the model run with hourly meteorology (red line) and daily meteorology (CH-experiment, green line).

The surface air temperature of highly urbanized regions is perturbed by the most various kinds of anthropogenic activities (heating, industry, private transports, electrification). The overestimation of snow-cover frequency in box 2 may signalize that urbanization influences the acceleration of snow melting in its surroundings. However, it is to note that the network of air temperature measurements in urbanized areas is particularly dense and, therefore, the influence of urbanization on the local climatology should be included in the meteorological input data.

7.4.5 Comparisons to the evapotranspiration records of the lysimeter in the Rietholzbach catchment

The long-term records of monthly evapotranspiration at the Rietholzbach lysimeter are used here for a qualitative verification of the CH-experiment. Figure 7.10 shows a comparison between simulated and observed evapotranspiration for the lysimeter site water balance for the period 1983-1998.

The CH-experiment time series for the lysimeter show, in the case of evapotranspiration (ET), a good agreement to both the observed records and the time series obtained by plot-scale simulations.

The year-to-year variability in the seasonal pattern of evapotranspiration is not particularly large. However, PREVAH is able to reproduce this small variability in both the plot-scale run and the CH-experiment with good agreement. As an example the year 1983 is characterized by high ET values in summer, while the summer in the years 1987 and 1993 is characterized by lower ET rates, when compared to the long-term average. The model results follow such year-to-year variability with good agreement.

7.4.6 Plausibility of the computed components of the natural water balance of Switzerland

Schädler and Weingartner (2002a and 2002b, hereafter referred as SW02) computed the components of the natural water balance for approximately 300 medium-scale Swiss catchments (100-200 km^2). The total extension of these catchments covers the whole of Switzerland. SW02 considered the period 1961-1990. Their determination of the natural water balance relies on the computation of precipitation from detailed observations of the natural discharge, from the evapotranspiration map of Menzel *et al.* (1999) and from publications on the long-term mass balance of Swiss glaciers.

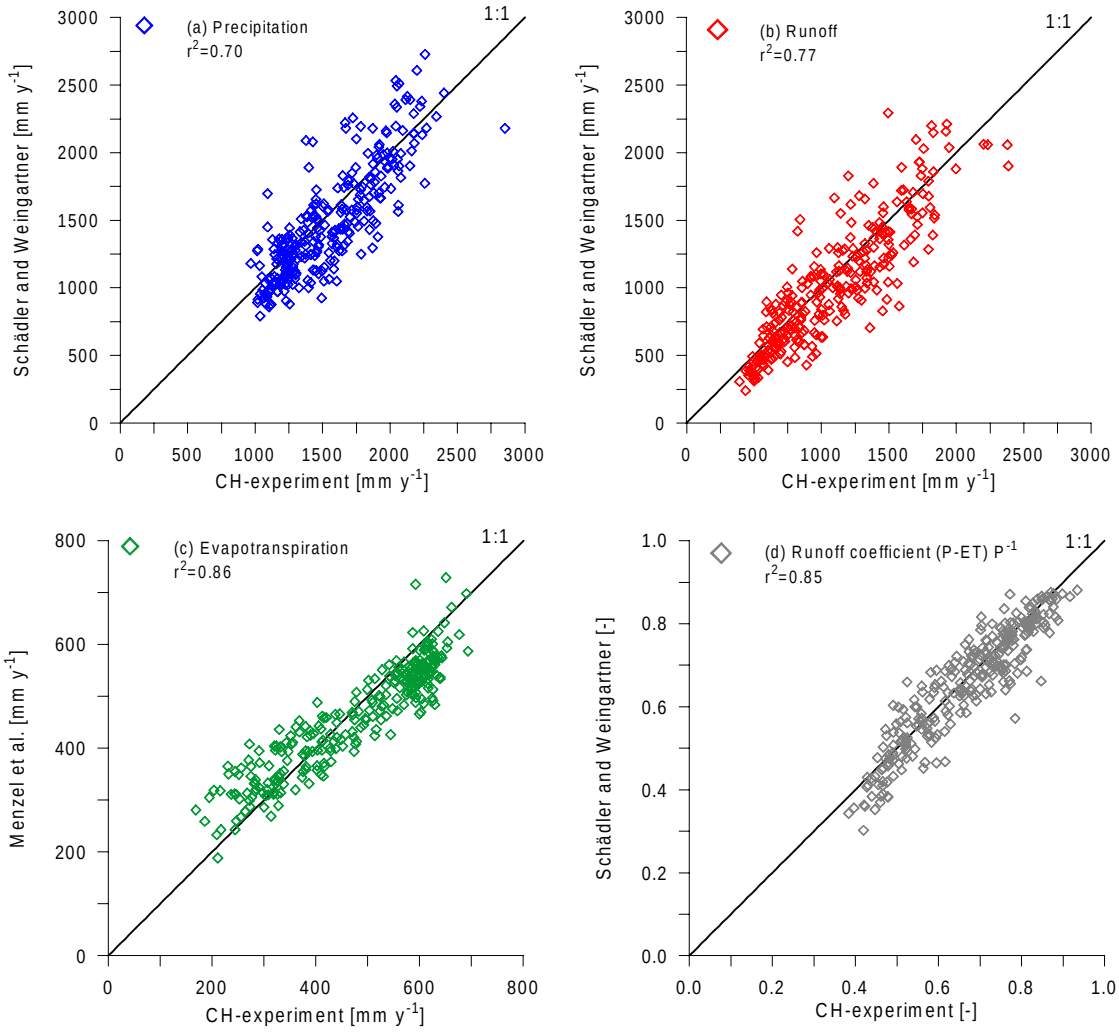

Figure 7.11 Comparison between the components of the natural water balance of medium-scale Swiss catchments as determined in this study (1981-2000) and as published by Schädler and Weingartner (2002a) for the period 1961-1990. (a) Assimilated precipitation (x) versus precipitation obtained from water balance considerations (y). (b) Simulated runoff (x) versus observed, regionally adjusted, runoff (y). (c) Simulated evapotranspiration with PREVAH versus simulated evapotranspiration with TRAIN (Menzel *et al.* 1999). (d) Runoff coefficient determined from the results of the CH-experiment versus the runoff coefficient proposed by Schädler and Weingartner (2002a).

The results of the CH-experiment were aggregated for the medium-scale catchments considered by SW02. The map of the medium-scale catchments was provided by FOWG. Figure 7.11 displays four scatter plots that summarize the results of the intercomparison between the CH-experiment and SW02. Such comparison may help to assess the plausibility of the spatially distributed simulations of the CH-experiment. The components of the natural water balance of the considered medium-scale catchments determined by the two studies are well aligned along the 1:1 line in case of precipitation (figure 7.11a), runoff (7.11b), evapotranspiration (7.11c) and runoff coefficient (7.11d). The r^2 correlation of linear regression is for all four scatter plots exceeds 0.7.

The qualitative comparison to SW02 indicates that PREVAH yields plausible average estimates of the natural water balance of Switzerland. The differences in natural water

balance of the considered medium-scale catchments are owed to a great extent to differences in the experimental settings between the two studies.

A first reason for the differences is the different periods, which were considered by two studies. Schädler and Weingartner (2002b) show that both precipitation and evapotranspiration show an increase of up to 5% between the two 30 year period averages 1946-1975 and 1961-1996. This analysis agrees with the hypothesis of an intensification of the mean hydrological cycle as a follow of the gradual increase of the average temperature over Europe formulated by Frei *et al.* (1998). The climatological variability could therefore explain differences of approximately 5% between the experimental results with PREVAH and SW02. SW02 assume that the evapotranspiration map of Menzel *et al.* 2002 yields plausible values for all the considered medium-scale catchments.

Perl (2002) completed detailed comparisons between Menzel *et al.* (1999) and the evapotranspiration map obtained through the CH-experiment. Menzel *et al.* (1999) computed higher evapotranspiration values for water bodies (+11%) and glacerized surfaces (+9%) and lower values for urban areas (-16%) when compared to CH-experiment. A regional analysis (Perl 2002) indicates that Menzel *et al.* (1999) computed higher evapotranspiration in the case of the climate units Wallis (+17%) and Ticino (+10%), while the values determined for the climate unit Jura (-14%) are distinctly lower when compared to the results of the CH-experiment. The scatter plot presented in figure 7.11c confirms the good correlation between both evapotranspiration maps. The r^2 correlation of linear regression is 0.86. PREVAH shows higher evapotranspiration values in the medium-scale catchments with higher average evapotranspiration. These are the catchments located in the lower elevation ranges with higher portion of urban areas. In the case of catchments located at higher elevation with lower average evapotranspiration, the results of Menzel *et al.* (1999) show slightly higher evapotranspiration values when compared to the results of PREVAH.

This behaviour is caused by the different parameterization of evapotranspiration from snow and from glaciated areas and, probably, by the different average duration of snow-cover between the two experiments. The duration of the snow cover at one location is governed by the amounts of precipitation and seasonal temperature cycle. A longer duration of snow cover causes lower evapotranspiration values during spring. This is due to the higher albedo of snow, which leads to a reduced availability of energy for evapotranspiration. Sections 7.4.3 and 7.4.4. showed that the simulations of snow cover for the whole of Switzerland are in good agreement with the observations in both time and space. Similar comparisons are not provided by Menzel *et al.* (1999). The climatological regionalization considered by Menzel *et al.* (1999) assumes that all the grid elements within the same 100 m elevation range of a climate unit have identical climatology. The work of Schwarb *et al.* (2001) demonstrates that the climatology of precipitation internally to the considered climate units is characterized by large small-scale variability. Figure 1.3 visualizes that this small-scale variability is particularly high in the climate units with alpine character (Wallis, Ticino, Alpine Rhine). From this point of view, the climatological regionalization and the adjustment of precipitation based on 2^{nd}-order sub-catchments and 200 m elevation ranges considered for the CH-experiment certainly represents an improvement when compared to Menzel *et al.* (1999). The evapotranspiration map obtained with the CH-experiment may therefore substitute the map of Menzel *et al.* (1999) for the diagnosis of the precipitation with the method proposed in Schädler and Weingartner (2002b).

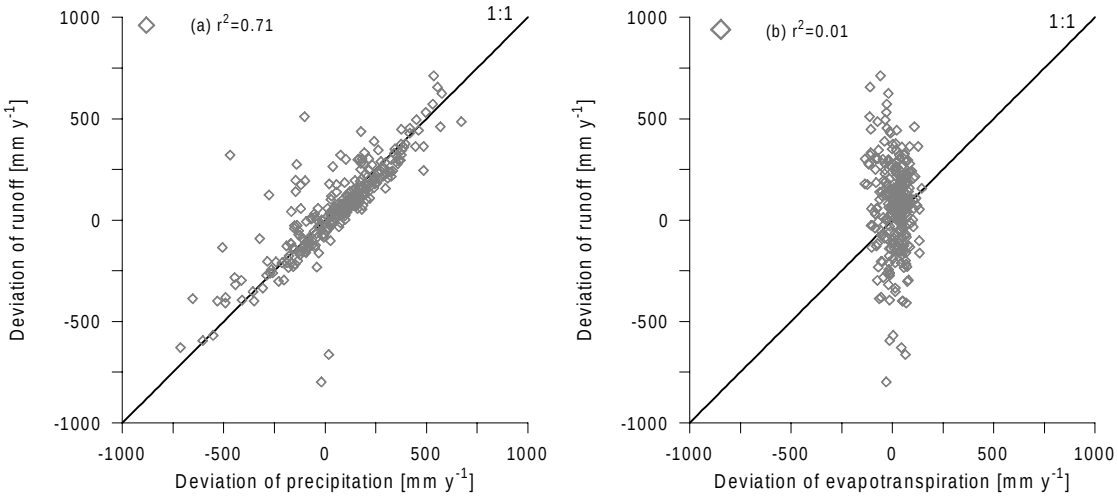

Figure 7.12 (a) Correlation between the deviation in average precipitation (CH-experiment minus SW02) and the deviation in average runoff. (b) Correlation between the deviation in average evapotranspiration and the deviation in average runoff.

The good correlation of the linear regression between the runoff coefficients determined by SW02 and by PREVAH ($r^2 = 0.85$) indicates that the correspondence of the average hydrological behaviour of the considered medium-size catchments is similar for both studies (figure 7.11d).

Figure 7.12a shows that the deviations in the average runoff and precipitation between the CH-experiment and SW02 are highly correlated, while figure 7.12b indicates that the differences in evapotranspiration are not correlated to the differences in the discharge. More than 70% of the differences in the average runoff can be explained by the differences in the average precipitation.

This finding might allow for an improved parameterization of the bias adjustment for precipitation (section 7.2) and for a better correspondence of the results of PREVAH to the regionalized map of the observed discharges prepared by SW02. This additional bias correction is justified to account for the reduction of the precipitation gradients in alpine and high-alpine regions. A similar conclusion was discussed in more detail in section 5.3.4.

7.5. A map for the basic natural runoff regimes of Switzerland

The dimensionless monthly Parde coefficients (*PC*, equation 13 in section 2.3.4) can be used to define a catchment discharge regime. The seasonal shape of the monthly *PC* allows for a classification of the regimes. Weingartner and Aschwanden (1989) published a plate on the natural (or slightly disturbed) discharge regimes of more than 80 Swiss catchments and respective tributaries in the Hydrological Atlas of Switzerland.

The completed CH-simulation provides spatially distributed information on runoff-generation with a resolution of 500x500 m^2, which is different from Weingartner and Aschwanden (1989), who only considered integral catchment regimes (as presented in figure 7.2). The monthly *PC* can be determined for each of the pixels, and used to determine the specific discharge regime at each pixel. A three steps decision scheme was introduced to classify the pixel-regimes:

- the determination of the season with average discharge maximum;
- the determination of the season with average discharge minimum;

- the classification of the magnitude M_Q of the average monthly discharge maximum Q_{max} [mm·month^{-1}], as defined by equation 29:

$$M_Q = INT\left[\log_{10}\left(2 \cdot Q_{\max}\right)\right] \tag{29}$$

Winter includes the months December, January and February (DJF, code '1'). Spring includes March, April and May (MAM, code '2'). Summer was defined in the months June, July and August (JJA, code '3'). September, October and November (SON, code '4') defined autumn. M_Q assumes integer values of '1' (low), '2' (moderate) or '3' (high). Thus, a three digits code was built. As an example, a pixel with maximum runoff-generation in April ('2', 1st digit), minimum runoff-generation in September ('4', 2nd digit) and a moderate M_Q ('2', 3rd digit) has a classified pixel regime defined by the code '*242*'.

The proposed three rules classification allows for the distinction of a maximum of 48 discharge regime classes. The code was determined on the basis of the declared decision scheme for all the pixels included in the computational domain of the CH-experiment, except for the pixels of large water bodies (lakes and large reservoirs). All pixels sharing the identical code are assumed to have the same basic-regime. The processing of the computed monthly averaged discharge of the CH-experiment showed that there only 26 effectively occurring regime-classes. The obtained classes can be considered as the basic regimes that govern the integral natural regime of Swiss catchments. Only 16 of the 26 regimes are shared by more than 400 pixels (10 km^2). Pixels with code regimes that occur less than 400 times have been assigned to another regime-classes with a similar code.

Table 7.3 Classification of typical basic-regimes of Switzerland based on a three-step decision scheme. D_{max} indicates the season where the average discharge maximum occurs. D_{min} indicates the season where the average discharge minimum occurs. M_Q is defined by equation 29 and indicates the magnitude of the average discharge maximum. The last column indicates the average portion of each of the 16 defined basic-regimes for the whole of Switzerland.

Type	D_{max}	D_{min}	M_Q	Portion [%]
Pluvial I	DJF	JJA	moderate	11.5
Pluvial II	MAM	SON	moderate	5.50
Pluvial III	DJF	MAM	low	0.45
Pluvial-sec I	DJF	SON	low	0.44
Pluvial-sec II	DJF	SON	moderate	2.64
Pluvial-sec III	MAM	SON	low	1.54
Pluvial prealpin	MAM	JJA	moderate	26.8
Pluvio-nival	MAM	MAM	moderate	0.57
Nivo-pluvial inferieur	MAM	DJF	moderate	24.7
Nivo-pluvial superieur	MAM	DJF	high	2.00
Nival inferieur	JJA	DJF	moderate	3.11
Nival superieur	JJA	MAM	high	3.92
Nivo-glacial inferieur	JJA	DJF	high	4.20
Nivo-glacial superieur	JJA	MAM	moderate	8.47
Pluvial meridional I	SON	JJA	moderate	0.24
Pluvial meridional II	SON	DJF	moderate	3.92

Table 7.3 defines the 16 basic-regimes occurring in Switzerland. Figure 7.13 displays the spatial distribution of the obtained 16 basic-regimes. The area of the 33 catchments considered for the previous analysis (section 7.4.2) is also visualized. The name of the regime types was assigned following, as far as possible, the definitions of Weingartner and Aschwanden (1989).

Half of the pixels are either classified as regime type *'pluvial prealpin'* (26.8%) or *'nivo-pluvial inferieur'* (24.7%). The *'pluvial pre-alpine'* basic-regime is characterized by high-flows in spring and limited runoff-generation in summer, when evapotranspiration is the dominant component of the hydrological cycle. The *'nivo-pluvial inferieur'* basic-regime is typical for regions with a small, but distinct snowmelt-season in spring and early summer. Further, the runoff-generation is controlled and limited by the evapotranspiration. The relatively high portion of those two regimes is due to the fact that they are typical for the elevation ranges between 400 and 1200 m a.s.l. The area in Switzerland (approximately 53%) is included between these two elevation ranges.

The highest urbanized areas of Switzerland are located along the Lake of Zürich and are characterized by a very steady regime (*'pluvial III'*). The most densely populated areas of northern Switzerland are, to a great extent, urbanized/industrialized and are characterized by a rainfed discharge regime (*'pluvial I'*). In a few rural and urbanized parts of Switzerland, at altitudes below 600 m a.s.l. (e.g. the floor of the climate unit Wallis), there are more dry regimes (*'pluvial sec I, II & III'*). In these regions the runoff-generation is largely reduced because the hydrological cycle is strongly dominated by evapotranspiration and reduced precipitation amounts (figure 1.3).

The typical alpine regimes show a very high dependence on elevation as a direct consequence of the timing of the main snowmelt season. The catchments Emme and Kleine-Emme (labels 19 and 20 on table 7.2) are typical for the transition between Prealps and Alps. Their discharge regime is determined by the combination of the basic-types *'pluvial prealpin'* and *'nivo-pluvial inferieur'*.

In the sub-catchment Lütschine (label 8 on table 7.2) of the climate unit Alpine Aare, a gradual transition from lowland to high alpine regime-types is generally evident. The floor of the main valley in the drainage system of the river Lütschine is characterized by a *'pluvial prealpin*' regime, which is basically rainfed. With increasing elevation, a succession of different regimes is found. The basic-regime type *'nivo-pluvial superieur'* shows a distinct snowmelt season between April and June, and a more rainfed regime in summer and autumn. At a higher elevation, the regimes are governed by both snowmelt (Mai to July) and melt from the ablation area of alpine glaciers (July to September). This is typical for the basic-regime- *'nivo-glacial inferieur'*. The highest elevations are characterized by firn and snowmelt (type *'nivo-glacial superieur'*). At these elevations, there is also large a accumulation of water. Parts of the accumulated snow survive past the snowmelt season and become firn.

The integral discharge regime of the Massa catchment (label 2) is composed of three basic-regimes: the types *'nivo-glacial inferieur', 'nivo-glacial superieur'* and *'nival superieur'*. The latter is typical in the areas of the Massa catchment along the equilibrium line altitude of the glacier, where there is reduced ablation from bare ice and reduced accumulation of firn.

A distinct difference is present between the regimes of the northern Alps and regimes in the climate unit Ticino. As previously discussed (section 5.3.4), the climate in the Ticino unit is characterized by a bimodal behaviour. There are two maximums of precipitation, the first is more moderate and occurs in spring, the other is larger and occurs in autumn.

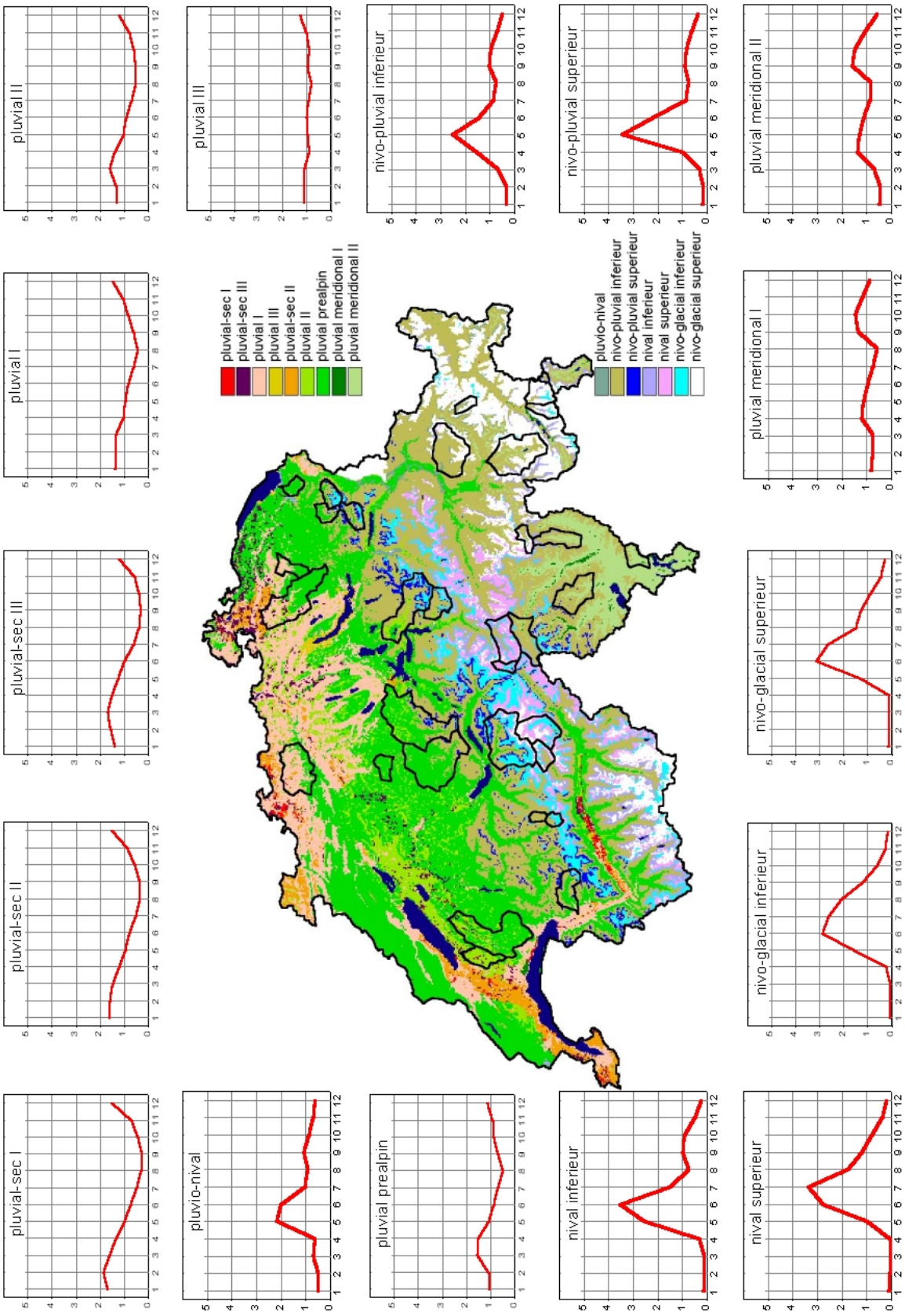

Figure 7.13 Pixel map of the basic natural discharge regimes of Switzerland. The black boundaries show the area of the catchments considered for the model verification (table 7.2). The label of the colours in the map indicates the 16 different basic regimes (table 7.3). The 16 graphs show the average monthly Parde coefficients of the pixels having the same regime.

This bimodal behaviour is also found in the case of the basic-regime types '*pluvial meridional I&II'*. These two regime types are generally only encountered in the climate unit Ticino. The type '*pluvial meridional II'* is governed by evapotranspiration in summer and is found in the valley floors. The type '*pluvial meridional II'* is governed by evapotranspiration to a lesser degree, and shows a slight nival character in winter and early spring. The integral regimes of the sub-catchments Verzasca and Calancasca (labels 32 and 29) are determined by the superimposition of runoff-generation from pixels showing basic-types '*pluvial meridional II'* and *'nivo-pluvial inferieur'*.

8. Overall conclusions and outlook

The collection of case studies in Switzerland and the Russian plain presented in the previous chapters covered a wide range of typical applications of hydrological models. The completed experiments verified a hydrological response units model from the plot-scale (section 5.1), through the catchment-scale (sections 5.2 and 5.3) up to a more regional scale (chapters 6 and 7). The step from plot-scale to distributed model application at catchment scale included a study on the sensitivity of the discharge simulation results on the resolution of the assimilated physiographic information (chapter 4).

The main message emerging from the discussions and conclusions of the completed experiments is that a hydrologist may benefit from a model verification based on more than just an integral assessment of the model quality with respect to observed discharge records. This study demonstrated that various options for alternative model evaluation are available. Different solutions for the assessment of the model quality were tested:

- soil moisture observations allowed for the assessment of the soil and evapotranspiration module quality;
- the long-term monitoring of the water balance at the lysimeter of the Rietholzbach test site provided a unique data set for verifying several model components;
- the analysis of the fluctuations of the groundwater levels yielded qualitative information on the dynamics of runoff generation in alpine catchments;
- the observations of snow water equivalent provided quantitative and qualitative information for the verification of the snowmelt modules;
- the use of processed remotely sensed images of snow patterns allowed for the evaluation of the quality of the spatially distributed simulation of snow cover.

The combination of these alternative options for a detailed multiple-response model verification with the integral verification obtained through comparisons between simulated and observed discharges showed that the different modules implemented in PREVAH are adequate for spatially distributed hydrological simulations in mountainous environments. The multiple-response evaluation of distributed hydrological models is the way to follow in the future of hydrological modelling with spatially distributed models. This also includes the completion of tests to assess both the integral and internal quality of the simulation results yielded by distributed models.

A high Nash and Sutcliffe score in the runoff simulation represents no guarantee that the physical formulation of the model is correct. With fitting, and over-fitting, it is not a particularly challenging task to get the runoff reasonably correct. More scientists should consider the introduction of multiple-efficiency scores to assess if the improvements in the simulation quality of one particular observation are plausible regarding the simulation of other variables. Seibert and McDonnell (2002) introduce such a score, the overall acceptability, to account for both ‘soft’ and ‘hard’ data in the determination of the quality of their simulation experiments. Their message is that the use of multiple-verification criteria, even if based on alternative indicators (‘soft data’) leads to simulation results closer to reality, even if the discharge simulation (‘hard’ data) may be less correct. Parameter estimation techniques and parameter optimization algorithms should therefore not exclusively be focussed on correctly simulating a catchment discharge. The automatic calibration must guarantee that other catchment internal variables are also consistent both with hard observations and with the perceptual knowledge of the dynamics of

hydrological processes acquired by means of field experiments (Menzel 1997, Vitvar 1998). This conclusion demonstrates the importance of the exchange of know-how and experience between modellers and experimentalists (Seibert and McDonnell 2002).

Overall, the achieved results show that the hydrological model PREVAH is a reliable tool for detailed hydrological studies in the Alpine region at different spatial scales. However, the different case studies showed that some improvements are needed:

- the simulation of the snow water equivalent at large scale was affected by large overestimation. A more local parameterization of the tuneable parameters of the snowmelt module has to be adopted. The use of a physically-based snowmelt module should be also taken into consideration. An experiment at catchment scale, showed that the physically-based snowmelt model, ESCIMO (Strasser *et al.* 2001), can yield reliable spatially distributed estimates of the snowmelt generation in alpine environments (Zappa *et al.* 2003);
- the computation of the water balance and runoff hydrograph of large catchments cannot assume that the runoff routing is instantaneous and tuneable by mean of the parameters of the runoff-generation. A separate routing module has to be implemented to account for the effective travel time of the water in the river.
- a reduction of the rain gauge bias correction and a comparison with areal precipitation estimations based on the water balance considerations (Schwarb 2001, Schädler and Weingartner 2002) has to be considered to allow for more plausible estimates of the snow water equivalents and of the water balance.
- the simulations at the high-alpine Dischmabach catchment and the hydrological research catchment Usadievsky showed that PREVAH could benefit from the integration of a routine for the simulation of soil freezing and thawing processes. Gusev and Nasonova (2002) propose a model that includes a soil freezing / thawing module. Such a module allowed for improved simulations at the Usadievsky catchment with the land surface scheme SWAP. The use of improved algorithms for the consideration of soil-freezing (Lunardini 1983) yielded positive feedbacks also in atmospheric models (Vidale *et al.* 2003);
- the implementation and use of a more physically-based soil-vegetation-atmosphere transfer scheme (SVAT) may improve the simulation of the energy fluxes. Schlosser *et al.* (2002) and Slater *et al.* (2002) show an intercomparison of several land-surface schemes that might be considered for the implementation in distributed hydrological models like PREVAH;
- the first results of the simulation experiment for the whole of Switzerland indicate that the simulation of runoff-generation would benefit from a regionalization of the tuneable parameters on the level of the medium-size catchments (Schädler and Weingartner 2002b);
- for the application of PREVAH at large-sized catchments, it should be considered that the simulation of the water fluxes within large water bodies must be described in more detail. This implies the implementation of a lake module and a routing module for the consideration of flood attenuation within lakes;
- the determination of the water balance of disturbed catchments requires the consideration of runoff diversion. This requires close collaboration with

hydropower companies, as already occurred in the study presented by Jasper *et al.* (2002).

This study showed that HRU based distributed hydrological models like PREVAH can be very flexible. Such models can be run as a black-box model for a small catchment, as a point model for a test site, and as a distributed model. Both the intercomparison of PREVAH to WaSiM-ETH and the experimental runs of PREVAH with different methods for spatial discretization (chapter 4) demonstrated that the aggregation of grid elements to HRUs is an efficient parameterization method for spatially distributed hydrological simulations in mountainous environments.

The findings presented in chapter 4 states that hydrological models might be calibrated on the basis of model runs at a relative coarse resolution and then applied at higher resolution in a limited number of runs. The presented results show that the model run based on the aggregation of grid-cells to HRU allowed similar results in the discharge simulation as the model run based on a discretization into regular grids. This means that further studies on the water balance for the whole of Switzerland may be continued with an HRU-related discretization and then applied in gridded mode at a higher resolution for the final runs. The presented formulation of the critical grid-size for spatially distributed hydrological simulations (equations 23 and 24) may yield a precious guideline for the determination of the adequate grid-size for the calibration runs.

Hydrological models can be driven by meteorological information from different sources, such as instrumented towers, fields of spatially and temporally interpolated surface observations and atmospheric models (chapter 6). The intercomparison of model runs driven by interpolated data and locally observed meteorological time series (section 5.1.1) showed that the interpolation techniques used fail to provide an accurate reproduction of the temporal dynamics of rainfall intensities for thunderstorms and local convective precipitation events. The errors in the estimation of rainfall intensities, particularly if using a daily time step, lead to, as an example, systematic errors in the computation of the soil water content and runoff-generation. The development of a more robust method for spatial rainfall interpolation should be considered for both plot-scale and spatially distributed applications. Garen and Marks (1999) and Susong *et al.* (2001) propose a promising technique based on detrended kriging. The use of climatological maps of precipitation (e.g. Schwarb 2001) to force and / or correct the interpolated precipitation fields can also lead to a enhancement of the quality of the spatially distributed hydrological simulation at large scale (chapter 7). The use of these climatological maps at seasonal resolution, as proposed by Kleinn (2002), may allow an enhancement of the large-scale simulation experiments with distributed hydrological models in the Alps.

Recent PhD-thesis at the Institute for Atmosphere and Climate ETH presented detailed studies on the one-way coupled application of atmospheric models with the spatially distributed hydrological model WaSiM-ETH. Jasper (2001) completed advanced offline flood forecasting simulation experiments by coupling WaSiM-ETH with selected Numerical Weather Predictions Models. Kleinn (2002) forced WaSiM-ETH with the meteorological fields obtained from a 6-year experiment with the Regional Climate Model CHRM (Vidale *et al.* 2003). PREVAH was coupled offline with the RCM CHRM and also with the general circulation model ECHAM4. For the current RCM, the model assimilates observed synoptic scale meteorological fields at its lateral boundaries, while the water cycle within the computational domain is completely simulated. This approach is fundamentally different from the GCM methodology, which is based upon the simulation

of the entire atmospheric climate. The usefulness of assimilated meteorological data has also been demonstrated in Central Asia, where observations are extremely sparse (Schär *et al.* 2002). The coupling experiment included in this thesis was completed in the framework of the hydrological simulations in the Upper Volga catchment (Oltchev *et al.* 2002). The interaction between climate conditions and the hydrological response of the Volga source area (Russia) was examined using a model chain approach (ECHAM4, CHRM, WaSiM-ETH and PREVAH). The experiments showed that additional investigations are needed to improve the assimilation of meteorological input from atmospheric models for large-scale studies. The most evident shortcoming was, in the case of the RCM, the correct representation of rainfall intensities in summer (a problem of predictability, Vidale *et al.* 2003), while the GCM failed to reproduce the local climatology of precipitation. Thus, the experiment with the RCM-forcing yielded more encouraging results than the experiment with a GCM-forcing. The availability of time series longer than 15-20 years is envisaged to make further progresses towards using RCMs experiments for hydrological studies with spatially distributed models.

The Upper Volga experiment also included the use of a prescribed monthly climate change scenario for the adaptation of the present climatology to predicted future climate conditions (Gurtz *et al.* 1997). The estimation of such scenarios is based on GCM studies (Wild *et al.* 1998). In the future, a new generation of climate scenarios for distributed hydrological simulations must be developed. The assimilation of the scenarios should account for the year-to-year, month-to-month and day-to-day variability of the possible climate changes when compared to the current climate.

Several future works with PREVAH can be envisaged. The promising results in the European Alps might be complemented with experiments in other mountainous regions of the earth. Collaboration is already established with the scientists involved in the People and Resource Dynamics of Mountain Watersheds (PARDYP) project Merz *et al.* (2000). Since 1997, PARDYP investigates five watersheds across the middle mountains of the Hindu Kush-Himalayan range. One of those catchments, the Jhikhu-Khola watershed in Nepal (111.4 km^2), will serve as first test-site for the application of PREVAH to a mountainous catchment with a monsoon climate. The first preliminary results show that PREVAH is a suitable tool to simulate the distinct difference in runoff-generation between dry and wet season at the Jhikhu-Khola watershed.

A more ambitious goal might be the inclusion of PREVAH in a system for the real time spatially distributed monitoring of the water balance elements of Switzerland. The development of such a system might allow for the preparation of detailed basic information and relevant start values for a new generation of flood prediction models.

Finally, it is expected that the results yielded by the simulation of the whole of Switzerland might provide valuable input to a wide range of other, not necessarily hydrology related, studies in the Swiss Alps. As an example, the derivation of quantitative and qualitative guidelines for the management of water resources of Switzerland from these simulation results would be a very challenging task for the years to come.

APPENDIX A

The interception module of PREVAH:
A simple bucket approach is used to conceptualize the process of canopy interception. A maximal interception storage capacity SI_{MAX} [mm] is assigned to each class of vegetation. Such maximal can be set to vary monthly (Gurtz *et al.* 1997a). The filling of the interception storage SI [mm] is computed as proposed by Menzel (1997):

$$SI(t) = SI_A(t-1) + (SI_{MAX} - SI_A(t-1)) \cdot \left(1 - e^{-cPI(t)}\right) \quad [\text{mm}] \quad \text{A1a}$$

$$c = SI_{MAX}^{-1} \quad [\text{mm}^{-1}] \quad \text{A1b}$$

t is here the computation time step, PI is the intensity of precipitation [mm] for the current time step. The consumption of SI occurs by evapotranspiration at potential rate.

Computation of potential evapotranspiration after Penman-Monteith:
The most widely adopted scheme for the estimation of evapotranspiration in distributed hydrological models rely on the Penman-Monteith equation (Monteith 1975, Menzel 1997, DVWK 1996, Gurtz *et al.* 1997a):

$$\lambda E = \frac{\Delta(R_N - G) + \rho c_p (e_s - e) / r_a}{\Delta + \gamma \left(1 + r_c / r_a\right)} \quad \text{A2}$$

E is here the potential evapotranspiration (latent heat flux) [kg·m^{-2}·s^{-1}] and λ the latent heat of evaporization of water [kJ·kg^{-1}]. The available energy is composed of net radiation R_n [W·m^{-2}] and soil heat flux G [W·m^{-2}]. Δ is the first derivative of the saturated vapour pressure curve [hPa·K^{-1}] and γ the psychometric constant [hPa·K^{-1}]. ρ is the density of dry air [kg·m^{-3}], c_p the specific heat of dry air at constant pressure [kJ·kg^{-1}·K^{-1}], r_a the aerodynamic diffusion resistance [s·m^{-1}], r_c the canopy (stomata) diffusion resistance [s·m^{-1}], e_s the saturated vapour pressure [hPa] at the actual temperature and e is the actual water vapour pressure [hPa]. For each vegetation type this approach uses time dependent (monthly) parameter values for albedo, minimum stomata diffusion resistance, aerodynamic roughness length, leaf area index and root depth. Time shifts in the seasonal vegetation development and conditional on an increasing altitude of location are also considered (Gurtz *et al.* 1997a, Schulla and Jasper 2000).

Other schemes for the estimation of potential evapotranspiration
The estimation of potential evapotranspiration (ETP) after Wendling (DVWK 1996) is applicable only if using a time step of one day or larger. The potential evapotranspiration using this approach is then given by:

$$ETP_{WENDLING} = (RG \cdot (1.1 - \alpha) + 93 \cdot f_k) \cdot \frac{(T + 22)}{150 \cdot (T + 123)} \quad [\text{mm·d}^{-1}] \quad \text{A3}$$

Table A1 Empirical coefficient $ETPF_{mon}$ for ETP_{TURC} (valid for central Europe).

Month	Jan	Feb	Mar	Apr	May	June	July	Aug	Sep	Oct	Nov	Dec
$ETPF_{mon}$	0.7	0.85	0.95	1.05	1.25	1.15	1.05	0.95	0.9	0.8	0.75	0.7

The Turc (DVWK 1996) scheme is applied in France and in arid/semi-arid regions when air temperature exceeds 5 °C. Also in these case the scheme is applicable only if using a time step of one day or larger. For temperatures below 5°C the schem of the scheme after IVANOV is used instead.

$$ETP_{TURC} = 0.0031 \cdot (RG + 209.4) \cdot \frac{T}{(T+15)} ETPF_{mon} \qquad T \geq 5°C \qquad [mm \cdot d^{-1}] \qquad A4a$$

$$ETP_{IVANOV} = f_k \cdot 0.00006 \cdot (T+25)^2 \cdot (100 - RH) \qquad T < 5°C \qquad [mm \cdot d^{-1}] \qquad A4b$$

The terms in equations A2 to A3 are defined as follows: *RG* is the global radiation [$J \cdot cm^{-2} \cdot d^{-1}$], α is the albedo, f_k is an empirical correction factor, (0.5 for northern Switzerland, Schulla and Jasper 2000) and *T* is the daily mean value of air temperature [°C]. $ETPF_{mon}$ is an empirical coefficient and varies monthly (table A1). *RH* is the relative humidity [%].

Determination of actual evapotranspiration

During dry periods the plant available soil moisture is consumed by evapotranspiration. This implies an increase of suction in the soil. Thus, the water molecules are strongly bind to the soils, the water demand of the vegetation cannot be completely provided and therefore reduced evapotranspiration values are expected. The concept for estimating such reduction relies on the relation between the plant available soil water content (Θ-Θ_{WP}) and the actual capillary pressure (suction, ψ). Evapotranspiration is reduced as a result of dry soils ($\Theta(\psi) < \Theta_{\psi_g}$):

$$ETR = 0 \qquad \Theta(\psi) < \Theta_{wp} \qquad A5a$$

$$ETR = ETP \cdot \frac{(\Theta(\psi) - \Theta_{wp})}{(\Theta_{\psi g} - \Theta_{wp})} \qquad \Theta_{wp} \leq \Theta(\psi) < \Theta_{\psi g} \qquad A5b$$

$$ETR = ETP \qquad \Theta_{\psi g} \leq \Theta \leq \Theta_{FC} \qquad A5c$$

Where ETR is the actual evapotranspiration [mm], *ETP* is the potential evapotranspiration [mm]. $\Theta(\psi)$ is the actual volumetric soil water content [%] at suction ψ [m]. Θ_{FC} is the volumetric water content of the soil at field capacity [%], Θ_{ψ_g} is the volumetric soil water content [%] at a given suction where *ETR* is assumed starting to reduce ($\approx 0.6\ \Theta_{FC}$) (Menzel 1997). Θ_{wp} is the volumetric water content of the soil [%] at permanent wilting point. In PREVAH Θ is not diagnosed as function of ψ but conceptualized through the content of the so-called plant available soil moisture storage in the aeration zone of the soil *SSM* [mm]:

$$SSM = (\Theta - \Theta_{WP}) \cdot SD \qquad [mm] \qquad A6a$$

$$SFC = (\Theta_{FC} - \Theta_{WP}) \cdot SD \qquad [mm] \qquad A6b$$

SD is the soil moisture active soil dept in [mm] and is parameterized as function of the soil type and the root depth (Gurtz *et al.* 1997a). Further, PREVAH reduces *ETP* if *SSM* is lower than the maximal plant available water content *SFC* [mm]:

$$ETR = ETP \qquad \varepsilon \cdot SFC \leq SSM \leq SFC \qquad [mm \cdot d^{-1}] \qquad A7a$$

$$ETR = (SSM)/(\varepsilon \cdot SFC) \cdot ETP \qquad 0 \leq SSM \leq \varepsilon \cdot SFC \qquad [mm \cdot d^{-1}] \qquad A7b$$

The dimensionless free parameter ε can range between 0.3 and 0.8 in the case of vegetated soils. ε is set equal to one in the case of bare soils and urban areas and equal to zero in the case of water surfaces and marsh.

The equations of the runoff-generation module

This paragraph presents the equations of the water flows within the runoff-generation module of PREVAH (section 2.2). The schematic representation of the flows is displayed by figures 2.4 and 2.5. and is computed for each HRU at each time step *dt* [h]. Table A3 summarizes the variables and parameters of the soil and runoff-generation modules.

Table A2 Main variables and parameters of the soil and runoff-generation modules.

Name	Unit	Definition
State Variables		
SFC	[mm]	Maximal plant available soil moisture storage
SSM	[mm]	Plant available soil moisture storage
DSUZ	[mm· dt^{-1}]	Inflow into the runoff-generation module
SUZ	[mm]	Upper storage reservoir
PERC	[mm· dt^{-1}]	Deep percolation rate
RS	[mm· dt^{-1}]	Surface runoff
RI	[mm· dt^{-1}]	Interflow
SG1	[mm]	Fast response groundwater reservoir
SG2	[mm]	1st order slow response groundwater reservoir
SG3	[mm]	2nd order slow response groundwater reservoir
GR1	[mm· dt^{-1}]	Recharge of SG1
GR2	[mm· dt^{-1}]	Recharge of SG2
GR3	[mm· dt^{-1}]	Recharge of SG3
RG1	[mm· dt^{-1}]	Fast response groundwater runoff component
RG2	[mm· dt^{-1}]	Delayed groundwater runoff component
R_{TOT}	[mm· dt^{-1}]	Total runoff
Tuneable parameters		
BETA	[-]	Soil moisture recharge parameter
SGR	[mm]	Threshold content of SUZ for generation of surface runoff
$SG1_{MAX}$	[mm]	Maximal content of the fast response groundwater reservoir SG1
K0	[h]	Storage coefficient for surface runoff
K1	[h]	Storage coefficient for interflow
K2	[h]	Storage coefficient for quick response baseflow
K3	[h]	Storage coefficient for delayed baseflow
$PERC_{MAX}$	[mm· dt^{-1}]	Maximal deep percolation rate

The inflow *DSUZ* into the storages of the runoff-generation module is regulated by *SFC*:

$$DSUZ(t) = P_b(t) \cdot \left(\frac{SSM(t-1)}{SFC} \right)^{BETA} \quad \text{A8}$$

Where *BETA* is a dimensionless non-linearity parameter that controls the redistribution of the available water amount for runoff generation P_b [mm·dt^{-1}] between the plant available soil moisture storage reservoir (*SSM*) and the upper storage reservoir of the unsaturated zone of the soil (*SUZ*).

This reservoir temporarily stores water amounts that can either drain by gravitation, or generate surface runoff and interflow. *SUZ* is the part of the soil moisture content that exceeds the field capacity and contributes to the runoff-generation (Figure 2.4). The soil moisture recharge (*SMR*) is the difference between P_b and *DSUZ*. *SMR* increases with increasing *BETA* (Uhlenbrook 1999).

At a first stage, the storage reservoir *SUZ* is incremented by *DSUZ*:

$$SUZ_1(t) = SUZ(t-1) + DSUZ(t) \cdot dt \quad \text{A9}$$

SUZ is emptied by deep percolation *PERC* into the reservoirs of the saturated zone of the soils *SG1*, *SG2*, *SG3*, by surface runoff RS, and by interflow RI:

$$SUZ_2(t) = SUZ_1(t) - PERC(t) \cdot dt \quad \text{A10}$$

$$with \quad PERC(t) = MIN\left[\left(SUZ_1(t) \cdot dt^{-1} \right), PERC_{MAX} \right] \quad \text{A11}$$

The maximum percolation rate $PERC_{MAX}$ is a tuneable parameter. *PERC* (eq. A11) is limited by the content of *SUZ* obtained from equation (A9). The generation of surface runoff *RS* (eq. A12) and interflow *RI* (A13) depends on the content of the linear reservoir *SUZ*, as obtained from Equation (A10):

$$RS(t) = \left(SUZ_2(t) - SGR \right) \cdot \left(1 - e^{-dt/K0} \right) \cdot dt^{-1} \quad if \quad SUZ_2(t) > SGR \quad \text{A12a}$$

$$RS(t) = 0 \quad if \quad SUZ_2(t) \le SGR \quad \text{A12b}$$

$$RI(t) = SUZ_2(t) \cdot \left(1 - e^{-dt/K1} \right) \cdot dt^{-1} \quad if \quad SUZ_2(t) > 0 \quad \text{A13a}$$

$$RI(t) = 0 \quad if \quad SUZ_2(t) = 0 \quad \text{A13b}$$

where *SGR* is a model parameter defining a threshold content of *SUZ* [mm] that must be exceeded to allow for surface runoff generation. The two storage coefficients *K0* and *K1* [h] are tuned through model calibration and adopted as catchment specific parameters to govern the generation of surface runoff and interflow, respectively.

The content of *SUZ* at the end of the time-step is equal to:

$$SUZ(t) = SUZ_2(t) - \left(RI(t) + RS(t) \right) \cdot dt \quad \text{A13}$$

The recharge rates *GR1*, *GR2* and *GR3* of the groundwater storage reservoirs *SG1*, *SG2* and *SG3* are determined as a function of the deep percolation rate *PERC*, obtained from equation (A11). The computation of the water flows within the groundwater storages and runoff components follows the method developed by Schwarze *et al.* (1999):

$$\begin{aligned} &if \quad SG1_{(t)} \geq SG1_{MAX} \quad && GR1_{(t)} = 0 \\ & && GR2_{(t)} = PERC_{(t)} \cdot 8/9 \\ & && GR3_{(t)} = PERC_{(t)} \cdot 1/9 \end{aligned} \qquad \text{A14}$$

$$\begin{aligned} &if \quad SG1_{(t)} < SG1_{MAX} \quad && GR1 = MIN\left(PERC_{(t)}, GR1_{MAX\,(t)}\right) \\ & && GR2 = \left(PERC_{(t)} - GR1\right) \cdot 8/9 \\ & && GR3_{(t)} = \left(PERC_{(t)} - GR1\right) \cdot 1/9 \end{aligned} \qquad \text{A15}$$

$$\text{with} \quad GR1_{MAX\,(t)} = \left[\frac{\left(SG1_{MAX} - SG1_{(t)}\right)}{K2_H} \right] \qquad \text{A16}$$

where $SG1_{MAX}$ is a threshold factor that restricts the content of the quick response groundwater reservoir *SG1*. Equation (A16) assures that $SG1_{MAX}$ is not exceeded during the time-step *dt*.

Equations A17 to A19 describe the computation of the change in storage of the three groundwater reservoir within *dt*.

$$SG1_{(t)} = SG1_{(t-1)} \cdot e^{-dt/K2} \quad + \quad \left[\left(1 - e^{-dt/k2}\right) \cdot GR1_{(t)} \cdot K2\right] \qquad \text{A17}$$

$$SG2_{(t)} = SG2_{(t-1)} \cdot e^{-dt/K3} \quad + \quad \left[\left(1 - e^{-dt/k3}\right) \cdot GR2_{(t)} \cdot K3\right] \qquad \text{A18}$$

$$SG3_{(t)} = SG3_{(t-1)} \cdot e^{-dt/K4} \quad + \quad \left[\left(1 - e^{-dt/k4}\right) \cdot GR3_{(t)} \cdot K4\right] \qquad \text{A19}$$

The generation of the groundwater runoff components is governed by tuneable storage coefficients:

$$RG1_{(t)} = \frac{SG1_{(t)}}{K2} \qquad \text{A20}$$

$$RG2_{(t)} = \frac{SG2_{(t)}}{K3} + \frac{SG3_{(t)}}{K4} \qquad \text{A21}$$

$$\text{with} \quad K4 = K3 \cdot 1/9 \qquad \text{A22}$$

K2 and *K3* are the storage coefficients [h] governing the generation quick response (*RG1*) and delayed (*RG2*) groundwater runoff, respectively. The additional reservoir *SG3* also generates a quick response groundwater component(*RG3*), whose storage coefficient *K4* is parameterized in function of *K3* (equation A22). The storage coefficients of the groundwater runoff components can be either tuned through model calibration or determined by an analysis of the hydrograph's recession curve (Schwarze *et al.* 1999).

The total runoff-generation R_{TOT} in the time-step *dt* is determined by adding all the components generated from the upper storage reservoir and the groundwater reservoirs:

$$R_{TOT}(t) = RS(t) + RI(t) + RG1(t) + RG2(t) \qquad \text{A23}$$

R_{TOT} is assumed to be instantaneously routed to the catchment outlet.

APPENDIX B

Add-in to section 5.1.1: Intercomparison of two meteorological time series:

Figure A1 and table A3 show the results of the comparisons between the meteorological data of the TOWER data set and the interpolated data set $ANETZ_H$.

Air temperature: The average interpolated temperature during the period from August to November is approximately 1 K higher than the observed values at 3 meters height in Claro (table A3). The correlation (R_{os}) between air temperature of the TOWER and interpolated air temperature of the other two meteorological time series is very high throughout the period. The interpolated air temperature data are aligned slightly above the 1:1 line with respect to the TOWER data (fig. A1a).

Global radiation: The average interpolated global radiation overestimates the observed average during the whole R-SOP period. The range of the differences is up to 11 $W \cdot m^{-2}$ (table A3). The scatter plot between observations at the TOWER and the interpolated radiation data shows a very good alignment along the 1:1 line (fig. A1b). The correlation (R_{OS}) between the observed TOWER values and the interpolated data is high.

Precipitation: As expected, the largest differences between the observed and the interpolated time series are present in the case of the precipitation data. R_{OS} between $ANETZ_H$ and the TOWER data set is above 0.85 (figure A1c), but the absolute values are underestimated in the period of calibration and overestimated during the period of evaluation (table A3). The cumulative precipitation during the whole observing period (fig. A1d) is 17% higher than the observations.

Although $ANETZ_H$ and ANETZ_D showed good correlation with the TOWER data set, there is some evidence that indicates that their relevance for this location is only qualitative. When compared to TOWER measurements, the interpolated $ANETZ_H$ time series are a bit warmer and wetter. The adopted methods for the spatial interpolation of the meteorological data from permanent stations of the MeteoSwiss network proved to be accurate for air temperature and global radiation. An accurate interpolation of precipitation was only possible in the case of advective rainfall events. The temporal dynamics of rainfall intensities for thunderstorms and local convective precipitation events was not accurately modelled. As well, a large overestimation of the total rainfall is present in the case of the interpolated data set with hourly time steps.

Table A3 Intercomparison of the two available meteorological time series with respect to the average air temperature (T), the average global radiation (RGL) and the precipitation sums (P).

Dataset	Variable	Unit	August	September	October	November	Total
$ANETZ_H$	T	°C	20.1	17.9	12.3	11.5	15.8
TOWER	T	°C	19.2	17.0	11.2	10.2	14.8
$ANETZ_H$	RGL	$W\ m^{-2}$	173	131	87	51	117
TOWER	RGL	$W\ m^{-2}$	162	123	85	48	110
$ANETZ_H$	P	mm	115	420	273	71	880
TOWER	P	mm	140	404	164	45	752

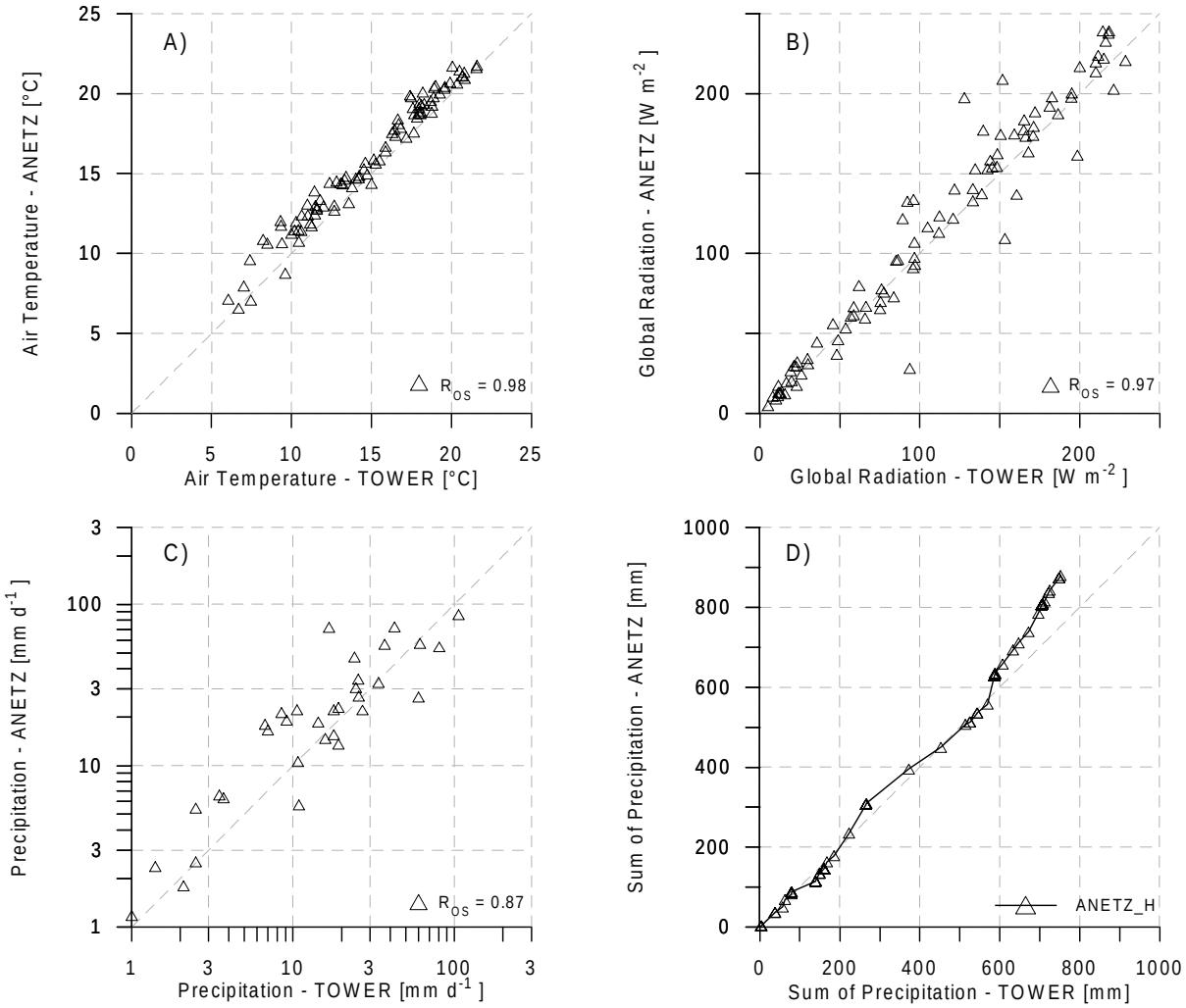

Figure A1 Correlation between the TOWER data set and the interpolated time series ($ANETZ_H$) during the whole MAP-Riviera campaign. a) average daily air temperature. b) average daily global radiation. c) daily precipitation rates. d) cumulative precipitation rates.

References

Abbott, M.B., Bathurst, J.C., Cunge, J.A., O'Connell, P.E. and Rasmussen, J. (1986a): An introduction to the European Hydrological System - Système Hydrologique Européen, 'SHE', 1: History and philosophy of a physically-based, distributed modelling system. *J. Hydrol.*, **87**, 45-59.

Abbott, M.B., Bathurst, J.C., Cunge, J.A., O'Connell, P.E. and Rasmussen, J. (1986b): An introduction to the European Hydrological System - Système Hydrologique Européen, 'SHE', 2: Structure of a physically-based, distributed modelling system. *J. Hydrol.*, **87**, 61-77.

Anderson, E.A. (1973): National Weather Service River Forecast System-Snow Accumulation and Ablation Model. *NOAA Tech. Memo.* NWS. U.S. Dep. of Commerce, Silver Spring.

Apfl, G., Barben, M., Baumgartner, M., Holzer, T. and Weingartner, R. (1995): *Variation of the Snow Line*. Plate 3.6 of the Hydrological Atlas of Switzerland.

Aschwanden, H., Weingartner, R. (1985): *Die Abflussregimes der Schweiz*. Publikation Gewässerkunde, **65**, Bern.

Aubinet, M., Grelle, A., Ibrom, A., Rannik, U., Moncrieff, J., Foken, T., Kowalski, A.S., Martin, P.H., Berbigier, P., Bernhofer, C., Clement, R., Elbers, J., Granier, A., Grunwald, T., Morgenstern, K., Pilegaard, K., Rebmann, C., Snijders, W., Valentini, R. and Vesala T. (2000): Estimates of the annual net carbon and water exchange of forests: The EUROFLUX methodology. *Advances in Ecological Research*, **30**, 113-17.

Badoux, A. (1999): *Untersuchung zur flächendifferenzierten Modellierung von Abfluss und Schmelze in teil-vergletscherten Einzugsgebieten*. Diploma thesis, ETH Zürich [available from the Institute for Atmospheric and Climate Science ETH, Winterthurerstr. 190, CH-8057 Zürich].

Becker, A. and Braun, P. (1999): Disaggregation, aggregation and spatial scaling in hydrological modelling. *J. Hydrol.*, **217**, 239-252.

Becker, A. and Nemec, J. (1987): Macroscale hydrologic models in support to climate research. In: Solomon, S.I., Beran, M., Hoog, W. (Eds.): *The Influence of Climate Change and Climatic Variability on the Hydrologic Regime and Water Resources*., IAHS Publication No. **168**, 431-445.

Benoit, R., Pellerin, P., Kouwen, N., Ritchie, H., Donaldson, N., Joe, P. and Soulis, E.D. (2000): Toward the use of coupled atmospheric and hydrologic models at regional scale, *Mon. Wea. Rev.*, **128**, 1681–1706.

Benoit, R., Schär, C., Binder, P., Chamberland, S., Davies H.C. *et al.* (2002): The real-time ultrafinescale forecast support during the Special Observing Period of the MAP. *Bull. Amer. Meteor. Soc.*, **83**, 85-109.

Bergström, S. (1976): Development and Application of a Conceptual Runoff Model for Scandinavian Catchments. *Bulletin Series A*, No. 52, University of Lund.

Bergström, S. (1992): The HBV model - its structure and applications. SMHI, RH No. 4, Norrköping, Sd.

Betts, A.K., Ball, J.H., Beljaars, A.C.M., Miller, M.J. and Viterbo, P.A. (1996): The land-surface atmosphere interaction: a review based on observational and global modeling perspectives. *J. Geophys. Res.*, **101**, 7209-7225.

Beven, K.J. (1989): Changing Ideas in Hydrology – The Case of Physically-Based Models. *J. Hydrol.*, **105**, 157-172.

Beven, K.J. (2000): *Rainfall-runoff modelling : the primer*, John Wiley & Sons LTD., Chichester, UK.

Beven, K.J. and Feyen, J. (2002): The future of distributed modelling: special issue, *Hydrol. Process.*, **16**, 169-172.

Beven, K.J., Kirkby M.J. (1979): A physically based, variable contributing area model of basin hydrology. *Hydrological Sciences Bulletin*, 24(1), 43–70.

BFLT (1991): *Digitales Höhenmodel RIMINI*. Bundesamt für Landestopographie, Wabern, Switzerland.

BFS (1995): *Die Bodennutzung der Schweiz. Arealstatistik 1979/85*. Bundesamt für Statistik, Bern, Switzerland.

BFR (1980): *Bodeneignungskarte der Schweiz. Grundlagen für die Raumplanung*. Bundesamt für Raumplanung, Bern, Switzerland.

Binder, P. (1996): MAP and surface hydrology, *MAP Newsletter*, **5**, 11-12. (available at: http://www.map.ethz.ch).

Blöschl, G. (1999): Scaling issues in snow hydrology. *Hydrol. Process.*, **13**, 2149-2175.

Blöschl, G. (2001): Scaling in hydrology. *Hydrol. Process.*, **15**, 709-711.

Blöschl, G. and Sivapalan, M. (1995): Scale issues in hydrological modelling - a review. *Hydrol. Process.*, **9**, 251-290.

Blöschl, G., Kirnbauer, R., and Gutknecht, D. (1991): Distributed snowmelt simulations in an alpine catchment: 1. Model evaluation on the basis of snow cover patterns. *Water Resour. Res.*, **27**, 3171-3179.

Blöschl, G. Kirnbauer, R., Jansa, J., Kraus, K., Kusching, D. Gutknecht, D. and Reszler, Ch. (2002): Using remote sensing methods for calibrating and verifying a spatially distributed snow model Österreichische Wasser- und Abfallwirtschaft. **54**, 16 pp. (in German).

Bohrer, M. (1998): Räumlich differenzierte Erfassung der Einzugsgebietskennwerte und Modellierung des Wasserhaushalts im Rietholzbachgebiet unter Nutzung eines GIS. Diploma thesis, ETH and UNI Zürich [available from the Institute for Atmospheric and Climate Science ETH, Winterthurerstr. 190, CH-8057 Zürich].

Bougeault, P. and Coauthors (2001): The MAP Special Observing Period. *Bull. Amer. Meteor. Soc.*, **82,** 433 –462.

Bowen, I.S. (1926): The ratio of heat losses by conduction and by evaporation from any water surface. *Phys. Rev*., **27**, 779-787.

Brasington, J. and Richards, K. (1998): Interactions between model predictions, parameters and DTM scales for TOPMODEL, *Computers & Geosciences*, **24**(4), 299-314.

Braun, L. (1985): *Simulation of Snowmelt-Runoff in Lowland and Lower Alpine Regions of Switzerland*. Zürcher Geographische Schriften, Heft 21, ETH Zürich [available from the Institute for Atmospheric and Climate Science ETH, Winterthurerstr. 190, CH-8057 Zürich].

Braun, L., Brun, E., Durand, Y. and Martin, E. (1994): Simulation of discharge using different methods of meteorological data distribution, basin discretization and snow modelling. *Nord. Hydrol.*, **25**, 129-144.

Bruneau, P., Gascuel-Odoux, C., Robin, P., Merot, P. and Beven, K.J. (1995): Sensitivity to space and time resolution of a hydrological model using digital elevation data, *Hydrol. Processes*, **9**, 69–81.

Carlaw, S. (2000): *Soil moisture accounting in distributed hydrological modelling*. MASc. Thesis, Dept. of Civil Engineering, University of Waterloo, Canada.

Cline, D.W., Bales, R.C. and Dozier, J. (1998): Estimating the spatial distribution of snow in mountain basins using remote sensing and energy balance modeling. *Water Resour. Res.*, **34**, 1275-1285.

Coughlan, M. and Avissar R. (1996): The Global Energy And Water Cycle Experiment (GEWEX) Continental-Scale International Project (GCIP): An Overview, *J. Geophys. Res.*, **101,** 7139-7147.

De Jong, C., List, F.K. and Ergezinger, P.J. (2002): Experimental hydrological analyses in the Dischma based on daily and seasonal evaporation. *Nordic Hydrol*., **33**(1), 1-14.

Doswell, C.A. III, Davies-Jones, R. and Keller, D.L. (1990): On summary measures of skill in rare event forecasting based on contingency tables. *Wea. Forecasting*, **5**, 576-586.

DVWK (1996): *Ermittlung der Verdunstung von Land- und Wasserflächen*. DVWK-Merkblätter zur Wasserwirtschaft, **238**.

Engel, B.A. (1996): Methodologies for development of hydrological response units based on terrain, land cover and soils data. In *GIS and environmental modeling*. New York: Oxford University Press, 123-128.

Essery, R., Martin, E., Douville, H., Fernandez, A. and Brun, E. (1999): A comparison of four snow models using observations from an alpine site. *Clim. Dyn.*, **15**, 583-593.

FOWG (2000): Swiss hydrological yearbook. Federal Office for Water and Geology. [available from http://www.bwg.admin.ch].

Fekete, B.M., Vörösmarty, C.J. and Lammers R.B. (2001): Scaling gridded river networks for macroscale hydrology: Development, analysis, and control of error. *Water Resour. Res.*, **37**, 1955-1967.

Ferguson, R.I. (1999): Snowmelt runoff models, *Progress In Physical Geography*, **23**(2), 205-227.

Flügel, W.A. (1995): Delineating hydrological response units by geographical inforamtion system analyses for regional hydrological modelling using PRMS / MMS in the drainage basin of the river Bröl, Germany. *Hydrol. Process.*, **9**, 423-436.

Flügel, W.A. (1997): Combining GIS with regional hydrological modelling using hydrologic response units (HRUs): An application from Germany, *Math. Comput. Simulat.*, **43**, 297-304.

Franchini, M. and Pacciani, M. (1991): Comparative analysis of several conceptual rainfall-runoff models. *Journal Of Hydrology*, **122**, 161-219.

Freeze, R.A. and Harlan, R.L.(1969): Blueprint for a physically-based digitally simulated hydrologic response model. *J. Hydrol.*, **9**, 237-258.

Frei, C. and Schär, C. (1998): A precipitation climatology of the Alps from high-resolution rain-gauge observations. *Int. J. Climatol.*, **18**, 873-900.

Frei, C., Davies, H.C., Gurtz, J. and Schär, C. (2000): Climate dynamics and extreme precipitation and flood events in Central Europe. *Integrated Assessment*, 1, 281-299.

Frei, C., Schär, C., Lüthi, D. and Davies, H.C. (1998): Heavy precipitation processes in a warmer climate. *Geophys. Res. Letters*, **25**, 1431-1434.

Garen, D. and Marks, D. (2001): Spatial fields of meteorological input data including forest canopy corrections for an energy budget snow simulation model. In: Dolman, A.J., Hall, A.J., Kavvas, M.L., Oki, T. and Pomeroy, J.W. (Eds.). *Soil-Vegetation-Atmosphere Transfer Schemes and Large Scale Hydrological Models*, IAHS Publication No. **270**, 349-353.

Gibson, J.K., Kallberg, P., Uppala, S., Nomura, A., Hernandez, A. and Serrano, E. (1997): ERA description, *Technical Report 1*, ECMWF Re-Analysis Project Report Series, Reading, UK.

Gilgen, H. and Ohmura, A. (1999): The Global Energy Balance Archive, *Bull. Amer. Meteor. Soc.*, **80**, 831-850.

Grayson, R. and Blöschl, G. (Eds.) (2001): *Spatial patterns in catchment hydrology : observations and modelling*. Cambridge University Press, Cambridge, UK.

Green, W.H., and Ampt, G.A. (1911): 'Studies on Soil Physics: I. The flow of air and water through soils. *Journal of Agricultural Sciences* **4**: 1-24.

Gurtz, J., Baltensweiler, A. and Lang, H. (1999): Spatially distributed hydrotope-based modelling of evapotranspiration and runoff in mountainous basins. *Hydrol. Process.*, **13**, 2751-2768.

Gurtz, J., Baltensweiler, A., Lang, H., Menzel, L. and Schulla, J. (1997a): Auswirkungen von klimatischen Variationen von Wasserhaushalt und Abfluss im Flussgebiet des Rheins. *Schlussbericht NFP 31:"Klimaänderungen und Naturkatastrophen"*, vdf Hochschulverlag AG ETH Zürich, 147 pp.

Gurtz, J., Schulla, J. and Lang, H. (1997b): Methodische Aspekte der Modellierung von Wasserhaushalt und Abfluss in Gebirgsgebieten. Symposium zur Modellierung in der Hydrologie, TU Dresden, 166-178.

Gurtz, J., Verbunt, M., Zappa, M., Moesch, M. and U. Moser (2003c): Long-term hydrometeorological measurements and model based analyses in the hydrological research catchment Rietholzbach. *Journal of Hydrology and Hydromechanics*, in print.

Gurtz, J., Zappa, M., Jasper, K., Lang, H., Verbunt, M., Badoux, A. and Vitvar, T. (2003a): A Comparative Study in Modelling Runoff and its Components in Two Mountainous Catchments. *Hydrol. Processes*, **17**, 297-311.

Gurtz, J., Zappa, M., Jasper, K., Verbunt, M., Badoux, A., Vitvar, T. and Lang, H. (2001): Modelling of runoff and its components and model validation in Swiss Pre-Alpine and Alpine catchments. Freiburger Schriften zur Hydrologie, **13**, 206-220.

Gurtz, J., Zappa, M., Verbunt, M. and K. Jasper (2003b): Advanced applications of distributed hydrological models in mountainous catchments. In: de Jong, C., Collins, D. and R. Ranzi (Editors): *Climate and Hydrology in Mountain Areas*. Wiley. Submitted Book Chapter.

Gusev, Y.M. and Nasonova, O.N. (2002) The simulation of heat and water exchange at the land–atmosphere interface for the boreal grassland by the land-surface model SWAP. *Hydrol. Processes*, **16**, 1893-1919.

Gyalistras, D., Schär, C., Davies, H.C. and Wanner, H. (1998): Future Alpine Climate. In: Cebon, P., Dahinden, U., Davies, H.C., Imboden, D.M., Jäger, C. (Editors): V*iews from the Alps: regional perspectives on climate change*. MIT press, Boston, 171-223.

Haddeland, I., Matheussen, B.V. and Lettenmaier, D.P. (2002): Influence of spatial resolution in a macroscale hydrologic model. *Water Resour. Res.,* **38**(7). 10 pp.

Heck, P., Lüthi, D., Wernli, H. and Schär, C. (2001): Climate impacts of European-scale anthropogenic vegetation changes: A sensitivity study using a regional climate model. *J. Geophys. Res.,* **106**, 7818-7835.

Henderson-Sellers, A., McGuffie, K. and Pitman, A.J. (1996): The Project for Intercomparison of Land-surface Parametrization Schemes (PILPS): 1992-1995. *Clim. Dyn.*, **12**, 849-859.

Henderson-Sellers, A., Yang, Z.L. and Dickinson, R.E. (1993): The Project for Intercomparison of Land-surface Parameterization Schemes, *Bull. of the Amer. Met. Soc.*, **74**, 1335-1349.

Higy, C. and Musy, A. (2000): Digital terrain analysis of the Haute-Mentue catchment and scale effect for hydrological modelling with TOPMODEL, *Hydrol. Earth System Sci.*, **4**, 225-238.

Hock, R. (1999): Distributed temperature-index ice- and snowmelt model including potential direct solar radiation. *J. Glaciol.*, **45**, 101-111.

Hock, R. (2003): Evaluation and recent developments in temperature index melt modelling in mountain regions. *Accepted by J. Hydrol.*, in print.

Horton, R.E. (1933): The role of infiltration in the hydrologic cycle. *Transaction of the American Geophysical Union*, **14**, 446-460.

IPCC (1992): Climate change, the IPCC scientific assessment. J. T. Houghton, B. A. Callander, S. K. Varney (Editors), Cambridge University Press, 200 pp.

Jasper K, Gurtz J, Lang H (2002): Advanced flood forecasting in Alpine watersheds by coupling meteorological observations and forecasts with a distributed hydrological model. *J. Hydrol.,* **267,** 40-52.

Jasper, K. (2001): Hydrological modelling of alpine river catchments using output variables from atmospheric models. PhD thesis. Swiss Federal Institute of Technology (ETH). Dissertation No. 14'385. [available from the Institute for Atmospheric and Climate Science ETH, Winterthurerstr. 190, CH-8057 Zürich].

Kenward, T., Lettenmaier, D.P., Wood, E.F. and Fielding, E. (2000): Effects of digital elevation model accuracy on hydrologic predictions. *Remote Sens. Environ.* **74,** 432–444.

Kirchhofer, W. and Sevruk, B. (1992): *Mean annual corrected precipitation depths 1951 – 1980*. Plate 2.3 of the Hydrological Atlas of Switzerland.

Kirnbauer, R., Blöschl, G. and Gutknecht, D. (1994): Entering the era of distributed snow models, *Nordic Hydr*ol., **25**, 1-24.

Kirnbauer, R., Lang, H. and Forster, F. (2000): Hydrological research basins - Sources of information for science and practice. Österreichische Wasser- und Abfallwirtschaft. **52**, 87-94. (in German).

Kite, G.W. (1997): Simulating Columbia river flows with data from regional-scale climate models, *Water Resour. Res.*, **33**, 1275-1285.

Kite, G.W. and Habertland, U. (1999): Atmospheric model data for macroscale hydrology, *J. Hydrol.*, **217**, 303-313.

Kleinn, J. (2002): Climate change and runoff statistics in the Rhine basin: A process study with a coupled climate-runoff Model. PhD thesis. Swiss Federal Institute of Technology (ETH). Dissertation No. 14'663. [available from the Institute for Atmospheric and Climate Science ETH, Winterthurerstr. 190, CH-8057 Zürich].

Klemeš, V. (1983): Conceptualisation and scale in hydrology. *J. Hydrol.*, **65**, 1–23.

Klemeš, V. (1990): The modelling of mountain hydrology: the ultimate challange. In: L. Molnar (Editor) *Hydrology of Mountanious Areas*, IAHS publication No. **190**, 29-43.

Klok, E.J., Jasper, K., Roelofsma, K.P., Badoux, A. and Gurtz, J. (2001): Distributed hydrological modelling of a glaciated Alpine river basin. *Hydrological Sciences Journal*, **46**, 553-570.

Konzelmann, T., Calanca, P., Menzel, L. and Müller, G. (1997): Energy balance and evapotranspiration in a high mountain area during summer. *J. Appl. Meteor.*, **36**, 966-973.

Kouwen, N., Seglenieks, F., Soulis, E.D., Benoit, R., Mailhot, J., Pellerin, P., Lee, V., Danard, M. and Chin, W.C. (1996): Modelling large watersheds with numerical weather data. *Scientific Meeting of the Canadian Geophysical Meeting, Banff, Alberta, May 5-9, 199*6. Abstract No. 26.

Krysanova, V., Bronstert, A. and Muller-Wohlfeil, D.I. (1999): Modelling river discharge for large drainage basins: from lumped to distributed approach, *Hydrolog. Sci. J.*, **44**, 313-331.

Kuo, W.L., Steenhuis, T.S., Mcculloch, C.E., Mohler, C.L., Weinstein, D.A., Degloria, S.D. and Swaney, D.P (1999): Effect of grid size on runoff and soil moisture for a variable-source-area hydrology model. *Wat. Resour. Res.* **35**(11): 3419-3428.

Lang, H. and Braun, L. (1990): On the information content of air temperature in the context of snow melt estimation, In: L. Molnar (Editor) *Hydrology of Mountanious Areas*, IAHS publication No. **190**, 347-354.

Leavesley, G.H. (1994): Modeling the effects of climate change on water resources - a review. *Climate Change*, **28**, 159-177.

Legates, D.R. and McCabe, G.J. (1999): Evaluating the use of "Goodness-of-Fit" measures in hydrologic and hydroclimatic model validation, *Water Resour. Res.*, **35**, 233-241.

Leibundgut, Ch., Uhlenbrook, S. and McDonnell, J. (Eds.) (2001): Runoff generation and implications for river basin modelling. Proceedings of the International Workshop 9-13 October 2000, *Freiburger Schriften zur Hydrologie* **13**, Institute of Hydrology, University of Freiburg i.Br., Germany.

Lunardini, V.J. (1983): *Heat transfer in cold climates*. Van Nostrand Reinhold, New York.

Lüthi, D., Cress, A., Davies, H.C., Frei, C. and Schär, C. (1996): Interannual variability and regional climate simulations, *Theor. Appl. Climatol.* **53**, 185-209.

Majewski, D. (1991): The Europa Modell of the Deutscher Wetterdienst. *ECMWF Seminar Proceedings on Numerical Methods in Atmospheric Models*, 16-18 Sept. 1991, Vol II., 147-190.

Matzinger, N., Andretta, M., van Gorsel, E., Vogt, R., Ohmura, A. and Rotach, M.W (2003): Surface Radiation Budget in an Alpine Valley. *Quarterly J. Roy. Meteorol. Soc.*, **129**, 877-895.

McGregor, J. L. (1997): Regional Climate Modelling, *Meteorol. Atmos. Phys.*, **63**, 105-117.

Menzel, L. (1995): Bodenfeuchtemessung mittels Time Domain Reflectometry (TDR) - Funktion und Anwendung, Berichte und Skripten **55**, ETH Zürich [available from the Institute for Atmospheric and Climate Science ETH, Winterthurerstr. 190, CH-8057 Zürich].

Menzel, L. (1997): Modellierung der Evapotranspiration im System Boden-Pflanze-Atmosphäre. *Zürcher Geographische Schriften*, Heft **67**, ETH Zürich [available from the Institute for Atmospheric and Climate Science ETH, Winterthurerstr. 190, CH-8057 Zürich].

Menzel, L. (1999): Flächenhafte Modellierung der Evapotranspiration mit TRAIN. [available from the Potsdam-Institut für Klimafolgenforschung e.V. PF 60 12 03, D-14412 Potsdam]

Menzel, L., Lang, H., and Rohmann, M. (1999): *Mean Annual Actual Evaporation 1973-1992*. Plate 4.1 of the Hydrological Atlas of Switzerland.

Merz, J., Dangol, P.M. and Dhakal, M.P. (2000): Comparison of climatological balances for the Jhikhu Kohla and Yarsha Kohla watersheds, Nepal. In Allen. R., Schreier, H., Brown, S. and Shah, P.B. (Editors): *The People and Resource Dynamics Project (PARDYP), the first there years (1996-1999)*. International Centre for Integrated Mountain Development (ICIMOD), 169-184.

Mihailovic, D.T., Lee, T.J., Pielke, R.A., Lalic, B., Arsenic, I.D., Rajkovic, B. and Vidale, P.L. (2000): Comparison of different boundary layer surface schemes using single point micrometeorological field data. *Theor. Appl. Climatol.*, **67**, 135-151.

Moesch, M. (2001): *Untersuchungen zur hydrologischen und klimatologischen Charakterisierung des Forschungsgebietes Rietholzbach. Auswertung des Beobachtungszeitraumes 1976-2000*. Diploma thesis, ETH Zürich [available from the Institute for Atmospheric and Climate Science ETH, Winterthurerstr. 190, CH-8057 Zürich].

Monteith, J. L. (1965): Evaporation and environment. *Symp. Soc. Exp. Biol.*, **19**, 205-234.

Monteith, J.L. (1975): *Vegetation and the atmosphere*, Vol. 1: Principles. Academic Press, London.

Monteith, J.L. (1981): Evaporation and surface temperature. *Quart J.R. Meteor. Soc.*, **107**, 1-27.

Moore, I.D., Turner, A.K., Wilson, J.P., Jenson, S. K. and Band, E.B. (1993): GIS and Land-Surface-Subsurface Process Modeling. In *Environmental Modeling with GIS*, New York: Oxford University Press, 196-230.

Müller, G., 1989: Methodische Untersuchungen zur Bestimmung der Verdunstung im voralpinen Raum. *Zürcher Geographische Schriften*, Heft 36, ETH, Zürich [available from the Institute for Atmospheric and Climate Science ETH, Winterthurerstr. 190, CH-8057 Zürich].

Murphy, A.H. and Epstein, E.S. (1989): Skill scores and correlation coefficients in model verification. *Mon. Wea. Rev.*, **117**, 572-581.

Nash, J.E. and Sutcliffe, J.V. (1970): River flow forecasting through conceptual models (1), a discussion of principles. *J. Hydrol.*, **10**, 282-290.

Nemec, J. (1993): *Comparison and selection of existing hydrological models for the simulation of the dynamic water balance processes in basins of different sizes and on different scales*. International Commission for the Hydrology of the Rhine basin, CHR/KHR-Report No. II-7.

Ohmura, A. (1982): Objective criteria for rejecting data for Bowen ratio flux calculations. *J. Appl. Meteor.*, **21**, 595-598.

Ohmura, A. (2001): Physical Basis for the Temperature-Based Melt-Index Method, *J. Appl. Meteor.*, **40**, 753-761.

Oltchev, A., Cermak, J., Gurtz, J., Keily, G., Nadezhdina, N., Tishenko, A., Zappa, M., Tishenko, N., Lebedeva, N., Vitvar, T., Albertson, J.D., Tatarinov, F., Tishenko, D., Nadezhdin, V., Kozlov, B., Ibrom, A., Vygodskaya, N. and Gravenhorst, G. (2001): The response of the water flows of the boreal forest region at the Volga's source area to climatic and land-use changes. *Phys. and Chem. of the Earth.*, Vol. **13**, 675-690.

Pardé, M. (1933): Le régime des cours d'eau de l'Europe orientale (en collaboration avec St.Kolupaila). *Revue Geographie alpine*, T.XXI,IV, 651-748.

Penman, H.L. (1948): Natural evaporation from open water, bare soil and grass. Proc. Roy. Meteorol. Soc., London, A **193**, 120-145.

Penman, H.L. (1956): Estimating evaporation. *Trans. Amer. Geophys. Union*, **37**, 43-46.

Perl, M. (2002): *Regionale Aspekte der räumlich differenzierten Verdunstungsberechnung in der Schweiz*. Diploma thesis, ETH and UNI Zürich [available from the Institute for Atmospheric and Climate Science ETH, Winterthurerstr. 190, CH-8057 Zürich].

Peschke, G. (1987): Soil moisture and runoff components from a physically founded approach. *Acta hydrophysica* **31**(3/4): 191-205.

Pos, F. (2001): *Spatially distributed modelling of snow accumulation and melt in pre-alpine and alpine catchments*. Diploma Thesis, Wageningen University. [available from the Institute for Atmospheric and Climate Science ETH, Winterthurerstr. 190, CH-8057 Zürich].

Quinn, P., Beven, K.J., Chevalier, P. and Planchon, O. (1991) The prediction of hillslope flow paths for distributed hydrological modelling using digital terrain models, *Hydrol. Process.*, **5**, 59-79.

Ranzi, R. (2001): Hydrological aspects in the Mesoscale Alpine Programme-SOP experiment: an overview. In: B. Bacchi and R. Ranzi (Editors): *Hydrological aspects in the Mesoscale Alpine Programme-SOP experiment*, Tech. Report Dept. of Civil Engineering-Univ. of Brescia, **10**(1).

Raschke, E., Karstens, U., Nolte-Holube, R., *et al.* (1998): The Baltic sea experiment BALTEX: A brief overview and some selected results of the authors, *Surv. Geophys.*, **19**, 1-22.

Razuvaev, V.N., Apasova, E.G. and Martuganov, R.A. (1995): Six-and three-hourly meteorological observations from 223 USSR Stations. ORNL/CDIAC-66, NDP-048. Carbon Dioxide Information Analysis Center, Oak Ridge National Laboratory, Oak Ridge, Tennessee.

Refsgaard, J.C. (1997): Parameterisation, calibration, validation of distributed hydrological models. *J. Hydrol.*, 198, 69-97.

Robock, A., Vinnikov, K.Ya, Srinivasan, G., Entin, J.K., Hollinger, S.E., Speranskaya, N.A., Liu, S. and Namkhai, A. (2000): The global soil moisture data bank. *Bull. Amer. Meteor. Soc.*, **81**, 1281-1299.

Roeckner, E., Arpe, K., Bengtsson, L., Christoph, M., Claussen, M., Dümenil, L., Esch, M., Giorgetta, M., Schlese, U. and Schulzweida, U. (1996): *The atmospheric general circulation model ECHAM4: Model description and simulation of present day climate*. Max Planck Institute for Meteorology Report No. 218, 171 pp.

Roeckner, E., Bengtsson, L., Feichter, J., Lelieveld, J. and Rodhe, H. (1999): Transient climate change simulations with a coupled atmosphere-ocean GCM including the tropospheric sulfur cycle. *J. Climate*, **12**, 3004-3032.

Rohrer, M.B., Braun, L.N. and Lang, H. (1994a): Long term records of snow cover water equivalent in the Swiss Alps: 1. Analysis, *Nordic Hydr*ology, **25**, 53-64.

Rohrer, M.B., Braun, L.N. and Lang, H. (1994b): Long Term records of snow cover water equivalent in the Swiss Alps: 1. Simulation, *Nordic Hydr*ology, **25**, 67-78.

Ross, B.B., Contractor, D.N. and Shanholtz, V.O. (1979): A Finite Element Model Of Overland And Channel Flow For Assessing The Hydrologic Impact Of Landuse Change. *J. Hydrol.*, **41**, 1-30.

Ross, C.N. (1921): The calculation of flood discharge by the use of time contour plan isochrones. *Transactions of the Institute of Engineers,* Australia. **2**. 85-92.

Rotach, M.W., Calanca, P., Graziani, G., Gurtz, J., Steyn, D., Vogt, R., Andretta, M., Christen, A., Cieslik, S., Conolly, R., De Wekker, S., Galmarini, S., van Gorsel, E., Kadygrov, E., Kadygrov, V., Miller, E., Neininger, B., Rucker, M., Weber, H., Weiss, A. and Zappa, M. (2003): The turbulence structure and exchange processes in an Alpine Valley: The Riviera Project. Submitted to *Bull. Amer. Meteorol. Soc.*

Roth, K., Schulin, R., Flühler, H. and Attinger, W. (1990): Calibration of Time Reflectometry for water content measurement using a composite dielectric approach. *Water Resour. Res*., **26**, 2267-2273.

Schädler, B. and Weingartner, R. (2002a): *The components of the natural water balance 1961–1990*. Plate 6.3 of the Hydrological Atlas of Switzerland.

Schädler, B. and Weingartner, R. (2002b): Ein detaillieter hydrologischer Hinblick auf die Wasserresourcen der Schweiz. *Wasser, Luft, Energie*. Jahrgang **94**, Heft 7/8, 189-197.

Schär, C., Vasilina, L. and Pertziger, F. (2002): *The use of weather prediction data to estimate winter snow cover accumulation in the Aral Sea Basin*. Research Report of the Regional Center of Hydrology, Tashkent, Uzbekistan, 23pp.

Schlosser, C.A., Robock, A., Vinnikov, K.Ya., Speranskaya, N.A. and Xue, Y. (1997): 18-year land surface hydrology model simulations for a midlatitude grassland catchment in Valdai, Russia, *Mon. Wea. Rev*., **125**, 3279-3296.

Schlosser, C.A., Slater, A.G., Robock, A., Pitman, A.J., Vinnikov, K.Ya., Henderson-Sellers, A., Speranskaya, N.A., Mitchell, K. and the PILPS 2(d) Contributors (2000): Simulations of Boreal Grassland Hydrology at Valdai, Russia: PILPS Phase 2(d). *Mon. Wea. Rev.*, **128**, 301–321.

Schulla, J. and Jasper, K. (2000): Model Description WaSiM-ETH (Water balance Simulation Model ETH). ETH Zürich [available from the Institute for Climate Research ETH, Winterthurerstr. 190, CH-8057 Zürich].

Schulla, J. (1997): Hydrologische Modellierung von Flussgebieten zur Abschätzung der Folgen von Klimaänderungen. *Zürcher Geographische Schriften*, Heft **69**, ETH Zürich. [available from the Institute for Atmospheric and Climate Science ETH, Winterthurerstr. 190, CH-8057 Zürich]

Schwarb, M. (2001): The Alpine Precipitation Climate. Evaluation of a High-Resolution Analysis Scheme Using Comprehensive Rain-Gauge Data. Diss. ETH No. 13911. *Zürcher Klima-Schriften*, Heft **80**, ETH Zürich. [CD available from the Institute for Atmospheric and Climate Science ETH, Winterthurerstr. 190, CH-8057 Zürich]

Schwarb, M., Daly, C., Frei, C. and Schär, C. (2001): *Mean Annual Precipitation throughout the European Alps 1971-1990*. Plates 2.6 and 2.7 of the Hydrological Atlas of Switzerland.

Schwarze, R., Droege, W. and Opherden, K. (1999): Regional analysis and modelling of groundwater runoff components from catchments in hard rock areas. In: Diekkrüger B, Kirkby MJ, Schröder U (Editors): *Regionalisation in hydrology*, IAHS Publication No. **254**, 221-232.

Seibert, J. and McDonnell, J.J. (2001): Towards a better process representation of catchment hydrology in conceptual runoff modelling. Freiburger Schriften zur Hydrologie 13, pp. 128-137.

Seibert, J. and McDonnell, J.J. (2002): On the dialog between experimentalist and modeler in catchment hydrology: Use of soft data for multi-criteria model calibration. *Water Resour. Res*. in press.

Sellers, P.J. *et al.* (1997b): Modeling the exchanges of energy, water, and carbon between continents and the atmosphere. *Science*, **275**, 502-509.

Sellers, P.J., Hall, F.G., Asrar, G., Strebel, D.E., and Murphy, R.E. (1988): The 1st ISLSCP Field Experiment (FIFE), *Bull. Amer. Meteor. Soc.*, **69**, 22-27.

Sellers, P.J., Hall, F.G., Kelly, R.D., Black, A., Baldocchi, D., Berry, J., Ryan, M., Ranson, K.J., Crill, P.M., Lettenmaier, D.P., Margolis, H., Cihlar, J., Newcomer, J., Fitzjarrald, D., Jarvis, P.G., Gower, S.T., Halliwell, D., Williams, D., Goodison, B., Wickland, D.E. and Guertin, F.E. (1997a): BOREAS in 1997: Experiment overview, scientific results, and future directions. *J. Geophys. Res.*, **102**, 28731-28769.

Sevruk, B. (ed.) (1986): Correction of Precipitation Measurements. ETH / IASH / WMO Workshop on the Correction of Precipitation Measurements. *Zürcher Geographische Schriften*, Heft **23**, ETH Zürich. [available from the Institute for Atmospheric and Climate Science ETH, Winterthurerstr. 190, CH-8057 Zürich].

Sevruk, B. and Kirchhofer, W. (1992): *Mean Annual Corrections of Measured Precipitation Depths 1951 – 1980*. Plate 2.3 of the Hydrological Atlas of Switzerland.

Singh, V.P. (1997): Effect of spatial and temporal variability in rainfall and watershed characteristics on stream flow hydrograph. *Hydrol. Process*., **11**, 1649-1669.

Singh, V.P. and Woolhiser, D.A. (2002): Mathematical modelling of watershed hydrology. *J. Hydrol. Eng.*, **7**, 270-292.

Slater, A.G., Schlosser, C.A., Desborough, C.E., Pitman, A.J., Henderson-Sellers, A., Robock, A., Vinnikov, K.Ya., Mitchell, K. and the PILPS 2(d) Contributors (2001): The representation of snow in land-surface schemes; results from PILPS 2(d). *J. Hydrometeorology*, **2**, 7-25

Strasser, U. and Mauser, W. (2001): Modelling the spatial and temporal variations of the water balance for the Weser catchment 1965-1994. *J. Hydrol.*, **254**, 199-214.

Strasser, U., Etchevers, P. and Lejeune, Y. (2002): Intercomparision of two snow models with different complexity using data from an alpine site. *Nordic Hydrol*., **33**, 15-26.

Susong, D., Marks, D. and Garen. D. (1999): Methods for developing time-series climate surfaces to drive topographically distributed energy- and water-balance models. *Hydrol. Process.*, **13**, 2003-2021.

Tishenko, A.P., Pirogow, Y.A., Kowalewskaya, O.W., Kozlow, B.V. and Tishenko, N.N. (1998): Delineation of the boundary of the central main watershed region of the Russain Plain. Thematical Report, State University of Tver, S. 124-133, in Russian.

Topp, G.C., Davis, J.L. and Annan, A.P. (1980). Electromagnetic determination of soil water content: measurements in coaxial transmission lines. *Water Resour. Res*., **16**, 574-582.

Uhlenbrook, S. (1999): *Untersuchung und Modellierung der Abflußbildung in einem mesoskaligen Einzugsgebiet*, Freiburger Schriften zur Hydrologie, **10**, Freiburg i. Br.

Uhlenbrook, S. and Hoeg, S. (2002): Quantifying uncertainties in tracer-based hydrograph separation: a case study for two-, three- and five-component separations in a mountainous catchment. *Hydrol. Processes*, **17**, 431-453.

Uhlenbrook, S. and Leibundgut, Ch. (2002): Process-oriented catchment modelling and multiple-response validation. *Hydrol. Process.*, **16**, 423-440.

Vàzquez, R.F., Feyen, L., Feyen, J. and Refsgaard, J.C. (2002): Effect of grid size on effective parameters and model performance of the MIKE-SHE code, *Hydrol. Process.*, **16**, 355–372.

Verbunt, M., Gurtz, J., Jasper, K., Lang, H., Warmerdam, P. and Zappa, M. (2003): The hydrological role of snow and glaciers in alpine river basins and their distributed modelling. *J. Hydrol.*, in print.

Vidale, P. L., Lüthi, D., Heck, P., Frei, C. and Schär, C. (1999): *The development of the Climate High-Resolution Model (C-HRM).* Quarterly Report of the Operational NWP-Models of the Deutscher Wetterdienst, No. **21**, 3-17. [available as pdf-file from http://www.dwd.de/research/publications/QuarterlyReport]

Vidale, P.L., Lüthi, D., Frei, C., Seneviratne, S. and Schär, C. (2003): Predictability and Uncertainty in a Regional Climate Model. Submitted to *J. Geophys. Res*.

Vitvar, T., 1998. Water residence times and runoff generation in a small prealpine catchement. *Zürcher Geographische Schriften*, Heft **71**, ETH Zürich [available from the Institute for Atmospheric and Climate Science ETH, Winterthurerstr. 190, CH-8057 Zürich].

von Storch, H. and Zwiers, F.W. (1999): *Statistical Analysis in Climate Research*, Cambridge University Press, 494 pp.

Walko, R.L., Band, L.E., Baron, J., Kittel, T.G.F., Lammers, R., Lee, T.J., Ojima, D., Pielke Sr., R.A., Taylor, C., Tague, C., Tremback, C.J. and Vidale, P.L., 2000. Coupled Atmosphere-Biophysics-Hydrology Models for Environmental Modeling, *J. Appl. Meteor.*, **39**, 931-944.

Weingartner, R. and Aschwanden, H. (1992): *Discharge regimes*. Plate 5.2 of the Hydrological Atlas of Switzerland.

Wendling, U. (1975): Zur Messung und Schätzung der potentiellen Verdunstung. *Zeitschrift für Meteorologie*, **25**, 103-111.

Western, A.W., Grayson, R.B., Blöschl, G., Willgoose, G.R. and T.A. McMahon (1999): Observed spatial organization of soil moisture and its relation to terrain indices, *Water Resour. Res.*, **35**, 797-810.

Wigmosta, M.S., Vail, L.W. and Lettenmaier, D.P. (1994): A distributed hydrology-vegetation model for complex terrain. *Water Resour. Res.*, **30**, 1665-1680.

Wild, M., Ohmura, A and Cubasch, U. (1997): GCM-Simulated surface energy fluxes in climate change experiments, *J. Climate*, **10**, 3093-3110.

Wild, M., Ohmura, A., Gilgen, H., Roeckner, E., Giorgetta, M. and Morcrette, J.J. (1998): The disposition of radiative energy in the global climate system: GCM-calculated versus observational estimates. *Climate Dynamics*, **14**, pp. 853-869.

WMO (1983): Guide to meteorological instruments and observing practices. WMO n° 8 (fifth edition), World Meteorological Organization, Geneva.

WMO (1986): Intercomparison of models of snowmelt runoff. Operational Hydrology Report **23**, World Meteorological Organization, Geneva.

Wolock, D.M. and Price, C.V. (1994): Effects of digital elevation model map scale and data resolution on a topography based watershed model', *Water Resour. Res.*, **30**, 3041-3052.

Wood, A.W., Lettenmaier, D.P. and Palmer, R.N. (1997): Assessing climate change implications for water resource planning, *Climatic Change*, **37**, 203-228.

Wood, E.F., Sivapalan, M., Beven, K.J. and Band, L. (1988): Effects of spatial variability and scale with implications to hydrologic modelling. *J. Hydrol.*, **102**, 29–47.

WSL (2001): Schweizerischer Landesforstinventar LFI. Datenbankauszug der Erhebung 1983-85 vom 24. April 2001. Ulrich Ulmer. Eidg. Forschungsanstalt WSL, Birmensdorf.

Zappa, M. (1999): *Untersuchungen zur Aufbereitung unterschiedlicher Rauminformationen für die flächendifferezierte Einzugsgebietsmodellierung*. Diploma thesis, ETH Zürich [available from the Institute for Atmospheric and Climate Science ETH, Winterthurerstr. 190, CH-8057 Zürich].

Zappa, M. and Gurtz, J. (2002): The spatial resolution of physiographic data as sensitive variable for distributed hydrological simulations in prealpine and alpine catchments. *In Water Resources and Environment Research*, Proceedings of ICWRER 2002,22-25 July 2002 Dresden, Germany, Band **28**, Volume I, pp. 101-105, 1.

Zappa, M. and Gurtz, J. (2003): Plot-scale simulation of soil moisture and evapotranspiration during the 1999 MAP-Riviera campaign. Submitted to *Hydrology and Earth System Sciences.*

Zappa, M., Badoux, A., and Gurtz, J. (2000): The application of a complex distributed hydrological model in an highly glaciated alpine river catchment. In: Horvatic, J. (Editor): *Proceedings of the 33rd Conference of International Association for Danube Research*, *Limnological Reports*, **33**, 23-28.

Zappa, M., Matzinger, N. and Gurtz, J. (2001): Hydrological and Meteorological Measurements at Claro (CH) - Lago Maggiore Target Area in the MAP-SOP 1999 RIVIERA Experiment - Including First Evaluation. In: B. Bacchi and R. Ranzi (Editors): *Hydrological aspects in the Mesoscale Alpine Programme-SOP experiment*, Tech. Report Dept. of Civil Engineering-Univ. of Brescia, **10**(2).

Zappa, M., Pos, F., Strasser, U. and J. Gurtz (2003): Seasonal water balance of an alpine catchment as evaluated by different methods for spatially distributed snow melt modelling. *Nordic Hydrology*, Vol. **34(3)**.

Zhang, W., and D.R. Montgomery (1994): Digital elevation model grid size, landscape representation, and hydrologic simulations, *Water Resour. Res.*, **30**, 1019-1028.

Acknowledgements to data providers

MeteoSwiss is acknowledged for supplying the meteorological data through the ETH database.

The Swiss Federal Institute for Snow and Avalanche Research SLF Davos provided the snow water equivalent data. "SLF Messdaten © SLF 1999"

The Swiss Federal Institute for Forest, Snow and Landscape Research WSL provided information on the Swiss Forests inventory (WSL 2001).

The Swiss Federal Office for Water and Geology provided the data on observed discharge.

The copyright of digital data of the Hydrological Atlas of Switzerland adopted for the analysis presented in section 7.4.6 is at the Swiss Federal Office for Water and Geology (agreements of December 17 2001 and October 2 2002).

The set of NOAA-AVHRR pictures used in section 7.4.4 were kindly provided by MFB-GeoConsulting (Bern - CH).

Acknowledgements

This thesis summarizes my work as a PhD student at the Institute for Atmospheric and Climate Research of the ETH. Many people, colleagues and friends contributed with precious advices and practical support. I would like to thank all of them for their contribution to this work. Grazie!

My supervisor Christoph Schär contributed with well-appreciated ideas and comments. His hints allowed a substantial improvement of the scientific substance of my work. Additionally, I want to thank Christoph for providing an ideal atmosphere of collaboration within his team.

It's challenging for me to find adequate words to thank my advisor and friend Joachim Gurtz. I'm grateful he assigned me this dissertation. I liked every single moment of my collaboration with him. It has been always fun for me to work with and for him and join him during conferences and excursions. The content of this thesis is the realization of some of his visions on the potentials of distributed hydrological models in mountainous regions.

I want to thank my external examiners Prof. Günter Blöschl and PD Dr. Rolf Weingartner. Their thorough know-how on hydrological issues was very appreciated. Both of them provided helpful reviews and comments. I particularly appreciated the invitation of Prof. Blöschl to Wien and the discussions with Rolf Weingartner at the railway station in Olten.

I want to address a particular thank to my former diploma students Philippe Achleitner, Nicolas Matzinger, Michael Moesch, Femke Pos, Madlaina Perl. Their help at different stages of this thesis allowed me for making important progresses.

Many thanks to the "MAP-Riviera team", especially to Mathias Rotach, Pierluigi Calanca, Marco Andretta, Karl Schroff and Shari Carlaw. MAP-Riviera has been founded by the Swiss National Science Foundation (Grant 20-63820.01).

The VOLGA FOREST project partners are acknowledged for the fruitful collaboration. The VOLGA FOREST Project has been founded by the European Commission (Grant ERBIC-15-CT98-0120) through the Swiss Federal Office for Education and Science (Bundesamt für Bildung und Wissenschaft, Grant BBW 98.0005). I thank Pier Luigi Vidale and Martin Wild for providing the results of their simulation with their atmospheric models.

Ulrich Strasser is acknowledged for providing the code of ESCIMO. Thanks to Ueli Moser for keeping the lysimeter working and for his engagement during our trips to the Rietholzbach catchment. I'm grateful to Prof. Herbert Lang for the friendly discussions. Special thanks to Raelene Sheppard for carefully correcting the English. William Sawyer also corrected parts of this manuscript

Thanks to Rae, Hendrik, Sebastian, Mark, André, Ludwig, Tomas, Alexandra, Sonia, Oli, Reto, Pia, Uta and all non-mentioned Institute members during my PhD project. I really enjoyed the life at the Institute, within and after the working hours. I will never forget the friendly atmosphere during the work, coffee breaks, Pegel parties and excursions.

Thanks to my parents and my sister for their endless love and support.

Thanks Karin.

May 2003, Massimiliano Zappa

Curriculum Vitae

Massimiliano Zappa, Altwiesenstrasse 152, CH-8051 Zürich
Born on April 12, 1975, in Viganello (TI)
Citizen of Onsernone (TI)

Education and Professional Training

1999- 2002	Scientific collaborator and Ph. D. Student Study at the Institute for Atmospheric and Climate Science, ETH Zürich, in the group headed by Prof. Ch. Schär.
May 1999	*Dipl. Sc. Nat. ETH.* Diploma Thesis under the guidance of Dr. habil. J. Gurtz: "Untersuchungen zur Aufbereitung unterschiedlicher Rauminformationen für die flächendifferezierte Einzugsgebietsmodellierung"
1994 - 1999	Graduate education at the Faculty of Natural Sciences (XC) of the Swiss Federal Institute of Technology (ETH) Zürich. Specialization in Hydrology and Climatology.
June 1994	*Matura Type B*
1990 - 1994	Liceo cantonale di Mendrisio (Ticino, Switzerland).
1981 - 1990	Primary education in Arzo and Mendrisio (Ticino, Switzerland).

International Conferences and Workshops

- Workshop "INCO COPERNICUS - Volga Forest - First year report", Göttingen, Germany, February 2000
- European Geophysical Society 25th General Assembly, Nice, France, April 2000
- 33rd Conference of International Association for Danube Research, Osijek, Croatia, September 2000
- International Workshop on runoff generation and implications for river basin modelling, Freiburg i. Br., Germany, October 2000
- Annual Meeting of SGHL / SANW, Winterthur, Switzerland, October 2000
- Annual Meeting of SGM / SANW, Winterthur, Switzerland, October 2000
- European Geophysical Society 26th General Assembly, Nice, France, March 2001
- Sommerschule Umweltphysik, Heidelberg, Germany, July 2001
- Phil.Alp 2002, Interacademic Commission Alpine Studies, Switzerland, March 2002
- Third International Conference on Water Resources and Environment Research ICWRER 2002, Dresden, Germany, July 2002.
- Annual Meeting of SGHL / SANW, Davos, Switzerland, September 2002